Petrogenesis of collision-related plutonic rocks, central Anatolia(Turkey)

Nurdane Ilbeyli

Petrogenesis of Collision-Related Plutonic Rocks, Central Anatolia (Turkey)

by

NURDANE ILBEYLI

A thesis submitted in partial fulfillment of the requirements for the degree of Doctor of Philosophy

Department of Geological Sciences

University of Durham

December 1998

Canım annem ve babama
Sevgilerimle

This work is dedicated to
my mum, Safiye, and my dad, Hasan,
for their love

ABSTRACT

Petrogenesis of Collision-Related Plutonic Rocks, Central Anatolia (Turkey)

Central Anatolia exhibits good examples of calc-alkaline and alkaline magmatism of similar age in a collision-related tectonic setting (continent-island arc collision). In the Central Anatolia region, post-collisional plutonic rocks (around 79.5 to 66.6 Ma) intrude Palaeozoic-Mesozoic metamorphic rocks overthrust by Upper Cretaceous ophiolitic units to make up the Central Anatolian Massif.

In the Massif, three different intrusive rock types are recognised based on their geochemical characteristics: (i) calc-alkaline (Behrekdag, Cefalikdag, Celebi-BCC); (ii) transitional (Baranadag-B); and (ii) alkaline (Hamit-H). The BCC and B plutonic rocks are metaluminous, I-Type ranging from monzodiorite to granite. The H plutonic rocks are metaluminous to peralkaline, predominantly A-Type ranging from nepheline monzosyenite to quartz syenite.

Two types of igneous enclave have been recognised in the BCC plutonic rocks; (i) fine-grained (Type-I); and (ii) medium-grained to porphyritic with feldspar megacrysts (Type-II). Field, petrographic and geochemical evidence suggest that the Type-I enclaves originated from injection of mafic magma into more silicic magma. Field, petrographic and mineralogical evidence together with major and trace element geochemistry suggest that the Type-II enclaves formed as cumulates of early-crystallised minerals (e.g. clinopyroxene, plagioclase, amphibole and biotite) from the granitoid magmas.

All intrusive rocks show enrichment in LILE and LREE relative to HFSE and have high $^{87}Sr/^{86}Sr$ and low $^{143}Nd/^{144}Nd$ ratios. These characteristics indicate an enriched mantle source region(s) carrying a subduction component inherited from pre-collision subduction events. Rb, Nb, Y versus SiO_2 diagrams and the tectonic discrimination diagram of Rb and the (Y+Nb) suggest that the BCC, B and H plutonic rocks have been affected by crustal assimilation combined with fractional crystallisation processes.

Coexistence of calc-alkaline and alkaline magmatism in the Central Anatolian Massif has been attributed to mantle source heterogeneity before collision. Either thermal perturbation of the metasomatised lithosphere by delamination of the thermal boundary layer (TBL) or removal of a subducted plate (slab breakoff) are the likely mechanisms for the initiation of the post-collisional magmatism in the Massif.

DECLARATION

I declare that this thesis, which I submit for the degree of Doctor of Philosophy at the University of Durham, is my own work and is not the same as any which has been previously been submitted for a degree at this or any other university.

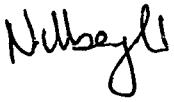

Nurdane Ilbeyli

University of Durham

Department of Geological Sciences

December 1998

ACKNOWLEDGEMENTS

Many people have been of great help during this study. First and foremost, I would like to thank to my supervisor, Dr. Julian A. Pearce for his helpful comments and criticisms. This thesis would not have been finished without his advice, support and encouragement. He read and offered suggestions on each chapter of this thesis, which make me rethink and clarify ideas in this study.

I would like to express my thanks to the Mustafa Kemal University and the Higher Educational Council (Turkey) for their generous financial support to carry out my research.

I am grateful to Yüksel Çakır, mayor of Kaman town, for providing me accommodation and also transport during my fieldtrips.

The original idea of this project stems from Prof. Dr. Okan Tekeli, who first aroused my interest in the intrusive rocks of the Central Anatolian Massif. I want to express my personal gratitude to him.

I owe great deal to Dr. Mehmet Keskin for his help, assistance and instruction in the preparation of XRF analysis.

I thank to Ron Hardy and Dr. Chris Ottley for their help and assistance of XRF and ICP-MS.

I am indebted to Drs. Peter Hill, Stuart Kearns and Simon Burgess for their assistance and instructions in the use of electron microprobe facilities at the University of Edinburgh.

I wish to thank to Prof. John Mitchell for carrying out radiometric (K-Ar) dating.

I am grateful to Dr. Matthew Thirlwall, Gary Ingram and Dr. Robin Gill for their help and assistance during performing isotopic analyses at the University of London, Royal Holloway.

I wish to thank to Cafer Şerifi for his help during one of my fieldtrips. Veysel Işık is thanked for providing me some samples from the Central Anatolian Massif.

I thank to TPAO geologist, Hasan Emiroğlu and MTA geologist, Haydar Kara for providing me maps of the Central Anatolian Massif.

There are so many people to whom I want to thank for their help and assistance during my study at the Durham University. The list starts with Prof. Maurice Tucker, Prof. Bob Thompson, Dr. Greenville Holland and Dr. Bob Holdsworth. Dr. Graham Pearson is thank to for helping me during the preparation of mineral analysis for ICP-MS. Ron Lambert and Julie Harrison are thanked for the preparation of countless thin sections of high quality; Gerry Dresser, Alan Carr for providing me great photograph services; Dave Asbury, Carol Blair and Claire Whitehill for their assistance; Dave Stevenson and George Ruth for their help to solve computer problems. I am indebted to Karen Atkinson for helping me prepare conference slides.

I thank to Affonso, Teresa, Vicky, Robin, Andy and Sarah(s) for their companionship, and special thanks to Belma and Ercan for their friendship and so many great chats.

Finally, and most importantly, my deepest thanks go to my family: my parents, Hasan and Safiye Ilbeyli, my brother, İsmail and my sisters, Nezaket, Zübeyde, Güldane whose constant love, support and understanding have helped me throughout all my life. I thank to my brother-in-law, Yalçın, my sister-in-law, Selamet and my niece, Aslı Nur for their support during this study. I owe special debt of gratitude to my brother, İsmail and my sister, Güldane for their help during my fieldtrips.

CONTENTS

CHAPTER 4: MINERAL GEOCHEMISTRY

CHAPTER 5: MAJOR AND TRACE ELEMENT GEOCHEMISTRY

CHAPTER 6: THE ENCLAVES

Chapter 1
INTRODUCTION

Granitic rocks can have a wide range of sources, from upper mantle to upper crust, displaying a significant correlation with tectonic setting (Pearce, 1996). These settings are; mid-ocean ridge, oceanic island arc, active continental margin, intraplate settings, particularly rift zone and collision zones.

Many collision zones (e.g. the Himalayas and Anatolia) display associations of calc-alkaline to alkaline magmatism which are closely related in space and time. The genesis of these calc-alkaline to alkaline magmatism has been the subject of debate, even though their origins still remain one of the most interesting and least well understood of all petrological problems. Bonin (1990) carried out some work on the intrusive rocks in the Alps, where magmatism changed from calc-alkaline to alkaline around the end of Permian. He argued that the source was roughly similar, and the change from calc-alkaline to alkaline magmatism was caused by decreasing water contents. When water is present, calc-alkaline magmas are produced from mantle; when water is unavailable, the same source generates alkaline magmas. Pearce et al. (1990) did some work on the collision-related volcanics in Eastern Anatolia. They argued that derivation from mantle above an earlier subduction gives a calc-alkaline character and derivation from the lithosphere beneath the passive margin gives an alkaline character.

The Central Anatolia region has been chosen for this study, as this region exhibits good examples of calc-alkaline and alkaline magmatism of similar age in a collision-related tectonic setting. In this work, attention is focused on the petrogenetic evolution of the Central Anatolian intrusive rocks.

1.1. Geological setting of the Central Anatolian Massif

Turkey is one of the important segments of the Tethyan orogenic collage, which lies between Eurasia in the north and Gondwanaland in the south. It is made up of a number of continental blocks separated by ophiolitic suture zones (Figure 1.1). This complex structure formed as the result of the closure of the different

branches of the Neotethyan ocean during the late Cretaceous-Eocene (Sengör and Yilmaz, 1981).

The studied area is situated in one of these blocks, the Central Anatolian Massif (Figure 1.1). The Massif is variously called the Kirsehir Massif, the Kizilirmak Massif (Erkan, 1981), the Kirsehir continent (Sengör et al., 1984) and the Central Anatolian Crystalline Complex (Göncüoglu et al., 1991). Two main models for the evolution of the Central Anatolian Massif have been proposed as follows:

(i) According to ***Sengör and Yilmaz (1981),*** the closure of Paleo-Tethys during the middle Jurassic meant that only two oceans were left in Turkey: the multi-branched northern, and the relatively simple, southern branch of Neo-Tethys (Figure 1.2). Sengör and Yilmaz (1981) postulated that the northern branches of Neo-Tethys consisted of the Izmir-Ankara-Erzincan, Intra-Pontide and the Inner Tauride oceans and that these separated the Anatolide-Tauride platform together with the Bitlis-Pötürge fragment from Eurasia (Figure 1.2). By contrast, the southern branch of Neo-Tethys separated the platform and fragment from the main body of Gondwanaland. According to Sengör and Yilmaz (1981), the Intra-Pontide and the Izmir-Ankara-Erzincan oceans isolated the Sakarya continent within the northern branches of Neo-Tethys.

The Izmir-Ankara-Erzincan ocean began opening between the Sakarya continent to the north and the Anatolide-Tauride platform to the south during the early Jurassic (Lias) (Figure 1.2a). The northern branches of the Neo-Tethyan ocean reached their maximum size during the early Cretaceous (Figure 1.2c).

The Izmir-Ankara-Erzincan ocean started to close at the beginning of the late Cretaceous along two north-dipping subduction zones beneath the Pontide arc (Sengör and Yilmaz, 1981) (Figure 1.2d). According to Sengör and Yilmaz (1981), the Rhodope-Pontide fragment collided with the Sakarya continent during the latest Cretaceous along the Intra-Pontide suture and acted as a single block-''the Pontides".

Ophiolite and ophiolitic mélange slivers from the Izmir-Ankara-Erzincan ocean, were obducted southwards onto the northern margin of the Anatolide-Tauride platform during the late Cretaceous (Figure 1.2d). Sengör and Yilmaz (1981) named these ophiolite and ophiolitic mélange slivers "the Bozkir ophiolite nappe".

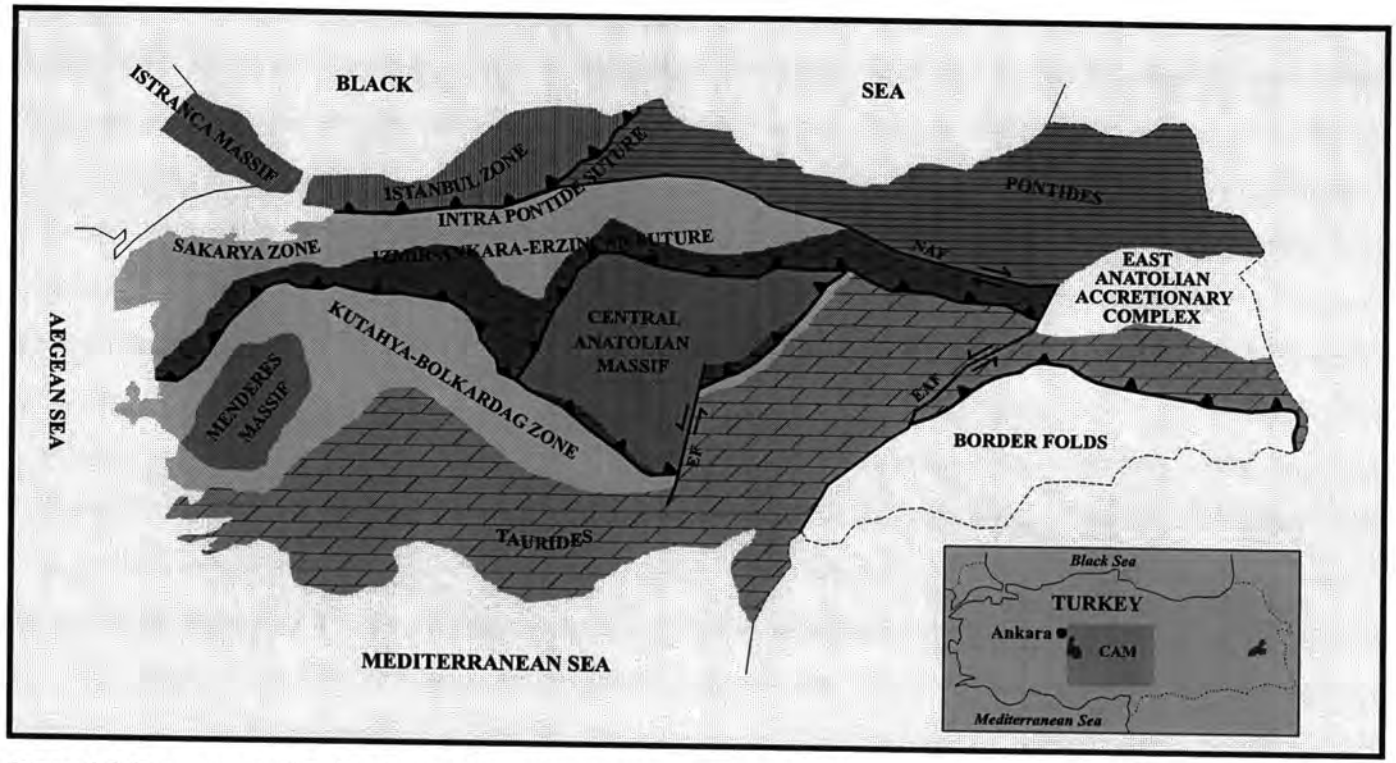

Figure 1.1. Tectonic map of Turkey showing the major tectonic zones, modified from Sengör and Yilmaz (1981). The inset map shows the Central Anatolian Massif in relation to the rest of Turkey. Abbreviations: CAM-Central Anatolian Massif, NAF-North Anatolian Fault, EAF-East Anatolian Fault and EF-Ecemis Fault. Heavier lines with black triangles show subduction zones and lines with half arrows display transform faults.

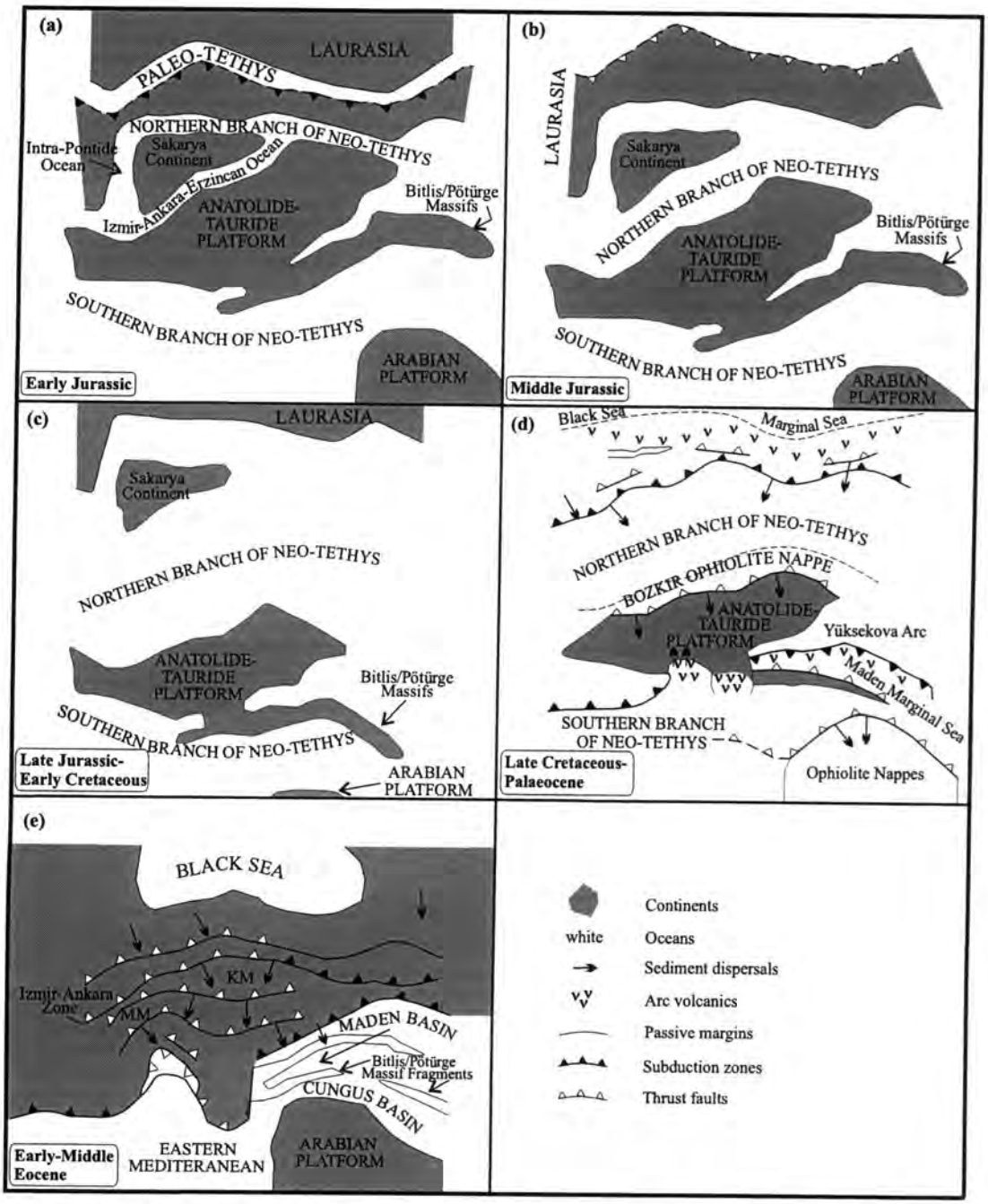

Figure 1.2. Paleotectonic maps depicting the tectonic evolution of Turkey simplified after Sengör and Yilmaz, 1981. Abbreviations: KM-Kirsehir Massif and MM-Menderes Massif.

This obduction caused crustal thickening, metamorphism and subsequent granite plutonism in the northern edge of the platform. The Anatolide-Tauride platform and the Pontides collided during the late early-middle Eocene (Sengör and Yilmaz, 1981). As a result of this collision, extensive internal deformations and uplifts of the Anatolide-Tauride platform took place (Figure 1.2e).

(ii) In contrast to the Sengör and Yilmaz (1981) model, ***Görür et al. (1984)*** assumed a distinct Inner Tauride ocean (Figure 1.3). In their model, the three major tectonic elements, the Pontides, the Menderes-Taurus and the Kirsehir Blocks, were all separated from one another by various branches of Neo-Tethys during the late Maastrichtian, with the exception of the contact between the toe of the Sakarya continent and the northwest corner of the Kirsehir Massif (Figure 1.3a).

North-dipping subduction of the northern branch of the Neo-Tethys began beneath both the Rhodope-Pontide fragment and the Sakarya continent during the Cenomanian and Turonian interval (Görür et al., 1984). After the Maastrichtian collision of the Sakarya continent with the Rhodope-Pontide fragment, a single, sinuous, north-dipping subduction zone remained along the southern boundary of the Pontides (Sakarya continent+Rhodope-Pontide fragment) (Figure 1.3a).

Görür et al. (1984) argued that the Baranadag plutonic complex, which follows the western margin of the Kirsehir Massif (Figure 1.4), began its intrusion during the Maastrichtian and continued through the Palaeocene. They suggested that the nearest subduction zone with appropriate age and orientation that could have generated this magmatic axis was the Inner Tauride suture (Sengör et al., 1982), located to the west and southwest of the Tuzgolu Basin (Figure 1.3b). Görür et al. (1984) argued that the Baranadag plutonic axis represents an Andean-type continental arc perched along the western margin of the Kirsehir Block as the latter moved westwards relative to the Menderes-Taurus Block.

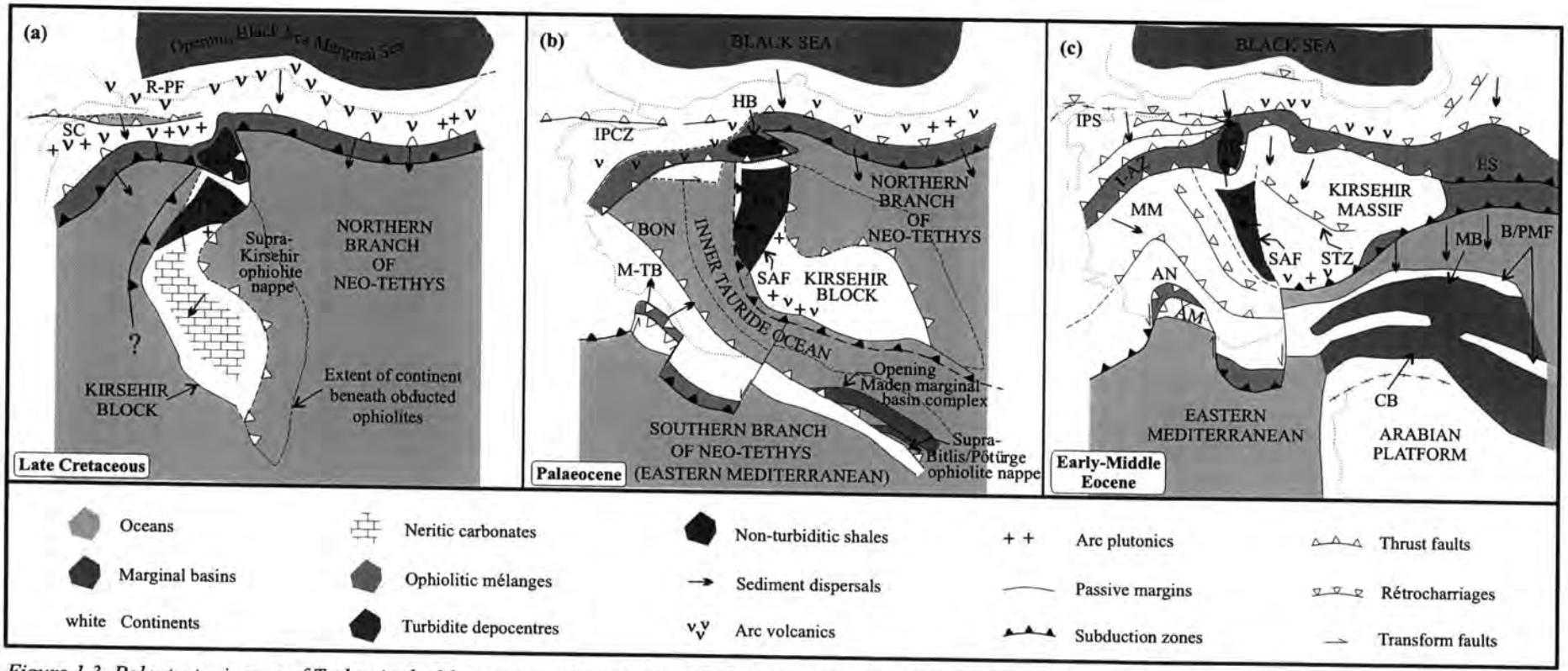

Figure 1.3. Paleotectonic map of Turkey in the Mesozoic and Tertiary simplified after Görür et al. (1984). Abbreviations: R-PF- Rhodope-Pontide Fragment, SC- Sakarya Continent, HB- Haymana Basin, TB-Tuzgolu Basin, IPCZ- Intra-Pontide Convergence Zone, BON- Bozkir Ophiolite Nappe, M-TB- Menderes-Taurus Block, SAF- Sereflikochisar-Aksaray Fault, IPS- Intra-Pontide Suture, I-AZ- Izmir-Ankara Zone, ES- Erzincan Suture, MM- Menderes Massif, B/PMF- Bitlis-Pötürge Fragments, STZ- Savcili Thrust Zone, MB- Maden Basin, CB- Cungus Basin, AM- Alanya Massif and AN- Antalya Nappe. Oceans are the various branches of Neo-Tethys; and Black Sea, Maden and Cungus Basins are the Neo-Tethys-related marginal basins.

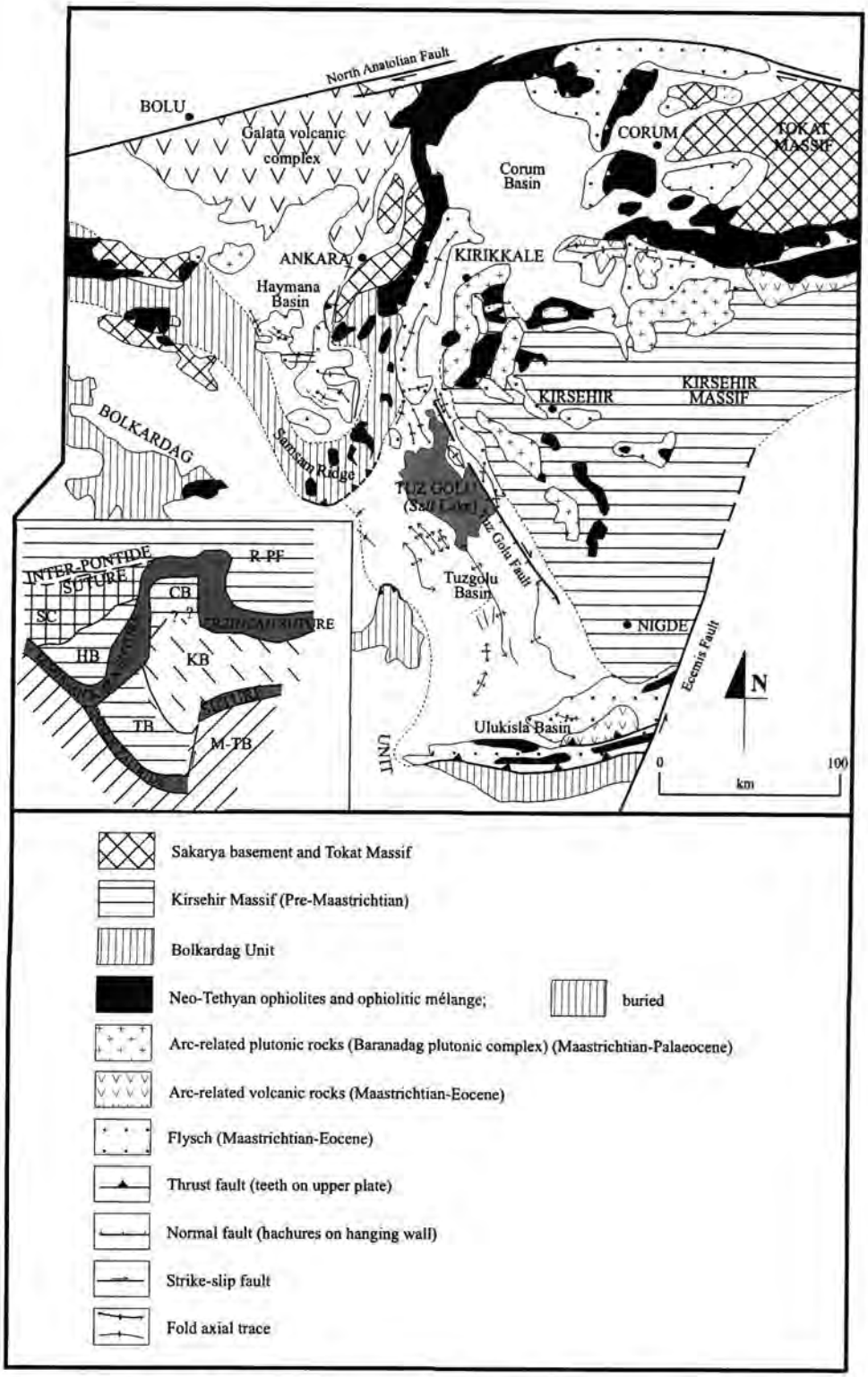

Figure 1.4. Simplified geological setting of the Central Anatolian Massif and surrounding regions (after Görür et al., 1984). White areas younger (Oligocene to Quaternary) cover. The inset map shows the first-order paleotectonic elements, i.e. continental blocks and suture zones in the area. Abbreviations: SC- Sakarya Continent, HB- Haymana Basin, TB- Tuzgolu Basin, CB- Corum Basin, R-PF- Rhodope-Pontide Fragment, KB- Kirsehir Block and M-TB- Menderes-Taurus Block.

During the late Maastrichtian, major parts of the Kirsehir Massif were covered by an ophiolitic nappe expelled from the northern branch of Neo-Tethys, now represented by the Erzincan suture. The initial contact between the Kirsehir Block and the Pontides took place during the late Maastrichtian (Figure 1.3a). Because arc magmatism both north of the Erzincan suture and along the western margin of the Kirsehir Massif continued into the Eocene (Figures 1.3a-c), thus neither the Erzincan nor the Inner Tauride sutures could have closed prior to the Palaeocene.

The collision of Sakarya and Kirsehir fore-arcs pinned the northwest corner of the Kirsehir Block to the Pontides, and around it the Kirsehir Massif began to rotate in an anticlockwise fashion until its entire present northern margin completely collided with the eastern Pontides along the Erzincan suture during the Priabonian (Seymen, 1975) (Figure 1.3c). The Inner Tauride suture closed during the late Eocene, thus completely isolating the Tuzgolu Basin among three converging continental blocks (Figure 1.3c).

The age of closure of the Izmir-Ankara-Erzincan ocean and the emplacement age of the Bozkir ophiolite nappe onto the Anatolide-Tauride platform are still the subject of debate. For the age of closure of the Izmir-Ankara-Erzincan ocean, Sengör and Yilmaz (1981) argue for a late Palaeocene-early Eocene collision between the Pontides and the platform. However, on the basis of blueschist evidence, Okay (1984a) postulated a late Cretaceous age for the final collision. He also added that the collision may have been diachronous, starting in the late Cretaceous in northwest Turkey and progressing eastward to the Eastern Sakarya Zone where island arc volcanism continued into the Eocene. Harris et al. (1994) argued that the obduction of the ophiolite fragments along the Izmir-Ankara-Erzincan suture zone indicate that the time of collision was certainly earlier than the middle Eocene and probably after the upper Cretaceous (Turonian).

Faunal data suggest that ophiolites in central Anatolia (Göncüoglu et al., 1992a; Yaliniz et al., 1996) and those in the Kütahya-Bolkardag Belt (Figure 1.1) (Ozcan et al., 1989; Göncüoglu, 1990) were emplaced by the pre-Upper Maastrichtian. Onen and Hall (1993) used stratigraphic evidence to postulate that ophiolite emplacement around the Kütahya region was completed by the Maastrichtian.

1.2. Previous studies in the Central Anatolian Massif

Most of the previous work in the Central Anatolian Massif has concentrated on the general geology and the metallogenic provinces of the Massif.

Ketin (1955, 1963) carried out some of the early work on general geology of central Anatolia. The term "Central Anatolian Massif" is used by him to refer to the crystalline rocks around Kirsehir. He (1963) revised and complied earlier and recent works on central Anatolia and prepared a map on a scale of 1:500 000.

Erkan (1976) studied the characteristics and conditions of metamorphism around Kirsehir. According to him, these rocks were metamorphosed under high temperature-medium pressure conditions and the degree of metamorphism increased from the south to the north-northeast of the Massif.

Göncüoglu (1977) did some work on the metamorphic rocks in the southern part of the Central Anatolian Massif. He named the Nigde group and argued that these rocks were the product of a medium-high grade of metamorphism.

Seymen (1981, 1982) studied the area between the Kirsehir and Kaman regions which comprises mainly the metamorphic rocks of the Central Anatolian Massif. He named these metamorphics "the Kaman group" and divided them into the Kalkanlidag, Tamadag and Bozcaldag formations. The Kalkanlidag formation is characterised by a complex of gneisses, biotite schists, pyroxene schists, quartzites and calc-silicate schists. The Tamadag formation is an intercalation of marbles, schists and gneisses. The Bozcaldag formation is primarily composed of marbles, meta-chert bearing marbles and meta-cherts. On the basis of their sedimentary characteristics, Seymen (1983, 1985) argued that the protoliths of the basal part of this sequence were flood plain-meandering river sediments, passing upward into shallow marine clastics followed by neritic platform carbonates. The protoliths of the uppermost lithologies of this unit were probably a flysch sequence. According to Seymen (1985), there is no direct evidence either for the age of the protoliths or for the age of metamorphism, although the unconformably overlying, non-metamorphic clastics define the upper age limit as the late Maastrichtian. The stratigraphy of the Central Anatolian Massif based on his work is given in Figure 1.5.

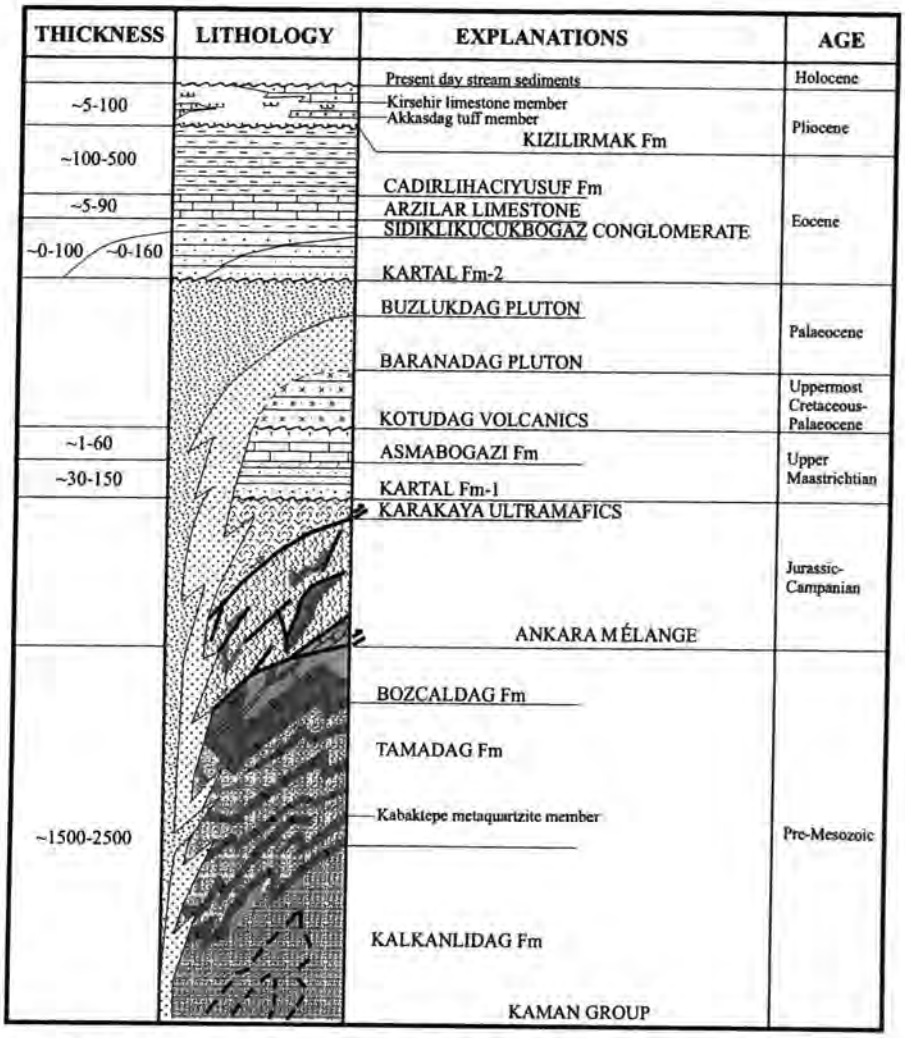

Figure 1.5. Generalised columnar section of the Central Anatolian Massif (after Seyman, 1982). Thicknesses are taken from Kara and Dönmez (1990). Abbreviation: FM-formation.

1.2.1. Previous studies on the intrusive rocks of the Central Anatolian Massif

Ayan (1963) made the first geochronological study on the plutonic rocks of the Massif. He used the total Pb method on a zircon crystal from the Baranadag monzonitic granite to obtain an age of intrusion of ~54 Ma. He also carried out some work on other intrusives in the northwestern part of the Central Anatolian Massif.

Ayan classified these intrusives as gabbro, granodiorite, granite, aplite granite, nepheline syenite, alkaline syenite, quartz syenite, nordmarkite and foyaite. According to Ayan, these rock types represented successive intrusions from the same magma chamber: first mafic rocks, then acidic rocks and finally alkaline rocks.

Ataman (1972) carried out a geochronological study of the Cefalikdag plutonic rocks using the Rb-Sr method on two whole-rock samples and a biotite separate. He obtained 71±1 Ma and ~80 Ma isochron ages. He postulated that the former was the cooling age of biotite, whereas the latter was the intrusion age. He argued that these plutonic rocks were derived from partial melting of arkose-greywacke types of sedimentary rocks.

Erkan and Ataman (1981) carried out K-Ar dating on regionally metamorphosed rocks (gneisses, mica-schists and amphibolites) from the northwest of Kirsehir. They obtained an age of 69.7±1.7 Ma, which is the average age of three biotite mineral separates, and 74.2±3.2 Ma for two hornblende separates. They argued that these values were not the ages of metamorphism but the cooling ages of the intrusive rocks.

Bayhan (1986, 1987) studied the petrographical, mineralogical and chemical characteristics of the Celebi, Cefalikdag and Baranadag plutons. He classified the Cefalikdag plutonic rocks as subalkaline and the Baranadag intrusive rocks as alkaline. He further classified the subalkaline rocks as monzonitic and I type, and the alkaline rocks as syenitic and A-type. On the basis of trace element data, he argued that the intrusive rocks from the Celebi, Cefalikdag and Baranadag plutons were formed by extensive crustal contamination of mantle-derived magma.

Göncüoglu (1986) carried out geochronological studies in the southern part of the Massif. Using the whole-rock Rb-Sr method, he obtained an age of 95±11 Ma (lower Cenomanian) for the Uckapili granitoid. The cooling ages of the granitoid and related gneisses obtained by the Rb-Sr whole-rock/mineral (biotite, muscovite) and K-Ar mineral (biotite) methods are 77.8±1.2 Ma and 76.5±1.1 Ma respectively.

Erler et al. (1991) studied a number of granitoids on the western margin (Kaman) and northern margin (Yozgat) of the Central Anatolia Massif. On the basis of petrographical and geochemical data, they argued that the intrusive rocks from the western margin of the Massif have I-type characteristics. In contrast, they noted that the plutonic rocks from the northern margin of the Massif show S-type features.

Akiman et al. (1993) argued that the granitoids of the western margin of the Massif, have metaluminous (I-type) and also peraluminous (S-type) characteristics and that these were derived from partial melting of crust. On the basis of trace element data, they suggested that the granitoids display syn- and post-collision granite characteristics. According to them, these granitoids were generated in two-stages: (i) an island arc, formed within the Izmir-Ankara-Erzincan oceanic crust by northward intra-oceanic subduction, collided with the northern part of the Anatolide-Tauride platform causing (a) obduction of ophiolite slivers onto the platform and (b) formation of the syn-collisional granitoids; and (ii) the Sakarya continent collided with the platform resulting in the intrusion of syn- and post-collisional granitoids.

1.3. Objectives of this thesis

The Behrekdag, Cefalikdag, Celebi, Baranadag and Hamit plutons from the Central Anatolian Massif have been selected for detailed study as they provide good examples of calc-alkaline and alkaline magmatism of similar age in a collision-related tectonic setting. Although these plutons have also been studied by other authors, mainly in terms of field relations and petrographic characteristics, the genesis of these intrusive rocks is still debated and poorly understood.

The aims of this project are:

(i) to characterise the intrusive rocks from the Massif and identify the differences between them in terms of their mineralogy, major and trace elements and Sr, Nd isotopic compositions;

(ii) to constrain the ages of emplacement for the intrusive rocks;

(iii) to identify the magmatic processes involved in their genesis, such as fractional crystallisation, assimilation and magma mixing and the extent of crustal assimilation in the evolution of these rock units;

(iv) to describe the composition of their source or sources and to place constraints upon the sources from which they were derived;

(v) to reveal the calc-alkaline and alkaline magmatism of a similar age in collision-related setting;

(vi) to present a petrogenetic model for the evolution of the collision-related Central Anatolian plutonics.

1.4. Analytical techniques used in this thesis

The techniques used in this study are summarised briefly below, also in Table 1.1. Methods of sample preparation, analytical conditions and estimates of precision and accuracy are presented in Appendices A and B.

XRF analysis

A total of 301 samples from the Central Anatolian Massif were crushed and then powdered using an agate ball mill. Their major element contents were analysed on both pressed powder pellets and fused glass discs but the latter results have been used in this study. Trace elements were analysed on pressed powder pellets. Major and trace elements were determined by an automated Philips PW 1400 XRF spectrometer with a Rh anode tube.

ICP-MS analysis

A subset of 50 representative samples were chosen for ICP-MS (Inductively Coupled Plasma Mass Spectrometry) analysis. Fused glass discs were analysed rather than powders to ensure dissolution of the intrusive rocks. In addition to these whole-rock samples, a total of 16 mineral separates (amphibole, biotite, plagioclase and alkali feldspar) were analysed by ICP-MS.

Electron Microprobe analysis

Electron microprobe analysis of a total of 33 representative samples was carried out using a Cameca CAMEBAX instrument at the University of Edinburgh. A total of 597 mineral grains were analysed of plagioclases, alkali feldspars, amphiboles, clinopyroxenes, biotites and Fe-Ti oxides.

K-Ar dating

3 mineral separates (hornblendes and biotite) were selected for dating and analysed by Dr. J. G. Mitchell in the Department of Physics at the University of Newcastle-upon Tyne.

Radiogenic isotope analysis

A subset of nine representative whole-rock samples from the Central Anatolian Massif were analysed. Sr and Nd radiogenic isotope analysis were performed using the automated VG 354 multicollector thermal ionisation mass spectrometer at the Department of Geology, Royal Holloway and Bedford New College, University of London.

ANALYTICAL TECHNIQUES	NUMBER OF SAMPLES	ELEMENTS	LABORATORY	EQUIPMENT
XRF (wr)	301	*Major elements* *Trace elements* (Sc, V, Cr, Co, Ni, Cu, Zn, Ga, Rb, Sr, Y, Zr, Nb, Ba, La, Ce, Nd, Pb, Th, U)	Durham University	Philips PW 1400
ICP-MS (wr)	50	Sc, V, Cr, Ni, Co, Cu, Zn, Ga, Rb, Sr, Y, Zr, Nb, Cs, Ba, La, Ce, Pr, Nd, Sm, Eu, Gd, Tb, Dy, Ho, Er, Tm, Yb, Lu, Hf, Ta, Pb, Th, U	Durham University	PE SCIEX ELAN 6000
ICP-MS (min)	16	Sc, Cr, V, Ni, Co, Zn, Ga, Rb, Sr, Y, Zr, Nb, Cs, Ba, La, Ce, Pr, Nd, Sm, Eu, Gd, Tb, Dy, Ho, Er, Tm, Yb, Lu, Hf, Ta, Pb, Th, U	Durham University	PE SCIEX ELAN 6000
ELECTRON MICROPROBE (min)	33 (597 points)	Major elements	Edinburgh University	Cameca CAMEBAX
K-Ar (min)	3	^{40}Ar	Newcastle University	
MASS SPECTROMETRY (wr)	9	$^{87}Sr/^{86}Sr$, $^{143}Nd/^{144}Nd$	University of London	VG 354 thermal ionisation mass spectrometry

Table 1.1. Summary of analytical techniques used for the Central Anatolian plutonics (wr-whole rock, min-mineral samples).

1.5. Description of the thesis

The thesis contains eight chapters. ***Chapter 2*** presents a field study of the intrusive rocks in the Central Anatolian Massif. ***Chapter 3*** describes the petrographic characteristics of the Central Anatolian plutonics. ***Chapter 4*** gives the mineral geochemistry of the plutonics. It is subdivided into two Sections. The first Section

deals with the classification of feldspar, amphibole, clinopyroxene, biotite and Fe-Ti oxides. Geothermo-barometer and oxygen fugacity calculations are the main subject of the second Section. ***Chapter 5*** presents the geochemical characteristics of the Central Anatolian plutonics. This chapter is also subdivided into two Sections. In the first Section, the plutonics are classified on the basis of their major element contents. The second Section presents the interpretation of their trace element characteristics, as shown by trace element variation diagrams, REE patterns, multi-element patterns and tectonic discrimination diagrams. ***Chapter 6*** describes the igneous enclaves in the Central Anatolian plutonics using their field, petrographic, mineralogical and geochemical characteristics. ***Chapter 7*** presents the petrogenetic modelling for the plutonics using their trace elements and Sr, Nd isotope compositions. ***Chapter 8*** gives the conclusions of this thesis.

Chapter 2
THE FIELD AREA

Introduction

The area chosen for study is situated in the Central Anatolian Massif. The Massif is roughly triangular-shaped and surrounded by the Izmir-Ankara-Erzincan Suture Zone to the north, the Tuz Golu fault to the west and the Ecemis fault to the east (Figure 2.1). It contains Palaeozoic-Mesozoic, medium-high grade metamorphic rocks overthrust by Upper Cretaceous ophiolitic units and intruded by a number of plutons. The Central Anatolian Massif is made up of three crystalline massifs: *(i) the Kirsehir Massif (around Kirsehir); (ii) the Akdagmadeni Massif (between Yozgat and Sivas); and (iii) the Nigde Massif (around Nigde).* Of these, the Kirsehir Massif is the largest and Nigde Massif the smallest (Figure 2.1).

The intrusive rocks in the Central Anatolian Massif cover an area of about 27000 km^2. They are exposed as bodies of various sizes at several locations within the Massif (Figure 2.1). The intrusive rocks can be subdivided into three groups:

(i) ***along the western margin of the Massif,*** a wide belt with large outcrops extending from northeast of Kirikkale in the north to Nigde in the south; this belt is 200-km-long, curving from NE-SW in the north to NW-SE in the south.

(ii) ***along the eastern margin,*** a narrow belt with small outcrops within metamorphic rocks, extending from Sivas in the north to Nigde in the south; this belt trends NE-SW.

(iii) ***along the northern margin,*** there is a granitoid outcrop around Yozgat.

This Chapter contains the result of fieldwork carried out in the western part of the Massif (Figures 2.1-2.3). Of the intrusive rocks in the region, the Behrekdag, Cefalikdag, Celebi, Baranadag and Hamit plutons have been studied. The fieldwork was carried out over three, two month field seasons. The plutons studied and sampled are shown in Figures 2.2, 2.3 and 2.5-2.7.

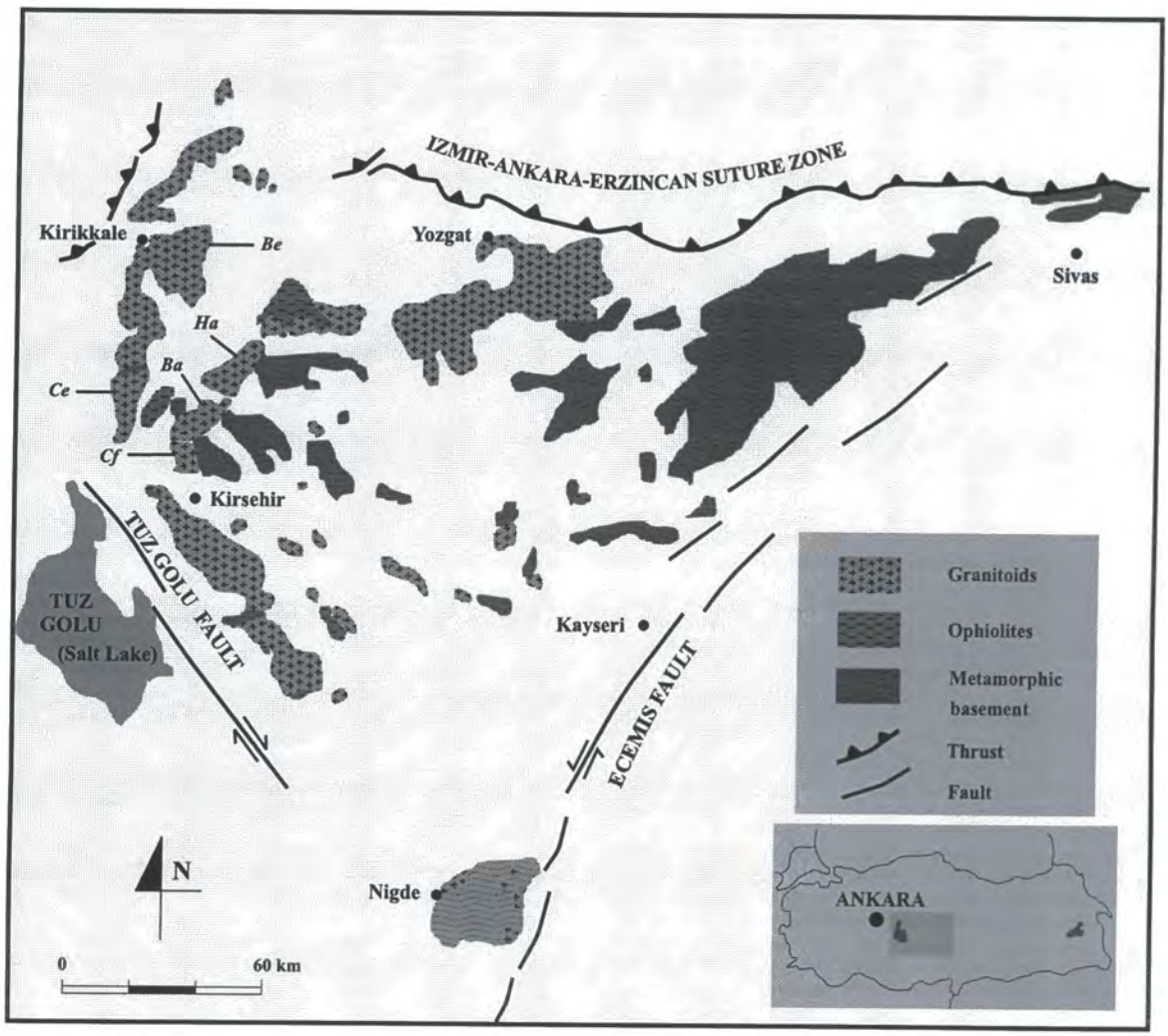

Figure 2.1. Geological setting of the Central Anatolian Massif (after Bingöl, 1989) (the inset map shows the Massif in relation to the rest of Turkey). Abbreviations: Ba- Baranadag, Be- Behrekdag, Ce- Celebi, Cf- Cefalikdag, Ha- Hamit and CAM- Central Anatolian Massif.

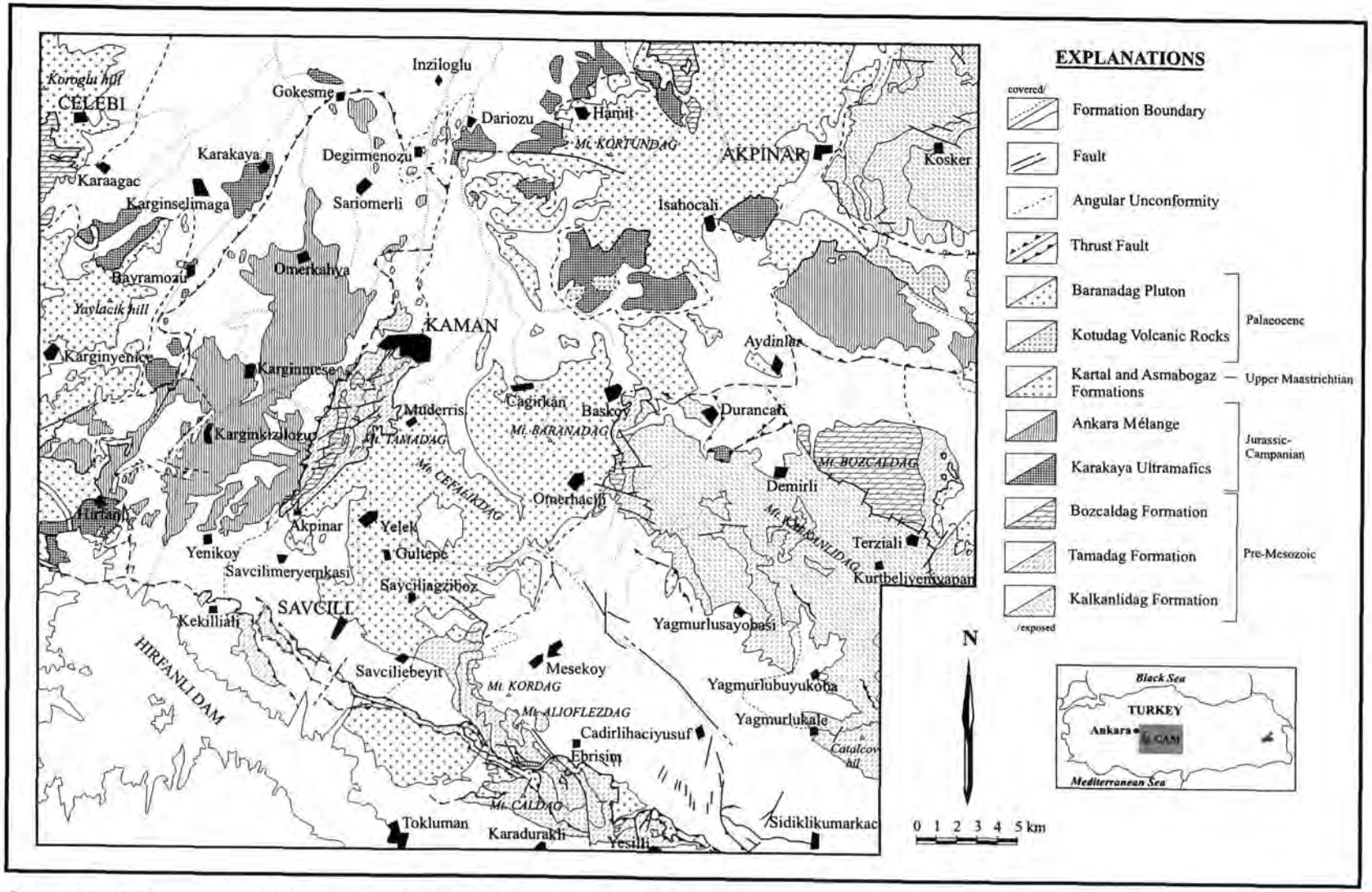

Figure 2.2. Geological map of the metamorphic and crystalline rocks in the Central Anatolian Massif around Kaman. Tertiary sedimentary cover is omitted (after Seymen, 1982). The inset map shows the Massif in relation to the rest of Turkey. Abbreviation: CAM- Central Anatolian Massif.

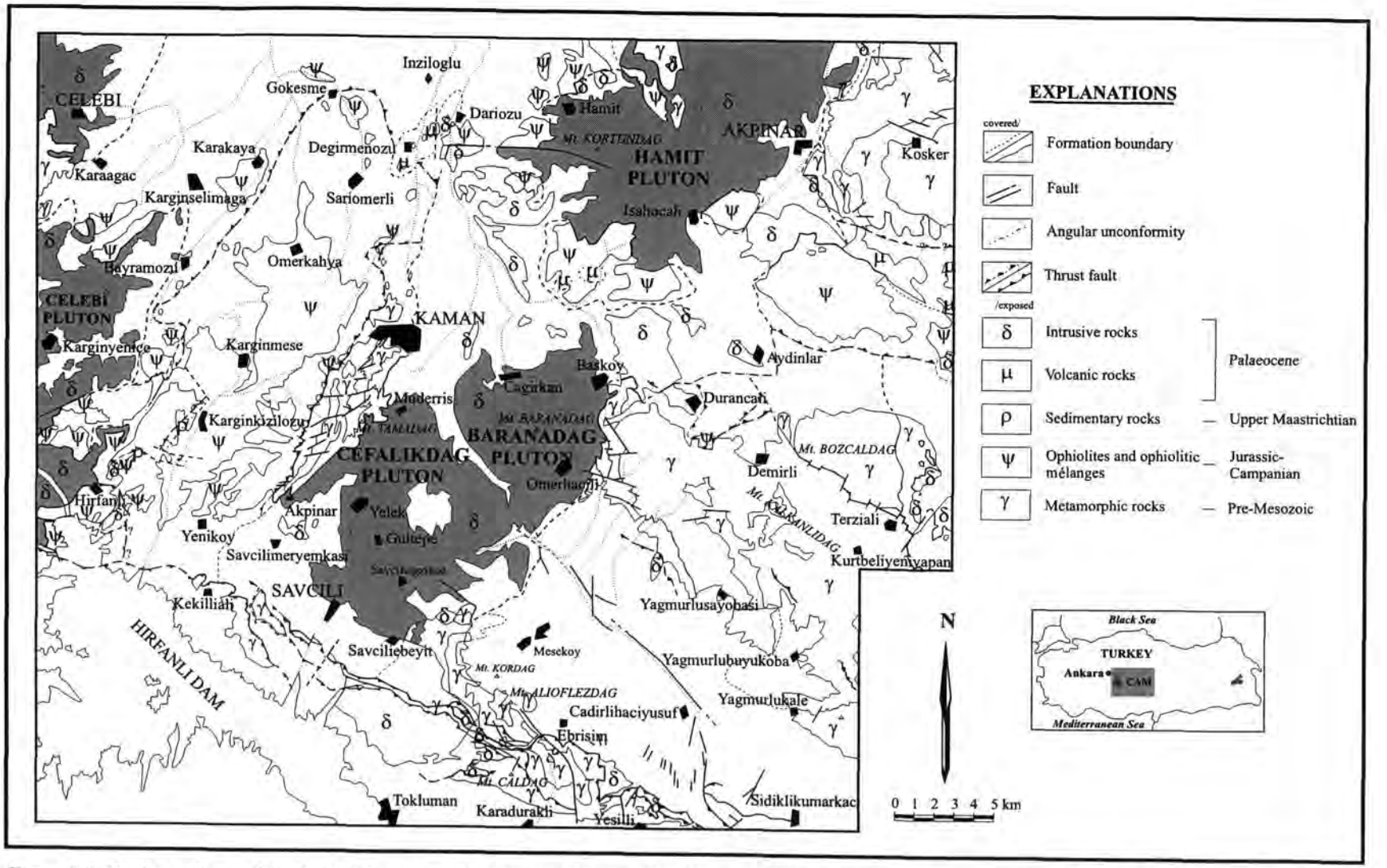

Figure 2.3. Geological map of the Central Anatolian Massif around Kaman (after Seymen, 1982) indicating the locations of the Baranadag, Cefalikdag, Celebi and Hamit plutons. Abbreviation: CAM- Central Anatolian Massif.

Figure 2.2 gives some general information about the geology of the intrusive rocks of the western part of the Massif. Figure 2.3 also provides general information about the geology of the four studied plutons (Baranadag, Cefalikdag, Celebi and Hamit). The geological settings of the Behrekdag, Cefalikdag and Hamit plutons are shown in Figures 2.5-2.7. Each pluton is well exposed. The primary aim of the field study was a number of traverses to study variations in each pluton. A number of small-scale traverses were also carried out in the country rocks to study the relationship between the plutons and the country rocks. A total of 550 representative samples were collected during the field study.

2.1. Classification of the intrusive rocks

The intrusive rocks from the Central Anatolian Massif have been classified according to the I.U.G.S. scheme (Streckeisen, 1976) as shown in Figure 2.4. The modal analyses on which it is based are given in Appendix C. On this diagram, the Behrekdag plutonics plot as quartz monzonite and granite. The Cefalikdag intrusives plot as a continuum of rock types from monzodiorite to granite. The Baranadag intrusives plot as monzonite and quartz monzonite and the Celebi intrusive rocks plot as quartz monzonite and granite. The Hamit plutonic rocks plot mainly as alkali feldspar syenite, quartz syenite and foid monzosyenite.

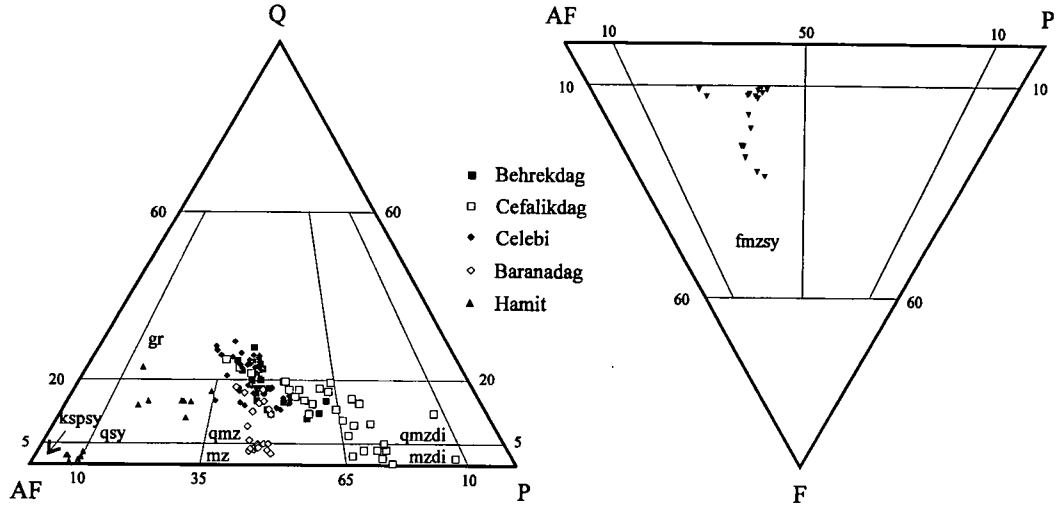

Figure 2.4. Modal classification of the intrusive rocks from the Central Anatolian Massif (after Streckeisen, 1976). The corners of the triangles are Q-quartz, AF-alkali feldspar, P-plagioclase and F-feldspathoid. Abbreviations: gr-granite, qsy-quartz syenite, qmz-quartz monzonite, qmzdi-quartz monzodiorite, kspsy-alkali feldspar syenite, mz-monzonite, mzdi-monzodiorite and fmzsy-foid monzosyenite.

2.2. Field relationships

2.2.1. The Behrekdag pluton

The Behrekdag pluton was described first by Taner (1974). Subsequently, Bayhan (1986) included its southern part in the Celebi intrusion and, later, Bayhan (1989) defined the same pluton as the Keskin intrusion. The pluton was mapped by Yadete (1990) (Figure 2.5).

The pluton trends north-south and is exposed over an area of about 230 km^2. It is bounded by the Celebi marble of the Bozcaldag formation (Kaman group) (Seymen, 1981) and by the cover units (Figure 2.5). In the Behrekdag pluton, jointing is well-developed (Photo 2.1) and leads to a distinctive topography. The prominent joint planes have been picked out by weathering. Joints commonly have NE strike and are SE dipping.

Photo 2.1. General view of the Behrekdag granite which shows well-developed jointing, Kizilirmak river, NW of Kopru village.

The Behrekdag pluton is made up (as noted earlier) of mainly quartz monzonite and granite. The quartz monzonite occupies the northeastern part and the granite covers western and southern parts, of the studied area (Figure 2.5).

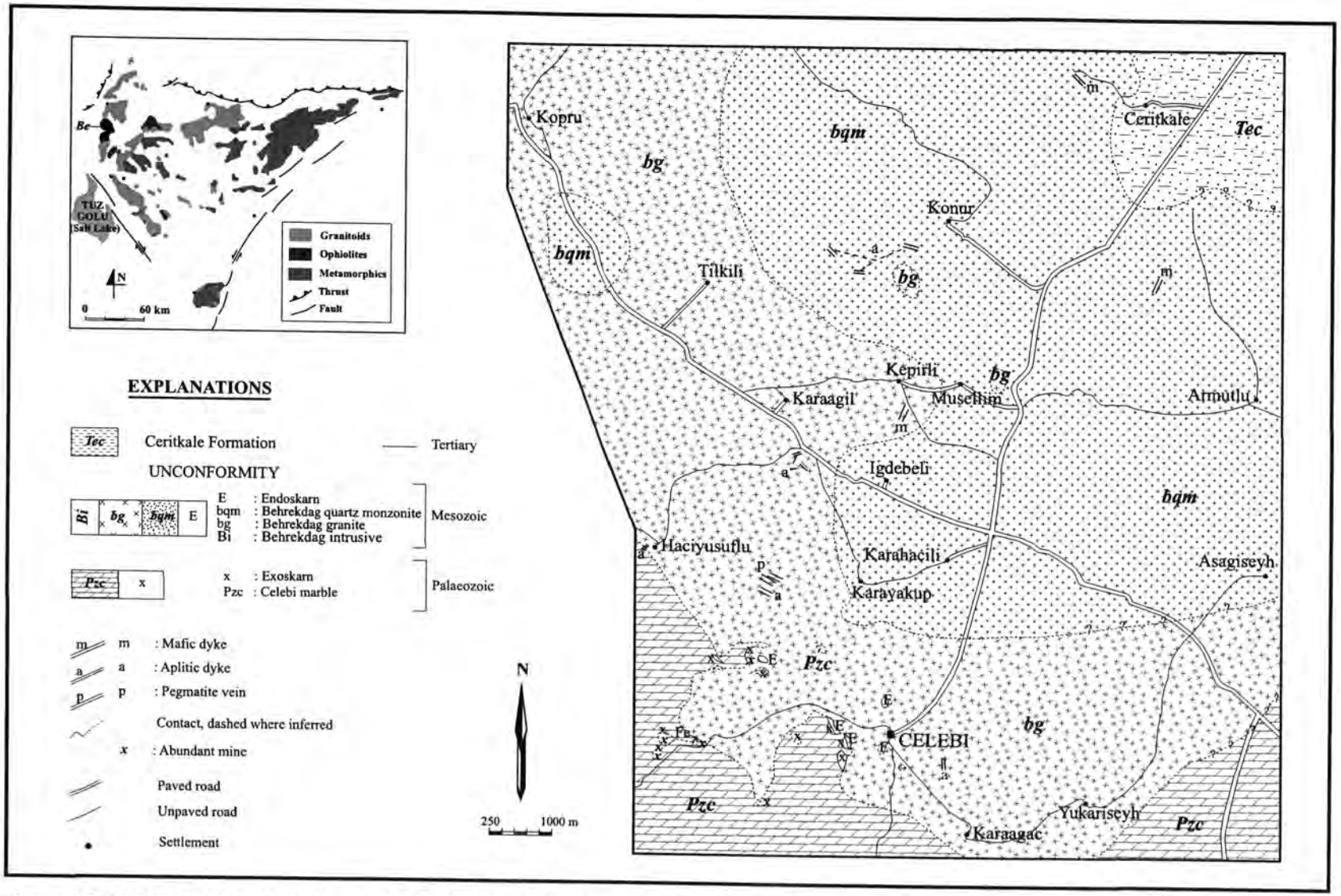

Figure 2.5. 1/25 000 scale geological map of the Behrekdag pluton (after Yadete, 1990). The inset map shows the pluton in relation to the rest of the Central Anatolian Massif (after Bingöl, 1989). Abbreviation: Be- Behrekdag pluton.

The quartz monzonite is grey-dark grey, coarse-grained and porphyritic with feldspar megacrysts. It is characterised by prismatic, white-coloured feldspar crystals set in a grey, medium-grained groundmass. The granite shows similar field characteristics to those of the quartz monzonite. Unlike the quartz monzonite, the granite has prismatic/tabular, light pink-coloured alkali feldspar megacrysts. In the field, no contact between the quartz monzonite and the granite has been observed. Macroscopically, they are both mainly composed of prismatic/tabular alkali feldspar, plagioclase, amphibole, biotite and quartz. In some places, they display flow foliation produced by elongate feldspar laths (Photo 2.2). The feldspar megacrysts are up to 8 cm across.

Photo 2.2. A slight preferred orientation is produced by feldspar megacrysts in the Behrekdag quartz monzonite, Igdebeli village. Orientation is in N20°E direction.

Enclaves are common throughout the pluton (see Chapter 6). The quartz monzonite and the granite are cross-cut by aplitic, pegmatitic and mafic dykes (see the dykes Section).

2.2.2. The Cefalikdag pluton

This pluton was named the Cefalikdag granodiorite by Ataman (1972), considered as part of the Baranadag pluton by Seymen (1982) and renamed as the Cefalikdag quartz monzonite by Erler et al. (1991). It was mapped by Geven (1992) as the Cefalikdag granitoid (Figure 2.6).

The Cefalikdag pluton is exposed over 76 km^2 and located in the northwest of the Central Anatolian Massif, trending roughly N-S from Kaman town to Savciliebeyit village (Figures 2.2, 2.3). It is bounded by the Baranadag pluton to the northeast, the Kaman metamorphics to the northwest and southeast and the cover units to the northeast, south and southwest (Figure 2.6). On the basis of petrographic studies, and also Geven's work (1992), the Cefalikdag plutonic rocks have been divided into three subunits: the Savciliebeyit monzodiorite; the Kucukcurtepe quartz monzonite; and the Kaletepe granite. The Savciliebeyit monzodiorite and Kucukcurtepe quartz monzonite were intruded by aplitic, pegmatitic, mafic and leucite phonolitic dykes. Unlike the Kaletepe granite, enclaves are common in the Savciliebeyit monzodiorite and the Kucukcurtepe quartz monzonite.

2.2.2.1 The Savciliebeyit monzodiorite

The Savciliebeyit monzodiorite was named by Geven (1992) as the Savciliebeyit hornblende granite after its best outcrops around Savciliebeyit village (Photo 2.3). Here, this rock type is renamed the Savciliebeyit monzodiorite as it is monzodiorite/quartz monzodiorite in composition rather than granite (Figure 2.4). It is mainly exposed around the contact zones of the Cefalikdag pluton (Figure 2.6). It is coarse-grained and porphyritic with feldspar megacrysts up to 10 cm across and dark grey-greenish in colour. Mesoscopically, it is composed of plagioclase, alkali feldspar, biotite and amphibole and is mainly characterised by a higher proportion of mafic minerals, especially biotite compared to the Kucukcurtepe quartz monzonite. Plagioclase laths in the monzodiorite show a slight to strong preferred NE orientation close to the pluton contact (especially around Savciliebeyit village) (Photo 2.4).

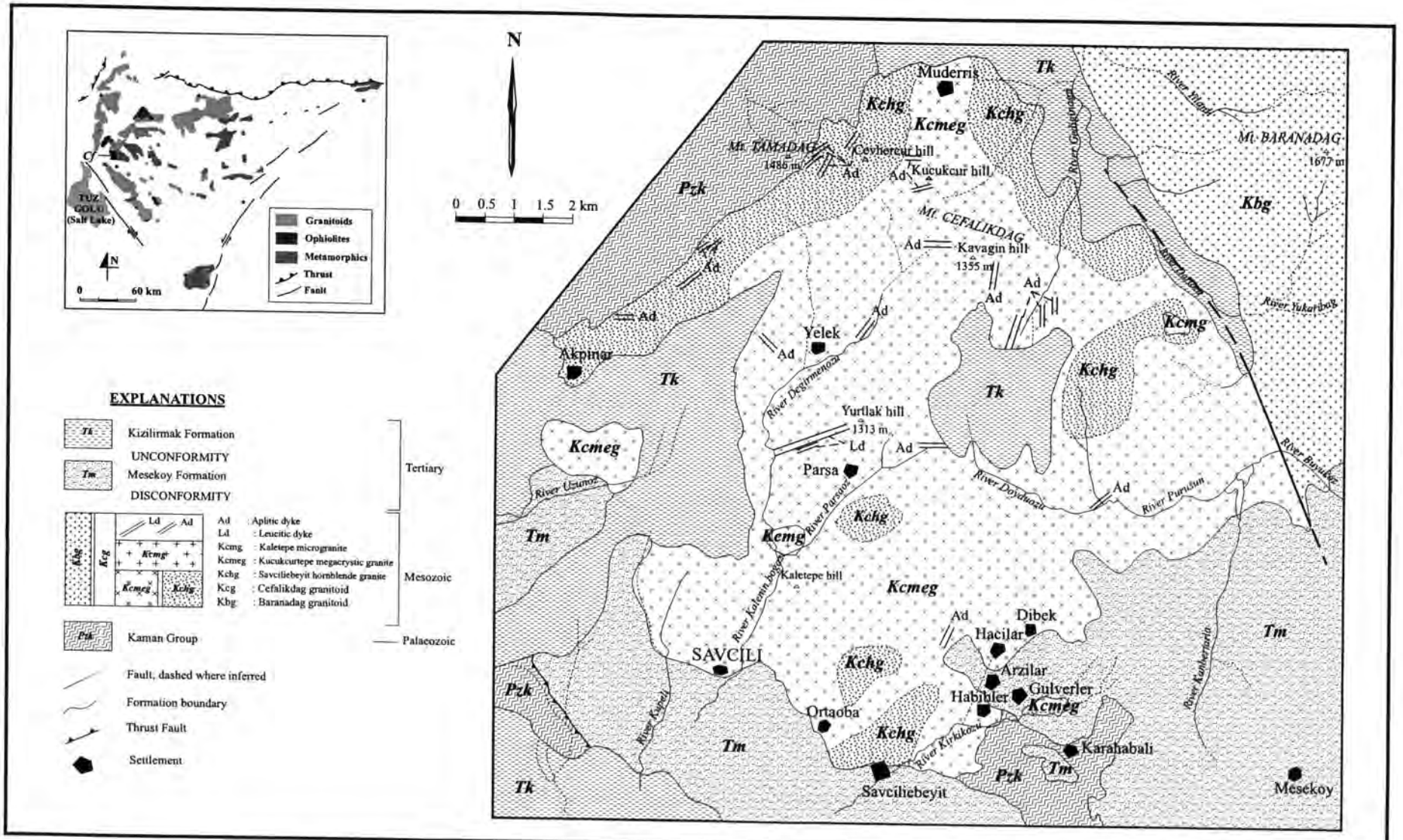

Figure 2.6. 1/25 000 scale geological map of the Cefalikdag pluton (after Geven, 1992). The inset map shows the pluton in relation to the rest of the Central Anatolian Massif (after Bingöl, 1989). Abbreviation: Cf- Cefalikdag pluton.

Photo 2.3. A general view of the Savciliebeyit monzodiorite, NE of Savciliebeyit village. The white-coloured unit is marble of the Kaman group and the dark brownish-coloured surface is the contact zone between the metamorphics and the monzodiorite.

Photo 2.4. A strong preferred orientation is produced by feldspar megacrysts in the Savciliebeyit monzodiorite, NE of Savciliebeyit village, River Kirkikozu.

2.2.2.2. The Kucukcurtepe quartz monzonite

The Kucukcurtepe quartz monzonite is the dominant lithology in the Cefalikdag pluton and crops out mainly in the central part of the intrusion (Figure 2.6). It was called the Kucukcurtepe megacrystic granite by Geven (1992). It is grey, coarse-grained and porphyritic with alkali feldspar (up to 10 cm across) megacrysts and contains amphibole as the predominant mafic mineral. It is characterised by euhedral, prismatic/tabular, light pink-coloured alkali feldspar megacrysts (Photo 2.5). The Kucukcurtepe quartz monzonite has a gradational contact with the Savciliebeyit monzodiorite with increasing proportions of alkali feldspar and decreasing proportions of mafic minerals, mainly biotite. In the field, the lighter grey colour, the lower proportion of mafic minerals and the higher proportions of light pinkish-coloured alkali feldspar distinguish the Kucukcurtepe quartz monzonite from the Savciliebeyit monzodiorite.

Photo 2.5. Pink prismatic/tabular alkali feldspar megacrysts developed in the Kucukcurtepe quartz monzonite, east of Kucukcurtepe hill.

2.2.2.3. The Kaletepe granite

The Kaletepe granite forms mini-stocks within the Savciliebeyit monzodiorite and Kucukcurtepe quartz monzonite towards the margin of the Cefalikdag pluton (Figure 2.6). It is characterised by an equigranular, fine-grained texture and light grey to white colour. It is mainly made up quartz, alkali feldspar, plagioclase and less than 5% mafic minerals.

2.2.3. The Celebi pluton

The Celebi pluton is also located at the northwestern part of the Central Anatolian Massif (Figures 2.1-2.3). It was defined as part of the Behrekdag pluton by Bayhan (1986). The pluton covers an area of approximately 150 km^2 and trends north-south. It lies to the south of the Behrekdag pluton (Figure 2.1) where it is bounded by the Celebi marble, the Ankara mélange, the Karakaya ultramafic rocks and the cover units. During the intrusion, the pluton produced the skarn belt of Kesikköprü (Bala-Ankara) (Bayhan, 1984).

Macroscopically, the Celebi pluton mainly comprises quartz monzonite and granite. In the field, there is no visible contact between these two rock types. They

are easily distinguished from one another on the basis of their colour and the composition of their megacrysts. The granite is the dominant lithology and occupies most of the pluton. It contains large, prismatic/tabular, pink, alkali feldspar megacrysts set in an equigranular, fine to medium-grained, darkish grey groundmass (Photo 2.6). Feldspar megacrysts are up to 3.5 cm across. The quartz monzonite tends to occur around the contact with the Celebi marble. It is grey to dark grey and medium-grained and porphyritic with white, feldspar megacrysts (Photo 2.7). Enclaves are common throughout the pluton. The Celebi plutonic rocks are cut by aplitic, pegmatitic and mafic dykes.

Photo 2.6. View of the Celebi granite, NW of Karginyenice village. Pink prismatic/tabular alkali feldspar megacrysts are set in an equigranular, medium-grained grey groundmass. The granite also contains enclaves.

Photo 2.7. White feldspar megacrysts developed in the Celebi quartz monzonite, NW of Tatik village. The rock is cross-cut by an aplitic dyke. Its thickness is about 3 cm with a strike of N70°E.

2.2.4. The Baranadag pluton

The pluton was described first by Seymen (1982) as a part of the Baranadag plutonic complex. It was defined by Erler et al. (1991) as a separate unit from other plutons of the Central Anatolian Massif. It was also called the Baranadag monzonite by Lünel (1985).

The pluton crops out over an area of 65 km^2 and produces a very steep topography (Photo 2.8). It is surrounded by the cover units to the north and south-southeast, the Kaman group to the east and the Cefalikdag pluton to the west-southwest (Figures 2.2, 2.3). The contact between the Baranadag and Cefalikdag plutons is a NW-SE trending fault zone (Figure 2.6).

The pluton mainly consists of monzonite and quartz monzonite. The monzonite is recognised in the field as a dark grey, coarse-grained and porphyritic rock with prismatic, white feldspar phenocrysts. In contrast, the quartz monzonite is coarse-grained and porphyritic with light pink-coloured alkali feldspar megacrysts set in medium-grained groundmass. The monzonite and quartz monzonite both contain amphibole and biotite as mafic minerals.

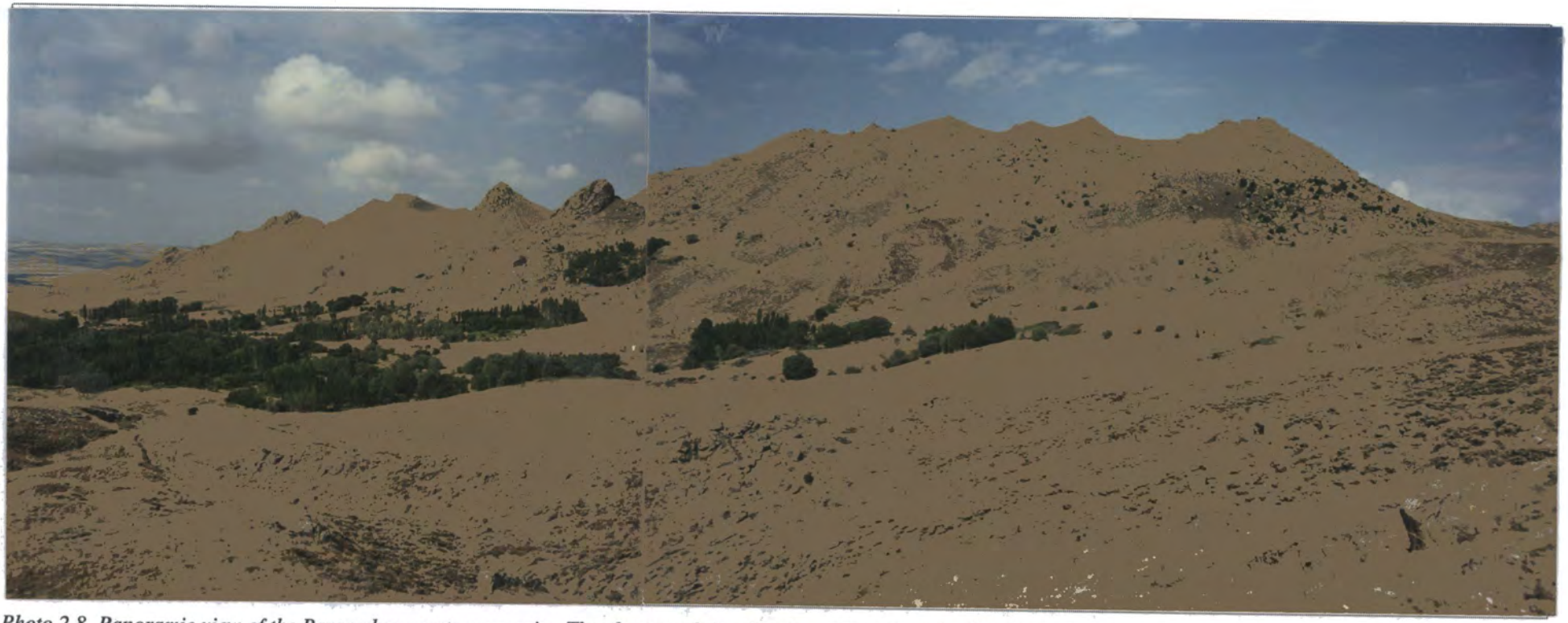

Photo 2.8. Panoramic view of the Baranadag quartz monzonite. The photograph is taken from NE of Omerhacili village. An open quarry can be seen in the photo. The intrusive rocks from the Central Anatolian Massif have been used as decorative building materials for years.

No contact between the monzonite and quartz monzonite has been observed in the field. They are distinguished from one another only on the basis of the colour of their megacrysts. Feldspar megacrysts in the Baranadag pluton are sometimes up to 5 cm across. The monzonite is mainly found in the north (around Cagirkan village) and the quartz monzonite in the south of the pluton (around Omerhacili village) (Figures 2.2, 2.3). Feldspar megacrysts in the pluton show a slight preferred orientation. As in other plutons, enclaves are abundant (see Chapter 6). The monzonite and quartz monzonite are cut by aplitic, pegmatitic and microsyenitic dykes (see the dykes Section).

2.2.5. The Hamit pluton

The Hamit pluton was defined as part of the Buzlukdag pluton by Seymen (1982). It was described as a separate unit by Erler et al. (1991). It was mapped by Akiman (1985) (Figure 2.7). It crops out to the northeast of Kaman and covers an area of about 120 km^2. The Hamit pluton is bounded by the Kaman group, the Karakaya ultramafic rocks and the cover units (Figures 2.2, 2.3).

Ridges and valleys are the main topographic features of the studied area. The greatest elevation is Camlik hill (1526 m) and the lowest is the flood plain of River Aci (900 m). Kirtis (1514 m), Domuduran (1463 m), Kale (1459 m), Sivriogul (1340 m), Yapanbel (1339 m) and Kel (1279 m) hills are the other high elevations in the studied area (Figure 2.7).

The Hamit pluton is composed of nepheline monzosyenite, pseudoleucite monzosyenite, alkali feldspar syenite and quartz syenite. In the field, these rock types are distinguished from each other mainly on the basis of their colour and the composition of their megacrysts. The dominant lithology in the Hamit pluton is the foid-bearing rocks (nepheline monzosyenite and pseudoleucite monzosyenite).

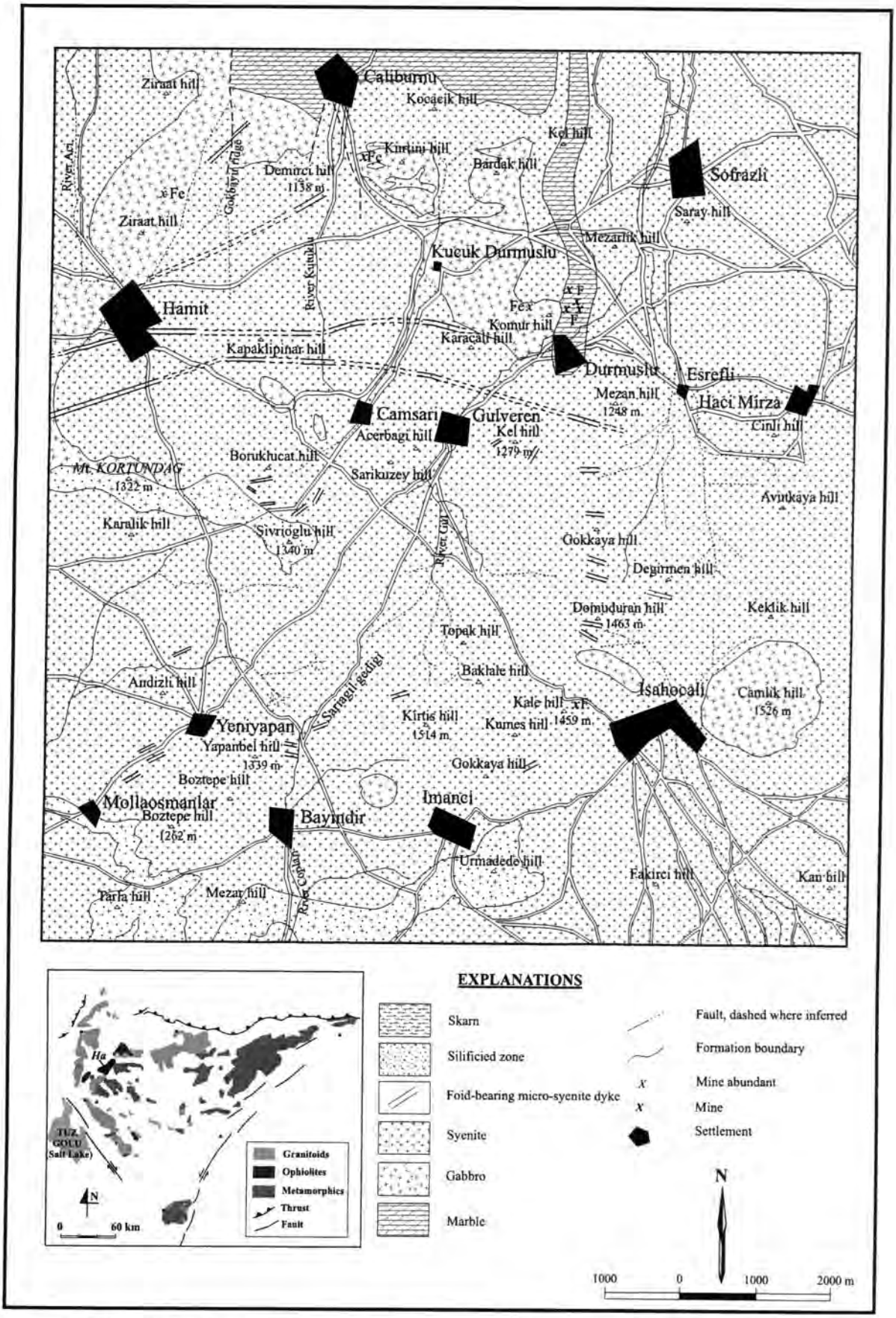

Figure 2.7. 1/25 000 scale geological map of the Hamit pluton (after Akiman, 1985). The inset map shows the pluton in relation to the rest of the Central Anatolian Massif (after Bingöl et al., 1989). Abbreviation: Ha- Hamit pluton.

The nepheline monzosyenite is dark grey-green, medium-grained, occasionally porphyritic with alkali feldspar. It contains a greater proportion of mafic minerals than the alkali feldspar syenite and quartz syenite. The nepheline monzosyenite and pseudoleucite monzosyenite tend to crop out in the central part of the pluton, whereas the quartz syenite roughly covers the rim of the pluton with the alkali feldspar syenite between them. The pseudoleucite monzosyenite is grey-dark grey and porphyritic with prismatic/tabular alkali feldspar and euhedral pseudoleucite megacrysts (Photo 2.9).

Photo 2.9. A general view from the Hamit pseudoleucite monzosyenite in which euhedral pseudoleucite and prismatic/tabular alkali feldspar megacrysts are set in fine to medium-grained groundmass. NE of Hamit town.

The alkali feldspar syenite is pink-coloured and medium-grained (Photo 2.10). The quartz syenite is cream-coloured, medium-grained and variably porphyritic with prismatic alkali feldspar (up to 4 cm across) (Photo 2.11). Alkali feldspar crystals show a slight preferred orientation. The alkali feldspar syenite and quartz syenite are cut by aplitic and silicic dykes. The nepheline monzosyenite and pseudoleucite monzosyenite are cut by foid-bearing micro-syenitic dykes. They trend E-W and NE-SW (Figure 2.7). They predominantly crop out in the northwestern part of the pluton. They are fine-grained, dark grey-green in colour and are mainly phonolite in composition. Their widths vary from centimetres to a few meters.

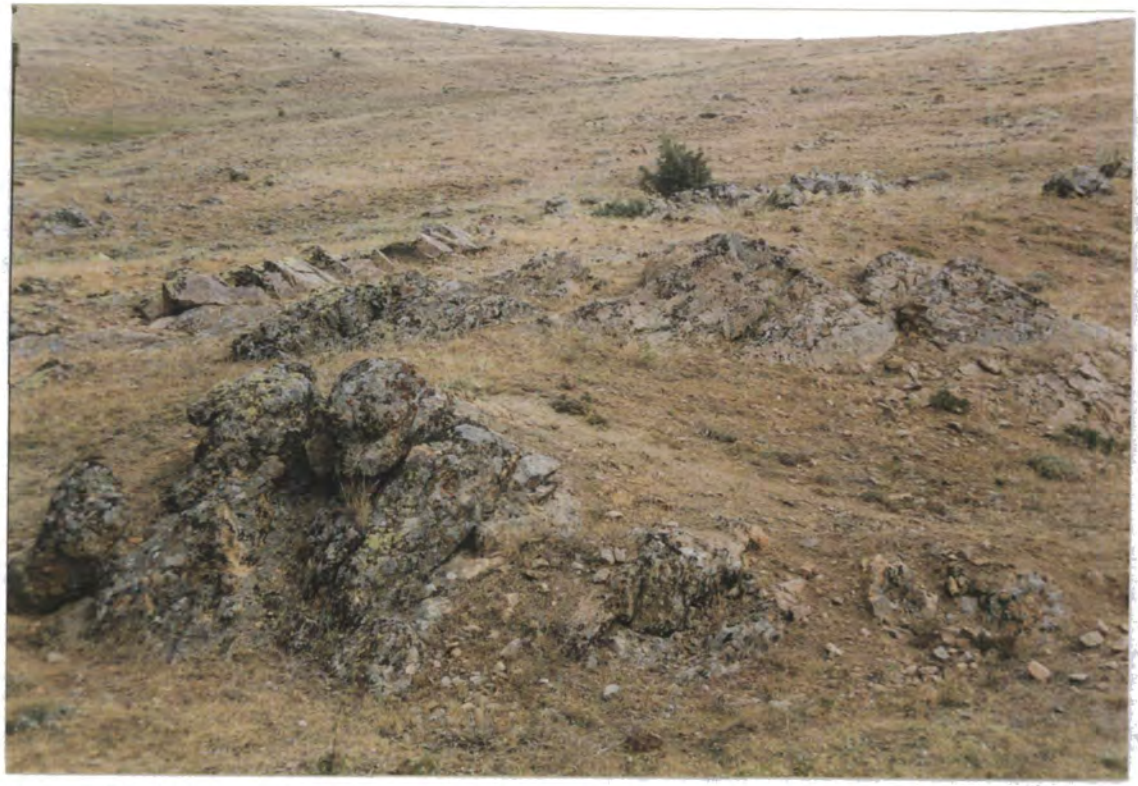

Photo 2.10. Field view of the alkali feldspar syenite from the Hamit pluton, SW of Camsari village, SE of Hamit town.

Photo 2.11. General field view of the Hamit quartz syenite. The photo is taken from east of Demirci hill, NE of Hamit town.

2.2.6. The dykes

The aplitic dykes cross-cut all intrusive rocks in the studied area. The pegmatitic dykes were found in all plutons except for the Hamit pluton. The aplitic dykes cut most of the main intrusive bodies. Their lengths vary from centimetres to hundreds of meters and widths from 1.5 cm to a few meters. Around Kucukcurtepe hill in the Cefalikdag pluton, the aplitic dykes reach their maximum width of 2-3 meters. The pegmatitic dykes are small in volume and less than about a few centimetres wide.

In hand specimen, fine-grained, equigranular, pinkish-yellowish coloured aplitic dykes are mostly granite composition and contain minor amounts of mafic minerals. Macroscopically, the pegmatitic dykes are composed of coarse-grained, smoky quartz, pinkish K-feldspar and a small amount of mica. The aplitic and pegmatitic dykes are most abundant around the contact zones of the plutons, especially the Celebi pluton.

The mafic dykes have been observed in the Behrekdag, Cefalikdag and Celebi plutons. In the Cefalikdag pluton, they tend to crop out around contact zones. They reach a few centimetres in length. They are fine-grained and dark green-coloured.

The micro-syenitic dykes have been found only in the Baranadag pluton. They are fine-grained and grey-dark grey coloured. They reach a few centimetres in length.

The leucite phonolitic dykes have been found in the Cefalikdag pluton. They are dark grey-green coloured and porphyritic with leucite minerals. These dykes crop out around the contact zone of the Cefalikdag pluton.

2.3. Age relations of the intrusive rocks in the Massif

The crystallisation ages for the Central Anatolian plutonics are still debated. Previous age determinations (whole-rock Rb-Sr) of different intrusive rocks in the Massif include 71±1 Ma (Cefalikdag pluton-Ataman, 1972), 95±11 Ma (Uckapili pluton-Göncüoglu, 1986), 110±5 Ma (Murmano pluton-Zeck and Unlü, 1987), 70±1.1 Ma (Bayindir pluton-Gündogdu et al., 1988) and 110±14 Ma (Gülec, 1994). In this study, three different intrusive rock samples have been dated by the K-Ar method on hornblende and biotite minerals. The K-Ar age data are presented in

Appendix C. K-Ar age determinations from the Behrekdag, Cefalikdag and Baranadag plutonic rocks have yielded K-Ar ages of 79.5±1.7, 66.6±1.3 and 76.4±1.3 Ma, broadly similar to the published ages of the Cefalikdag and Bayindir intrusions.

2.4. Summary

The Behrekdag, Cefalikdag, Celebi, Baranadag and Hamit plutons of the Central Anatolian Massif have been the subject of this study. The characteristics of these plutonic rocks have been listed in Table 2.1.

PLUTON	BEHREKDAG	CEFALIKDAG	CELEBI	BARANADAG	HAMIT
ROCK UNIT	quartz monzonite, granite	monzodiorite (1), quartz monzonite (2), granite (3)	quartz monzonite, granite	monzonite, quartz monzonite	nepheline monzosyenite (1), pseudoleucite monzosyenite (2), alkali feldspar syenite (3), quartz syenite (4)
GRAIN SIZE	coarse-grained and porphyritic with feldspar	coarse-grained and porphyritic with feldspar (1, 2); and fine-grained (3)	medium grained and porphyritic with feldspar	coarse-grained and porphyritic with feldspar	medium-grained (1, 3, 4); porphyritic with pseudoleucite and alkali feldspar (2); or alkali feldspar (4)
ORIENTATION	slight by feldspar	slight to strong by feldspar (1, 2)	slight by feldspar	slight by feldspar	slight by alkali feldspar (4)
ENCLAVES	common	common (except 3)	common	common	none
AGE	79.5±1.7 Ma (this study)	66.6±1 Ma (this study)		76.4±1.3 Ma (this study)	70.7±1.1 Ma (Gündogdu et al., 1988)

Table 2.1. Summary of the field relations and geochronology of the intrusive rocks from the Central Anatolian Massif.

Chapter 3
PETROGRAPHY

Introduction

This chapter aims to describe and interpret the petrography of the Behrekdag, Cefalikdag, Celebi, Baranadag and Hamit plutons. In order to model the chemical variations in the intrusive rocks, it is necessary first to identify the crystallising phases. It is particularly important to recognise texturally which minerals are early crystallising phases (cumulates), and which crystallised from trapped interstitial melt. It is also important to describe subsolidus modification which may affect magma in that its original mineralogy is changed considerably.

3.1. The Behrekdag pluton

The Behrekdag pluton is made up of quartz monzonite and granite. The quartz monzonite and the granite show similar characteristics, even though the latter has slightly higher proportions of quartz. In addition, the megacrysts in the granite are mostly plagioclase feldspars whereas in the quartz monzonite they are alkali feldspars. The quartz monzonite and the granite will be discussed together in the following paragraphs.

Modal estimates for the pluton are 25%-43% plagioclase and alkali feldspar, 9%-26% quartz, 2%-24% amphibole, <5% biotite, and <2% clinopyroxene. The rock units are medium to coarse-grained with a hypidiomorphic, granular texture. The alkali feldspar is mostly orthoclase but microcline has been also observed in lesser amounts. Alkali feldspar crystals are up to 8 mm across and show a microperthitic texture (Photo 3.1). Alkali feldspar megacrysts are subhedral-anhedral in shape and poikilitically enclose plagioclase, amphibole, biotite, apatite and opaque minerals. Plagioclase inclusions are often orientated subparallel to the rims of the alkali feldspars. Plagioclase megacrysts (up to 7 mm across) are lath-shaped or prismatic, euhedral to subhedral and show normal and complex oscillatory zoning (Photo 3.2). Small grains of biotite, apatite and opaque minerals are enclosed by plagioclase feldspar. Some plagioclase feldspar crystals occasionally have a sieve texture caused

by small inclusions of biotite. Quartz is subhedral to anhedral and sometimes poikilitically encloses earlier crystallised minerals. Quartz is predominantly interstitial and has accommodated small amounts of strain, as revealed by undulose extinction. It occasionally forms vermicular intergrowths with plagioclase.

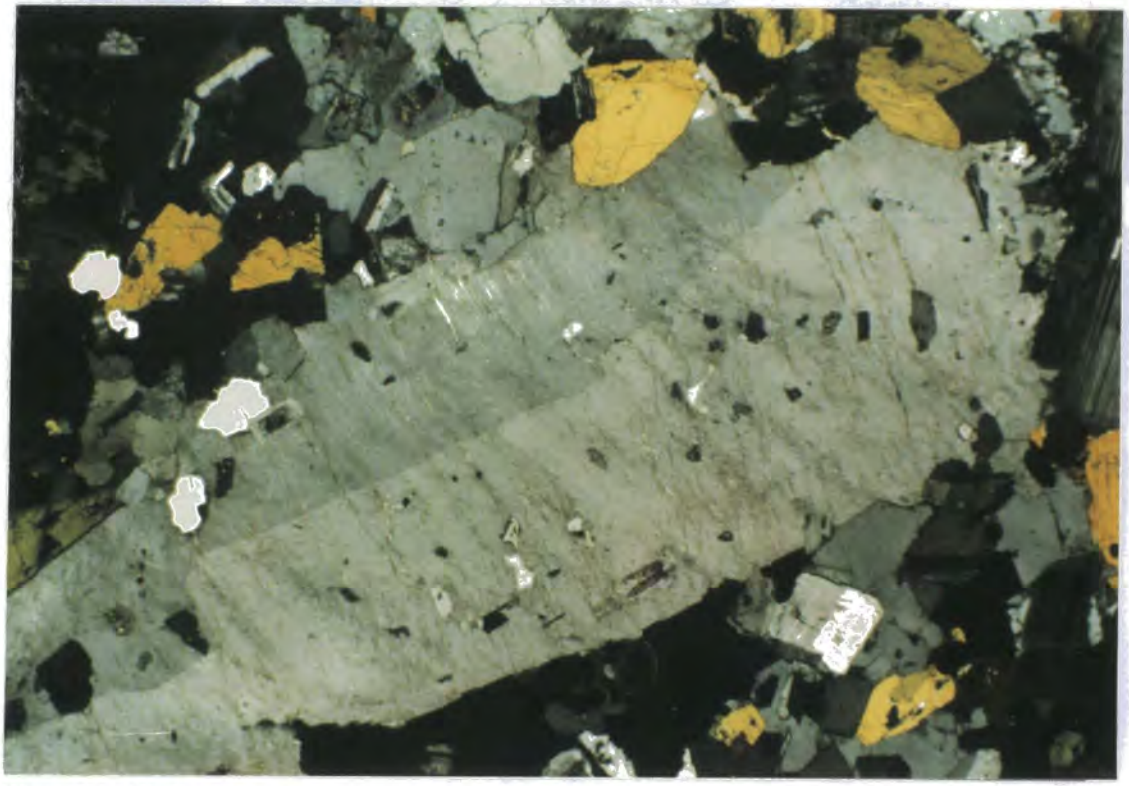

Photo 3.1. Alkali feldspar megacryst in the granite (sample N9) encloses small grains of plagioclase feldspar. Alkali feldspar shows a microperthitic texture and simple twinning. Magnification: 6x3.7 mm, XPL.

Amphibole and biotite are the main mafic minerals, the former being the more common. Amphibole is found as euhedral to subhedral crystals, reaches up to 4 mm in size. It occasionally encloses inclusions of plagioclase feldspar, titanite, apatite and opaques. Biotite is subhedral in shape and is in minor amounts compared to amphibole. Clinopyroxene occurs as relics within amphibole. Amphibole and biotite have inclusions of accessory phases such as titanite, opaques, apatite and zircon. Titanite is euhedral and fine to coarse-grained. The opaque minerals present are magnetite, ilmenite and pyrite.

Sericitisation and chloritisation are the most common alteration types in the Behrekdag plutonic rocks. The former has affected both types of feldspar. It is most intense within the core of the plagioclase feldspar crystals. Plagioclase is occasionally replaced by carbonate. Biotite has been slightly to moderately affected by chloritisation.

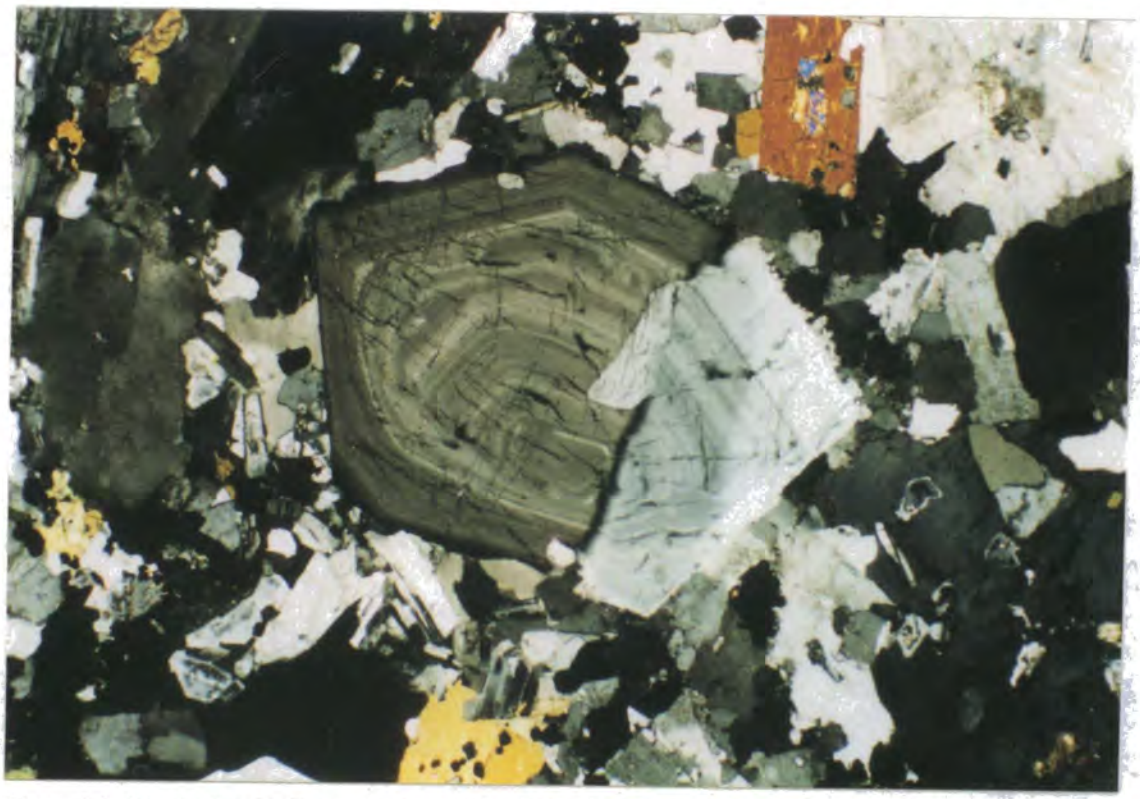

Photo 3.2. Plagioclase feldspar in the granite (N9) displays complex oscillatory zoning. Subhedral amphibole crystal to the bottom left of the plagioclase feldspar encloses clinopyroxene relics. Magnification: 6x3.7 mm, XPL.

Oscillatory zoning in minerals is a common phenomenon (e.g. Shore and Fowler, 1996), and has been reported from a variety of geological environments. The rich structure represented by such zoning patterns contains potentially valuable information about crystal growth processes as well as changes in environments in which the crystals grow. Attempts to explain complex mineral zoning patterns commonly have been based on two assumptions: (i) the zonation is a result of internal crystal growth processes (e.g. Allégre et al., 1981; Wang and Merino, 1992; L'Heureux and Fowler, 1994); and (ii) the zonation mainly reflects changes in the external geological environment during crystal growth (e.g. Yardley et al., 1991; Jamtveit et al., 1993).

3.2. The Cefalikdag pluton

As mentioned in Chapter 2, the Cefalikdag pluton is composed of the Savciliebeyit monzodiorite, the Kucukcurtepe quartz monzonite and the Kaletepe granite.

3.2.1. The Savciliebeyit monzodiorite

The Savciliebeyit monzodiorite varies modally between monzodiorite and quartz monzodiorite, and has a modal mineralogy of 39-57% plagioclase, 8-32% alkali feldspar, 1-29% amphibole and biotite, up to 17% quartz, and <5% clinopyroxene. It is medium to coarse-grained with a hypidiomorphic, granular texture (Photo 3.3).

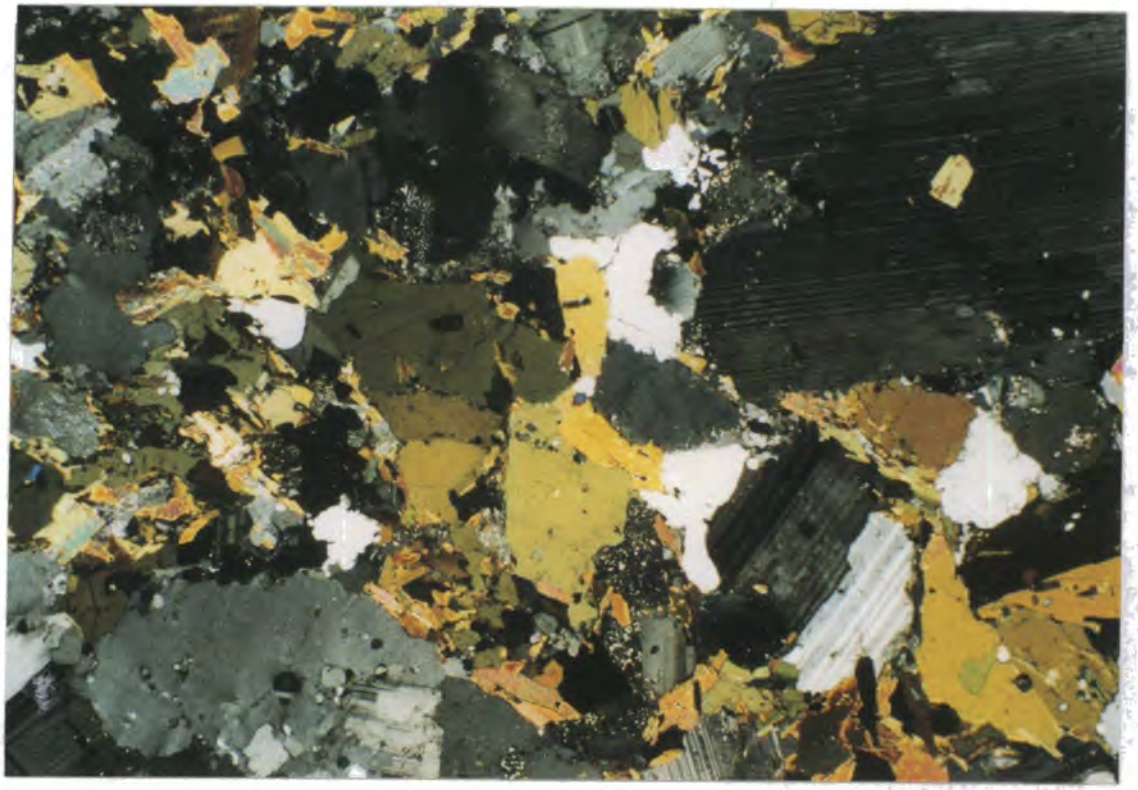

Photo 3.3. Microphotograph of the Savciliebeyit monzodiorite (sample N231). Myrmekite is common and most minerals display undulose extinction due to strain. Magnification: 6x3.7 mm, XPL.

Plagioclase feldspar is characterised by no zoning or by normal and oscillatory zoning. Its size reaches 8 mm across. Alkali feldspar is mainly orthoclase and a microperthitic texture is characteristic. Alkali feldspar encloses predominantly plagioclase, amphibole, biotite, apatite and opaque minerals. Quartz occasionally shows a poikilitic texture. It is also present as interlocking grains with sutured boundaries and appears to have crystallised late. It shows undulose extinction.

The mafic phases are amphibole, biotite and clinopyroxene. Subhedral amphibole crystals enclose inclusions of plagioclase feldspar, titanite, apatite and opaques. Biotite is found as fresh, subhedral crystals and also as inclusions in other minerals. It has typically a foxy-red brown colour. Biotite has zircon inclusions which produce pleochroic haloes due to their high content of radioactive elements.

Clinopyroxene is also present, either as relics within amphibole cores or as subhedral, medium-grained discrete crystals. Titanite, opaques, apatite and zircon are accessory minerals. The opaque minerals present are magnetite, ilmenite and pyrite.

The most common subsolidus modification in the monzodiorite is sericitic alteration. It has affected both alkali feldspar and plagioclase feldspar. A few plagioclase grains are also altered to carbonate. Amphibole crystals are sometimes replaced by biotite.

3.2.2. The Kucukcurtepe quartz monzonite

The Kucukcurtepe quartz monzonite is medium to coarse-grained with a hypidiomorphic, granular texture. Modal estimates are 35%-48% plagioclase, 28%-33% alkali feldspar, 12%-17% quartz, 5%-11% amphibole, and up to 7% biotite. Alkali feldspar is mostly orthoclase with a microperthitic texture. A poikilitic texture is developed when subhedral, alkali feldspar megacrysts (up to 1.2 cm across) enclose small grains of earlier phases such as plagioclase, amphibole, biotite, apatite and opaque minerals. Plagioclase is subhedral and shows normal, oscillatory and patchy zoning. Small grains of biotite are enclosed by plagioclase feldspar. Quartz is late and has undulose extinction. It is also common as myrmekite, forming vermicular intergrowths with plagioclase.

Subhedral amphibole, with clinopyroxene cores, is the main mafic phase for the Kucukcurtepe quartz monzonite (Photo 3.4). Amphibole crystals reach 3 mm across. Biotite in the quartz monzonite is in minor amounts compared to amphibole. It contains no inclusions apart from tiny zircon grains which produce pleochroic haloes. Titanite and apatite are mainly found as euhedral crystals. The opaque minerals present are magnetite and ilmenite.

Sericite is the most common alteration products in the monzodiorite. Sericitic alteration occurs mainly along the zoning planes and around central parts of the feldspar crystals. Plagioclase is occasionally altered to carbonate. Chlorite is found as alteration products after biotite. Amphibole is occasionally replaced by biotite.

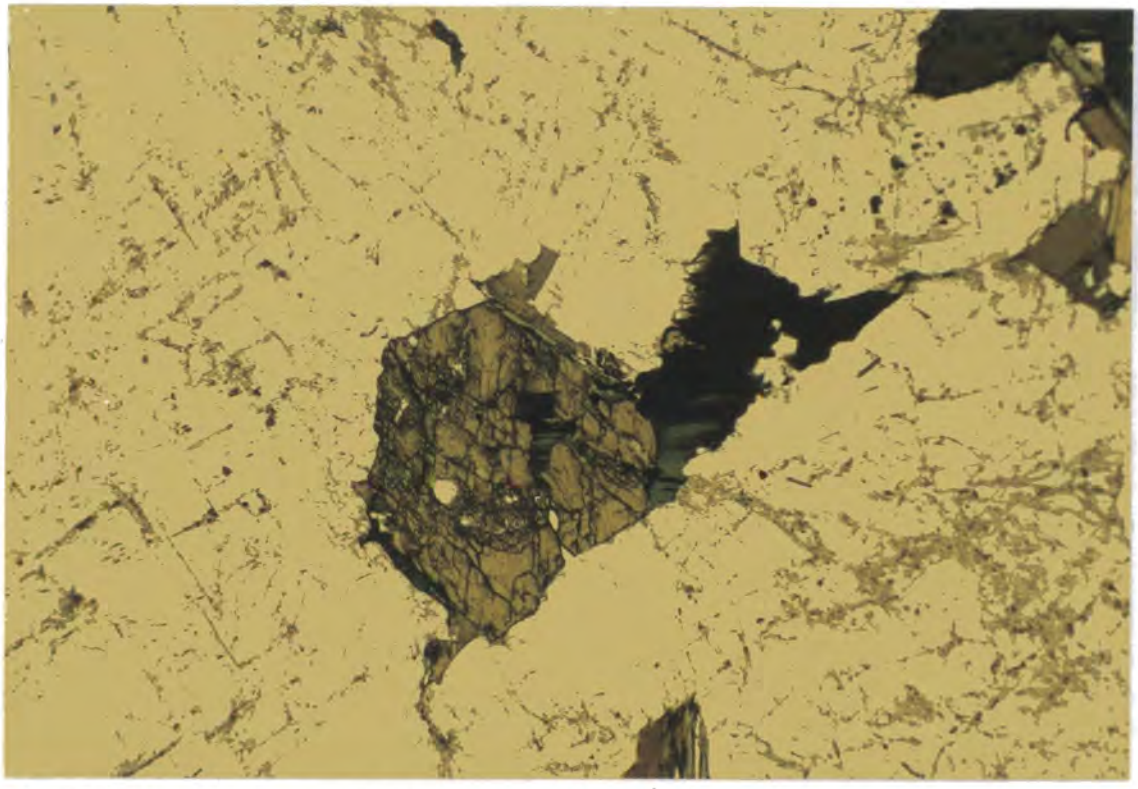

Photo 3.4. Photo shows an amphibole and an anhedral biotite mineral in the Kucukcurtepe quartz monzonite (sample N83). Biotite is moderately chloritised. Magnification: 3x1.9 mm, PPL.

3.2.3. The Kaletepe granite

The Kaletepe granite is fine to medium-grained and has an allotriomorphic, granular texture (Photo 3.5). Modal estimates are 42%-45% alkali feldspar, 26%-32% plagioclase, 20-23% quartz, and <7% biotite. The contents of plagioclase and mafic minerals decrease from the Savciliebeyit monzodiorite to the Kaletepe granite, while alkali feldspar and quartz increase.

Alkali feldspar is most commonly found as microperthitic microcline which shows typical tartan twinning. It poikilitically encloses biotite, plagioclase and quartz. Euhedral-subhedral plagioclase feldspar is zoned and is the earliest phase. Quartz is subhedral to anhedral and also fills the interstices between the early formed minerals. It has sutured boundaries and shows undulose extinction. Quartz displays graphic intergrowths with alkali feldspar and myrmekitic intergrowths with plagioclase feldspar. Biotite is the only mafic mineral. Accessory minerals in the Kaletepe granite are titanite, opaques, apatite, zircon and allanite.

Sericite is found as replacement products of both feldspars. Biotite is occasionally replaced by chlorite.

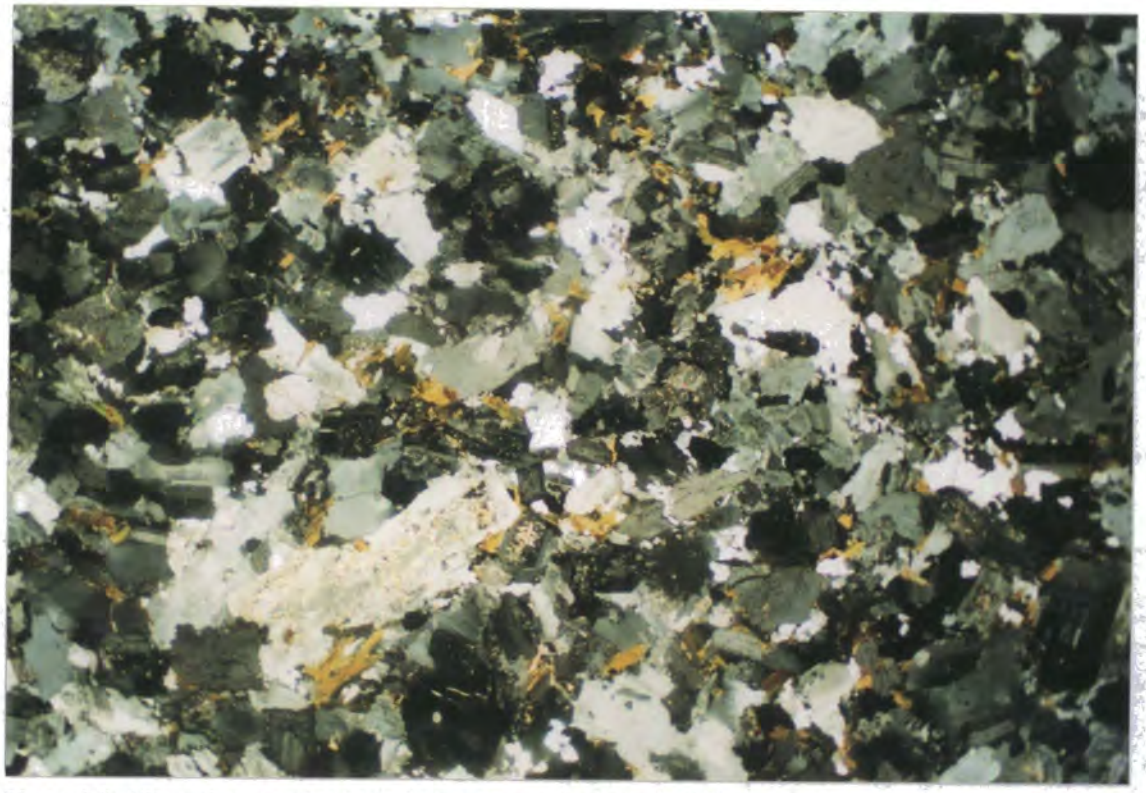

Photo 3.5. Microphotograph of the Kaletepe granite (sample N394) showing microperthitic alkali feldspar, zoned plagioclase feldspar, quartz and biotite crystals. Magnification: 12x7.2 mm, XPL.

3.3. The Celebi pluton

The Celebi pluton comprises quartz monzonite and granite. The Celebi quartz monzonite is medium to coarse-grained with a hypidiomorphic, granular texture. Modal estimates are 25%-45% alkali and plagioclase feldspars, 11-17% quartz, 4%-13% amphibole, and up to 7% biotite.

Microperthitic alkali feldspar in the quartz monzonite is mostly orthoclase but microcline has been also observed. Alkali feldspar megacrysts (up to 1.1 cm across) are subhedral-anhedral and enclose plagioclase, amphibole, biotite, opaques and apatite. Fine plagioclase inclusions in alkali feldspar have a preferred orientation, subparallel to the rims of the alkali feldspars. Plagioclase megacrysts are euhedral to subhedral and show normal and oscillatory zoning. Plagioclase reaches 8 mm across in the quartz monzonite. Plagioclase feldspar encloses amphibole, biotite, apatite and opaque minerals. Quartz is always present as interlocking grains with sutured boundaries and shows undulose extinction. It occasionally encloses other mineral phases of the rock indicating late crystallisation (Photo 3.6). Quartz forms intergrowths with plagioclase.

The mafic phases in the quartz monzonite are amphibole and biotite. The main mafic phase is euhedral to subhedral amphibole. Biotite is subhedral in shape. Clinopyroxene is generally found as relics within amphibole cores. Amphibole and biotite enclose titanite, opaques, apatite and zircon. The opaque minerals include magnetite, ilmenite and pyrite.

Sericite and epidote have been observed as secondary minerals after plagioclase. The former is most common along the zoning planes and the latter is found mainly within the cores of the plagioclase feldspar. Chlorite is also found as alteration products after biotite.

Photo 3.6. Quartz in the Celebi quartz monzonite (sample N23) poikilitically encloses plagioclase feldspars. Magnification: 6x3.7 mm, XPL.

Thin section study of the Celebi granite yields an estimate of the modal mineralogy of 34-46% alkali feldspar, 24-33% plagioclase, 18-26% quartz, 2-12% amphibole, and <2% biotite. The rock is medium to coarse-grained, locally porphyritic with a hypidiomorphic, granular texture. In the porphyritic samples, alkali feldspar, plagioclase, quartz, amphibole and biotite form the phenocrysts. The matrix is made up of alkali feldspar, plagioclase, quartz and biotite.

In the non-porphyritic samples, alkali feldspar megacrysts are subhedral-anhedral and are mostly orthoclase with a microperthitic texture. They are up to 1 cm

across and often form a poikilitic texture with inclusions of plagioclase, amphibole, biotite, apatite and opaques. Plagioclase inclusions are concentrated around the rims of the alkali feldspar crystals and some have a preferred orientation. Alkali feldspar shows graphic intergrowths with quartz. Plagioclase feldspar is euhedral to subhedral. Its size is up to 7 mm across and it shows normal and oscillatory zoning. Myrmekite is developed on the rims of the plagioclase feldspar and within the smaller grains. Quartz appears as a late phase and is subhedral to anhedral. Earlier crystallised phases are included in quartz, and quartz occasionally fills interstices between other phases of the rock. It is slightly strained, as revealed by undulose extinction.

Amphibole is always euhedral and prismatic, most commonly acicular in shape (Photo 3.7, 3.8). It is occasionally poikilitic with inclusions of apatite, titanite and opaques. Biotite is in minor amounts relative to amphibole and subhedral in shape. Clinopyroxene has been observed as relics within amphibole cores. Common accessory phases are fine to medium-grained titanite, together with opaques, apatite and zircon.

The most common alteration products in the granite are sericite and epidote after plagioclase feldspar. Chlorite is found as secondary minerals after amphibole and biotite.

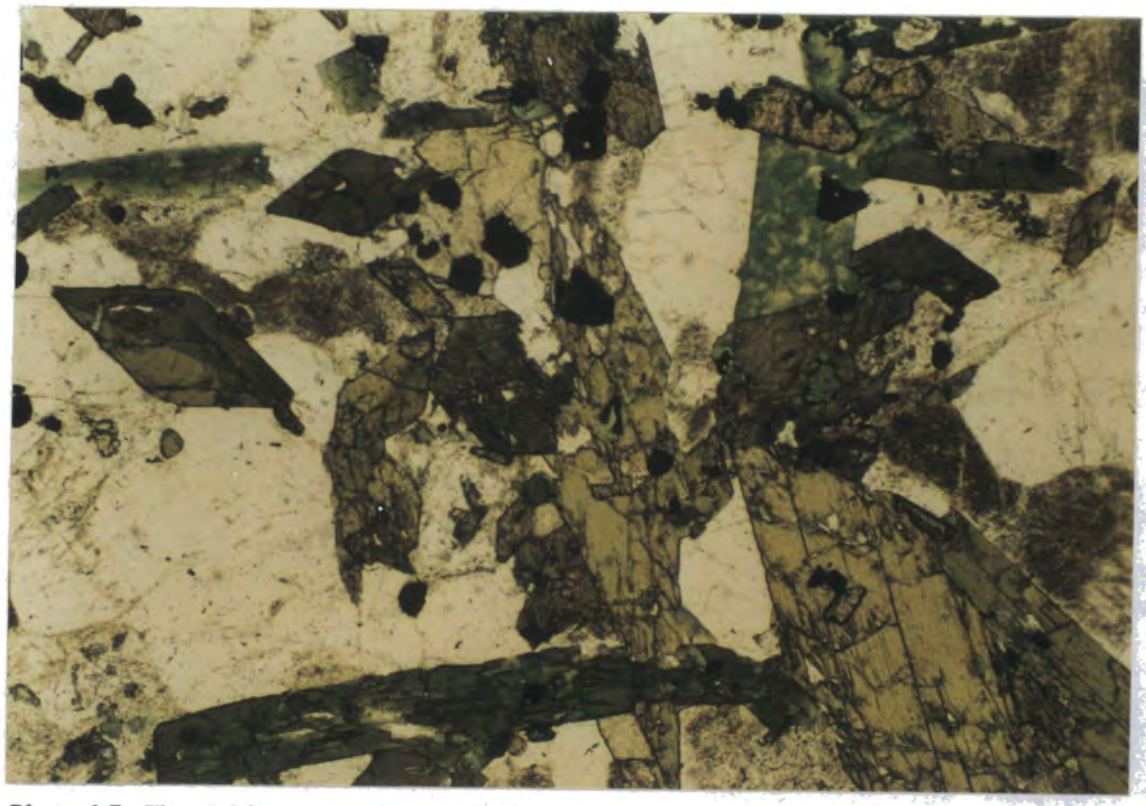

Photo 3.7. The Celebi granite (sample N75) with euhedral, prismatic amphiboles. Subhedral, anhedral crystals at the upper right of the field are titanites and the green-coloured mineral next to titanites was originally amphibole which is extensively altered to chlorite. The yellow-coloured crystal above the centre of the field is epidote. Magnification: 3x1.9 mm, PPL.

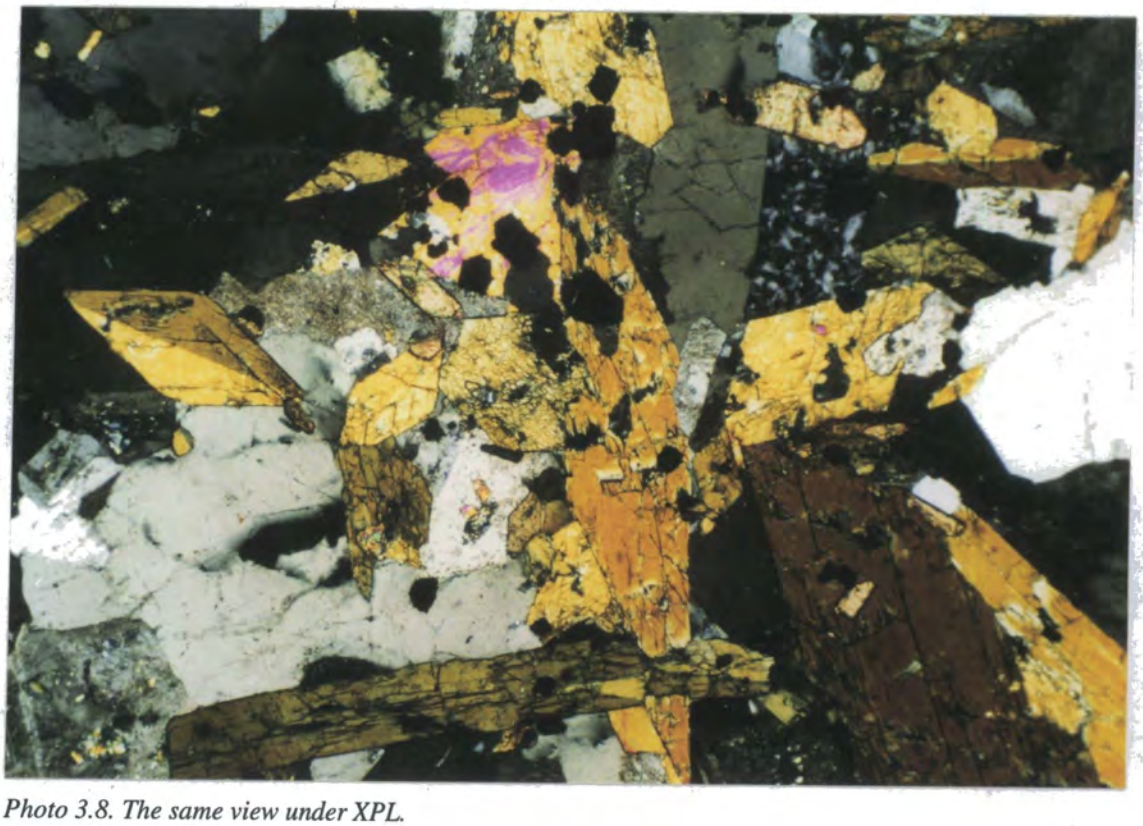

Photo 3.8. The same view under XPL.

3.4. The Baranadag pluton

The Baranadag pluton is made up of monzonite and quartz monzonite. In thin sections, the monzonite and the quartz monzonite show similar characteristics, although the latter has slightly higher proportions of quartz. The monzonite and the quartz monzonite will be discussed together in the following paragraphs. Modal estimates are 39%-46% alkali feldspar, 31%-39% plagioclase, 3%-15% amphibole, 2%-17% quartz, up to 8% clinopyroxene, and <2% biotite. The Baranadag plutonic rocks are medium to coarse-grained with a hypidiomorphic, granular texture.

Alkali feldspar is most commonly orthoclase and occasionally microcline with a microperthitic texture (Photo 3.9). Alkali feldspar megacrysts (up to 1.5 cm across) are subhedral to anhedral and contain inclusions of plagioclase, amphibole, biotite, apatite and opaques. Plagioclase inclusions in alkali feldspar are often orientated and concentrated around rims of the host crystal. Plagioclase megacrysts are subhedral and commonly zoned. Plagioclase often shows a myrmekitic texture. Biotite, apatite and opaque minerals are enclosed by plagioclase feldspar. Quartz is generally interstitial indicating late crystallisation and also shows a poikilitic texture enclosing earlier phases. Quartz occasionally displays a graphic texture and also shows undulose extinction.

Amphibole, clinopyroxene and biotite are the mafic minerals. The main mafic phase is subhedral amphibole which encloses plagioclase feldspar, titanite, apatite and opaques. Clinopyroxene is most commonly found as subhedral, prismatic and medium-grained (up to 2 mm across) crystals (Photo 3.10). It is occasionally within amphibole cores. Biotite is in minor amounts compared to amphibole and clinopyroxene. Titanite, apatite, opaques, zircon and allanite are found as accessory minerals (Photo 3.11).

Sericite and chlorite are found as common alteration products after feldspar and biotite in the Baranadag intrusive rocks. Amphibole is occasionally replaced by biotite.

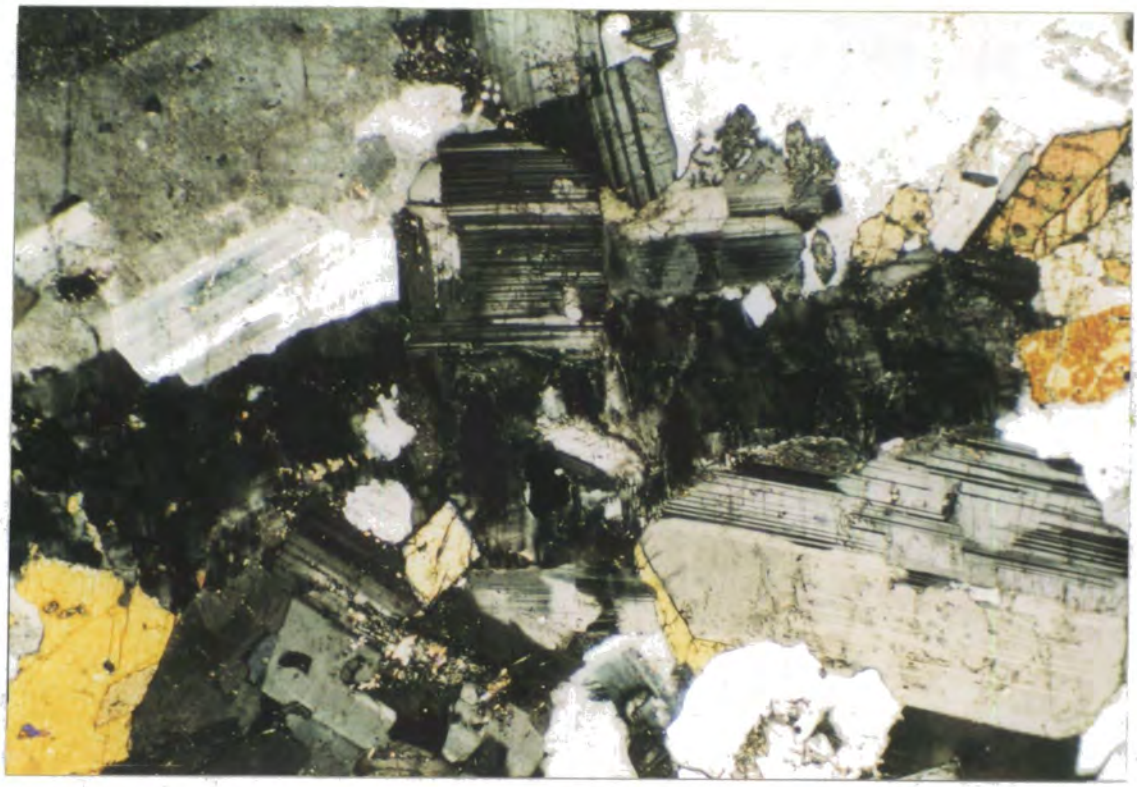

Photo 3.9. Microcline in the monzonite (sample N304) encloses plagioclase feldspars and shows a microperthitic texture. Magnification: 3x1.9 mm, XPL.

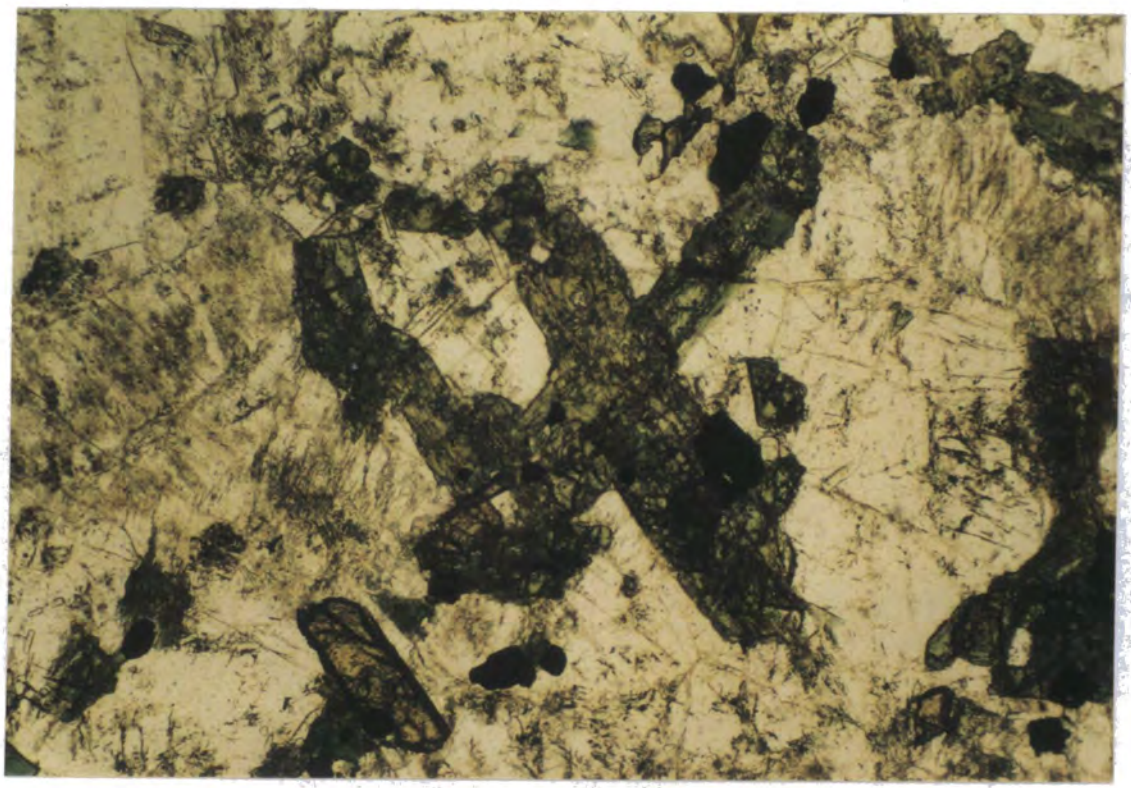

Photo 3.10. Subhedral, prismatic clinopyroxenes in the monzonite (sample N28). Magnification: 3x1.9 mm, PPL.

Photo 3.11. Euhedral, prismatic, dark brown-coloured allanite in the quartz monzonite (sample N135) showing zoning. In the field view, there are also titanite, apatite and biotite minerals. The latter is chloritised. Magnification: 1.3x0.77 mm, PPL.

3.5. The Hamit pluton

The Hamit pluton comprises nepheline monzosyenite, pseudoleucite monzosyenite, alkali feldspar syenite and quartz syenite. The nepheline monzosyenite and pseudoleucite monzosyenite are cut by the foid-bearing microsyenitic dykes.

The nepheline monzosyenite is medium-grained with a hypidiomorphic, granular texture. It has higher proportion of mafic minerals than the alkali feldspar syenite and the quartz syenite. Alkali feldspar is the dominant mineral in the nepheline monzosyenite and is most commonly orthoclase. Microperthitic alkali feldspar is euhedral to subhedral. The alkali feldspar encloses inclusions of plagioclase, biotite, titanite and opaques. The interstices between other crystals of the rock are generally filled by nepheline. Alkali feldspar and nepheline form intergrowths in places. Plagioclase feldspar is euhedral to subhedral and zoned. It encloses apatite, titanite and clinopyroxene.

Clinopyroxene, amphibole and biotite are the mafic minerals. Clinopyroxene is euhedral to subhedral and reaches 4 mm across. It is often zoned and sometimes

rimmed by amphibole (Photo 3.12). Clinopyroxene occasionally has a colourless core but a green-coloured rim. Amphibole is found as subhedral-anhedral crystals. Subhedral amphibole poikilitically encloses titanite, apatite and opaques. Amphibole crystals in the nepheline monzosyenite are strongly pleochroic. Biotite is in minor amounts compared to clinopyroxene and amphibole. It is commonly subhedral or interstitial. Biotite contains inclusions of accessory minerals such as titanite, apatite, zircon, fluorite and opaques. Garnet has been also observed as euhedral crystals and shows zoning (Photo 3.13). Titanite is found as inclusions enclosed within amphibole, alkali feldspar and biotite or as fine-grained discrete crystals. Apatite is fine-grained and forms elongated prismatic crystals or hexagonal crystals. Fluorite is found as inclusions mostly in clinopyroxene. Opaque minerals are generally magnetites.

Photo 3.12. The nepheline monzosyenite (sample N32) from the Hamit pluton with a zoned prismatic clinopyroxene. The remaining minerals seen in the view are alkali feldspar, nepheline and plagioclase feldspars. Magnification: 3x1.9 mm, XPL.

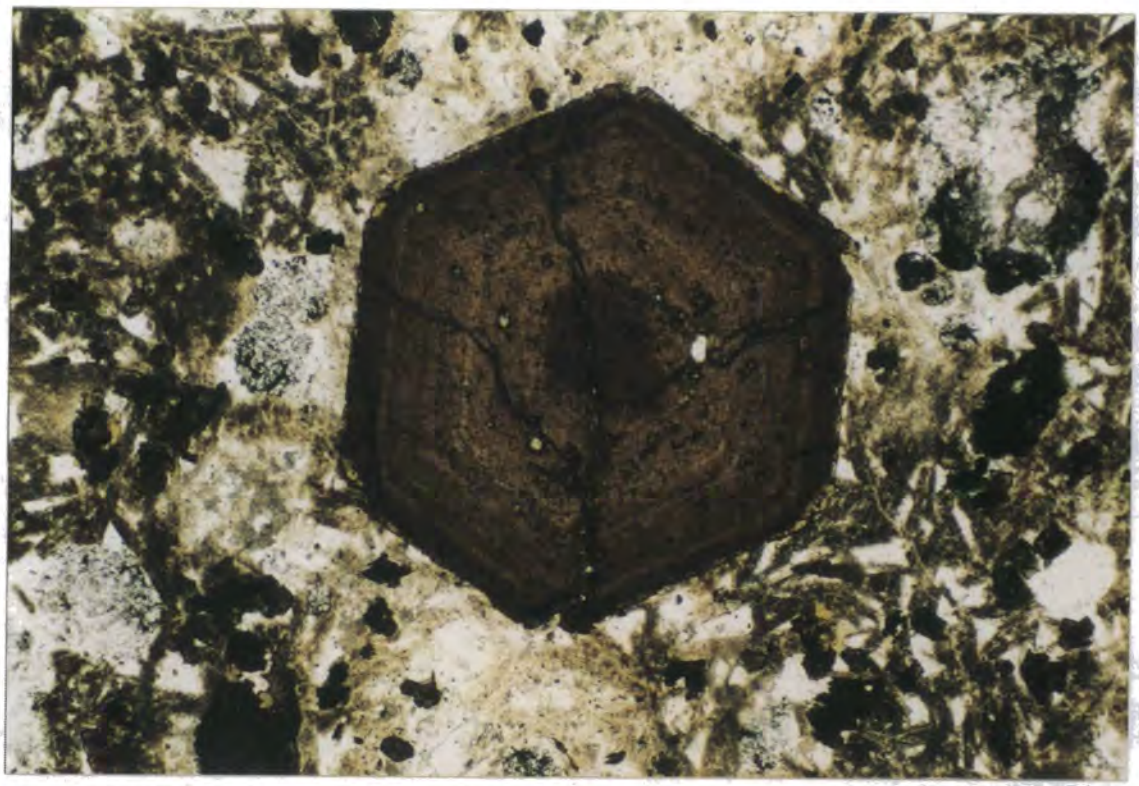

Photo 3.13. Euhedral garnet phenocryst in the nepheline monzosyenite (sample N50) shows oscillatory zoning. Magnification: 3x1.9 mm, PPL.

The most common alteration product is cancrinite after nepheline. Sericite and chlorite are also observed as secondary minerals. Alkali feldspar and plagioclase feldspar are partially sericitised. Biotite is slightly to moderately chloritised. Amphibole is occasionally replaced by biotite.

The pseudoleucite monzosyenite is porphyritic with a hypidiomorphic, granular texture. Phenocrysts are pseudoleucite, plagioclase, alkali feldspar, clinopyroxene and, occasionally, amphibole and garnet. The matrix is fine to medium-grained containing nepheline, nosean, garnet and plagioclase feldspar. The dominant phase in the rock is alkali feldspar which is euhedral to subhedral with a microperthitic texture and is, most commonly, orthoclase. Plagioclase, biotite, titanite and opaques are enclosed by alkali feldspar. Nepheline appears as a late phase filling the interstices between the earlier-formed phases. Plagioclase feldspar (up to 7 mm across) is euhedral to subhedral and zoned.

Clinopyroxene is euhedral to subhedral and shows oscillatory zoning. It has either a colourless core with a green rim or a green core with a colourless rim. Colourless clinopyroxene has been also found. Accessory minerals, such as titanite, apatite, opaques and fluorite; are embedded in clinopyroxene. Pseudoleucite hass

resulted from an intergrowth of nepheline and alkali feldspar and has well-defined boundaries (Photo 3.14). Garnet is generally euhedral with a poikilitic texture and occasionally zoned. Nosean is euhedral to subhedral with dark rims due to iron oxide inclusions. Amphibole is occasionally found as reaction rims around clinopyroxene crystals. Subhedral amphibole poikilitically encloses biotite, titanite, apatite and opaques. Biotite is subhedral and contains inclusions of zircon, apatite, titanite, fluorite and opaques.

Cancrinite is the most common secondary mineral after nepheline. Nepheline is generally extensively altered to cancrinite and is, rarely, altered to gieseckite. Biotite is slightly to moderately chloritised.

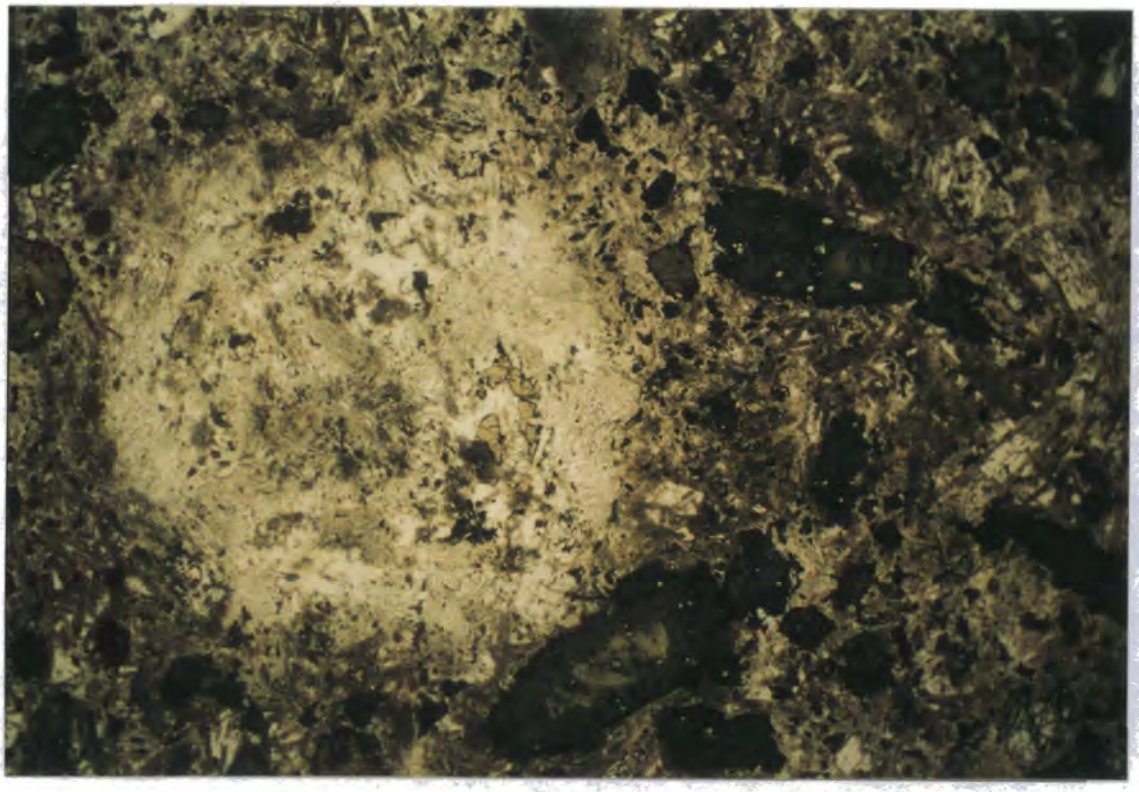

Photo 3.14. Pseudoleucite phenocryst in the pseudoleucite monzosyenite (sample N45) from the Hamit pluton together with euhedral clinopyroxenes. Magnification: 12x7.2 mm, PPL.

The alkali feldspar syenite is medium-grained, equigranular with a hypidiomorphic, granular texture. The dominant mineral is alkali feldspar, which occurs as tabular, euhedral to subhedral crystals, and forms up to 90% of the rock by volume (Photo 3.15). The alkali feldspar is mostly orthoclase and occasionally microcline. It almost always shows a microperthitic texture. Plagioclase feldspar is euhedral to subhedral and forms about 10% of the rock. Feldspar crystals show a preferred orientation. Quartz is interstitial and in minor amounts. The alkali feldspar

syenite contains small quantities of amphibole, clinopyroxene and biotite. In some thin sections, subhedral amphibole encloses small grains of plagioclase feldspar, titanite and opaque minerals. The amphibole is up to 2 mm across. Subhedral to anhedral clinopyroxene encloses apatite and opaque minerals. Garnet is occasionally found as a primary mineral. Accessory minerals are quartz, clinopyroxene, biotite, titanite, opaques, apatite, zircon and allanite. The titanite crystals are euhedral, fine-grained and often associated with opaque minerals.

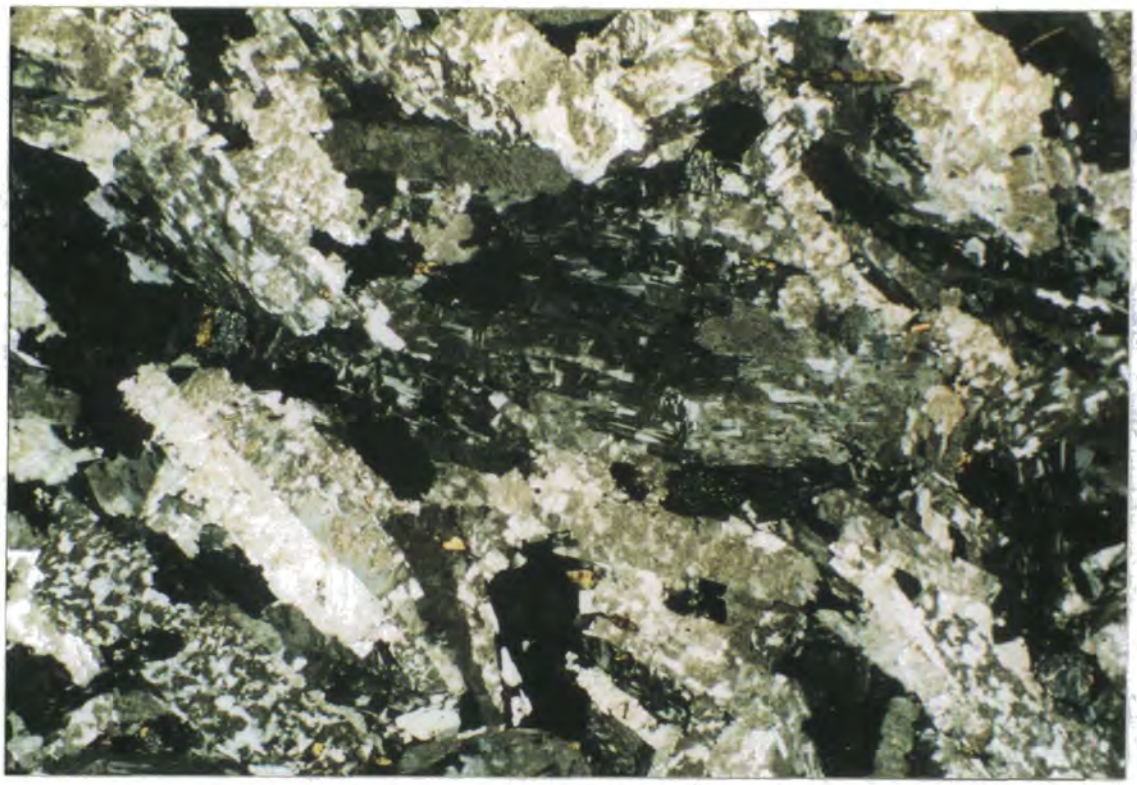

Photo 3.15. Tabular alkali feldspars in the alkali feldspar syenite (sample N40) show strong microperthitic texture. Alkali feldspars also display typical simple twinning. Magnification: 6x3.7 mm, XPL.

Muscovite and epidote are found as alteration products after plagioclase. Plagioclase is occasionally extensively sericitised. Alkali feldspar also shows sericitic alteration.

The quartz syenite shows similar characteristics to the alkali feldspar syenite but with higher proportions of quartz and mafic minerals (Photo 3.16). Modal estimates are 50%-70% alkali feldspar, 12%-26% plagioclase, 11%-23% quartz, and <8% amphibole, biotite and clinopyroxene. The alkali feldspar is mainly orthoclase but microcline has been also observed. The alkali feldspar is found as tabular and euhedral to subhedral crystals, up to 1.5 cm across and always displays a microperthitic texture. Its microperthitic texture is not so intense as in the alkali

feldspar syenite. It poikilitically encloses plagioclase, biotite, titanite and opaque minerals. Plagioclase feldspar is euhedral to subhedral and exhibits complex oscillatory zoning. As in the alkali feldspar syenite, feldspar crystals show a preferred orientation. The plagioclase feldspar encloses biotite, apatite and opaque minerals. Quartz appears as a late phase and fills interstices between the other phases. It is slightly strained, as revealed by undulose extinction. Quartz is intergrown with both plagioclase and also with alkali feldspar.

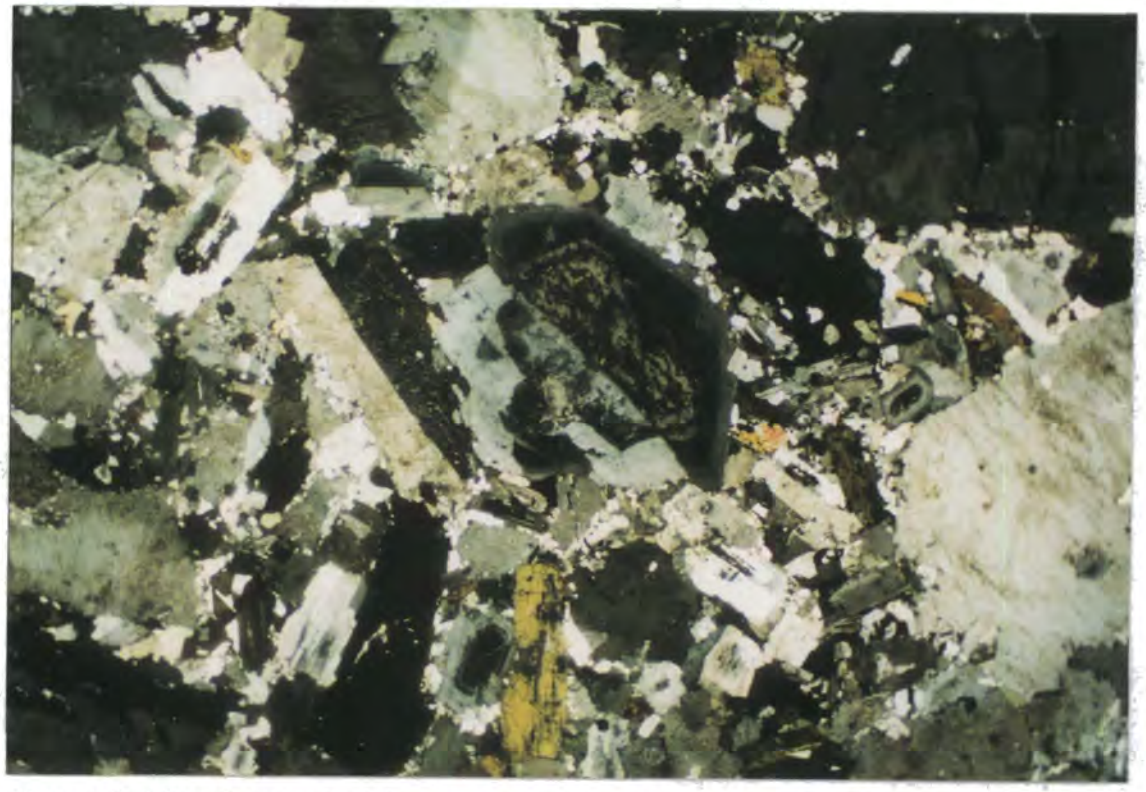

Photo 3.16. Microphotograph of the quartz syenite (sample N49) from the Hamit pluton. Tabular alkali feldspars are seen showing microperthitic texture. Plagioclase feldspars display complex zoning. The remaining minerals are quartz and amphibole. Magnification: 12x7.2 mm, XPL.

Amphibole, clinopyroxene and biotite are found as mafic minerals. Subhedral amphibole encloses inclusions of apatite, titanite and opaques. Biotite has inclusions of zircon, apatite, titanite and opaque minerals. Clinopyroxene is in smaller amounts than amphibole and biotite. Accessory minerals are titanite, opaques, apatite and zircon. Titanite is generally euhedral and fine to coarse-grained.

Sericite is found as a secondary mineral after plagioclase. Alkali feldspar also displays sericitic alteration. Biotite is slightly to moderately replaced by chlorite.

The foid-bearing microsyenitic dykes are, in general, phonolite in composition. They show a well-developed porphyritic texture with plagioclase, clinopyroxene, alkali feldspar and nepheline phenocrysts. The groundmass is made

up of nepheline, plagioclase, alkali feldspar, biotite and nosean. The plagioclase feldspar is generally euhedral to subhedral, lath-shaped, and forming a glomeroporphyritic texture. The clinopyroxene phenocrysts are generally euhedral and green. The alkali feldspar is commonly subhedral and slightly altered to sericite. The nepheline crystals in the groundmass are subhedral and prismatic. The nepheline crystals are often altered to cancrinite and, rarely, gieseckite. Fluorite, titanite and opaques are the main accessory minerals.

3.6. The dykes

The aplitic dykes are fine-grained with an allotriomorphic, granular texture. Alkali feldspar, plagioclase and quartz are the dominant minerals. Quartz is anhedral and shows undulose extinction. It displays graphic intergrowths with alkali feldspar. Alkali feldspar is most commonly found as microperthitic microcline which shows typical tartan twinning but orthoclase is also present. Plagioclase is subhedral to anhedral and shows zoning. The accessory minerals are biotite, apatite, titanite and opaque minerals.

The mafic dykes are fine-grained with a hypidiomorphic, granular texture. The dominant minerals are plagioclase, clinopyroxene, amphibole, quartz, biotite and alkali feldspar. Clinopyroxene is the main mafic phase and is most commonly found as subhedral and prismatic crystals. Amphibole is subhedral to anhedral and prismatic. Plagioclase is subhedral and shows zoning. It is commonly altered to sericite, carbonate and epidote. Biotite is slight to moderately chloritised. Quartz is subhedral to anhedral and shows undulose extinction. Titanite, opaques and zircon are accessory phases. Quartz is intergrown with both plagioclase and alkali feldspar.

The micro-syenitic dykes are fine-grained with a hypidiomorphic, granular texture. The dominant mineral is alkali feldspar, which forms subhedral to anhedral crystals. The alkali feldspar is mostly orthoclase and occasionally sericitised. It shows a microperthitic texture. Plagioclase feldspar is subhedral and shows zoning. Quartz is interstitial and in minor amounts. Accessory minerals are biotite, titanite and opaques.

3.7. Summary

The thin section features of the Behrekdag, Cefalikdag, Celebi, Baranadag and Hamit plutons have been summarised in Table 3.1.

PLUTON	BEHREKDAG	CEFALIKDAG	CELEBI	BARANADAG	HAMIT
ROCK UNIT	quartz monzonite, granite	monzodiorite (1), quartz monzonite (2), granite (3)	quartz monzonite (1), granite (2)	monzonite, quartz monzonite	nepheline monzosyenite (1), pseudoleucite monzosyenite (2), alkali feldspar syenite (3), quartz syenite (4)
TEXTURE	hypidiomorphic	hypidiomorphic (1, 2); allotriomorphic (3)	hypidiomorphic (1, 2); hypidiomorphic porphyritic (2)	hypidiomorphic	hypidiomorphic (1, 3, 4); hypidiomorphic, porphyritic (2)
GRAIN SIZE	medium-coarse	medium-coarse (1, 2); and fine (3)	medium-coarse	medium-coarse	medium-coarse
MAFIC PHASE	amp, bi, (±) cpx	amp, bi, cpx (1); amp, bi, (±) cpx (2); bi (3)	amp, bi, (±) cpx (1); amp, bi, cpx (2)	amp, cpx, bi	cpx, amp, bi, (±) gt (1); cpx, amp, bi, gt (2); (±) amp, (±) cpx, (±) bi (3, 4)
ACCESSORY PHASE	titanite, opaques, apatite, zircon	titanite, opaques, apatite, zircon, allanite (only 3)	titanite, opaques, apatite, zircon	titanite, opaques, apatite, zircon, allanite	titanite (1-4), opaques (1-4), apatite (1-4), zircon (1-4), allanite (3), fluorite (1, 2), quartz (3), clinopyroxene (3), biotite (3)
QUARTZ AND FELDSPAR TEXTURE	microperthite, zoning, myrmekite	microperthite, zoning, myrmekite, graphic (1, 3)	microperthite, zoning, myrmekite	microperthite, zoning, myrmekite, graphic	microperthite, zoning, myrmekite (4)
ALTERATION	sericite, chlorite, carbonate	sericite, chlorite, carbonate	sericite, chlorite, epidote	sericite, chlorite	cancrinite (1, 2), gieseckite (2), sericite (1-4), chlorite (1-4), garnet (3, 4), epidote (3)

Table 3.1. Summary of the petrographic characteristics of the intrusive rocks from the Central Anatolian Massif. Abbreviations: amp-amphibole, bi-biotite, cpx-clinopyroxene and gt-garnet.

Chapter 4
MINERAL GEOCHEMISTRY

Introduction

This chapter interprets the electron microprobe analyses of the mineral phases (plagioclase, alkali feldspar, amphibole, clinopyroxene, biotite and Ti-Fe oxides) from the Central Anatolian plutonics. The analyses were undertaken to assess how the whole-rock major element variations were reflected in individual minerals and also to investigate conditions of crystallisation. A total of 539 point analyses were performed on 29 representative samples from the Behrekdag, Cefalikdag, Celebi, Baranadag and Hamit plutons using a Cameca CAMEBAX electron microprobe at the University of Edinburgh. The full electron microprobe data set is listed in Appendix D.

This chapter is presented in two main Sections:

4.1. Classification of mineral phases: this Section classifies the mineral phases using the International Mineralogical Association (IMA) methodologies.

4.2. Geothermo-barometry and oxygen fugacity: this Section presents determination of crystallisation temperatures, pressures and oxygen fugacities and hence provides vital information about the emplacement conditions of the granitic magmas.

4.1. Classification of mineral phases

4.1.1. Feldspars

28 representative samples from the Behrekdag, Cefalikdag, Celebi, Baranadag and Hamit plutons were chosen for electron microprobe analysis (Table 4.1). A total of 266 feldspar crystals were analysed. Feldspars (plagioclase and alkali feldspar) are, in general, the most abundant mineral phases of the Central Anatolian plutonics. Alkali feldspar can make up nearly 90% of the alkali feldspar syenite from the Hamit pluton. Because plagioclase feldspars in the Central Anatolian plutonics

are generally zoned, analyses of at least two points (one near the margin and the other near the core) were performed on these zoned crystals (Figure 4.1-4.6). The mole fractions of the feldspar end-members (albite, orthoclase, anorthite) were calculated using the Na, K and Ca contents of feldspar (in atoms per formula unit). The data were then plotted on albite-orthoclase-anorthite ternary classification diagrams (Figure 4.1-4.5).

PLUTON	ROCK UNIT
BEHREKDAG	quartz monzonite granite
CEFALIKDAG	Savciliebeyit monzodiorite Kucukcurtepe quartz monzonite Kaletepe granite
CELEBI	quartz monzonite granite

PLUTON	ROCK UNIT
BARANADAG	monzonite quartz monzonite
HAMIT	nepheline monzosyenite pseudoleucite monzosyenite alkali feldspar syenite quartz syenite

Table 4.1. Table showing the studied plutons from the Central Anatolian Massif from which representative samples were chosen for electron microprobe analyses.

Plagioclase crystals from the Central Anatolian plutonics vary from An_{71} to An_1 (these maximum and minimum values both belong to the Hamit pluton). The average anorthite content of the plutonics, based on 183 analyses, is 38.17 mol.% and the standard deviation of these analyses is 10.77%. This means that 95% of the anorthite contents of the plutonics lie in the range 38.17±21.5. Or (orthoclase) contents are consistently low, rarely exceeding 2 mol.% for plagioclases from the Behrekdag, Cefalikdag, Celebi and Baranadag intrusive rocks. On the other hand, those in plagioclases are generally high in the Hamit plutonic rocks (up to 9.3 mol.%).

As noted in Chapter 3, alkali feldspars generally show a microperthitic texture. In the Hamit pluton (especially in the alkali feldspar syenite), this texture is quite coarse which causes problems in trying to obtain representative values. To eliminate this problem, and also the possibility of sample decomposition (especially Na and K-bearing minerals, e.g. feldspar and biotite), the electron beam was defocused to about 15μ.

4.1.1.1. Chemical variations

The Behrekdag pluton comprises quartz monzonite and granite. Figure 4.1 shows that the plagioclases from the quartz monzonite and granite are mainly andesine, the exception being an oligoclase from one granite sample. The main compositional range of plagioclase is restricted in the quartz monzonite (An_{50-38}) but slightly wider in the granite (An_{47-27}). Potassium feldspar in the quartz monzonite has compositions of Or_{79-89} and that in the granite Or_{81-84}.

The Cefalikdag pluton is made up of the Savciliebeyit monzodiorite, Kucukcurtepe quartz monzonite and Kaletepe granite. Plagioclases from the Savciliebeyit monzodiorite are mainly andesine in composition (An_{52-40}), except for two samples falling in the labradorite field (Figure 4.2). The Kucukcurtepe quartz monzonite has a compositional range of An_{47} and An_{30}, which has a similar mean but slightly greater standard deviation than that of the Savciliebeyit monzodiorite. There are only five plagioclase analyses from the Kaletepe granite and these plot in the oligoclase and andesine fields (An_{30-27}). Potassium feldspars in the Savciliebeyit monzodiorite and Kucukcurtepe quartz monzonite are characterised by similar compositions (Or_{82-95}). There are no alkali feldspar analyses from the Kaletepe granite.

The Celebi pluton consists of quartz monzonite and granite. Plagioclase from the quartz monzonite and granite is mainly andesine, the one exception being oligoclase (Figure 4.3). The quartz monzonite contains plagioclase with a compositional range of An_{48-33} compared with the granite range of An_{46-25}. The main compositional range of orthoclase is restricted in the granite (Or_{73-81}) but slightly wider in the quartz monzonite (Or_{76-91}).

The Baranadag pluton contains monzonite and quartz monzonite. Plagioclase from the monzonite and quartz monzonite is mainly andesine and oligoclase (Figure 4.4). Plagioclases in the monzonite lie in the range An_{37-29} whereas the range in the quartz monzonite is wider at An_{38-17}. Alkali feldspars in the monzonite show almost the same compositional range as the quartz monzonite (Or_{77-93}).

The Hamit pluton is made up of nepheline monzosyenite, pseudoleucite monzosyenite, alkali feldspar syenite and quartz syenite. In Figure 4.5, plagioclase from the nepheline monzosyenite plots in the labradorite, andesine and oligoclase fields (An_{49-24}). Apart from one bytownite sample, plagioclase from the

pseudoleucite monzosyenite is mainly labradorite in composition (An_{71-48}). Most plagioclase crystals, from the nepheline monzosyenite and pseudoleucite monzosyenite have higher orthoclase contents than other rock units in the Hamit pluton (up to 9.3 mol.%). These higher values can be explained by the development of antiperthite, although this has not been observed microscopically. The alkali feldspar syenite and quartz syenite from the Hamit pluton contain much more sodic plagioclase than the nepheline monzosyenite and pseudoleucite monzosyenite. Plagioclase in the alkali feldspar syenite is mainly albite (An_{9-1}). Plagioclase in the quartz syenite is albite and oligoclase (An_{20-1}), with one andesine sample (An_{37}). Alkali feldspar from the Hamit pluton has a large compositional range compared to that from the Behrekdag, Cefalikdag, Celebi and Baranadag plutons, possibly because of exsolved lamellae of perthite. Alkali feldspars from the Hamit pluton plot in the sanidine field (Or_{60-95}).

Figure 4.6 illustrates the plagioclase compositions of the cores and rims of zoned plagioclase crystals from the Central Anatolian plutonics. An additional point analysis, here called the "inner-zone", was sometimes carried out between the rim and core of some plagioclase crystals. It is evident from this Figure that oscillatory zoning is quite common in the plagioclase of the plutonics. As it was mentioned in Chapter 3, the plagioclase generally shows normal, oscillatory and, rarely, patchy zoning patterns.

In Figure 4.7, the anorthite compositions of plagioclases are plotted against the SiO_2 wt.% contents of the host rocks. As can be seen from Figure 4.7, the anorthite contents generally decrease with increasing silica. For comparison a linear regression line has been plotted through all plagioclase data for the plutonic rocks. The anorthite contents of plagioclase crystals from the Behrekdag, Cefalikdag, Baranadag and Hamit intrusive rocks decrease with silica, forming linear trends, whereas those from the Celebi intrusives increase with silica, forming also linear trends. In theory, if they had been crystallised in equilibrium with the magma, their anorthite contents would have been decreased progressively with increasing silica, forming a linear or sublinear trend with a negative gradient and without substantial scatter. The negative linear trends shown by the Behrekdag, Cefalikdag, Baranadag and Hamit plutonic rocks indicate that most of the plagioclase crystals in these plutonic rocks are in equilibrium with magma/magmas.

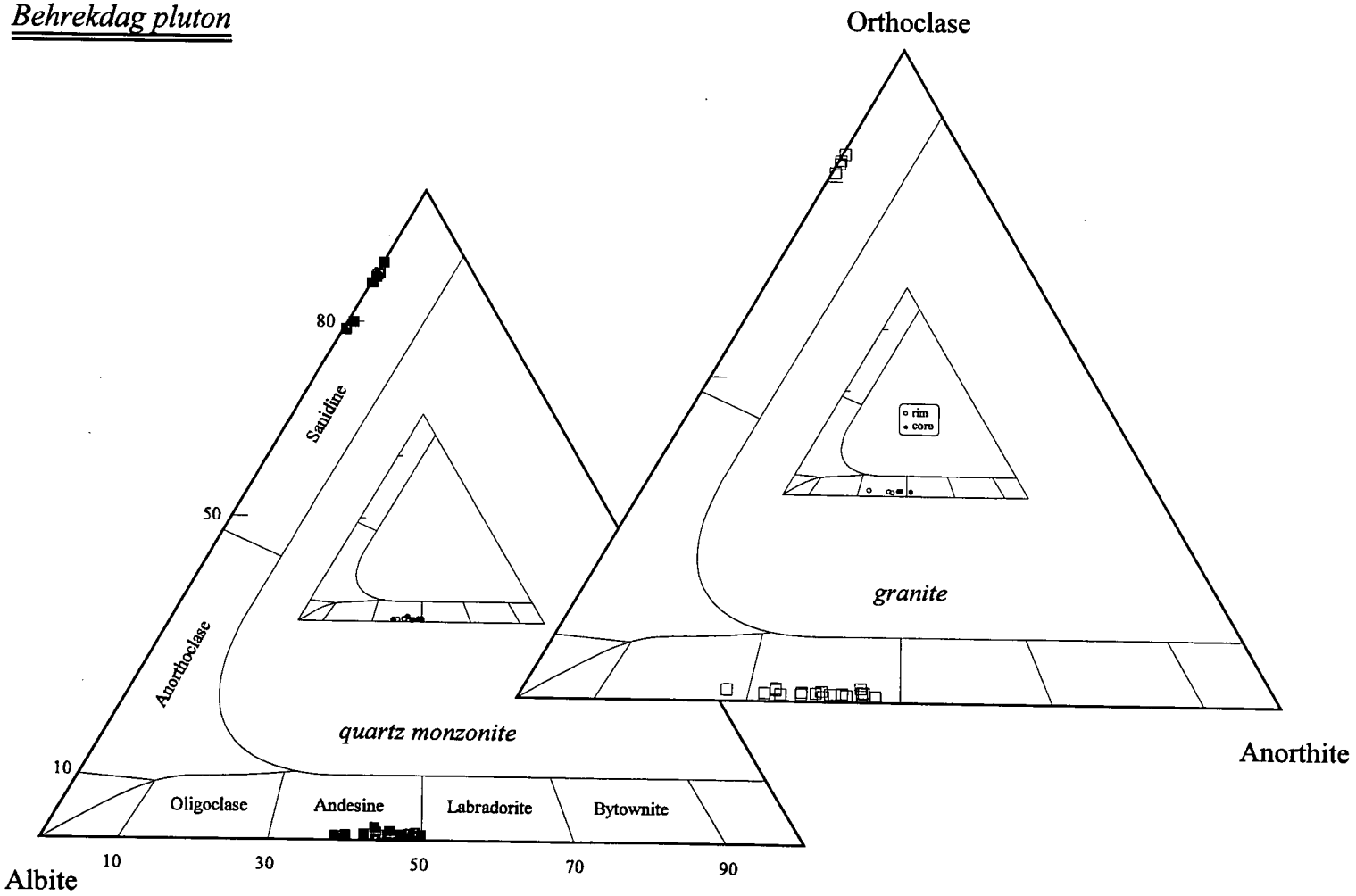

Figure 4.1. Compositions of feldspars in the Behrekdag plutonic rocks in plots of orthoclase, albite and anorthite ternary.

Cefalikdag pluton

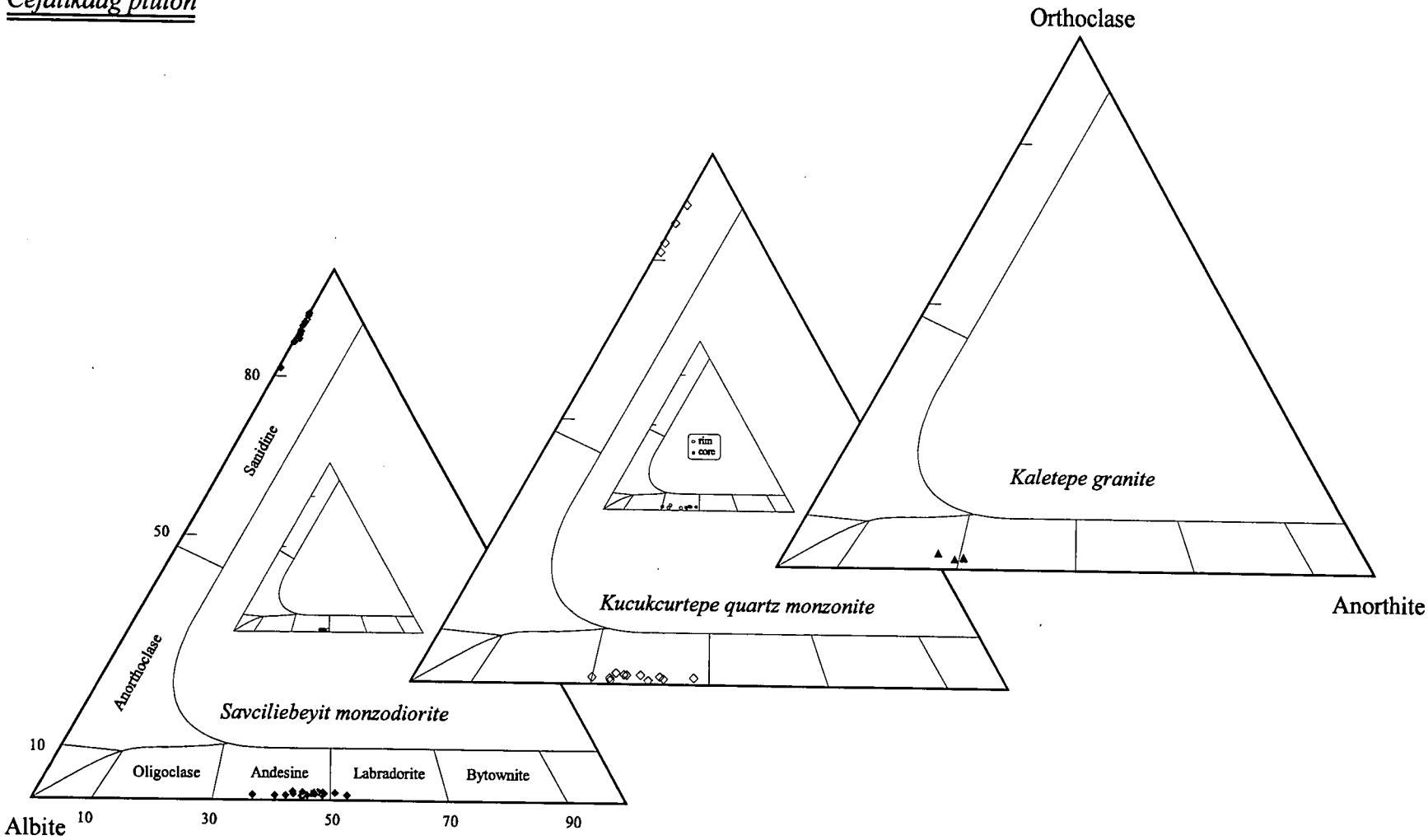

Figure 4.2. Diagram displaying compositions of feldspars in the Cefalikdag pluton.

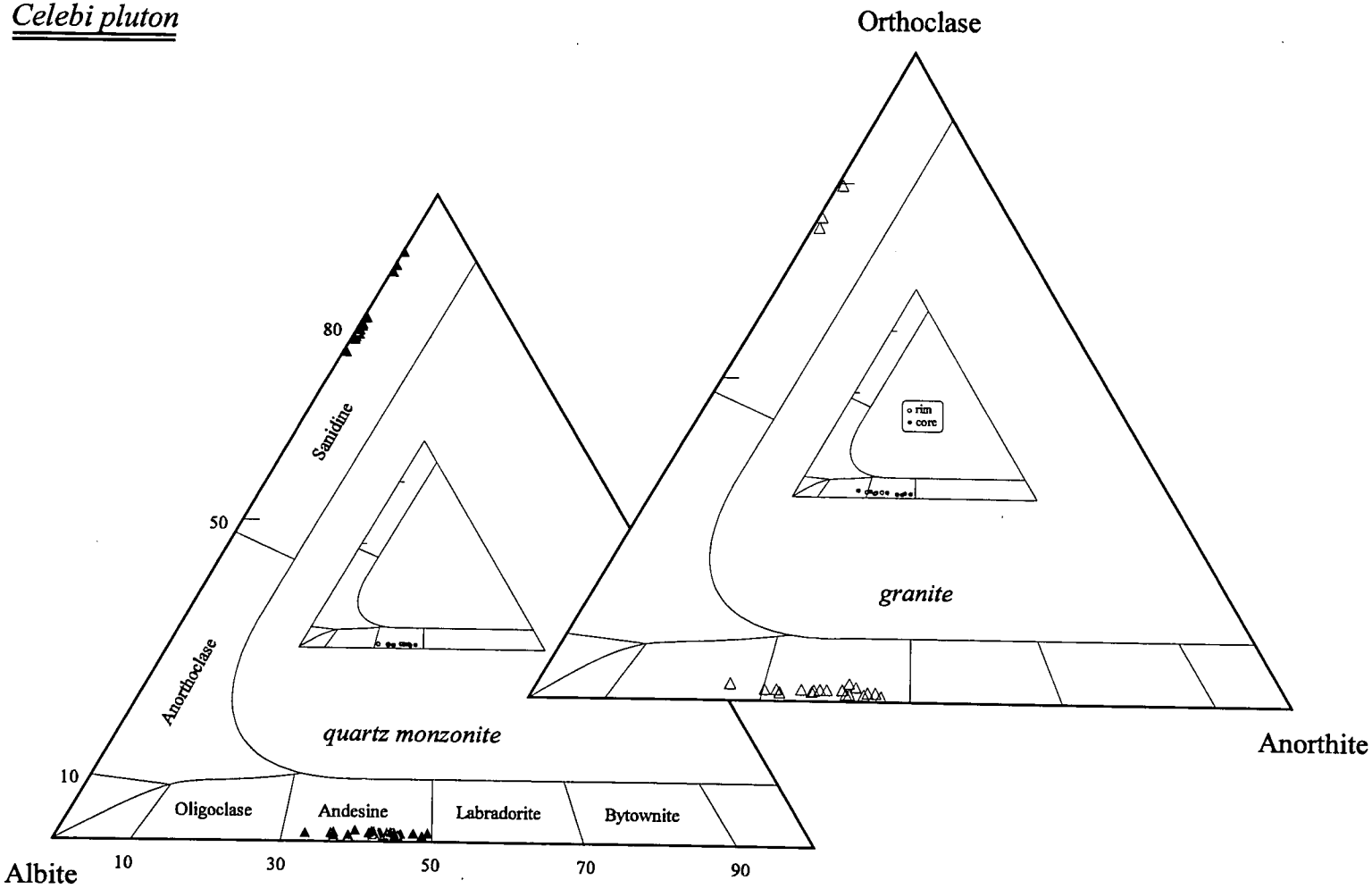

Figure 4.3. Distribution of feldspar compositions in the Celebi pluton.

Baranadag pluton

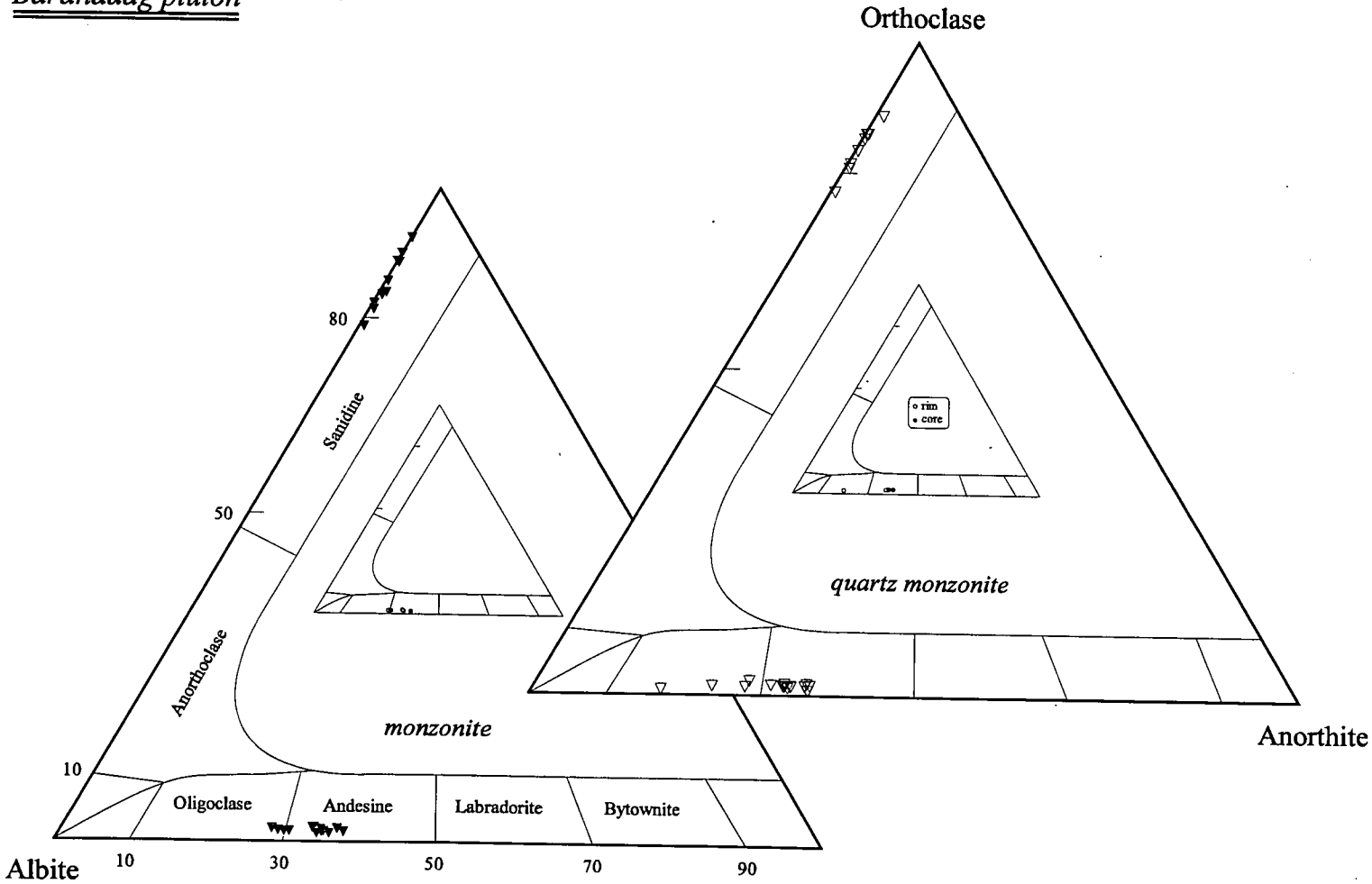

Figure 4.4. Compositional variation in feldspars from the Baranadag plutonic rocks.

Hamit pluton

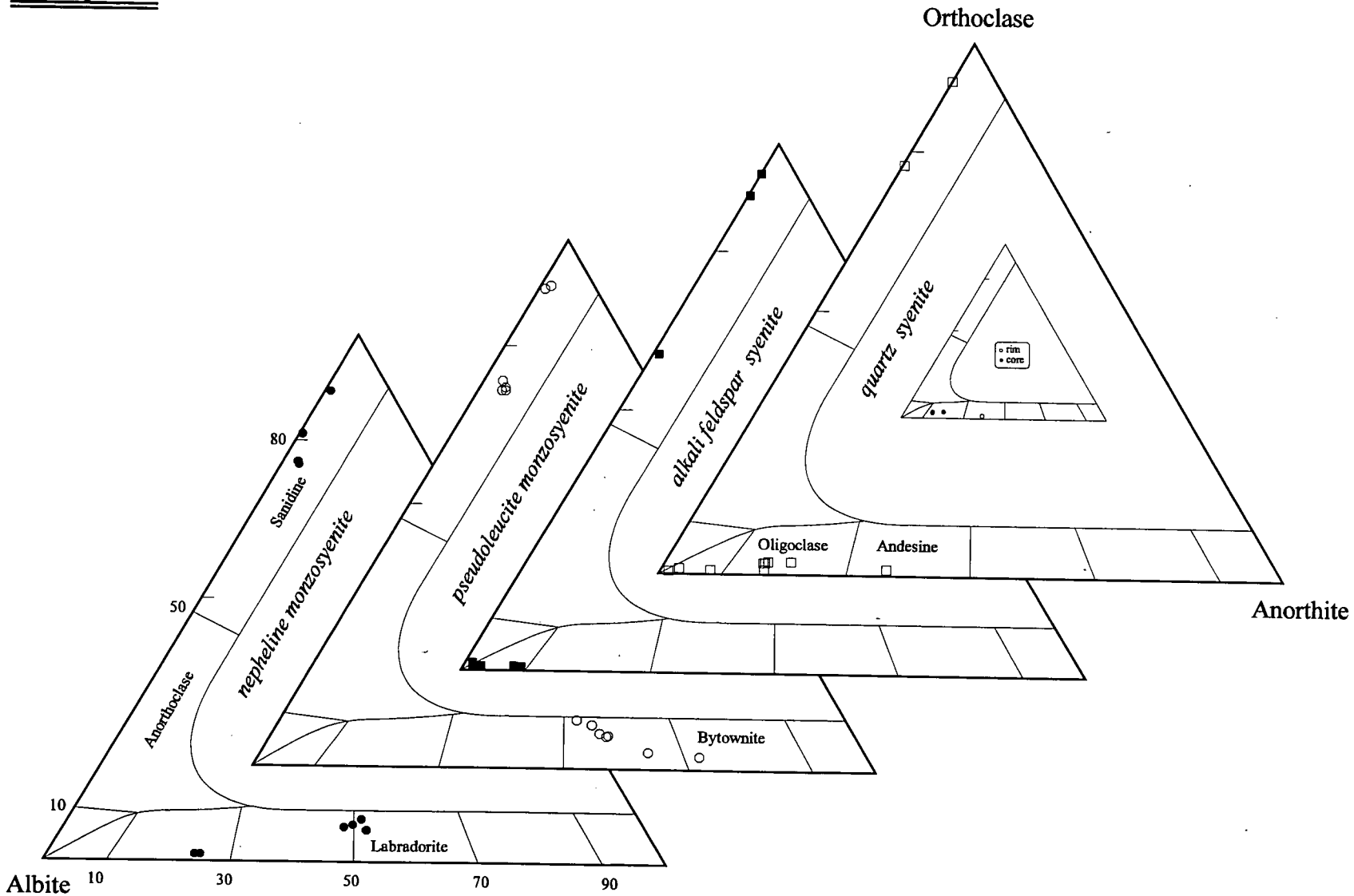

Figure 4.5. Distribution of feldspar compositions in the Hamit pluton.

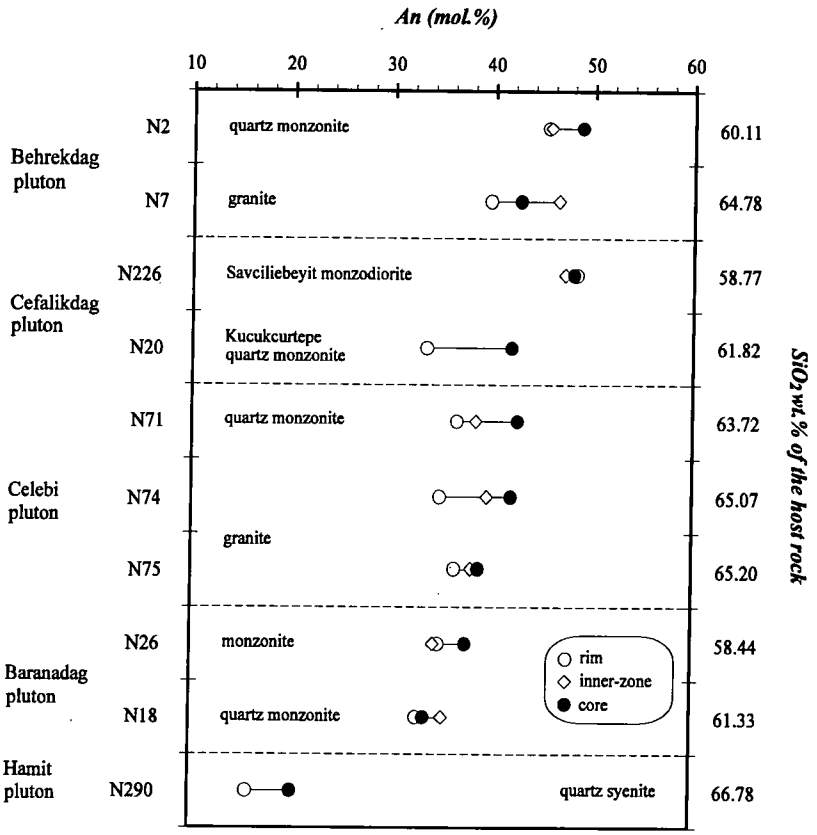

Figure 4.6. Diagram shows plagioclase compositional ranges from the Central Anatolian plutonics. Sample numbers are listed on the left side; whole-rock SiO_2 wt.% content on the right side.

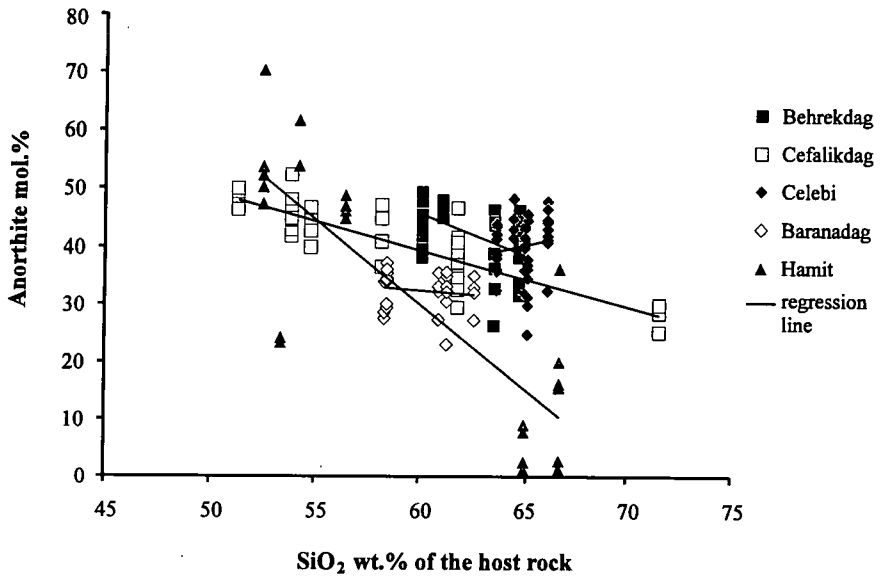

Figure 4.7. Variation in plagioclase An content (mol.%) with SiO_2 wt.% content of their host rock.

4.1.2. Amphiboles

4.1.2.1. Calculations of amphibole end-members

Amphiboles are a highly complex group of minerals, because of the wide variety of cation sites available. Their compositional space is defined by A, B, C and T site occupancies. These sites are subdivided into 13 tetrahedral domains which comprise the amphibole end-members (Currie, 1991) (Table 4.2).

tremolite *(A) (B) (C) (T)* ( ) (Ca_2) (Mg_5) (Si_8)	ferro-actinolite ferro-anthophyllite tirodite dannemorite
winchite ( ) (CaNa) (Mg_4Al) (Si_8)	ferro-alumino ferro-ferri magnesio-ferri
riebeckite ( ) (Na_2) ($Fe^{3+}{}_2Fe^{3+}$) (Si_8)	magnesio-riebeckite ferro-glaucophane glaucophane holmquistite
hornblende ( ) (Ca_2) (Mg_4Al) (Si_7Al)	ferro-alumino ferro-ferri magnesio-ferri
barroisite ( ) (CaNa) (Mg_3Al_2) (Si_7Al)	magnesio-alumino ferro-alumino ferro-ferri magnesio-ferri
tschermakite ( ) (Ca_2) (Mg_3Al_2) (Si_6Al_2)	magnesio-alumino ferro-alumino ferro-ferri magnesio-ferri
richterite (Na) (CaNa) (Mg_5) (Si_8)	ferro-richterite

arfvedsonite *(A) (B) (C) (T)* (Na) (Na_2) ($Fe^{3+}Fe^{2+}{}_4$) (Si_8)	magnesio-arfvedsonite eckermannite ferro-eckermannite kozulite
edenite (Na) (Ca_2) (Mg_5) (Si_8)	magnesio-edenite ferro-edenite
kataphorite (Na) (CaNa) (Mg_4Al) (Si_7Al)	magnesio-alumino ferro-alumino ferro-ferri magnesio-ferri
nyboite (Na) (Na_2) (Mg_3Al_2) (Si_7Al)	magnesio-alumino ferro-alumino ferro-ferri magnesio-ferri
pargasite (Na) (Ca_2) (Mg_4Al) (Si_6Al_2)	ferro-pargasite hastingsite magnesio-hastingsite
taramite (Na) (Na_2) (Mg_3Al_2) (Si_6Al_2)	magnesio-alumino ferro-alumino ferro-ferri magnesio-ferri

Table 4.2. Table displaying amphibole end-members used in the calculation scheme of Currie (1991).

The nomenclature of amphiboles has been established by the Subcommittee on Amphiboles of International Mineralogical Association (IMA) (Leake, 1978; Rock and Leake, 1984; Leake et al., 1997). On this basis, the amphibole formula may be written as:

$$A_{0\text{-}1}B_2C_5T_8O_{22}(OH,F,Cl)_2$$

A (8 to 10-fold site): Na, K to total between 0.00 and 1.00,

B (6 to 8-fold site) : Na, Li, Ca, Mn, Fe^{2+}, Mg to total 2.00,

C (octahedral site) : Mg, Fe^{2+}, Mn, Al, Fe^{3+}, Ti to total 5.00,

T (tetrahedral site) : Si, Al to total 8.00.

Mole fractions of amphibole end-members can be calculated by using analyses of amphiboles as source data and by site assignments (A, B, C and T). However this requires complex calculations because of the wide variety of cation sites and valencies of elements. Another problem is to reduce the results of electron microprobe analysis lacking H_2O and Fe^{3+} determinations. To recalculate chemical analysis of amphiboles on the basis of their structural formulae and also classify them according to the IMA guidelines, Richard and Clarke (1990) and Currie (1991) developed computer programs. A CLASAMPH program written by Currie (1991) starts from an amphibole composition and attains site assignments of end-members followed by calculation of mole fractions based on these assignments. He argues that the calculation is relatively insensitive to a lack of water and ferrous iron determinations.

4.1.2.2. Chemical variations

Amphibole is, in general, the most abundant mafic mineral in the Central Anatolian plutonics. A total of 132 electron microprobe analyses from five plutons (Behrekdag, Cefalikdag, Celebi, Baranadag and Hamit) were made from a sum of 20 representative samples. Their end-member calculations on the basis of Currie's software are presented in Appendix D. Amphibole end-member calculations from the Hamit pluton were carried out only on those from the quartz syenite, as the calculations assume that there are no vacancies in the A site of amphiboles from the nepheline monzosyenite, pseudoleucite monzosyenite and alkali feldspar syenite.

Average amphibole end-member compositions for the Behrekdag, Cefalikdag, Celebi, Baranadag and Hamit plutons are plotted in Figure 4.8. As can be seen from Figure 4.8, amphiboles from the Central Anatolian plutonics are mainly edenite, tschermakite and hornblende in composition. Amphiboles generally exhibit considerable variation within the Central Anatolian plutonics. For example, amphibole crystals from the Behrekdag, Cefalikdag and Celebi plutons are mainly made up of edenite, tschermakite, predominantly hornblende and barroisite and, rarely, taramite and kaersutite. These plutons do not contain any A1B4Si6 at all. Amphiboles from the Baranadag and Hamit plutons predominantly contain A1B4Si6. Amphiboles from the Baranadag pluton consist of mostly edenite and tschermakite, predominantly taramite, kaersutite and A1B4Si6 and, rarely, barroisite. Unlike other

plutons, the Baranadag and Hamit plutons do not contain hornblende. The quartz syenite from the Hamit pluton, like the monzonite from the Baranadag pluton, also does not contain barroisite and mostly contains edenite and tschermakite.

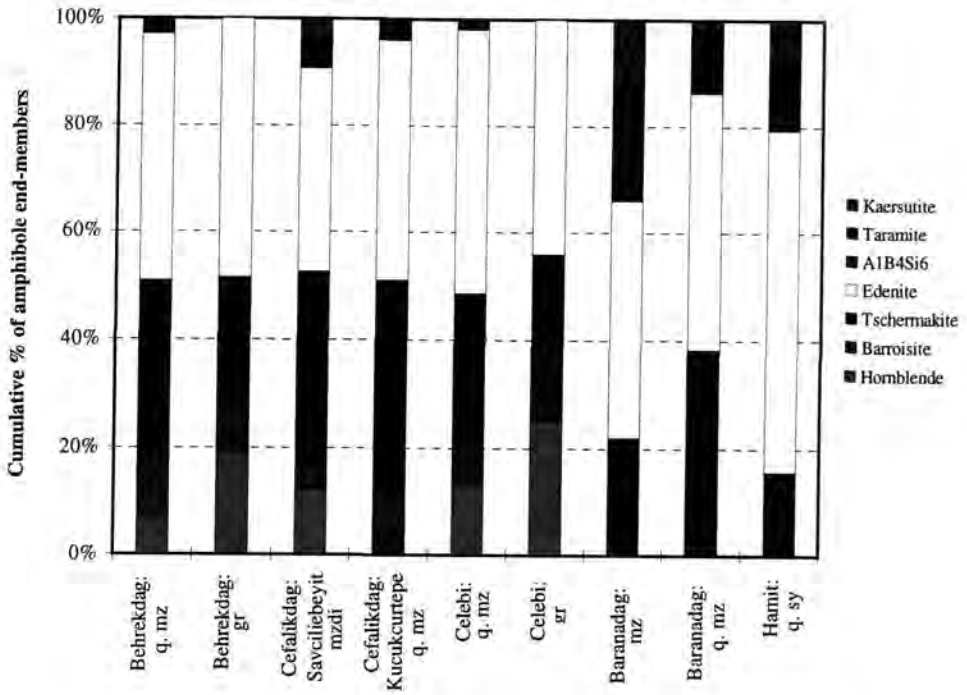

Figure 4.8. Average end-member compositions of amphibole crystals from the Central Anatolian plutonics. Abbreviations: q-quartz, mzdi-monzodiorite, mz-monzonite, gr-granite and sy-syenite.

The microprobe data have been also plotted on the classification diagram of Leake et al. (1997) (Figure 4.9). All samples from the Central Anatolian plutonics are classified as calcic amphiboles, mainly edenite, magnesio-hornblende and, predominantly, magnesio-hastingsite and hastingsite. Amphiboles from the Behrekdag, Cefalikdag and Celebi plutonic rocks are plotted into two diagrams on the basis of $(Na+K)_A \geq 0.50$ and $(Na+K)_A \leq 0.50$ (Figures 4.9a,b) following the IMA classification scheme (Leake et al., 1997). Amphiboles from these plutons are mainly edenite and magnesio-hornblende in composition.

Amphiboles from the Baranadag pluton fall in both the edenite and magnesio-hastingsite fields. The data from the Hamit pluton appear to have high and low Mg/(Mg+Fe) values, and thus the compositions of amphiboles from the Hamit pluton

fall in discrete areas which principally include hastingsite and edenite. Amphiboles from the quartz syenite have high Mg/(Mg+Fe) values, whereas those from the nepheline monzosyenite, pseudoleucite monzosyenite and alkali feldspar syenite in the Hamit pluton have low Mg/(Mg+Fe) contents.

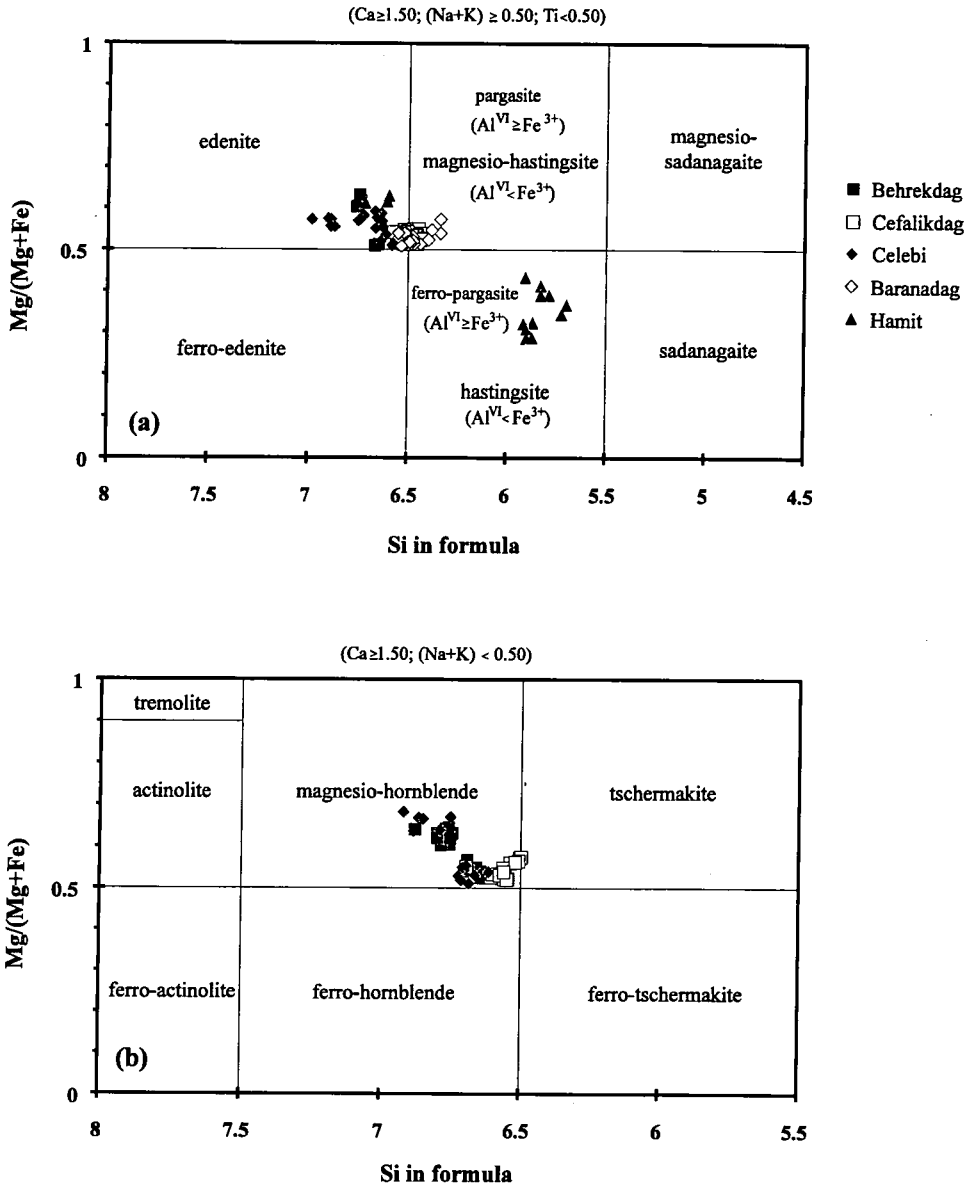

Figure 4.9. (a) Amphibole crystals from the Behrekdag, Cefalikdag, Celebi, Baranadag and Hamit plutons plotted on the classification diagram of Leake et al. (1997) on the basis of (Na+K) ≥ 0.50. (b) Amphiboles from the Behrekdag, Cefalikdag and Celebi plutons according to (Na+K) ≤ 0.50.

The compositional differences of amphiboles from the Central Anatolian plutonics can be also seen on a plot of Na (formula unit) versus the SiO_2 wt.% of their host rocks (Figure 4.10a). Amphiboles from the Behrekdag, Cefalikdag and Celebi plutons have the lowest Na values, whereas those from the Hamit pluton have high Na contents. Amphiboles from the Baranadag pluton have intermediate Na values between these rocks. Similar relationships can be also seen from the plot of K (formula unit) against the SiO_2 wt.% of their host rocks (Figure 4.10b).

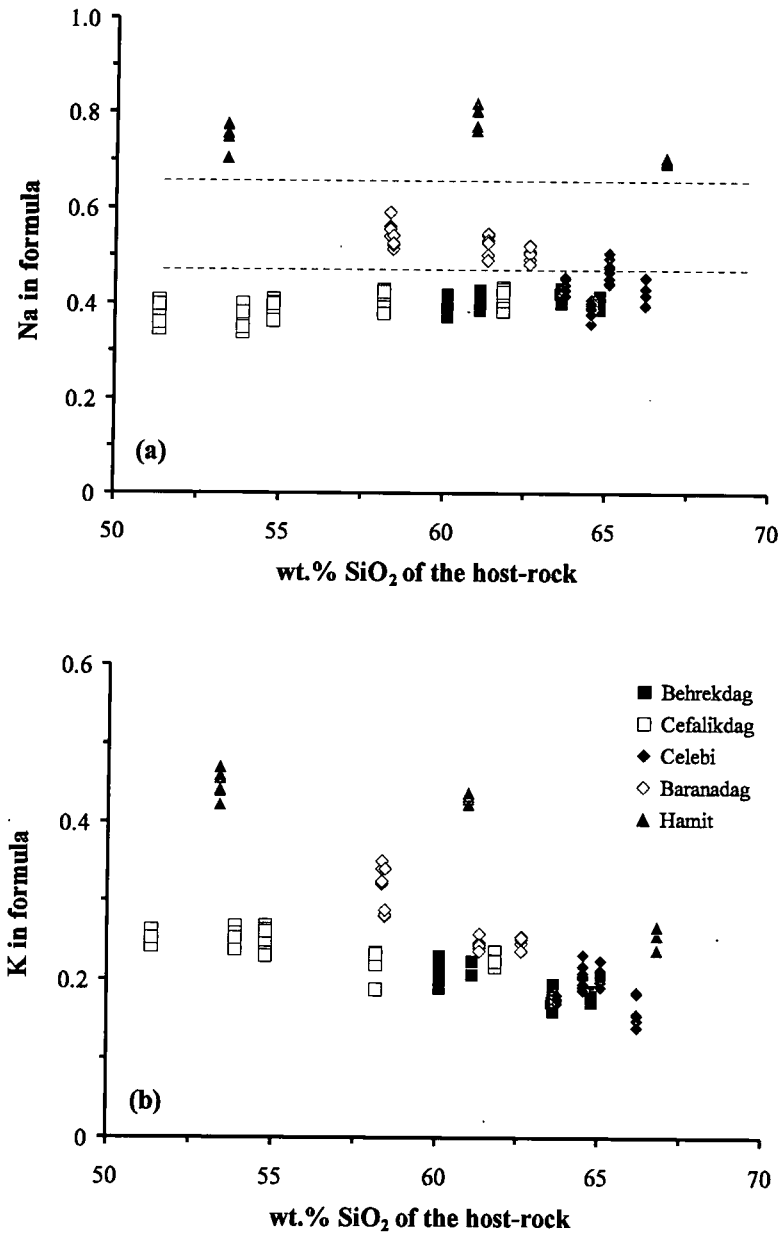

Figure 4.10. Na (a) and K (b) formula units of amphiboles from the Central Anatolian plutonics plotted against the SiO_2 wt.% content of their host rocks.

4.1.3. Clinopyroxenes

4.1.3.1. Calculations of clinopyroxene end-members and classification

Although clinopyroxene is the most common mafic mineral in the foid-bearing Hamit rock units (nepheline monzosyenite, pseudoleucite monzosyenite), it is generally found only as relics in amphibole cores in the Behrekdag, Cefalikdag, Celebi and Baranadag plutonic rocks.

Several methods have been proposed for the calculation of pyroxene end-members. Most of them are sequential schemes that usually differ in the order of the calculation sequence and this may lead to an overestimation of the component calculated first. To solve this problem, Dietrich and Petrakakis (1986) developed an algebraic method which allows the calculation of 11 linearly-independent pyroxene components. However, on the basis of crystal-chemistry experiments, Lindsley (1986) showed that some of those end-members have little chemical justification.

These pyroxene end-member calculations had a drawback since electron microprobe analysis cannot detect the two oxidation states of iron separately. Cawthorn and Collerson (1974) proposed an alternative scheme which minimises the significance of Fe_2O_3 contents and allows for a more rigorous determination of end-member concentrations. Several methods have also been developed to calculate the structural formulae of the pyroxenes (e.g. Dollase and Newman, 1984; Guiraud, 1986).

The Subcommittee on Pyroxenes (Commission on New Minerals and Mineral Names of the International Mineralogical Association-IMA) has recently approved the new classification and nomenclature for pyroxene minerals (Morimoto, 1989). The IMA proposes that, if Fe_2O_3 is not available, the formula should be calculated to four cations to estimate Fe^{3+} by charge balance. Cations are then allocated to their structural sites. According to the IMA suggestions, Si^{4+} and particular amounts of Al^{3+} and Fe^{3+} are situated in tetrahedral sites. The remaining cations are considered to belong to the M1 or M2 sites. Each pyroxene is then assigned to one of four chemical groups defined by Morimoto and Kitamura (1983): (i) Ca-Mg-Fe pyroxenes (Quad); (ii) Na-Ca pyroxenes (Na-Ca); (iii) Na pyroxenes (Na); and (iv) other pyroxenes (Other). The Quad pyroxenes are classified in the enstatite-ferrosilite-diopside-hedenbergite (En-Fs-Di-Hd) quadrilateral, whereas the Na-Ca and Na pyroxenes are plotted in the Quad-Jd-Ae triangle. Despite the use of this new

classification system, the calculation of pyroxene end-members remains necessary for many studies. Some authors (e.g. McHone, 1987 and Gómez, 1990) have developed computer programs for this purpose. The PX program (Gómez, 1990) classifies pyroxenes on the basis of the IMA scheme and also calculates the two normalisation schemes of Kushiro (1962) and Cawthorn and Collerson (1974). In addition, the program calculates the wollastonite, enstatite and ferrosilite parameters following the scheme of Lindsley and Anderson (1983).

4.1.3.2. Chemical variations

A total of 54 point analyses was carried out on a sum of 12 samples selected from the Behrekdag, Cefalikdag, Celebi, Baranadag and Hamit plutons. Mineral formulae were calculated using the PX program of Gómez (1990) (Appendix D). They were then plotted on the Quad (enstatite-ferrosilite-diopside-hedenbergite) diagrams. Classification of clinopyroxenes from the Central Anatolian plutonics is presented in Figure 4.11 and a more detailed classification is also shown in Figure 4.12.

As can be seen from Figure 4.11 and 4.12, clinopyroxenes from the Behrekdag, Cefalikdag, Celebi and Baranadag plutons have a limited compositional range and plot in the salite field apart from one Celebi quartz monzonite sample that falls into the augite field. Clinopyroxenes from the Baranadag pluton are slightly more calcic than those from the Behrekdag, Cefalikdag and Celebi plutons.

Clinopyroxenes from the Hamit pluton show a rather wider compositional range and predominantly plot in the salite field (Figure 4.11, 4.12). The Hamit rocks mainly contain more calcic clinopyroxenes than the Behrekdag, Cefalikdag, Celebi and Baranadag intrusive units. In addition, of the nonquadrilateral cations, clinopyroxenes from the Hamit pluton tend to be richer in Al, Ti and Na than the clinopyroxenes from other plutons.

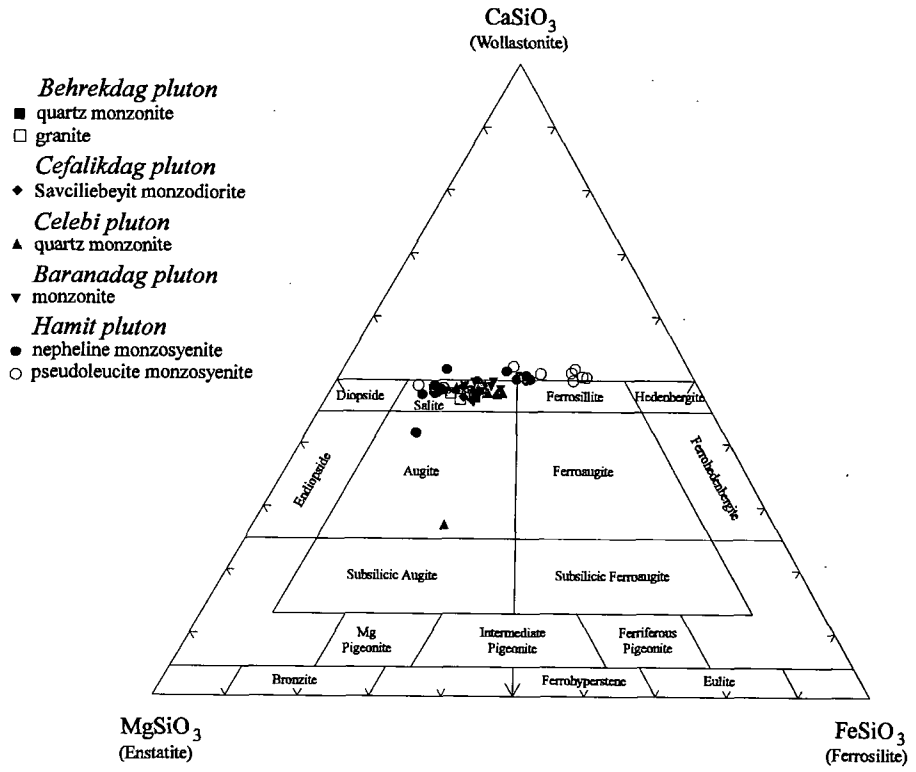

Figure 4.11. Distribution of the composition of clinopyroxenes from the Central Anatolian plutonics.

Recent reviews of the mineralogy of orogenic volcanic rocks have suggested that the clinopyroxenes in potash-rich rocks may differ from those in lower-K calc-alkali rocks. Ewart (1982) noted that, whereas augite is characteristic of most calc-alkalic rocks, there is a 'tendency to extend into diopside and salite compositions in the higher K magmas'. Gill (1981) found a general 'increase in Wo (wollastonite) content of augite as K-enrichment of the whole rock increases', and showed that some clinopyroxenes in potash-rich andesites have high Al_2O_3 contents.

4.1.4. Biotites

Biotite is as common a ferro-magnesian mineral as amphibole in the Savciliebeyit monzodiorite and Kucukcurtepe quartz monzonite (Cefalikdag pluton). On the other hand, it is less abundant in the Behrekdag, Celebi and Baranadag intrusive rocks and it is a scarce mineral phase in the Hamit rocks.

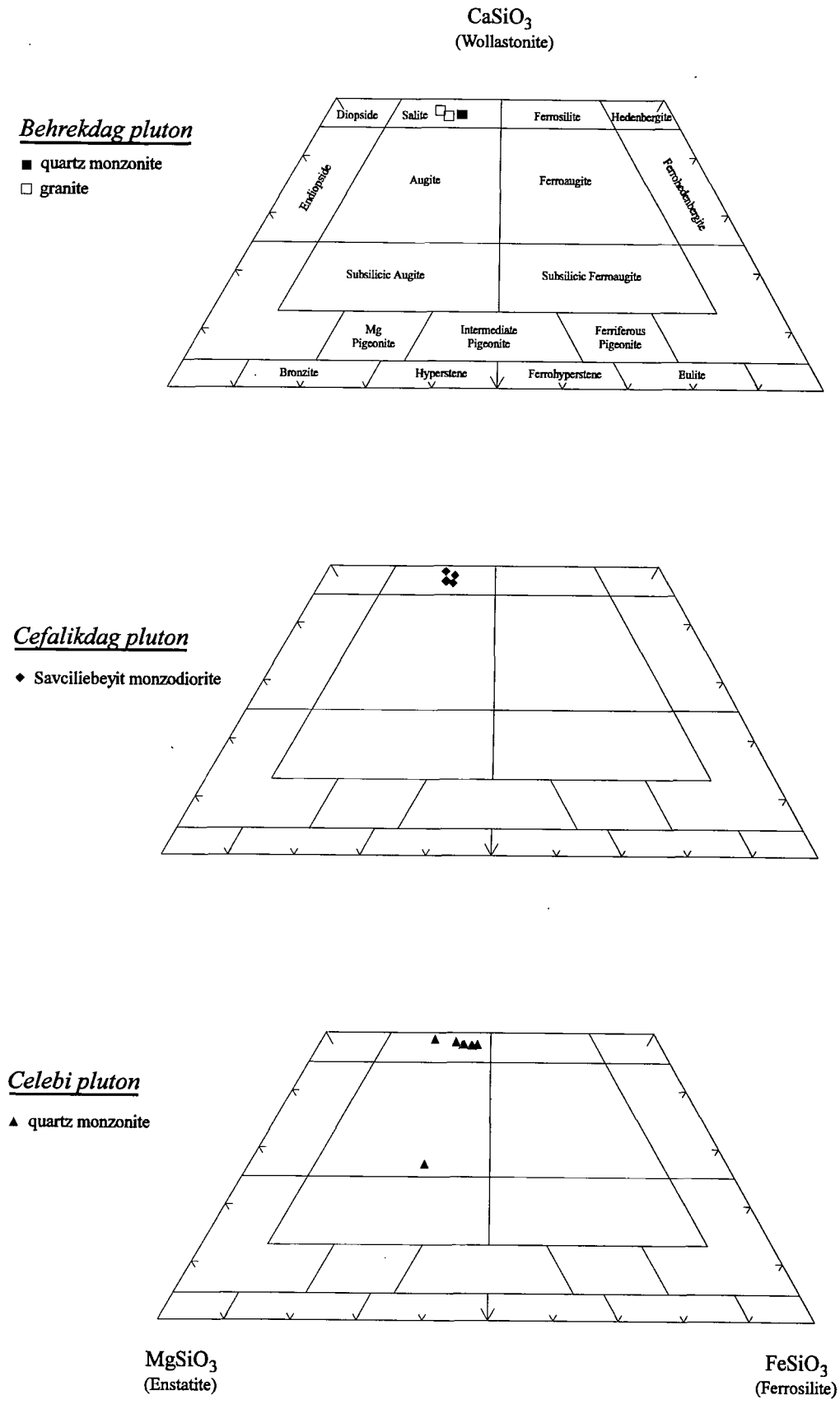

Figure 4.12. Clinopyroxene compositions from the Behrekdag, Cefalikdag and Celebi plutons.

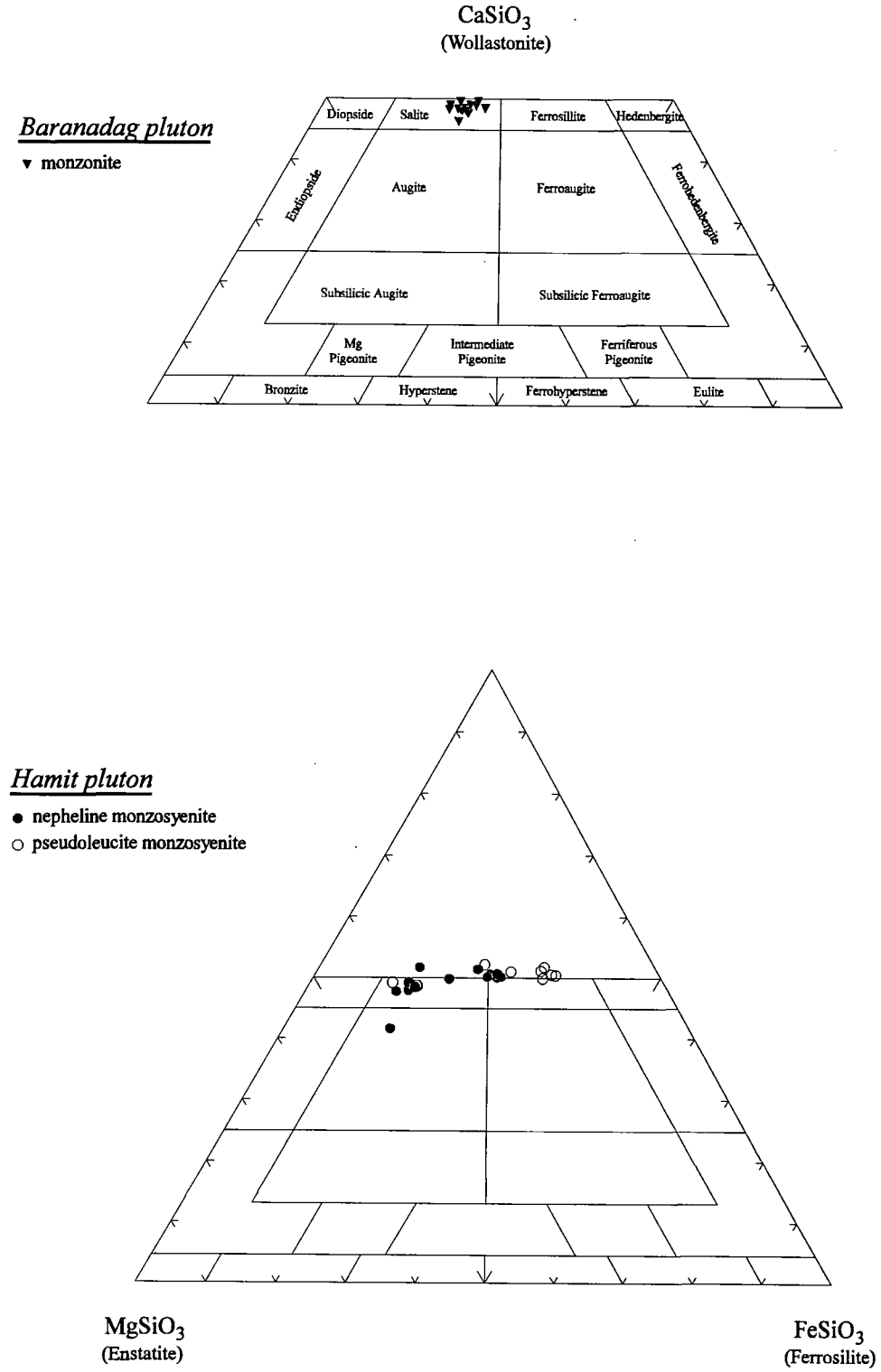

Figure 4.12 (continued). Diagram shows clinopyroxene compositions from the Baranadag and Hamit plutons.

A total of 28 point analyses were carried out on a sum of 9 samples from the Behrekdag, Cefalikdag, Celebi, Baranadag and Hamit plutons (Appendix D). Except for biotites from the Hamit pluton, biotites from the Central Anatolian plutonics are rich in TiO_2, with contents of 2.75-5.01 wt.% in the Cefalikdag pluton, 4.99 wt.% in the Behrekdag pluton, 4.00 wt.% in the Celebi pluton and 3.16-4.11 wt.% in the Baranadag pluton. In addition, biotites from the Cefalikdag pluton are slightly more aluminous than those from the Behrekdag, Celebi, Baranadag and Hamit plutons. Unlike biotites from the Hamit pluton, the range of Fe/(Fe+Mg) is quite small, with an average of approximately 0.54 for the Behrekdag, Cefalikdag, Celebi and Baranadag intrusives. Minor constituents show no correlation with Fe/(Fe+Mg).

4.1.5. Fe-Ti oxides

A total of 27 analyses were performed on 11 samples from the Behrekdag, Cefalikdag, Celebi, Baranadag and Hamit plutons (Appendix D). Only magnetite and ilmenite from these plutons have been studied in detail as the other opaque minerals (chalcopyrite and pyrite) are restricted in occurrence. Unlike magnetite, ilmenite is quite scarce in the Hamit rocks. Magnetites from the Central Anatolian plutonics have 0-0.8 wt.% TiO_2 and 0.05-1.06 wt.% Al_2O_3. Ilmenites from the plutonics contain 2.4-9.7 wt.% MnO ($pyrophanite_{ss}$) and up to ~0.2 wt.% MgO.

Takasashi et al. (1980) have compared Ishahara's (1977) classification of granites as magnetite- and ilmenite-bearing with the I- and S-type granite classification of Chappell and White (1974). I-type granites generally contain magnetite and less commonly ilmenite without magnetite. The absence of magnetite is often associated with S-type granites, because of the C (graphite) content of the sedimentary source.

4.2. Calculations of pressures, temperatures and oxygen fugacities of the Central Anatolian plutonics

The mineral compositions of the granitic plutons enable the use of a large number of thermometers and barometers that characterise emplacement conditions. However, only a portion of mineral compositions in igneous rocks represents true solidus conditions since some mineral phases continue to react during subsolidus cooling (e.g. feldspar, Fe-Ti oxides).

Water fugacity (f_{H2O}) and oxygen fugacity (f_{O2}) are two of the intensive properties that also control the crystallisation paths of a magma. Determination of these variables at magmatic conditions is also difficult because of phase and compositional changes caused by subsolidus re-equilibration (e.g. Czamanske and Wones, 1973; Wones, 1981). Nevertheless, there are several ways to estimate the pressure, temperature and oxygen fugacity during crystallisation of the Central Anatolian plutonics. These are:

4.2.1. Amphibole-plagioclase geothermometer and barometer:

4.2.1.1. Al-in-hornblende barometer (Schmidt, 1992)

4.2.1.2. Amphibole-plagioclase geothermometer (Blundy and Holland, 1990)

4.2.2. Feldspar geothermometer:

4.2.2.1. Two-feldspar geothermometry (Wen and Nekvasil, 1994)

4.2.3. Oxygen and water fugacities:

4.2.3.1. Oxygen fugacity (Wones, 1989)

4.2.1. Amphibole-plagioclase geothermometer and barometer

4.2.1.1. Al-in-hornblende barometer

Hammerstrom and Zen (1986) first experimentally determined that the Al content of hornblende in calc-alkaline granitoids varies linearly with pressure of crystallisation, thereby providing a means of determining depth of pluton emplacement (Equation 4.1):

$$P(\pm 3\ \text{kbar}) = -3.92 + 5.03\ Al^{tot}_{hbl} \qquad r^2 = 0.80 \qquad \text{(Eq. 4.1)}$$

Hollister et al. (1987) discussed the thermodynamic basis for this barometer and refined the empirical calibration of Hammerstrom and Zen (1986) with additional hornblende compositional data from intrusives that crystallised at intermediate pressures (Equation 4.2):

$$P(\pm 1\ \text{kbar}) = -4.76 + 5.64\ Al^{tot}_{hbl} \qquad r^2 = 0.97 \qquad \text{(Eq. 4.2)}$$

Both empirical calibrations (Equation 4.1, 4.2) are based on pressures generally derived from contact-aureole geobarometry. Hammerstrom and Zen (1986) and

Hollister et al. (1987) emphasised that the barometer is restricted to calc-alkaline rocks containing the specific assemblage "quartz + plagioclase + potassium feldspar + hornblende + biotite + titanite + Fe-Ti oxide phase(s) (magnetite or ilmenite)".

Johnson and Rutherford (1989) equilibrated the specified assemblage (using natural samples of both volcanic and plutonic rocks) in reversed, f_{O2}-buffered, vapour-present experiments over the range from 2 to 8 kbar at 740-780 °C (Equation 4.3):

$$P(\pm 0.5 \text{ kbar}) = -3.46 + 4.23\ Al^{tot}_{hbl} \qquad r^2 = 0.99 \qquad \text{(Eq. 4.3)}$$

Schmidt (1992) calibrated the Al-in-hornblende barometer experimentally under water-saturated conditions at pressures of 2.5-13 kbar and temperatures of 700-655 °C (Equation 4.4):

$$P(\pm 0.6 \text{ kbar}) = -3.01 + 4.76\ Al^{tot}_{hbl} \qquad r^2 = 0.99 \qquad \text{(Eq. 4.4)}$$

The Al-in-hornblende geobarometer has been criticised by Anderson and Smith (1995) and Anderson (1996). They pointed out that many granitic intrusions are emplaced under conditions inconsistent with those of existing experimental calibrations, including f_{O2}<NNO (nickel-nickel oxide) and/or variable to high temperature. They also noted that the barometer fails by yielding elevated pressures for low-f_{O2} plutons with iron-rich hornblendes. Thus they recommend that the barometer is used for hornblende with Fe/(Fe+Mg)<0.65.

132 point analyses of amphiboles from the Central Anatolian plutonics were performed on a subset of 20 representative samples. Pressure calculations were carried out only for the quartz syenite in the Hamit pluton. The foid-bearing syenite (nepheline monzosyenite and pseudoleucite monzosyenite) and alkali feldspar syenite from the Hamit pluton are excluded because amphiboles from these rock units have the ratios of Fe/(Fe+Mg)>0.65. Thus crystallisation pressures were determined only on 122 analyses from 18 samples from the Behrekdag, Cefalikdag, Celebi, Baranadag and Hamit plutons using the Schmidt's calibration. The results are presented in Table 4.3 and Appendix D.

PLUTON	PRESSURE (kbar) (±0.6)
Behrekdag pluton	
quartz monzonite	3.6 - 4.3
granite	2.6 - 3.4
Cefalikdag pluton	
Savciliebeyit monzodiorite/quartz monzodiorite	3.5 - 5.2
Kucukcurtepe quartz monzonite	4.2 - 4.6
Celebi pluton	
quartz monzonite	2.9 - 4.0
granite	2.6 - 3.8
Baranadag pluton	
monzonite	4.5 - 5.3
quartz monzonite	4.1 - 4.6
Hamit pluton	
quartz syenite	3.4 - 3.9

Table 4.3. Table displaying crystallisation pressures of the plutonics in the Central Anatolian Massif.

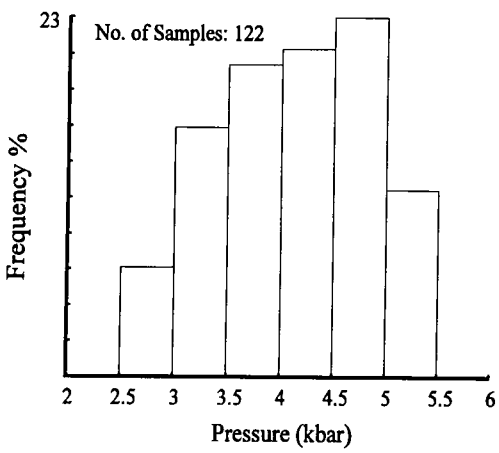

Figure 4.13. Histogram showing the frequency distribution of crystallisation pressures in the Central Anatolian plutonics.

As can be seen from Table 4.3, the Savciliebeyit monzodiorite from the Cefalikdag pluton and also the monzonite from the Baranadag pluton yield considerably higher pressures (3.5-5.3 kbar) than the other rock units in the Massif. The granite from both the Behrekdag and Celebi plutons have the lowest crystallisation pressures. Figure 4.13 shows the distribution of the crystallisation pressures in the Central Anatolian plutonics. As shown by the histogram, most of the plutonics have crystallisation pressures between 3 to 5 kbar. Only about 10% of the plutonic rocks have pressures between 2.5 and 3 kbar and about 15% of those have pressures ranging from 5 to 5.5 kbar.

4.2.1.2. Amphibole-plagioclase geothermometer

Experimental studies performed using synthetic amphibole from a wide range of starting materials and pressures and temperatures demonstrated that amphibole

also has potential for indicating crystallisation temperatures. Spear (1980, 1981) described early calibrations of the hornblende-plagioclase thermometer based on pairs (hornblende-plagioclase) in metamorphic rocks for which temperature was already known. Nabelek and Lindsley (1985) proposed an experimentally-based thermometer using variations in Al^{IV} of hornblende. Blundy and Holland (1990) developed a new amphibole-plagioclase geothermometer using a combined set of experimental and empirical data and have formulated a calibration for the equilibria:

edenite + 4 quartz = tremolite + albite

pargasite + 4 quartz = hornblende + albite

and their calibration is:

$$T = \frac{0.677P - 48.98 + Y}{-0.0429 - 0.008314 \ln K} \qquad \text{(Eq. 4.5)}$$

where;

$$K = \left(\frac{Si - 4}{8 - Si}\right) X_{Ab}^{Plag}$$

Si: number of atoms per formula unit in amphibole

P: pressure (kbar)

T: temperature (Kelvin)

Y: plagioclase non-ideality

$Y = 0$ *for* $X_{ab} > 0.5$ *and* $Y = -8.6 + 25.5(1-X_{ab})^2$ *for* $X_{ab} < 0.5$

They determined that the amphibole-plagioclase thermometer is robust to ferric iron recalculation from electron microprobe data and should yield temperatures of equilibration for hornblende-plagioclase assemblages with uncertainties of around ±75 °C for rocks equilibrated at temperatures in the range 500-1100 °C. They also demonstrated that the thermometer should only be used in this temperature range and for assemblages with plagioclase less calcic than An_{92} and with amphiboles containing less than 7.8 Si atoms per formula unit.

The Blundy and Holland's (1990) calibration was criticised by Hammerstrom and Zen (1992), Rutherford and Johnson (1992) and Poli and Schmidt (1992) generally on thermodynamic grounds.

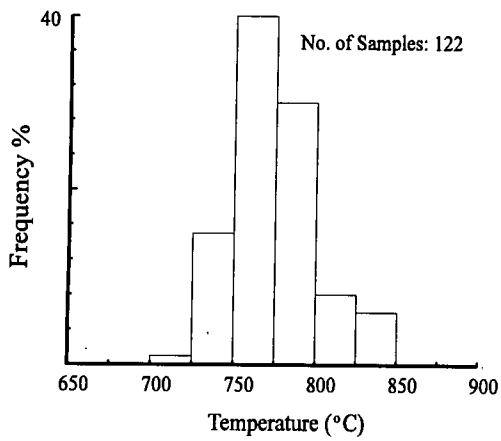

Figure 4.14. Histogram displaying the frequency distribution of crystallisation temperatures in the plutonics.

Temperatures obtained for the Central Anatolian plutonics using the Blundy and Holland (1990) calibration of the hornblende-plagioclase geothermometer range from 716 to 858 °C.

Figure 4.14 shows the distribution of crystallisation temperatures in the plutonics. As can be seen from the histogram, most of the plutonics have crystallisation temperatures ranging from 750 to 800 °C. About 1-2% of the plutonics have temperatures between 700 and 725 °C.

Figure 4.15 displays the relationship between the distribution of temperatures and the SiO_2 wt.% contents of their host rocks. Notably, temperatures from these plutons decrease with increasing silica contents of their host rocks.

Figure 4.16 shows the relationship between pressures and temperatures for the plutonics. As can be seen from Figure 4.16, there is a positive linear correlation between temperatures and pressures calculated for the Behrekdag, Cefalikdag, Celebi, Baranadag and Hamit plutons. The monzodiorite from the Cefalikdag pluton have the highest temperatures, whereas the granite from the Behrekdag and the quartz monzonite and granite from the Celebi plutons have the lowest temperatures.

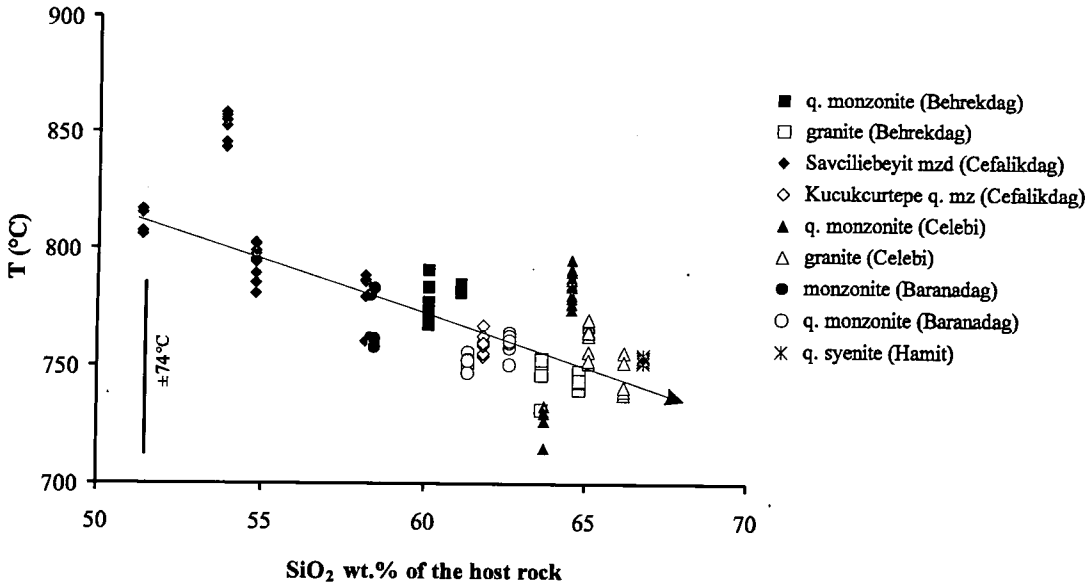

Figure 4.15. Distribution of amphibole-plagioclase geothermometer calculations from the Behrekdag, Cefalikdag, Celebi, Baranadag and Hamit plutons plotted against SiO_2 contents of their host rocks. Abbreviations: q-quartz, mz-monzonite and mzd-monzodiorite.

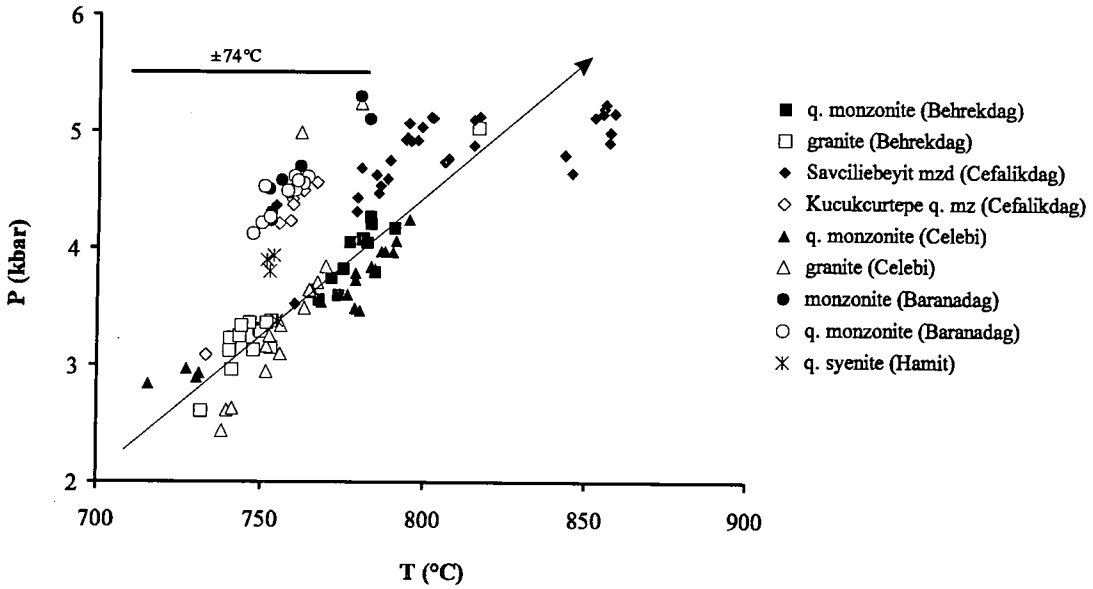

Figure 4.16. Diagram displaying a positive correlation between pressures and temperatures from the Behrekdag, Cefalikdag, Celebi, Baranadag and Hamit plutons calculated by using the Schmidt's (1992) and Blundy and Holland's (1990) formulations. Abbreviations: q-quartz, mz-monzonite and mzd-monzodiorite.

4.2.2. Feldspar geothermometer

4.2.2.1. Two-feldspar geothermometry

Feldspars have been given much attention over the past decades mainly for the purpose of geothermometry. Barth (1951) first suggested that the distribution of the albite component between coexisting plagioclase and alkali feldspar could be used to estimate the temperature of equilibration. Several more recent feldspar thermometers (e.g. Stormer, 1975; Powell and Powell, 1977; Whitney and Stormer, 1977; and Haselton et al., 1983) have been calibrated using the equilibrium of a single component between coexisting feldspars. Brown and Parsons (1977) suggested that thermodynamic models of feldspar equilibria should account for the equilibria between all three components (albite-orthoclase-anorthite) in coexisting feldspars. More recent publications, including Ghiorso (1984), Green and Usdansky (1986), Nekvasil and Burnham (1987), Fuhrman and Lindsley (1988) and Elkins and Grove (1990) offer three calibrations for each feldspar pair based on the exchange of albite, anorthite and orthoclase components, respectively. However, each of these models has both advantages and weakness. Anderson (1996) argues that the results using anorthite and orthoclase components are subject to analytical error given that the proportions of the anorthite component in K-feldspar and of the orthoclase component in plagioclase are usually very low.

Wen and Nekvasil (1994) developed a computer program, SOLVCALC. The program calculates isothermal sections of the ternary feldspar solvus using Ghiorso (1984), Green and Usdansky (1986), Nekvasil and Burnham (1987), Fuhrman and Lindsley (1988) and Elkins and Grove (1990) geothermometers.

16 representative samples from the Behrekdag, Cefalikdag, Celebi, Baranadag and Hamit (only quartz syenite samples) plutons were selected to calculate crystallisation temperatures. Pressures from these plutons were determined using the Schmidt's (1992) Al-in-hornblende equation. The results of two-feldspar geothermometers are given in Table 4.4 and also Figure 4.17.

Temperatures estimated from the Central Anatolian plutonics using the two-feldspar geothermometer range from 485 to 742 °C. As can be seen from Table 4.4 and Figure 4.17, the quartz syenite from the Hamit pluton has the lowest temperatures among the Central Anatolian plutonics. It seems likely that feldspars from the quartz syenite have undergone subsolidus re-equilibration.

		Two-feldspar geothermometry (°C)					
Pluton	Sample no	Ghiorso, 1984	Green & Usdansky, 1986	Nekvasil & Burnham, 1987	Fuhrman & Lindsley, 1988	Lindsley & Nekvasil, 1988	Elkins & Grove, 1990
Behrekdag	**N2**	730	710	679	703	655	706
	N7	684	649	651	663	665	629
Cefalikdag	**N85**	708	723	670	683	650	699
	N20	680	681	653	660	621	656
Celebi	**N71**	728	690	670	713	678	718
	N75	742	715	685	722	686	729
Baranadag	**N26**	684	678	645	666	624	656
	N18	669	671	661	666	636	661
Hamit	**N290**	526	478	570	510	487	485

Table 4.4. The results of two-feldspar geothermometer for the Central Anatolian plutonics calculated using the SOLVCALC program (Wen and Nekvasil, 1994).

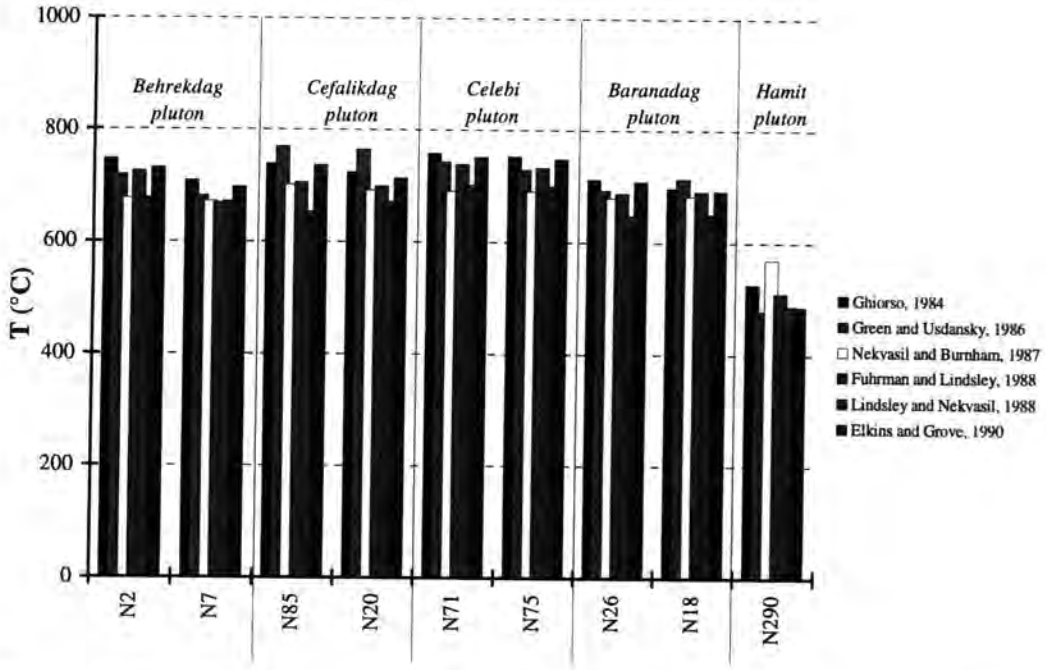

Figure 4.17. Comparison of two-feldspar geothermometers for the Central Anatolian plutonics.

4.2.2.2. Comparison of geothermometers calculated using different methods

The Central Anatolian plutonics, unfortunately, have an insufficient range of mineral assemblages to allow the comparison of large number of geothermometers. Figure 4.18 demonstrates the comparison of geothermometer results for individual samples chosen from the studied plutons (Behrekdag, Cefalikdag, Celebi, Baranadag

and Hamit) in the Central Anatolian Massif. Temperatures from these plutons were calculated using Blundy and Holland's (1990) amphibole-plagioclase geothermometer and Wen and Nekvasil's (1994) two-feldspar geothermometers. As can be seen from Figure 4.18, Wen and Nekvasil's two-feldspar geothermometers agree to ±10°C with the Blundy and Holland's amphibole-plagioclase geothermometer for the Behrekdag, Cefalikdag, Celebi and Baranadag plutonic rocks. In contrast, the amphibole-plagioclase geothermometer of Blundy and Holland (1990) gives temperatures which are higher than those obtained by the two-feldspar geothermometer of Wen and Nekvasil (1994) for the quartz syenite from the Hamit pluton.

4.2.3. Oxygen and water fugacities

4.2.3.1. Oxygen fugacity

Determination of oxygen fugacity (f_{O2}), at the P and T of crystallisation of granitic rocks is often constrained by subsolidus re-equilibration and/or alteration. During late-stage re-equilibration in granitic plutons, magnetite typically loses Ti and ilmenite undergoes one or more stages of oxidation-exsolution. Therefore, the application of ilmenite-magnetite geothermometry cannot be used to ascertain oxygen fugacities during crystallisation of the magmas (Buddington and Lindsley, 1964; Haggerty, 1976).

The assemblage titanite+magnetite+quartz in volcanic or granitic rocks permits an estimate of relative oxygen fugacity. Verhoogen (1962) demonstrated that the equilibrium;

$$\text{titanite} + \text{magnetite} + \text{quartz} = \text{wollastonite} + \text{ilmenite} + O_2 \qquad \text{(Eq. 4.6)}$$

separates an oxidised titanite + magnetite assemblage from a reduced wollastonite + ilmenite assemblage.

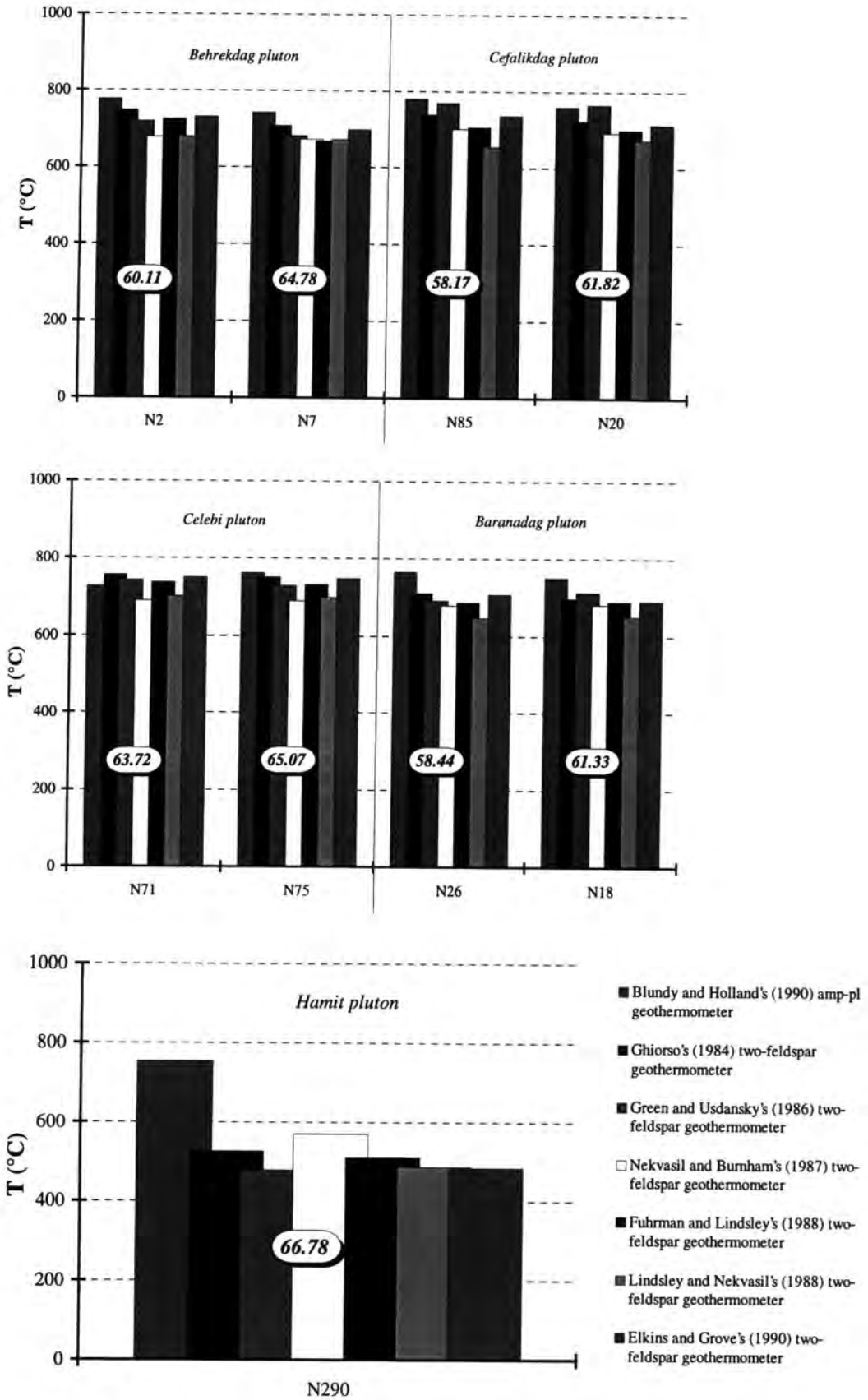

Figure 4.18. Comparison of geothermometers applied to the Central Anatolian plutonics. SiO_2 wt.% contents of their host rocks are given on the labels on each bar. Abbreviations: amp-amphibole and pl-plagioclase.

By adding SiO_2, the equilibrium can be written as:

titanite + magnetite + quartz = hedenbergite + ilmenite + O_2 (Eq. 4.7)

in which hedenbergite and ilmenite represent the reduced assemblages (Wones, 1989). Wones (1989) also suggested that an equilibrium comparable to Equation 4.7, but involving amphibole, can be written:

titanite + magnetite + quartz + H_2O = ferrotremolite + ilmenite + O_2 (Eq. 4.8)

According to Wones (1989), Equation 4.8 can be used to distinguish relatively oxidised granitoids containing titanite + magnetite + quartz from those that are more reduced and contain amphibole + ilmenite. The temperature dependency of oxygen fugacity (Equations 4.9 and 4.10) can be approximated by:

$$\log f_{O2} = -\frac{A}{T} + B + \frac{C\,(P-1)}{T} \qquad \text{(Eq. 4.9)}$$

using calculated values for A, B and C (Wones, 1989) we get:

$$\log f_{O2} = -\frac{30930}{T} + 14.98 + \frac{0.142*(P-1)}{T} \qquad \text{(Eq. 4.10)}$$

P: pressure (bar)
T: temperature (Kelvin)

To calculate f_{O2}, Wones (1989) equation (Equation 4.10) has been applied to 18 representative samples from the Behrekdag, Cefalikdag, Celebi, Baranadag and Hamit (only quartz syenite samples) plutons. The average pressures and crystallisation temperatures of the plutonics were obtained using the Schmidt (1992) and Holland and Blundy (1990) equations. The estimated T-f_{O2} conditions for the crystallisation of the Central Anatolian plutonics are given in Figure 4.19.

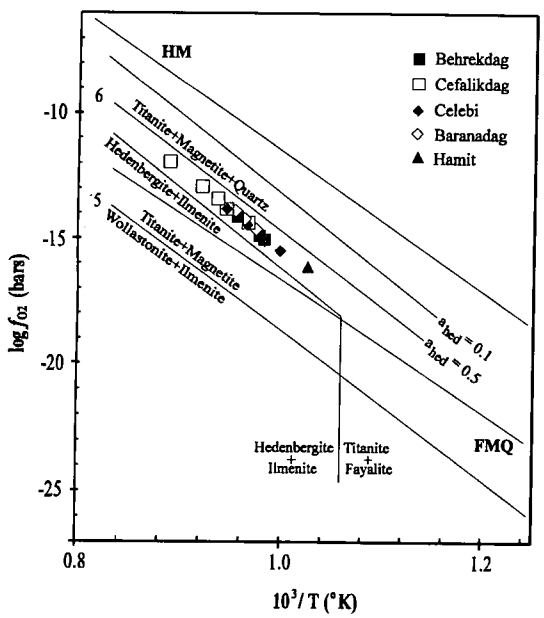

Figure 4.19. Logarithmic plot of f_{O2} versus temperature for the Behrekdag, Cefalikdag, Celebi, Baranadag and Hamit intrusive assemblages. Abbreviations: HM=Hematite-Magnetite, FMQ=Fayalite-Magnetite-Quartz and hed-hedenbergite.

As can be seen from Figure 4.19, the plutonics crystallised under conditions between the HM (Hematite-Magnetite) and FMQ (Fayalite-Magnetite-Quartz) buffers. The rock units from the Behrekdag, Cefalikdag, Celebi, Baranadag and Hamit plutons plot between the titanite + magnetite + quartz and hedenbergite lines. The Cefalikdag plutonic rocks have slightly higher f_{O2} than the other units in the Central Anatolian Massif.

Many arc-related batholiths crystallise near the experimental Ni-NiO buffer (Czamanske et al., 1981; Speer, 1987). Others, particularly ilmenite series and fayalite-bearing granites (Anderson, 1983; Emslie and Stirling, 1993), crystallise near the quartz-fayalite-magnetite buffer; and a few high f_{O2}, magnetite series granites (Barth et al., 1995) crystallise a few log units below the hematite-magnetite buffer. Thus, the observed range of f_{O2} in granites spans seven orders of magnitude and this duplicates the range of f_{O2} measurements for rapidly erupted volcanic rocks (Ewart et al., 1975; Luhr et al., 1984; Carmichael, 1991).

4.3. Summary

The mineral phase characteristics and also geothermo-barometry of the Behrekdag, Cefalikdag, Celebi, Baranadag and Hamit plutons have been summarised in Table 4.5.

PLUTON	BEHREKDAG	CEFALIKDAG	CELEBI	BARANADAG	HAMIT
ROCK UNIT	quartz monzonite (1), granite (2)	monzodiorite (1), quartz monzonite (2), granite (3)	quartz monzonite (1), granite (2)	monzonite (1), quartz monzonite (2)	nepheline monzosyenite (1), pseudoleucite monzosyenite (2), alkali feldspar syenite (3), quartz syenite (4)
PLAGIOCLASE	mainly andesine (1, 2)	andesine and labradorite (1); andesine (2); oligoclase and andesine (3)	andesine (1, 2)	oligoclase and andesine	oligoclase, andesine and labradorite (1); mainly labradorite (2); albite (3); albite, oligoclase and andesine (4)
AMPHIBOLE	hornblende, barroisite, tschermakite, edenite and taramite (only 1)	hornblende (only 1), barroisite, tschermakite, edenite, taramite and kaersutite (only 1)	hornblende, barroisite, tschermakite, edenite and taramite (only 1)	barroisite (only 2), tschermakite, edenite, A1B4Si6 (only 1), taramite and kaersutite	tschermakite, edenite, A1B4Si6, taramite and kaersutite (these amphibole compositions only for 4; more explanation see Section 4.1.2.2)
CLINOPYROXENE	salite	salite	salite	salite	salite
PRESSURE (kbar)*	3.6-4.3 (1); 2.6-3.4 (2)	3.5-5.2 (1); 4.2-4.6 (2)	2.9-4.0 (1); 2.6-3.8 (2)	4.5-5.3 (1); 4.1-4.6 (2)	3.4-3.9 (4)
TEMPERATURE (°C) #	768-791 (1); 741-753 (2)	760-858 (1); 754-767 (2)	716-791 (1); 740-770 (2)	759-783 (1); 747-764 (2)	698-711 (4)

*Table 4.5. Summary of the mineral phase features and geothermo-barometry of the intrusive rocks from the Central Anatolian Massif. *-Pressures were calculated using the Schmidt's calibration (1992) and #-temperatures were calculated using the Blundy and Holland's calibration (1990).*

Chapter 5
MAJOR AND TRACE ELEMENT GEOCHEMISTRY

Introduction

Whole-rock XRF major and trace element data are presented for 301 rock samples from the Central Anatolian Massif. The trace elements determined were Sc, V, Cr, Co, Ni, Cu, Zn, Ga, Rb, Sr, Y, Zr, Nb, Ba, La, Ce, Nd, Pb, Th and U. A subset of representative samples were also analysed for Rb, Sr, Y, Zr, Nb, Cs, Ba, Rare Earth Elements (REE), Hf, Ta, Pb, Th and U by ICP-MS. Appendix A documents the analytical techniques while Appendix B lists the accuracy and precision of the analytical data. The set of XRF and ICP-MS data is given in the Appendix C.

This chapter contains two Sections:

5.1. The first Section classifies the Central Anatolian plutonics on the basis of their major element contents and examines the major element variation diagrams.

5.2. The second Section concentrates on the trace element characteristics, as shown by trace element variation diagrams, REE patterns, multi-element patterns and tectonic discrimination diagrams.

5.1. Major element characterisation of the Central Anatolian plutonics

5.1.1. Classification of the intrusive rocks using major element geochemistry

The Central Anatolian plutonics have a broad petrological range from monzodiorite to granite/syenite, as illustrated on the Streckeisen diagram (Figure 2.4). They have been classified chemically using the total alkali versus SiO_2 diagram of Middlemost (1994) (Figure 5.1).

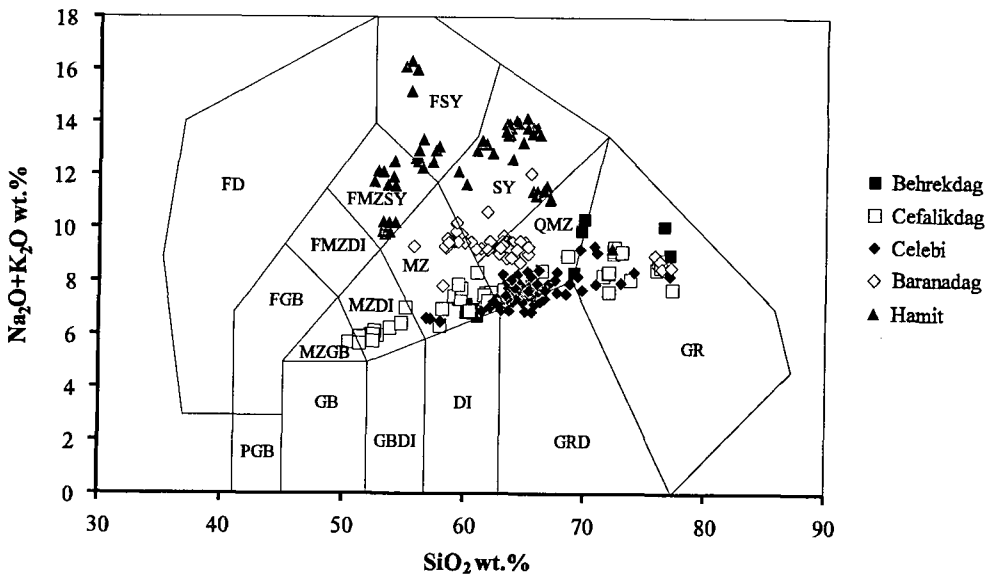

Figure 5.1. The intrusive rocks from the Central Anatolian Massif plotted on the total alkali versus SiO_2 diagram of Middlemost (1994). Abbreviations: FD-foidolite, FSY-foid syenite, FMZSY-foid monzosyenite, FMZDI-foid monzodiorite, FGB-foid gabbro, SY-syenite, MZ-monzonite, MZDI-monzodiorite, MZGB-monzogabbro, QMZ-quartz monzonite, PGB-peridotgabbro, GB-gabbro, GBDI-gabbroic diorite, DI-diorite, GRD-granodiorite and GR-granite.

The data from the Central Anatolian plutonics fall in three distinct areas of this diagram. The first area, which includes the data from the intrusive rocks from the Behrekdag, Cefalikdag and Celebi plutons, covers a linear compositional spectrum from monzogabbro with 50.45 wt.% SiO_2 through monzonite/quartz monzonite to granite with 77.26 wt.% SiO_2. The second area includes the intrusive rocks from the Baranadag pluton that plot within the monzonite, quartz monzonite, syenite and granite fields. The third area is characterised by high total alkali values and contains the rocks from the Hamit pluton. The samples from this pluton mainly plot from the foid monzosyenite through the foid syenite to the syenite fields, but they do extend into the quartz monzonite and granite fields.

The Middlemost (1994) diagram is displayed in Figure 5.2 in five parts (a-e) to show the compositional differences between the rock types in more detail. The intrusive rocks from the Behrekdag pluton, which is made up of quartz monzonite and granite according to the Streckeisen classification (Figure 2.4), plot in the monzonite, quartz monzonite and granite fields (Figure 5.2a).

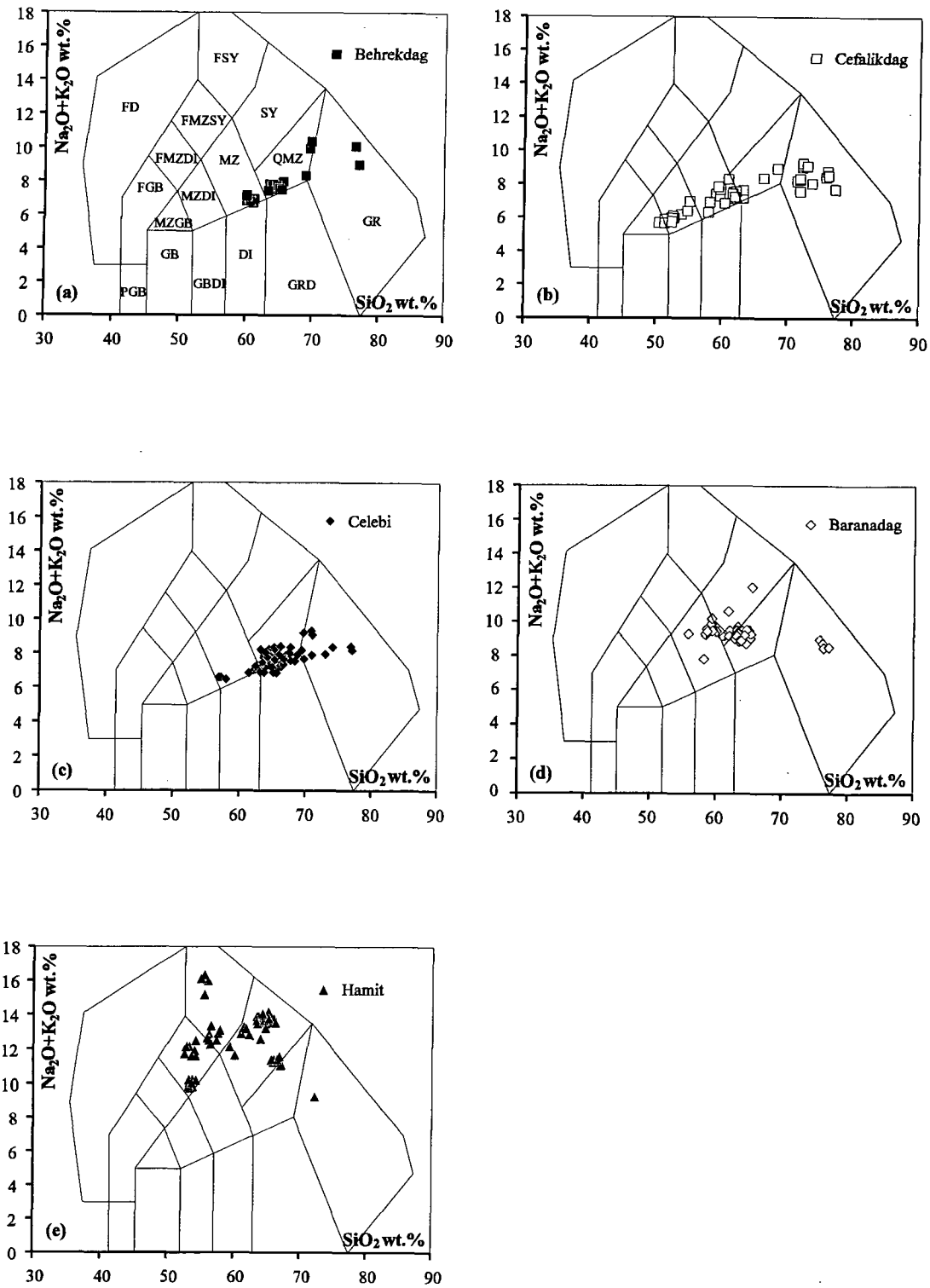

Figure 5.2. Classification of the Central Anatolian plutonics using the classification diagrams of Middlemost (1994). Abbreviations: FD-foidolite, FSY-foid syenite, FMZSY-foid monzosyenite, FMZDI-foid monzodiorite, FGB-foid gabbro, SY-syenite, MZ-monzonite, MZDI-monzodiorite, MZGB-monzogabbro, QMZ-quartz monzonite, PGB-peridotgabbro, GB-gabbro, GBDI-gabbroic diorite, DI-diorite, GRD-granodiorite and GR-granite.

The Cefalikdag pluton is composed of monzodiorite/quartz monzodiorite, quartz monzonite and granite (Figure 2.4). In Figure 5.2b, these rock units form a well-defined trend from the monzogabbro through the monzonite to the granite fields. The Celebi intrusives are plotted in Figure 5.2c and fall predominantly in the quartz monzonite and granodiorite fields. The Baranadag plutonics plot in the monzonite, quartz monzonite, syenite and granite fields (Figure 5.2d). The granite field only includes the aplitic granites. The rocks from the Hamit pluton fall in the foid monzosyenite, foid syenite and syenite fields, apart from two samples falling in the quartz monzonite and granite fields (Figure 5.2e).

In addition, the intrusive rocks have been classified as high-K types according to their K_2O and silica contents (Le Maitre et al., 1989) (Figure 5.3). The three distinct areas described above can be also seen in this diagram. In Figure 5.3, the Behrekdag, Cefalikdag and Celebi intrusive rocks have the lowest K_2O (2.56-7.97 wt.%) and a well-defined positive correlation, whereas the rocks from the Baranadag pluton have intermediate K_2O (5.14-7.94 wt.%), and a negative correlation with silica. The highest values for the Behrekdag, Cefalikdag, Celebi and Baranadag plutonic rocks mainly belong to the aplitic dyke samples. The Hamit rocks from the Massif have the highest K_2O (5.86-11.30 wt.%). The K_2O abundance increases until ~64 wt.% SiO_2 and then decreases sharply.

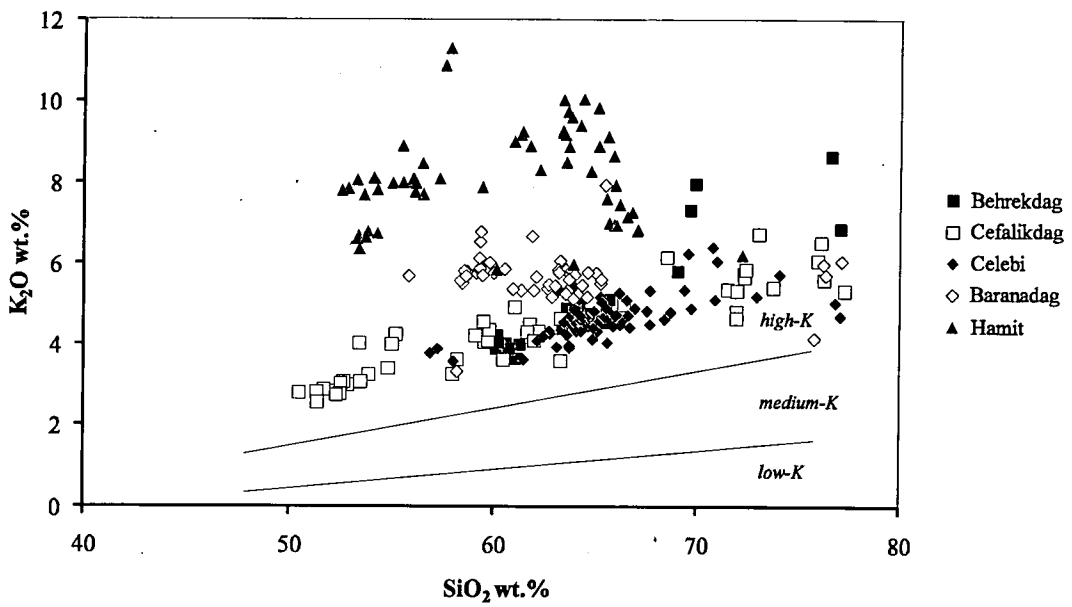

Figure 5.3. K_2O versus SiO_2 diagram of Le Maitre et al. (1989) for the Central Anatolian plutonics.

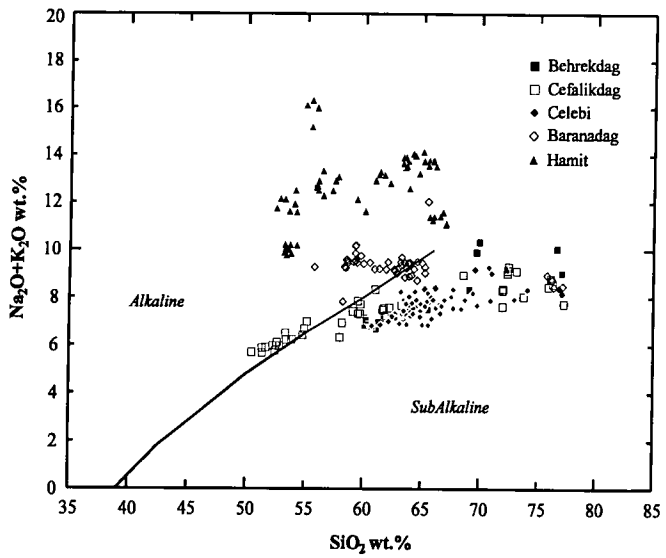

Figure 5.4. The plutonics plotted on the classification diagram of Irvine and Baragar (1971).

On the basis of the total alkali versus silica diagram of Irvine and Baragar (1971) (Figure 5.4), the intrusive rocks from the Behrekdag and Celebi plutons fall in the subalkaline field. The Cefalikdag intrusives plot mainly in the subalkaline field except for the least acidic samples which fall in the alkaline field. Although the Baranadag intrusive rocks lie between the subalkaline and alkaline fields, they predominantly plot in the alkaline field. On the other hand, the Hamit rocks plot in the alkaline field.

The intrusive rocks from the Central Anatolian Massif plot within the calc-alkaline field on the ternary AFM diagram of Irvine and Baragar (1971) (Figure 5.5) where no iron enrichment is observable. The Hamit intrusive rocks plot almost on the A corner of the AFM diagram showing alkali enrichment compared to the other intrusives in the Massif.

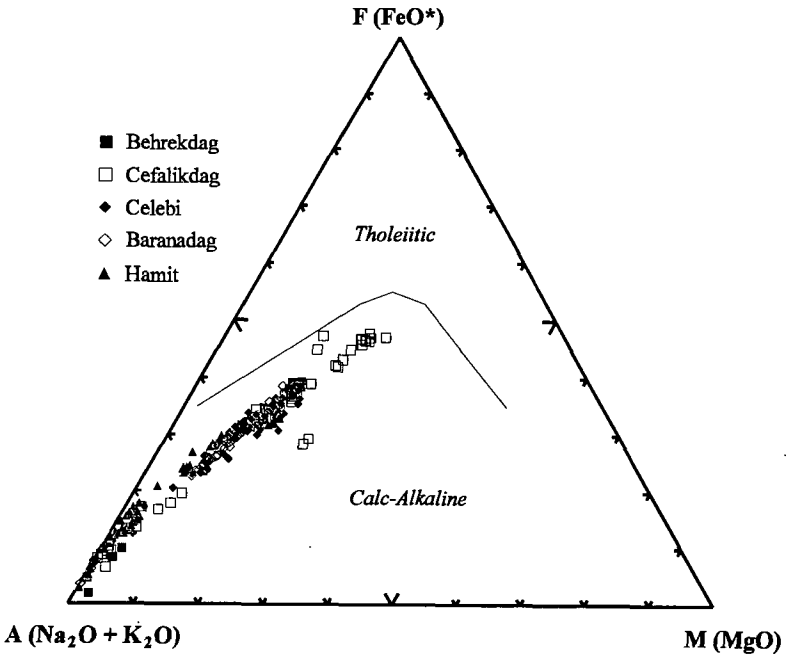

Figure 5.5. Ternary alkali-total iron-magnesia (AFM) diagram (Irvine and Baragar, 1971) of the Central Anatolian plutonics.

One of the most important early contributions to the recognition and classification of magmatic rock series was that of Peacock (1931). Peacock's classification is made up of two Harker plots on the same diagram: SiO_2 versus (Na_2O+K_2O) and then versus CaO. The critical value on this diagram is the SiO_2 value at the point where best-fit curves through the two trends intersect which is called "alkali-lime index". Four rock series are defined in Peacock's plot: alkalic, alkali-calcic, calc-alkalic and calcic. On the basis of the Peacock diagram (1931) (Figure 5.6), the Central Anatolian plutonics form three different kinds of series:

(i) Calc-alkalic series: the Behrekdag, Cefalikdag and Celebi plutonic rocks have an alkali-lime index of 57±1.

(ii) Alkali-calcic series: the Baranadag intrusive rocks have an alkali-lime index of 52±1.

(iii) Alkalic series: the Hamit rocks have an alkali-lime index of 45±1.

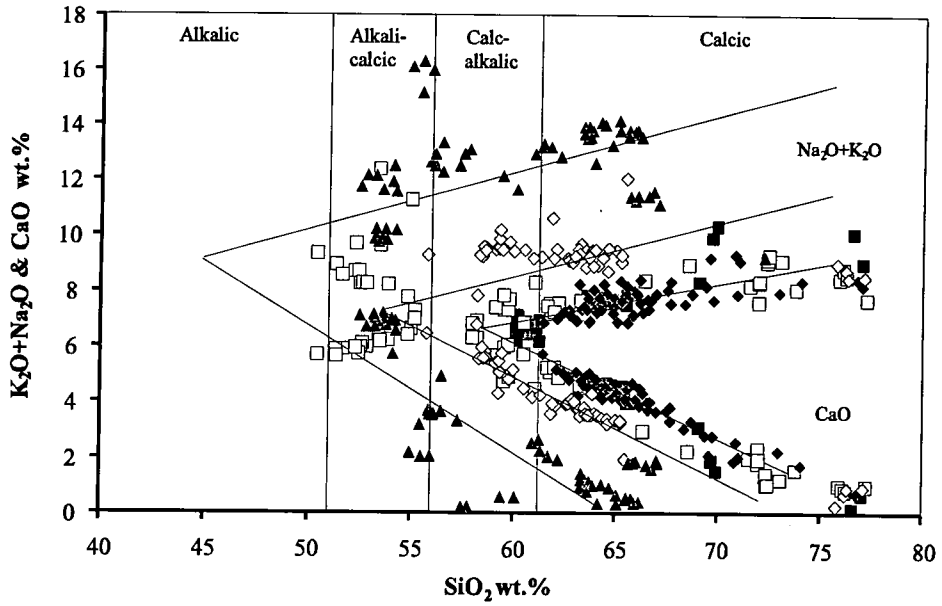

Figure 5.6. Peacock's (1931) alkali-lime diagram of the Central Anatolian plutonics (key symbols as in Figure 5.5).

On the basis of the alumina saturation diagram of Shand (1951) (Figure 5.7), the intrusive rocks from the Central Anatolian Massif are mainly metaluminous. The Behrekdag, Cefalikdag, Celebi and Baranadag plutonic rocks are metaluminous except for four samples from the Cefalikdag pluton which are peraluminous. The foid-bearing rocks (nepheline monzosyenite, pseudoleucite monzosyenite) from the Hamit pluton are metaluminous, whereas the alkali feldspar syenite and quartz syenite are peralkaline. A few samples from the Hamit pluton are peraluminous.

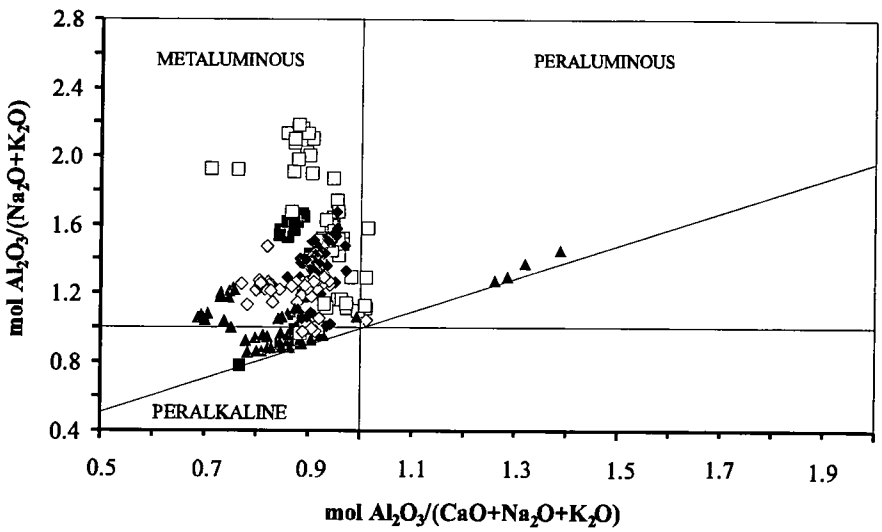

Figure 5.7. Alumina saturation diagram (Shand, 1951) of the Central Anatolian plutonics (symbols as in Figure 5.5).

5.1.1.1. I-, S- and A-type granite classification

Chappell and White (1974) classified the granitoids of the Lachlan fold belt into two groups based on their source characteristics (Table 5.1): (i) I-type and (ii) S-type. They suggested that metaluminous "I-type" granitoids are derived from igneous (or meta-igneous) sources, whereas peraluminous "S-type" granitoids are derived from metasedimentary sources. Even though this classification has been extensively used to interpret the nature of the source of granitoids, it has some drawbacks. For example: a granitoid may be derived from a combination of igneous and sedimentary sources; or the composition of source regions within continental crust may vary from amphibolite/granulite to greywacke rock types.

I-type	*S-type*	***Behrekdag, Cefalikdag, Celebi and Baranadag plutons***
Metaluminous to weakly peraluminous	Strongly peraluminous	Metaluminous
Amphibole common and cordierite absent; accessory titanite common	Biotite and muscovite predominate, cordierite present; monazite may be accessory	Amphibole common and cordierite absent; accessory titanite common
Normative diopside or <1% normative corundum	>1% normative corundum	Normative diopside
Magnetite common	Ilmenite common	Magnetite common
High Na_2O>3.2% for felsic varieties; >2.2% for mafic varieties	Low Na_2O<3.2% when K_2O=5%; >2.2% when K_2O=2%	High Na_2O>3.2% for intermediate and felsic varieties
Relatively high Ca and Sr	Relatively low Ca and Sr	Relatively high Ca and Sr
Regular inter-element variation within plutons and near linear variation diagrams	Variations diagram more irregular	Near linear variation diagrams (see Sections 5.1.2; 5.2.1)
Mafic to felsic	Mainly felsic	Intermediate to felsic
Shallow to deep level	Shallow level	Shallow level (see Chapter 4)
Amphibole-bearing enclaves common	Metasedimentary enclaves common	Amphibole-bearing enclaves common; no sedimentary enclaves (see Chapter 6)
Low initial $^{87}Sr/^{86}Sr$ ~0.704-0.706	High initial $^{87}Sr/^{86}Sr$ >0.708	Initial $^{87}Sr/^{86}Sr$ =0.7090-0.7096 (see Chapter 7)

Table 5.1. Comparison of I- and S-type granites (Chappell and White, 1974; White and Chappell, 1983) with the intrusive rocks from the Behrekdag, Cefalikdag, Celebi and Baranadag plutons.

A-type granite was used first by Loisella and Wones (1979) to describe "alkaline, anorogenic and anhydrous granites". Collins et al. (1982) have described a set of chemical criteria for the anorogenic granites of the Lachlan Fold Belt of the southeastern Australia. The chemical and other characteristics of A-type granites

are listed in Table 5.2 which also compares to the most silicic rocks from the Hamit pluton.

A-type	***Hamit pluton (alkali feldspar syenite/quartz syenite)***
Low Al, Mg and Ca	Low Mg and Ca
High Na_2O+K_2O	High Na_2O+K_2O (11.27-14.16 wt.%)
Low Sr and Ba	Low Sr and Ba
High abundances of large highly charged cations e.g. Zr, Nb, Y and REE (except Eu)	Relatively high Zr, Nb and REE
Feldspar is mainly alkali feldspar commonly albite-orthoclase solid solutions or intergrowths	Feldspar is mainly alkali feldspar and for other petrographic characteristics see Chapter 3
Cl high in peralkaline and F high in metaluminous magmas reduces viscosity	Fluorite present

Table 5.2. Comparison of A-type granites with the most silicic rock types from the Hamit pluton (after Collins et al., 1982; and Whalen et al., 1987).

To sum up, the general characteristics of the plutonics are given in Table 5.3, which is on the basis of major element geochemistry and mineralogy.

Pluton	***Behrekdag, Cefalikdag, Celebi (BCC)***	***Baranadag (B)***	***Hamit (H)***
Alkali-lime index (Peacock, 1931)	calc-alkalic	alkali-calcic	alkalic
Shand's index (1951)	metaluminous	metaluminous	peralkaline
Mineral composition	Ksp+pl+q+amp+bi±cpx	Ksp+pl+q+amp+bi (+)/±cpx	Ksp+pl(±)/+q±amp±bi ±cpx
Na_2O+K_2O (wt.%)	5.66-10.34	8.85-12.05	11.27-14.16
Rock type(s)	mzdi, qmzdi, mz, qmz, gr	mz, qmz	kspsy, qsy
Granite type	I	I/A	A

*Table 5.3. Classification of the Central Anatolian plutonics on the basis of major element geochemistry and mineralogy. *Abbreviations: ksp-alkali feldspar, pl-plagioclase, q-quartz, amp-amphibole, bi-biotite, cpx-clinopyroxene, mzdi-monzodiorite, qmzdi-quartz monzodiorite, mz-monzonite, qmz-quartz monzonite, gr-granite, kspsy-alkali feldspar syenite and qsy-quartz syenite.*

In the following sections, major and trace element characteristics of the Central Anatolian plutonics will be examined in the framework of this classification namely the ***BCC (Behrekdag, Cefalikdag, Celebi), B (Baranadag) and H (Hamit)*** plutonic rocks.

5.1.2. Harker diagrams of major elements

The intrusive rocks from the Central Anatolian Massif are plotted on Figure 5.8 with silica as the index of differentiation. The intrusive rocks from the Massif have a range of silica contents from approximately 50 to 77 wt.%, corresponding to a compositional variation from monzogabbro to granite/syenite (Figures 5.1, 5.2).

As can be seen from Figure 5.8, the BCC (Behrekdag, Cefalikdag, Celebi), B (Baranadag) and H (Hamit) intrusive rocks from the Massif generally form three distinctive differentiation trends on most of the diagrams. Samples from these plutons fall on negatively correlated linear arrays on Harker variation diagrams for TiO_2, Al_2O_3, Fe_2O_3 (total), MnO, MgO, CaO and P_2O_5.

The concentrations of TiO_2, Fe_2O_3, MnO, MgO and CaO are higher in the BCC intrusive rocks, compared to the B and H rocks. In addition, the least acidic samples from the BCC (mainly from the Cefalikdag pluton) intrusive rocks have higher TiO_2, Fe_2O_3, MnO, MgO and CaO contents than those of the other BCC intrusions.

On the other hand, the concentrations of Al_2O_3 and Na_2O are generally higher in the H plutonic rocks than the B and the BCC intrusive rocks, whereas the concentrations of P_2O_5 are higher only in the least acidic members of the H rocks.

Moreover, the B intrusive rocks from the Central Anatolian plutonics have transitional values between the BCC and the H rocks for all major elements. Na_2O remains constant for the BCC and the B intrusive rocks until about 68 wt.% and then decreases. The latter includes mainly aplitic samples of these plutons. On the other hand, Na_2O describes a more scattered trend for the H rocks.

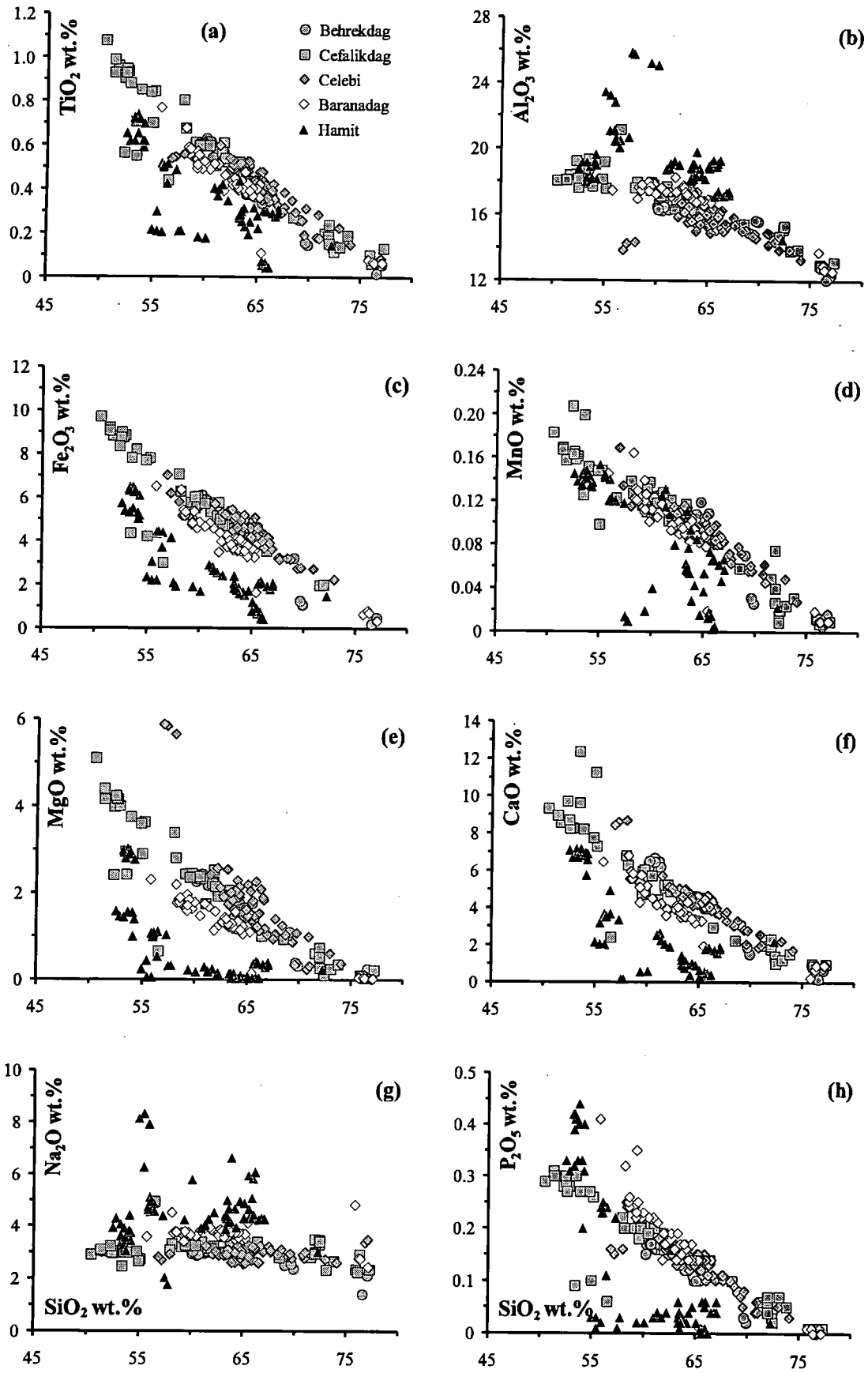

Figure 5.8. Harker variation diagrams of the intrusive rocks from the Central Anatolian Massif.

5.2. Trace element characteristics of the plutonics

5.2.1. Trace element variation diagrams

Harker diagrams of trace elements plotted against silica are presented as log-normal diagrams for all the plutons in Figure 5.9. Like major element diagrams, the BCC (Behrekdag, Cefalikdag, Celebi), B (Baranadag) and H (Hamit) intrusive rocks generally form three distinctive differentiation trends on most of the diagrams (Figure 5.9).

As can be seen from Figure 5.9, the BCC intrusive rocks are enriched in the transition elements, Sc, V, Cr, Co compared to the B and H intrusive rocks. On the other hand, the H rocks are enriched in LILEs (e.g. Rb, Sr, LREE, Pb, Th, U) and HFSEs (e.g. Zr, Nb). The B plutonic rocks have generally intermediate values of those elements between the BCC and H rocks.

Sc, V, Cr, Co, Ni, Cu, Zn and Ga have a negative correlation with silica in the BCC and H rocks. Of these elements, Cr and Ga have a positive correlation until ~65 wt.% SiO_2 and then negative correlation in the B plutonic rocks.

Rb shows a constant positive correlation for the BCC intrusive rocks. It remains almost constant for the B plutonic rocks. It increases slightly for the H rocks.

Sr decreases steadily with increasing silica for the BCC and the B intrusive rocks. However, Sr has two distinct ranges for the H rocks: (i) the foid-bearing rocks (nepheline monzosyenite, pseudoleucite monzosyenite) have generally higher concentrations of Sr (1453-1066 ppm); and (ii) the alkali feldspar syenite and quartz syenite have lower concentrations of Sr (284-59 ppm). Sr remains almost constant for both rock types.

Y is almost constant until ~70 wt.% SiO_2 and then decreases sharply in the BCC plutonic rocks. The latter mainly includes the aplitic rocks from these plutons. Y shows a negative correlation with silica in the B and H rocks.

Zr demonstrates a constant decrease with silica until ~75 wt.% and then falls rapidly for the BCC and B intrusive rocks (Figure 5.9l). Zr increases until ~60 wt.% SiO_2 for the foid-bearing syenite (nepheline monzosyenite, pseudoleucite monzosyenite) and then decreases for the alkali feldspar syenite and quartz syenite in the H plutonic rocks.

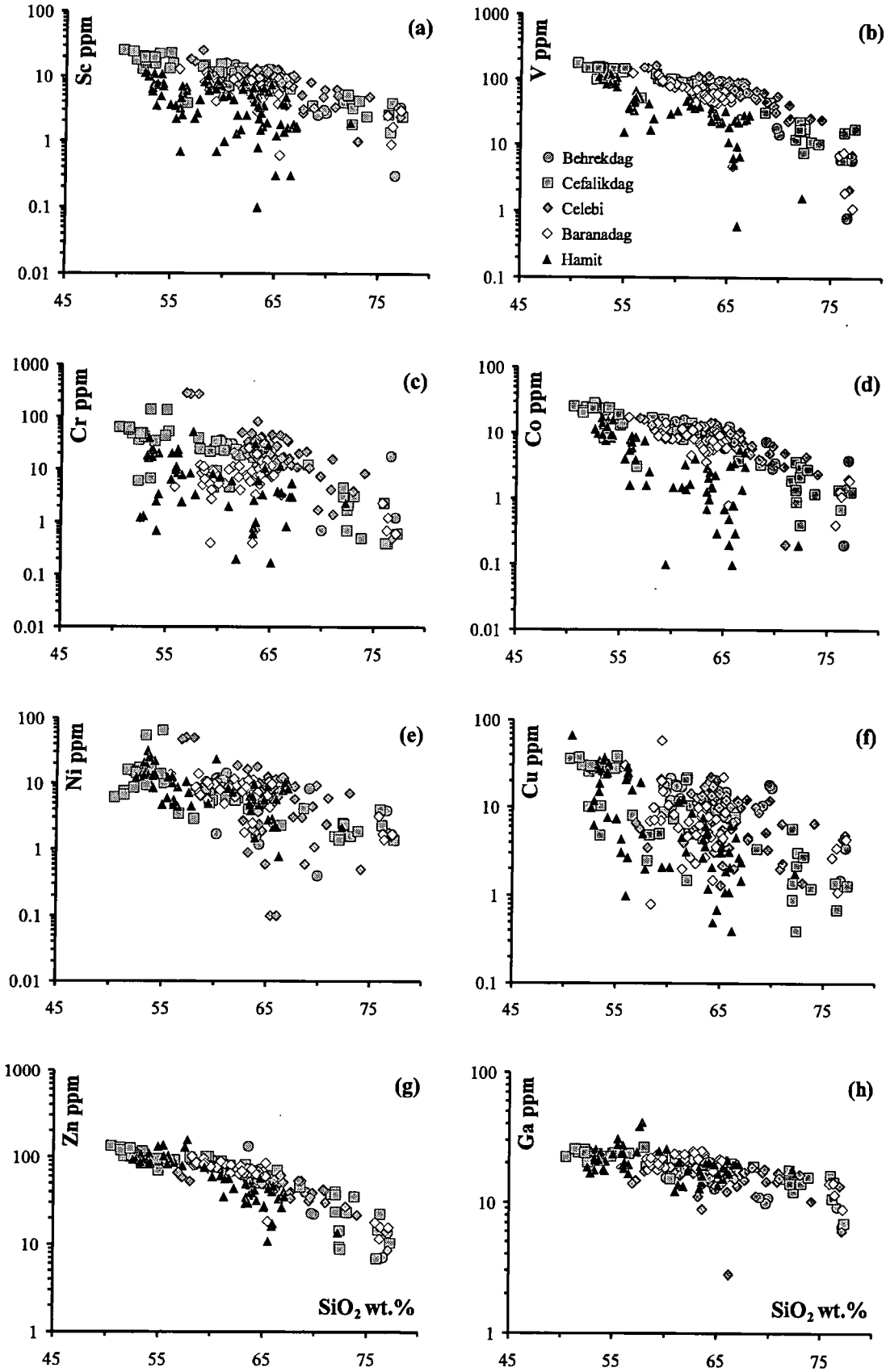

Figure 5.9. Log-normal plots of Sc, V, Cr, Co, Ni, Cu, Zn, Ga, Rb, Sr, Y, Zr, Nb, Ba, La, Ce, Nd, Pb, Th and U against silica displaying differences between the intrusive rocks from the Central Anatolian Massif.

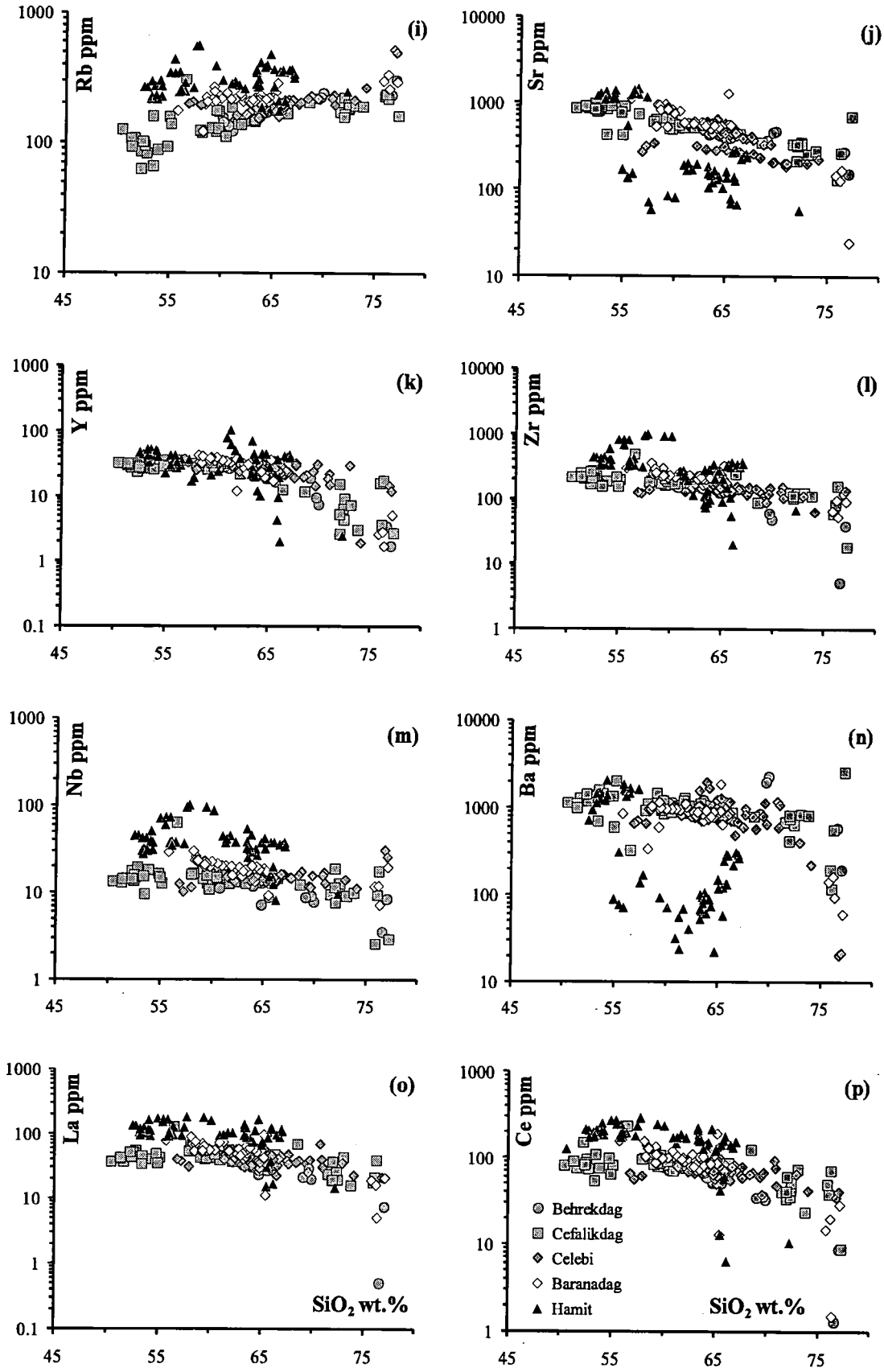

Figure 5.9. (continued).

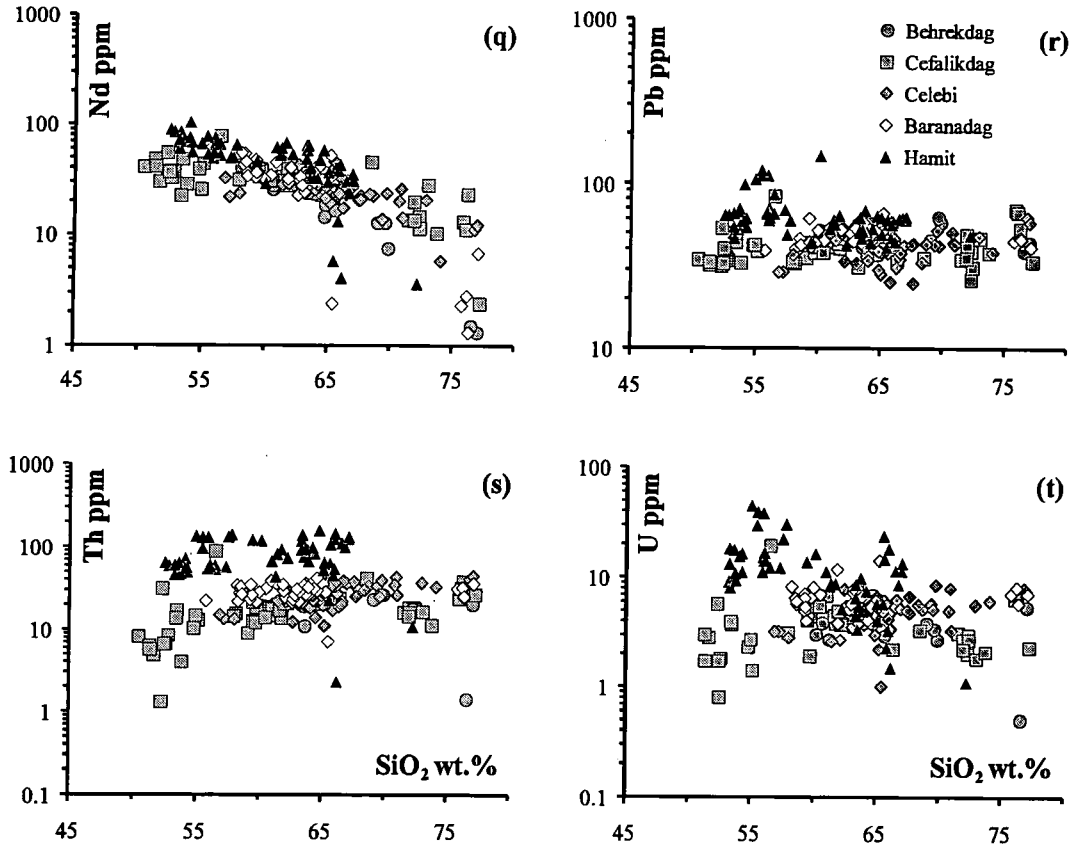

Figure 5.9. (continued).

Nb remains constant until ~67 wt.% SiO_2 and decreases for the BCC plutonic rocks. It shows a constant negative correlation with silica for the B intrusive rocks. Nb increases until ~60 wt.% SiO_2 for the foid-bearing syenite and then decreases for the alkali feldspar syenite and quartz syenite in the H plutonic rocks.

Ba decreases slightly with silica until ~72 wt.% and then decreases sharply for the BCC plutonic rocks. However, it shows a constant negative correlation for the B intrusive rocks. Ba has two distinct ranges for the H rocks: (i) the foid-bearing rocks have predominantly higher concentrations of Ba (2082-1134 ppm); and (ii) the alkali feldspar syenite and quartz syenite have lower concentrations of Ba (309-22 ppm). Ba decreases for both rock types.

La, Ce and Nd decrease slightly for all the intrusive rock types from the Massif.

Th and U have a positive correlation for the BCC and B plutonic rocks. However, U decrease with silica and Th increases slightly for the H rocks. Pb remains almost constant for the BCC, B and H rocks.

5.2.2. Rare earth element geochemistry

The rare earth elements (REE) are a group of 15 elements with atomic numbers of 57 to 71 from lanthanum (La) to lutetium (Lu); of which all but Promethium-Pm occur naturally. The REE with lower atomic numbers are generally referred to as the light REE, LREE (La, Ce, Pr, Nd), those with higher atomic numbers as the heavy REE, HREE (Dy, Ho, Er, Tm, Yb, Lu), and with intermediate numbers as the middle REE, MREE (Sm, Eu, Gd, Tb).

The REEs have similar chemical and physical properties because they form stable 3+ ions of similar size. A small number of the REE also exists in oxidation states other than 3+, notably Ce^{4+} and Eu^{2+}. The REEs show differences in their mass and ionic radius due to small but steady decrease in ionic size with increasing atomic number. These small differences in their size and behaviour cause the REEs to become fractionated relative to each other in a number of petrological processes. Thus, the REEs are used in geochemistry to probe the genesis of igneous rocks.

The extent of fractional crystallisation is related to mineral/melt partition coefficients (K_d). The K_d's for olivine are so low that its crystallisation causes the equivalent enrichment of all the REEs. Feldspars have low K_d's for the REE, except Eu therefore, they have a minor effect on the REE pattern of the melt. Garnet has low K_d's for the LREEs and has increasingly larger K_d's for the HREEs. Therefore, the fractional crystallisation of garnet causes the depletion of the HREEs in the melt. Ortho- and clinopyroxene, in general, have K_d's that are lower than 1 for the REEs. For pyroxenes, the K_d's of the LREEs are slightly lower than those of the MREEs and HREEs. Therefore, fractional crystallisation of pyroxenes causes a LREE enrichment in the melt in most cases. The K_d's for hornblende are strongly dependent on composition and greater than 10 for the MREEs and HREEs in silica-rich systems. Thus, hornblende crystallisation causes the depletion of the MREEs and HREEs. Biotite has K_d's values lower than 1 for the REEs. Therefore, its presence has a relatively little effect on the REE pattern of the melt.

Whereas the REE partition coefficients for most rock-forming minerals are <10, those for accessory minerals may be up to three orders of magnitude higher. Studies of the distribution of REEs in granitoids have shown that the REE are largely accommodated in accessory minerals such as monazite, allanite, zircon, titanite and apatite (e.g. Miller and Mittlefehldt, 1982; Gromet and Silver, 1983;

Sawka, 1988). Zircon has very large K_d's (on order of 100's) for the HREE. However, its low abundance (generally less than 0.1%) leads to only a minor depletion of the HREE in the melt. Apatite and titanite have similar K_d patterns for the REE with K_d's greater than 1 for all of the REE. Their generally low abundance reduces the effect of their large K_d's. Both apatite and titanite cause enrichment of the LREEs and HREEs relative to the MREEs.

Apatite, titanite and most likely monazite and allanite have K_d's much greater than 1 for the LREEs and may deplete the LREEs in the melt if they are present in abundance during melting or fractional crystallisation. The MREEs in a melt will be less enriched or even depleted relative to the LREEs and HREEs principally by the fractionation of apatite and titanite.

5.2.2.1. REE abundances in minerals of the Central Anatolian plutonics and individual mineral contributions to the whole-rock REE system

Mineral separates of amphibole, biotite, plagioclase and alkali feldspar from the BBC (Behrekdag, Cefalikdag, Celebi) and B (Baranadag) plutonics were analysed by ICP-MS. Details of the analytical procedures are given in Appendix A and the data set is presented in Appendix C. Chondrite- and whole-rock normalised REE patterns of these mineral separates are displayed in Figure 5.10. These mineral separates are normalised to their whole-rocks since in intrusive rocks, a whole-rock sample is accepted as representative of a melt composition.

Published partition coefficients (e.g. Dudas et al., 1971; Nagasawa and Schnetzler, 1971; Arth, 1976; Leeman and Phelps, 1981; Mahood and Hildreth, 1983; Nash and Crecraft, 1985) are presented in inset diagrams for comparison.

As can be seen from the chondrite-normalised REE patterns in Figure 5.10, amphibole and biotite separates show LREE-enriched patterns with negative Eu anomalies. Both plagioclase and alkali feldspar have very similar patterns with steep slopes in the LREE, large positive Eu anomalies and low concentrations of HREEs.

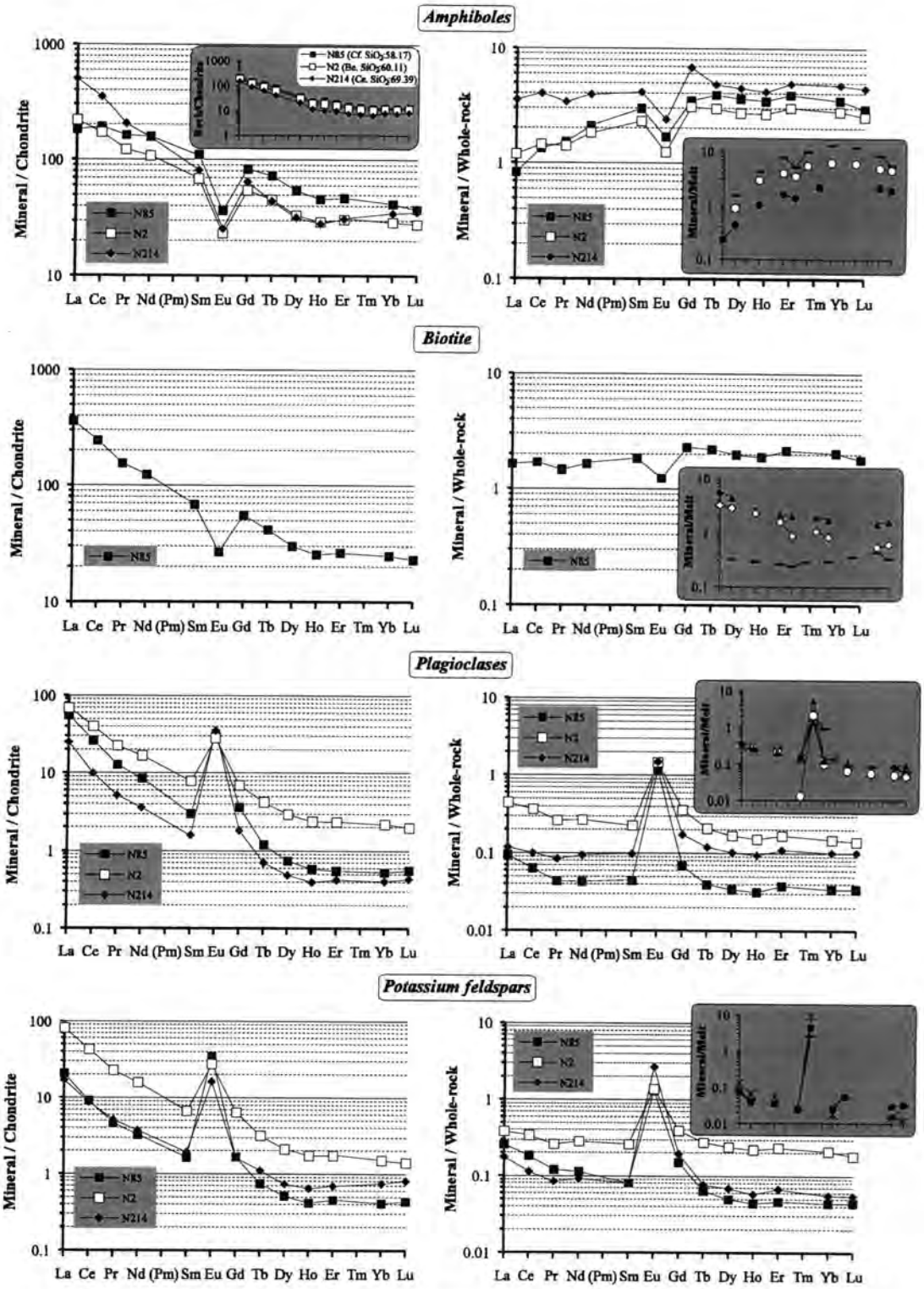

Figure 5.10. Chondrite- and whole-rock normalised REE patterns of mineral separates in the Central Anatolian plutonics. Chondrite normalisation factors are taken from Boynton (1984). The inset graph on the left side of diagrams shows the chondrite-normalised REE patterns of whole-rocks of mineral separates. In addition, compiled partition coefficients are displayed in the inset graphs for comparison. Abbreviations: Cf-Cefalikdag, Be-Behrekdag and Ce-Celebi plutons.

The whole-rock normalised REE patterns for amphibole separates (N85 and N2) are LREE-depleted with negative Eu anomalies. They have nearly flat MREE and HREE patterns. On the other hand, an amphibole separate from sample N214 shows a nearly flat LREE pattern with a negative Eu anomaly. The whole-rock normalised REE patterns for amphiboles in Figure 5.10 are generally in good agreement with published partition coefficients for amphiboles except for sample N214.

The whole-rock normalised REE pattern for a biotite separate (Figure 5.10) exhibits a nearly flat REE pattern except for a negative Eu anomaly. The whole-rock normalised REE pattern for a biotite plots about in the limits of published partition coefficient ranges.

Plagioclase and alkali feldspar both show REE patterns with characteristic positive Eu anomalies. In Figure 5.10, the whole-rock normalised REE patterns of plagioclase and alkali feldspar separates from the plutonics closely resemble phenocryst/groundmass REE distributions measured in silicic volcanic rocks (e.g. Dudas et al., 1971; Arth, 1976; Mahood and Hildreth, 1983; Nash and Crecraft, 1985).

Mineral/whole-rock abundance ratios measured from the Central Anatolian plutonics do not represent actual mineral/melt (K_d) values. The relationship between the minerals composing intrusive rocks and the minerals involved during differentiation of the precursor liquids (i.e. early liquidus minerals) is unclear, as the cooling history of intrusive rocks may alter the compositions of what were originally early liquidus minerals. Unlike intrusive rocks, partition coefficient values can be determined by analysing phenocrysts and their glassy matrix in volcanic rocks. These values measured from volcanic rocks are more reliable than those from intrusive rocks.

5.2.2.2. REE abundances in whole-rocks of the Central Anatolian plutonics

In addition to mineral separates, a set of representative whole-rock samples was analysed for the REEs by Inductively Coupled Plasma-Mass Spectrometry (ICP-MS). Samples plotted in accordance with the increasing silica content of the rock samples are presented on the legend of each diagram. LREE/MREE and MREE/HREE ratios are calculated using the normalised ratios of $(La/Eu^*)_N$ and

$(Eu^*/Yb)_N$ respectively. Eu* represents the extrapolated value calculated using the normalised values of Sm and Gd.

The REE patterns of the Central Anatolian plutonics are presented in four diagrams (Figures 5.11a-d). Three of these diagrams (Figures 5.11 a-c) demonstrate REE characteristics of the BCC (Behrekdag, Cefalikdag, Celebi), B (Baranadag) and H (Hamit) plutonic rocks, whereas Figure 5.11d shows the comparison between these rock types. As can be seen from Figure 5.11, the BCC, B and H plutonic rocks display generally similar REE patterns. In general, the intrusive rocks from the Central Anatolian Massif are LREE-enriched with small/moderate negative Eu anomalies.

The samples from the BCC plutonic rocks have LREE-enriched patterns (La_N/Yb_N=10.33-19.45) (Figure 5.11a) with small to moderate negative Eu anomalies (Eu/Eu*=0.68-0.85) indicating probable plagioclase and/or alkali feldspar fractionation. They have a LREE/MREE ratio of about 5.05-13.06 and MREE/HREE ratio of about 1.27-2.44. In these rock samples, the Eu anomaly generally increases slightly with increasing silica content in response to feldspar crystallisation. The BCC rock samples, in general, have the lowest total REE contents of the plutonics.

The B intrusive samples have slightly steeper LREE-enriched patterns (La_N/Yb_N=15.98-22.83) than the BCC samples but they have similar small to moderate negative anomalies (Eu/Eu*=0.66-0.82) (Figure 5.11b). The samples from the B pluton have broadly similar LREE/MREE profiles to those of the BCC plutons, with $(La/Eu^*)_N$ values varying between 7.60 and 11.98. These samples have total REE contents between those of the BCC and H rocks.

The H rock samples have higher abundances of LREE and MREE (Figure 5.11c) than the BCC and B samples. Like other plutons, the rocks from the H pluton show LREE enrichment (La_N/Yb_N=27.44-56.10 for the least acidic and 22.61-41.68) for the most acidic samples with small to moderate negative Eu anomalies (Eu/Eu*=0.68-0.85 for the former and 0.58-0.67 for the latter). The H intrusive rocks have a LREE/MREE ratio of about 8.19-14.48 for the least acidic and 19.66-33.56 for the most acidic samples and a MREE/HREE ratio of about 3.27-3.87 for the former and 1.15-3.12 for the latter. The H intrusive samples have the highest total REE values in the Central Anatolian plutonics.

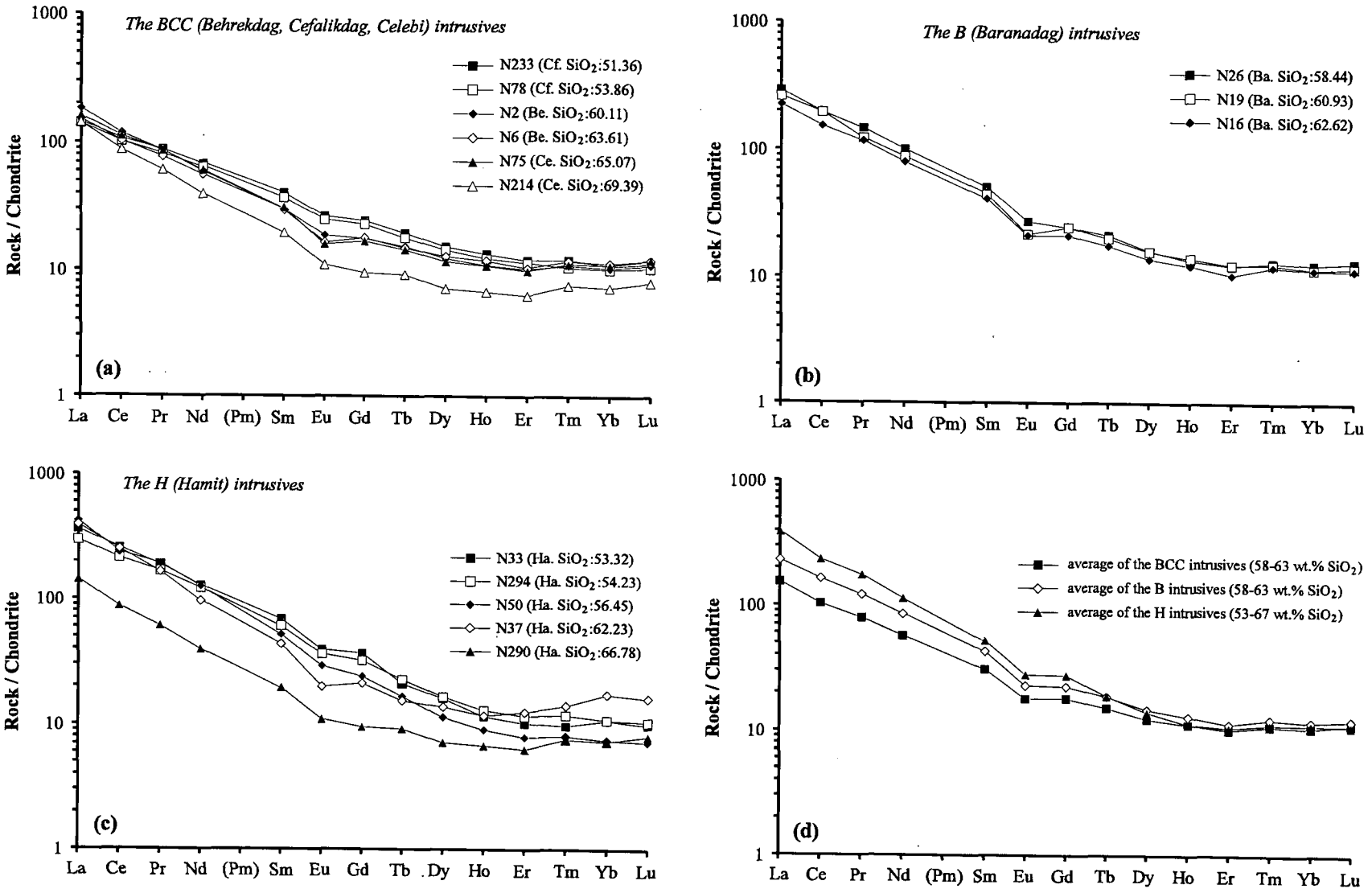

Figure 5.11. Chondrite-normalised REE patterns for the representative intrusive samples from the Central Anatolian Massif. Normalisation factors are taken from Boynton (1984). Abbreviations: Be-Behrekdag, Ce-Celebi, Cf-Cefalikdag, Ba-Baranadag and Ha-Hamit plutons.

Figure 5.11d generally shows that the LREEs and MREEs contents of the Central Anatolian plutonics increase from the BCC to the H rocks whereas the HREEs are constant.

5.2.3. Multi-element patterns

5.2.3.1. ORG-normalised diagrams

Pearce et al. (1984) proposed a spider diagram for granites to classify them on the basis of their tectonic settings. Trace element abundances are normalised to a hypothetical ocean ridge granite (ORG) produced by assuming 75% fractional crystallisation of average N-type mid-ocean ridge basaltic magma (MORB) (Pearce et al., 1984). The chosen trace elements for this pattern were restricted to those that behave incompatibly during fractionation of MORB to acid composition, therefore Ti, P, Eu and Sr were excluded from these diagrams. Pearce et al. (1984) ordered the chosen elements on the basis of their relative incompatibility during MORB genesis (which increases from Yb to Rb) and K_2O was added to the LHS of the pattern. Ce, Sm and Yb were used to represent REE. The normalising conditions, therefore, represent the composition of a granite would have had were it: (i) derived from upper mantle unaffected by any mantle enrichment event; (ii) derived from basalt by fractional crystallisation of A plagioclase-olivine-clinopyroxene-magnetite assemblage; and (iii) unaffected by crustal melting or assimilation or by volatile-dominated processes (Pearce et al., 1984).

Representative intrusive rock samples (samples >5% of modal quartz) from the Central Anatolian Massif are normalised to the hypothetical ocean ridge granite (ORG), the results are shown in Figure 5.12. Rb, Ba, Th, Ta, Nb, Ce, Hf, Zr, Sm, Y and Yb data are ICP-MS analyses whereas K_2O is analysed by XRF. The plots are presented in four multi-element diagrams (Figures 5.12 a-d). Three of these (Figures 5.12 a-c) show trace element characteristics of the BCC (Behrekdag, Cefalikdag, Celebi), B (Baranadag) and H (Hamit) rocks, whereas Figure 5.12d compares these three rock units. The inset diagram in Figure 5.12d also compares these three units to well-known granites from the volcanic arc and collision settings.

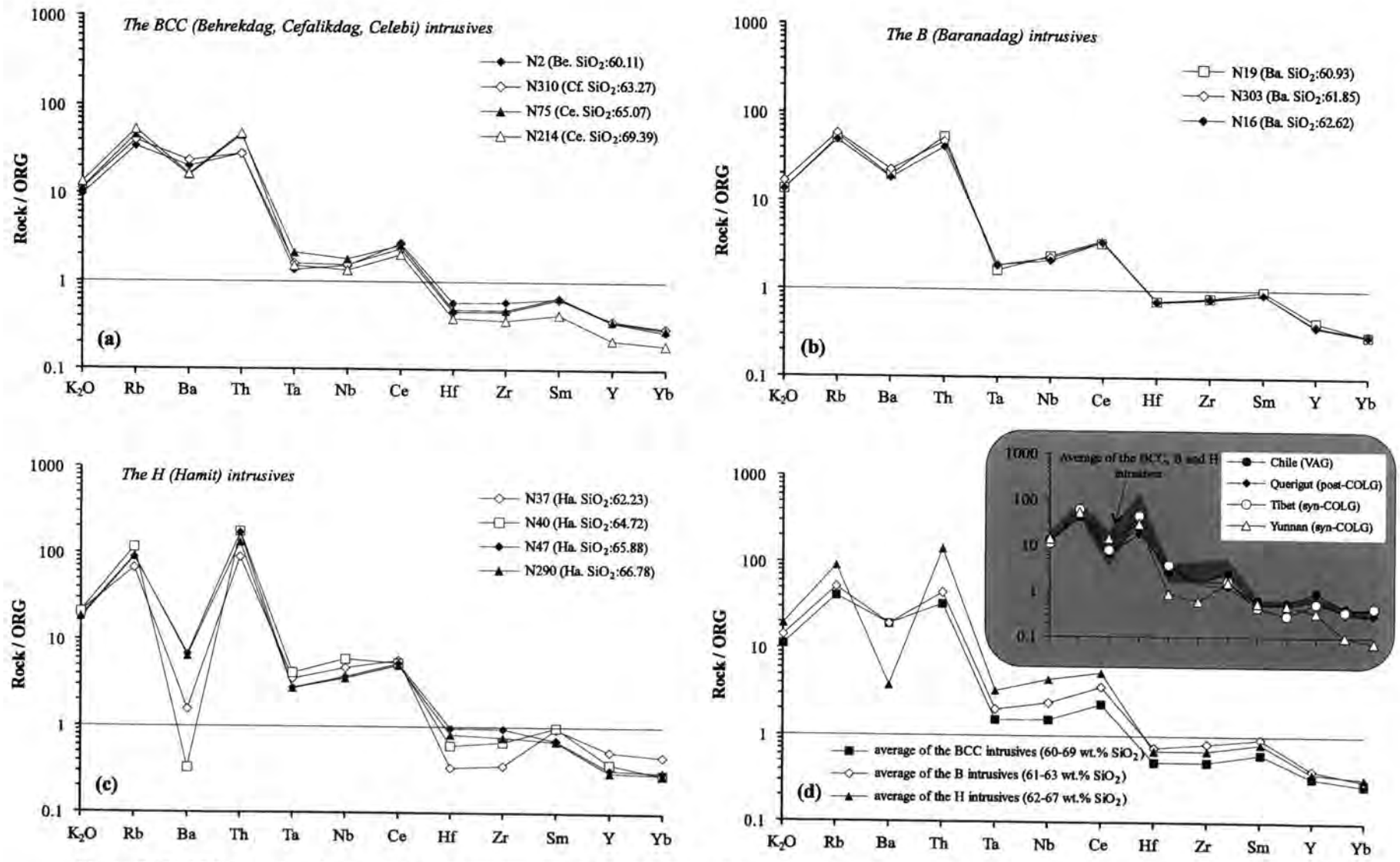

Figure 5.12. ORG-normalised patterns for the intrusive rocks from the Central Anatolian Massif. Normalisation factors are taken from Pearce et al. (1984). The inset graph compares three rock units from the Massif to well-known granites from the volcanic arc and collision settings. Abbreviations: VAG-volcanic arc granite, syn-COLG-syn-collisional granite, post-COLG-post-collisional granite, Be-Behrekdag, Ce-Celebi, Cf-Cefalikdag, Ba-Baranadag and Ha-Hamit.

All samples are characterised by enrichments in LILEs (K, Rb, Ba, Th) and LREEs (Ce, Sm) relative to HFSEs (Ta, Nb, Hf, Zr, Y and Yb) (Figure 5.12). In addition, they have low values of Y and Yb relative to the normalising compositions. There is also a relative enrichment of all elements except Ba from the BCC to the H rocks (Figure 5.12d).

The patterns of the BCC, B and H rocks are broadly similar in shape, differing mainly in the absolute abundances of the elements. There are nonetheless some features which are peculiar to particular rock types. For example, the most acidic rocks from the H pluton (Figure 5.12c) are more depleted in Ba than the other rock series, reflecting the dominant control of alkali feldspar. The shapes of the patterns resemble those for the volcanic arc (VAG) and collision granites (syn- and post-COLG) of Pearce et al. (1984) (Figure 5.12d).

5.2.4. Tectonic discrimination diagrams

The most commonly used tectonic discrimination diagrams for granites were introduced by Pearce et al. (1984). The concept that trace element compositions of granites can be used to indicate tectonic setting is particularly attractive because the tectonic history of an orogen can be reconstructed by studying the changing compositions of the granites which are associated with it. Perhaps for this reason, the tectonic discrimination diagrams of Pearce et al. (1984) are commonly used.

Pearce et al. (1984) examined the relationship between the chemical compositions of granites and the tectonic setting in which they occur. They noted that the granite composition is fundamentally controlled by source rock composition and not by tectonic setting, but they also demonstrated empirically that granites from different tectonic settings have distinct trace element characteristics. Pearce et al. (1984) used Nb (or Ta), Rb and Y (or Yb) to show the link between sources and tectonic settings.

Over 600 trace element data of granites taken from known tectonic settings were used by Pearce et al. (1984) in a series of discrimination diagrams to characterise granites to one of four tectonic settings: (i) ocean-ridge; (ii) volcanic arc; (iii) within-plate; and (iv) collision (syn- and post-).

The samples from the Central Anatolian plutonics (>5% of modal quartz) (excluding aplitic rocks) are plotted on the tectonic discrimination diagrams of Pearce et al. (1984) (Figure 5.13). In the Nb versus Y diagram (Figure 5.13a), the BCC (Behrekdag, Cefalikdag, Celebi) intrusive rocks fall into the volcanic arc granite (VAG) and syn-COLG fields. In contrast, the B (Baranadag) plutonic rocks plot between the volcanic arc granite (VAG) and syn-COLG and within-plate granite (WPG) fields. The H (Hamit) rocks fall in the within plate granite (WPG) field.

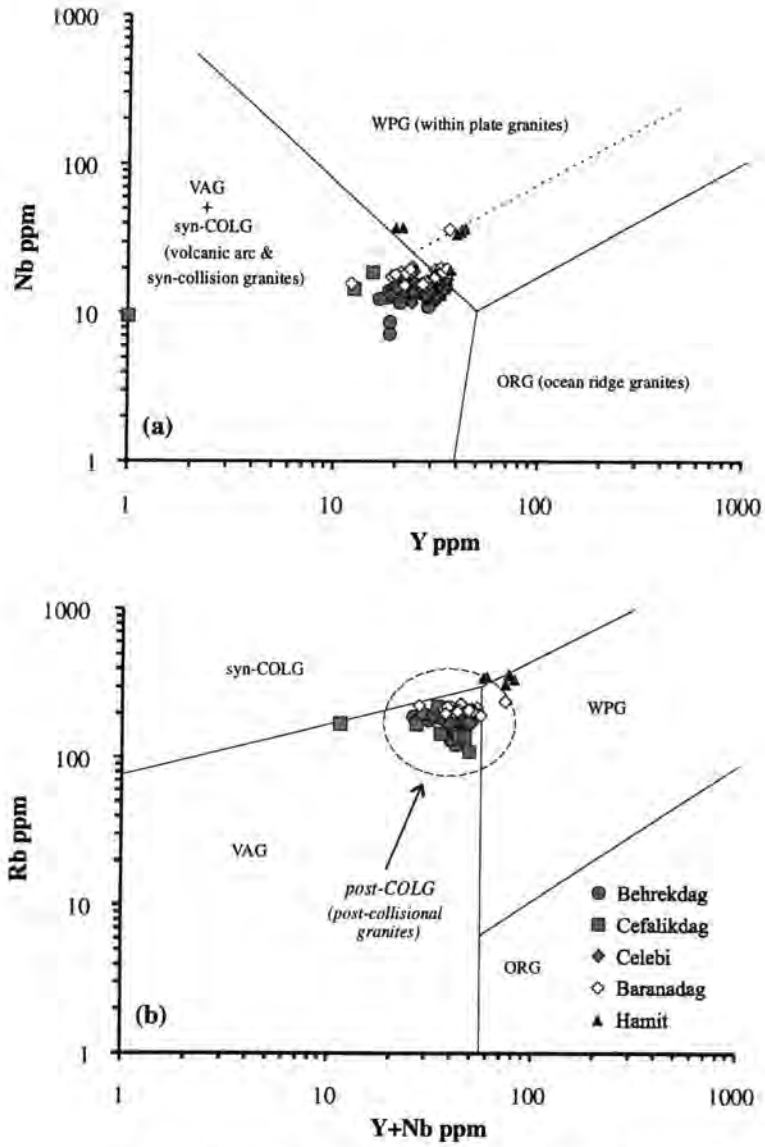

Figure 5.13. Nb versus Y (Figure 5.13a) and Rb versus (Y+Nb) (Figure 5.13b) discrimination diagrams for the Central Anatolian plutonics (>5% modal quartz) (after Pearce et al., 1984).

In the Rb against (Y+Nb) discrimination diagram (Figure 5.13b), most of the intrusive samples from the Central Anatolian Massif plot within the post-COLG field as described by Pearce et al. (1984) and Pearce (1996). The BCC rocks plot in the volcanic arc field. The B plutonic rocks fall within the volcanic arc field apart from one sample which falls in the within-plate granite field. In contrast, the H rocks plot between the syn-collision and within plate granite fields.

5.3. Summary

The geochemical characteristics of the BCC (Behrekdag, Cefalikdag, Celebi), B (Baranadag) and H (Hamit) plutonic rocks have been summarised in Table 5.4.

PLUTON	*BEHREKDAG, CEFALIKDAG, CELEBI (BCC)*	*BARANADAG (B)*	*HAMIT (H)*
Rock type	monzodiorite, monzonite, quartz monzonite, granite	monzonite, quartz monzonite	nepheline monzosyenite (1), pseudoleucite monzosyenite (2), alkali feldspar syenite (3), quartz syenite (4)
Shand's index (1949)	metaluminous	metaluminous	metaluminous (1, 2); peralkaline (3, 4)
Alkali-lime index (Peacock, 1931)	calc-alkalic	alkali-calcic	alkalic
Major elements	high TiO_2, Fe_2O_3, MnO, MgO and CaO	transitional between the BCC and H rocks	high Al_2O_3 and P_2O_5
Trace elements	enrichment in LILEs relative to HFSEs	enrichment in LILEs relative to HFSEs	enrichment in LILEs relative to HFSEs
Rare earth elements	enrichment in LREEs (LREEs and MREEs contents increase from the BCC to the H rocks)	enrichment in LREEs (LREEs and MREEs contents transitional between the BCC and H rocks)	enrichment in LREEs (LREEs and MREEs contents higher compared to the BCC and B rocks)
Tectonic discrimination (Pearce et al., 1984)	*in the Nb versus Y diagram*: the VAG+syn-COLG field; *in the Rb versus Y+Nb diagram*: the post-COLG field	*in the Nb versus Y diagram*: between the VAG+syn-COLG and the WPG fields; *in the Rb versus Y+Nb diagram*: the post-COLG field	*in the Nb versus Y diagram (3 and mainly 4)*: the WPG field; *in the Rb versus Y+Nb diagram*: between the WPG and syn-COLG fields
Granite type	I	I/A	A (only 3 and 4)

Table 5.4. Summary of the geochemical characteristics of the Central Anatolian plutonics.

Chapter 6
THE ENCLAVES

Introduction

Igneous enclaves are a widespread feature of granitoid intrusions (e.g. Pabst, 1928; Didier, 1973) and silicic volcanic rocks (e.g. Bacon, 1986). Their compositions range from gabbro to granodiorite but they are usually of quartz diorite to tonalite composition. Igneous enclaves have igneous microstructures and generally show strong affinities with their host rocks in terms of mineralogy, mineral composition and bulk chemistry (e.g. Didier, 1973; Vernon, 1983).

Igneous enclaves have been interpreted in four principal ways: as partially reacted and digested fragments (xenoliths) of wall rocks (e.g. Tindle and Pearce, 1983); as cognate fragments of cumulate minerals (e.g. Arculus and Wills, 1980); as refractory 'restite' blocks inherited from the source region of partial melting (e.g. White and Chappell, 1977; Chappell et al., 1987); and as magma mixing/mingling products representing blobs of mafic magma injected into a felsic magma (e.g. Vernon, 1983; Castro et al., 1990). These genetic types may vary between occurrences and, conceivably, several types could coexist in the same pluton.

This Chapter describes the igneous enclaves taken from the Behrekdag, Cefalikdag and Celebi plutons in the Central Anatolian Massif and attempts to identify their origin using their field, petrographic, mineralogical and geochemical characteristics.

6.1. Field occurrence of enclaves

Enclaves are very abundant in all the plutons studied except the Hamit pluton. Although the Baranadag plutonic rocks contain a few enclaves, only the enclaves from the BCC (Behrekdag, Cefalikdag, Celebi) plutonic rocks will be discussed in the following sections. The abundance of enclaves in the BCC plutons is not related to the proximity of the margin or to any other particular part of the plutons: the enclaves are evenly dispersed throughout the whole plutons. Most of the enclaves are ellipsoidal in shape with a wide range of sizes. Contacts with host rocks are generally

sharp and chilled rims are occasionally present. Two types of igneous enclave may be recognised (Table 6.1): (i) fine-grained (Type-I); and (ii) medium-grained to porphyritic with feldspar megacrysts (Type-II). No sedimentary enclaves have been found.

(i) Fine-grained varieties (Type-I)

These enclaves are consistently finer-grained and darker than the host. They are generally ellipsoidal with their long axis in the range of ~0.5 to ~45 cm. Contacts with host rocks are generally sharp and, occasionally, have crenulated fine-grained margins. These margins have high proportions of mafic minerals, especially amphibole.

(ii) Medium-grained to porphyritic varieties (Type-II)

These are found mainly in the Savciliebeyit monzodiorite of the Cefalikdag pluton. They are generally ellipsoidal with their long axis in the range of ~5 cm to ~1 m. Flattened enclaves have been found only around the contact zone of the pluton (around Savciliebeyit village) (Photo 6.1). They are medium-grained and porphyritic with plagioclase or amphibole crystals. They are darker than the host and contacts with host rocks are sharp (Photo 6.2). The Savciliebeyit monzodiorite and enclaves show a slight to strong preferred orientation (commonly NE strike) defined by parallel alignment of plagioclase feldspar laths which is strongest near the pluton contacts.

	Type-I enclaves	***Type-II enclaves***
size	~0.5 to ~45 cm	~5 cm to ~1 m
shape	rounded to ellipsoidal (generally elipsoidal)	rounded to ellipsoidal (generally elipsoidal)
grain size	fine-grained	medium-grained and porphyritic with pl sometimes amp
contact	sharp (occasionally crenulated fine-grained margins)	sharp
host	monzodiorite to granite	

Table 6.1. The macroscopic characteristics of the enclaves from Central Anatolian Massif. Abbreviations: pl-plagioclase and amp-amphibole.

Photo 6.1. Field view of flattened enclaves, NE of Savciliebeyit village, River Kirkikozu.

Photo 6.2. The Kucukcurtepe quartz monzonite around Kucukcurtepe hill containing porphyritic enclaves which vary in size (12 cm across in the photo).

6.2. Petrography

On a modal quartz-alkali feldspar-plagioclase (QAP) diagram (Streckeisen, 1976) (Figure 6.1), the fine-grained enclaves (Type-I) mainly plot in the quartz diorite and quartz monzodiorite fields. However, the medium-grained to porphyritic enclaves (Type-II) plot in the quartz diorite and gabbro fields.

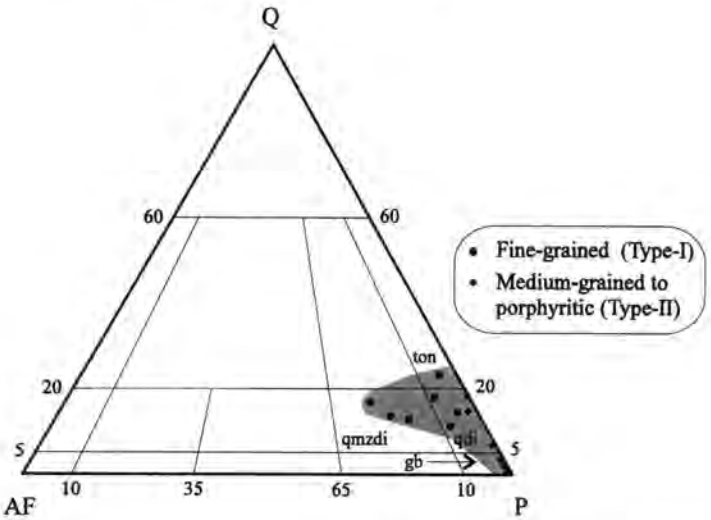

Figure 6.1. Modal classification of the enclaves from the Central Anatolian Massif (after Streckeisen, 1976). The corners of the triangles are Q-quartz, AF-alkali feldspar and P-plagioclase. Abbreviations: ton-tonalite, qmzdi-quartz monzodiorite, qdi-quartz diorite and gb-gabbro.

(i) Fine-grained varieties (Type-I)

The enclaves are fine-grained and, rarely, porphyritic with a hypidiomorphic, granular texture. They are made up of plagioclase, alkali feldspar, clinopyroxene, amphibole, biotite and quartz.

Plagioclase feldspar is generally lath-like, or prismatic, with sericitised cores. It is euhedral to subhedral, exhibiting normal, patchy and oscillatory zoning. The rims are free from inclusions while cores partially or wholly enclose biotite. Alkali feldspar is microperthitic and anhedral and poikilitically encloses other phases (Photo 6.3). Clinopyroxene occurs as four types: subhedral large grains (2.4 mm); subhedral-anhedral fine grains; needles scattered throughout the rock; and irregular patches included within amphibole. Amphibole is subhedral to anhedral and encloses plagioclase crystals. Biotite is foxy-red coloured and subhedral. Quartz is generally anhedral and shows undulose extinction. It often encloses small grains of the other phases. Quartz is intergrown with both plagioclase feldspar and alkali feldspar.

Accessory phases include apatite, titanite, zircon and opaques. Apatite forms short-prisms or needles. It occurs either as a separate phase or as inclusions. Opaque minerals are most commonly euhedral and are scattered throughout the rock. Titanite is often euhedral and prismatic zircon almost always occurs as inclusions in biotite.

Epidote and sericite are common alteration products of plagioclase feldspar. Clinopyroxene is occasionally altered to uralitic amphibole or chlorite. Biotite is also slightly altered to chlorite.

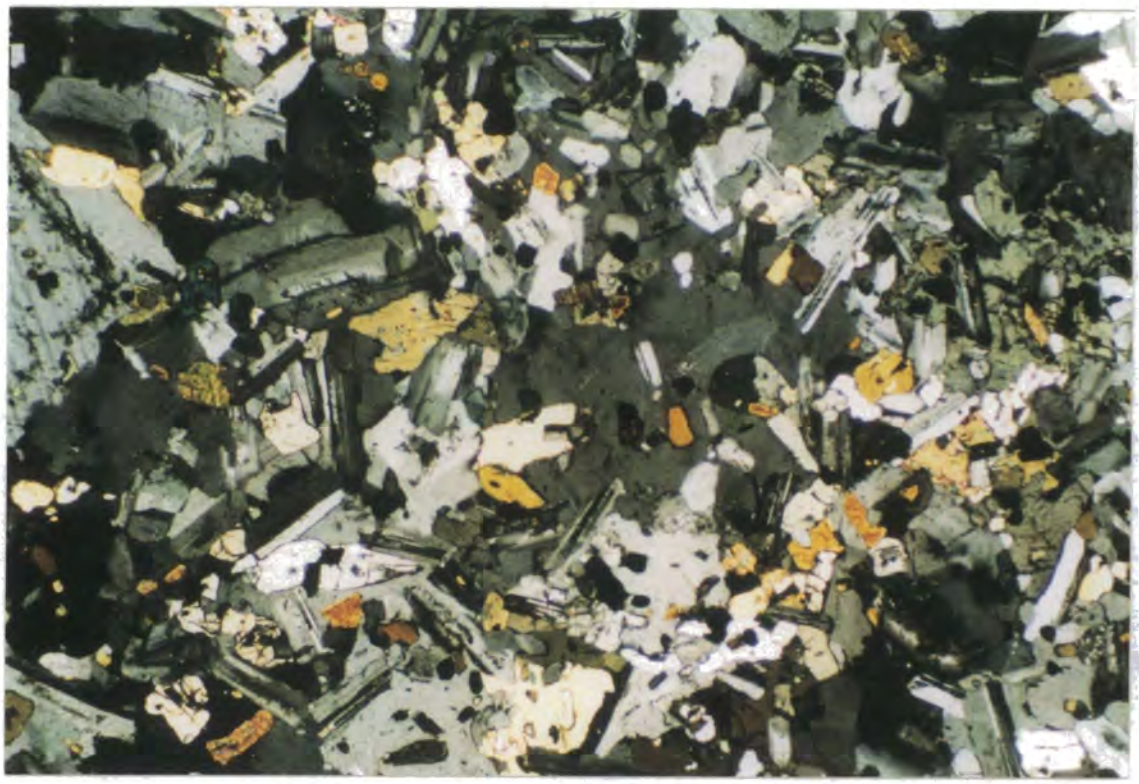

Photo 6.3. View showing poikilitic alkali feldspar (centre of the view), quartz (on the left side of the view) and amphibole (right corner of the field) enclosing predominantly plagioclase and other phases of the enclave (sample N103). Magnification: 3x1.9 mm, XPL.

(ii) Medium-grained to porphyritic varieties (Type-II)

The medium-grained enclaves are made up of plagioclase, amphibole, biotite, clinopyroxene, alkali feldspar and quartz. These enclaves show cumulate textures (Photo 6.4).

Plagioclase is euhedral to subhedral and shows zoning. Amphibole (up to 9 mm across) is generally present as prismatic, euhedral to subhedral crystals. Biotite is foxy-red coloured and subhedral. Clinopyroxene is occasionally colourless and is subhedral to anhedral. Alkali feldspar is microperthitic and interstitial. It encloses

biotite, plagioclase and clinopyroxene. Quartz is interstitial and shows undulose extinction. Accessory minerals are apatite, titanite, zircon and opaques.

Epidote, carbonate and chlorite are found as alteration minerals. The former is replaced by plagioclase and the latter is by amphibole and biotite.

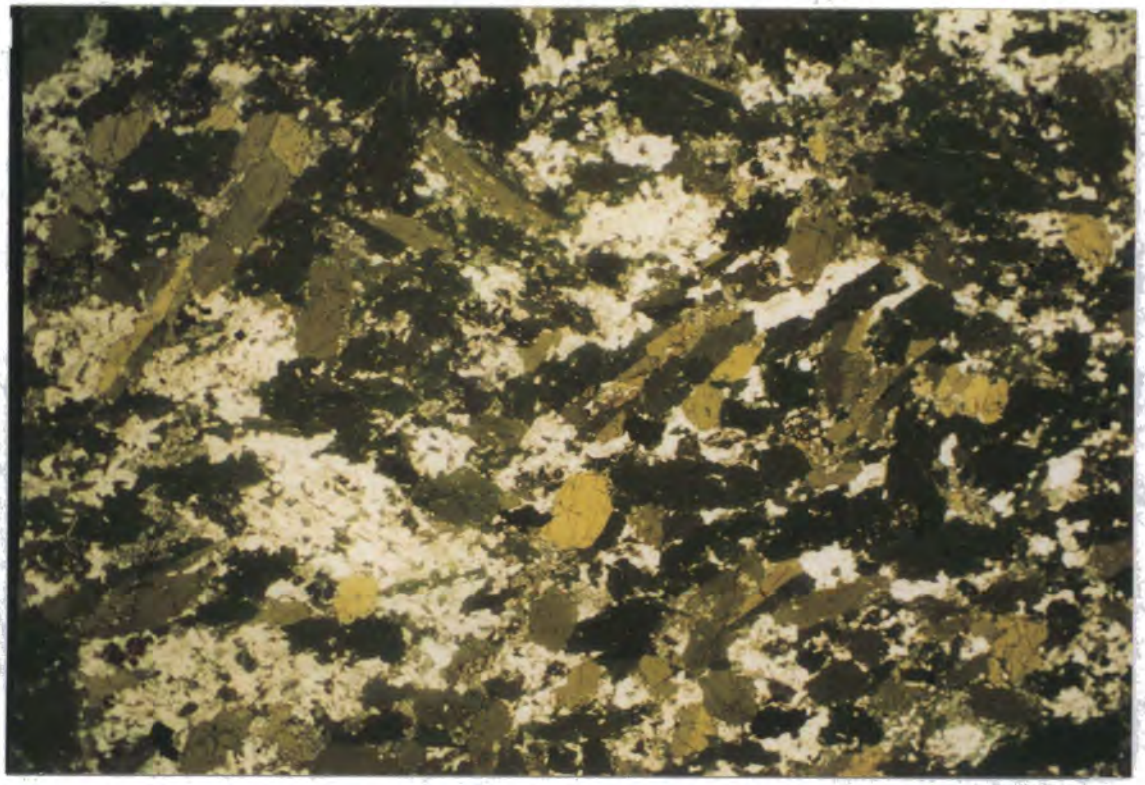

Photo 6.4. Microphotograph of the medium-grained enclave in the Savciliebeyit monzodiorite (sample N509) showing a cumulate texture. The green-coloured crystals in the view are amphiboles. Magnification: 12x7.2 mm, PPL.

The porphyritic enclaves have a hypidiomorphic, granular texture (Photo 6.5). Phenocrysts are plagioclase feldspar, clinopyroxene, amphibole and biotite. Matrix minerals are plagioclase, clinopyroxene, amphibole, biotite, quartz and alkali feldspar. Modal estimates give 40-50% plagioclase, 15-30% clinopyroxene, amphibole and biotite, 15-20% quartz, and <5% alkali feldspar.

The plagioclase phenocrysts (up to 2.1 mm) are generally present as tabular, euhedral to subhedral crystals. Some crystals show zoning of normal and oscillatory type. They occasionally enclose fine-grained biotite and, rarely, clinopyroxene which are mainly concentrated in plagioclase cores. Clinopyroxenes in the enclaves from the Savciliebeyit monzodiorite have three forms: irregular patches included within amphibole; small grains enclosed within plagioclase feldspar; and colourless, anhedral small grains scattered throughout the matrix. Amphibole crystals are commonly present as subhedral crystals, but some are euhedral and anhedral. In

some cases, they enclose fine-grained plagioclase crystals suggesting that amphibole crystals grew later than the enclosed minerals. Some amphibole crystals contain patches of clinopyroxene. Biotite is often foxy-red coloured and ranges in size up to 1.1 mm. It occurs as subhedral flakes enclosing zircon crystals. Some biotites occasionally have undulose extinction and are kinked. The small greenish biotites occasionally replace amphiboles along cleavages and are apparently a later product. Quartz occurs as small grains in the matrix and is often anhedral in shape indicating late crystallisation. Alkali feldspar is generally interstitial indicating late crystallisation. Accessory minerals are zircon, apatite, opaques and, rarely, titanite. Opaque minerals include magnetite and ilmenite. These minerals are normally fine-grained and scattered throughout the rock.

Plagioclase and alkali feldspar are altered to sericite. Clinopyroxenes are, rarely, altered to chlorite ånd carbonate.

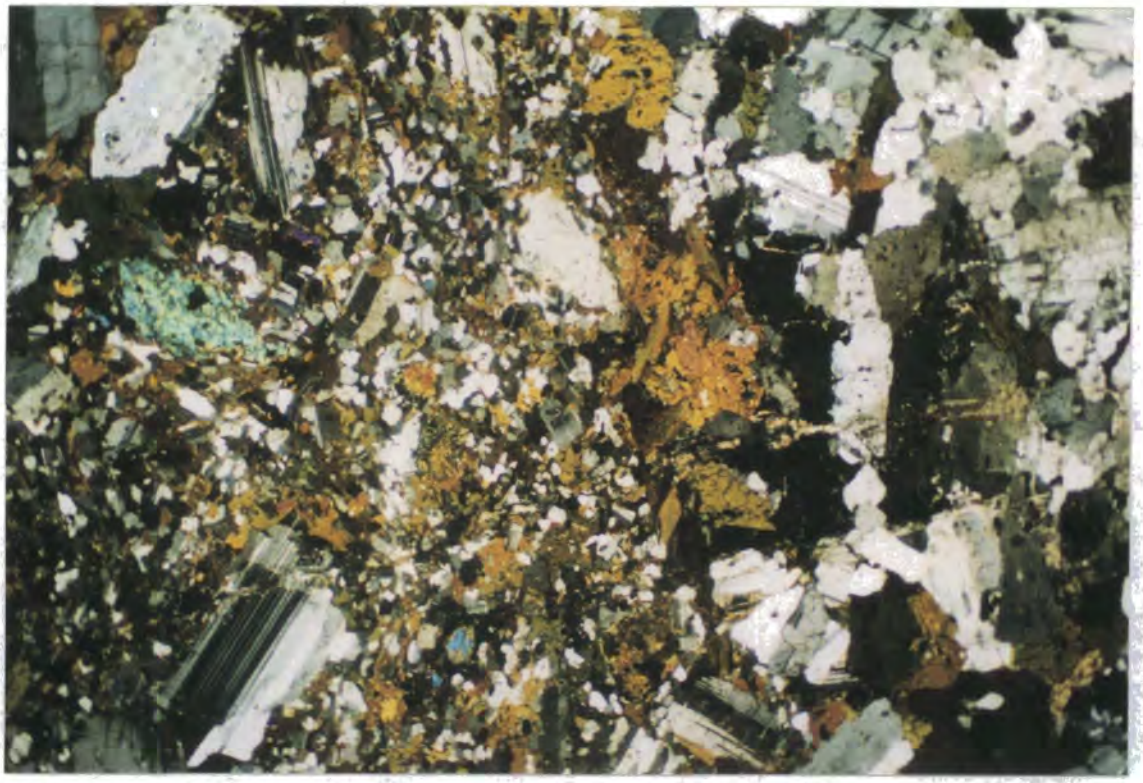

Photo 6.5. View from the boundary between the porphyritic enclave and host (sample N80). The former contains abundant biotite and amphibole. Magnification: 3x1.9 mm, XPL.

6.3. Mineral chemistry

6.3.1. Plagioclase

Plagioclase is generally the most abundant phase in the Type-I and Type-II enclaves. Plagioclase from *the Type-I enclaves* and host rocks is mainly andesine in

composition (Figure 6.2). They contain plagioclase with a compositional range of An_{55-35} compared with the host rocks range of An_{47-33}. Plagioclase cores in the host rocks lie in the range of An_{44-36}, whereas the range in the Type-I enclaves wider at An_{54-36}.

Plagioclase from *the Type-II enclaves* is mainly andesine in composition (An_{51-42}), except for one sample falling in the labradorite field (Figure 6.2). The host rocks have a compositional range of An_{50-40}, which has a similar mean but slightly greater standard deviation than that of the Type-II enclaves. Plagioclase cores in the Type-II enclaves show almost the same compositional range as the host rocks (An_{51-45}).

6.3.2. Amphiboles

Amphiboles from *the Type-I enclaves* have a restricted Al_2O_3 content of 7.05 to 7.51 wt.% and a SiO_2 content of 45 to 46 wt.%. They are characterised by a mg# (Mg/Mg+Fe) ratio between 0.44 and 0.48. On the other hand, amphiboles from the host rocks have the same Al_2O_3 content as the enclaves with a range of 6.90 to 8.30 wt.%. However, amphiboles from the host rocks have a slightly greater range of SiO_2 (43 to 46 wt.%) than those from the enclaves. In addition, amphiboles from the host rocks are slightly more magnesian (mg# = 0.51-0.57) than those from the Type-I enclaves. On the IMA classification scheme (Leake et al., 1997), amphiboles from the enclaves and host rocks are classified as edenite (Figure 6.3a).

Amphibole is the most abundant mafic phase in *the Type-II enclaves.* Amphiboles from the Type-II enclaves have a restricted Al_2O_3 content of 8.79 to 10.42 wt.% and a SiO_2 content of 41 to 43 wt.%. They are characterised by a mg# (Mg/Mg+Fe) ratio between 0.42 and 0.48.

In contrast, amphiboles from the host rocks have an Al_2O_3 content of 8.91 to 9.37 wt.% and a SiO_2 content of 42 wt.%. The host rocks are slightly more magnesian (mg# = 0.51-0.55) than the enclaves. On the IMA classification scheme (Leake et al., 1997) (Figure 6.3b), amphiboles from the Type-II enclaves predominantly fall in the ferro-edenite field. On the other hand, those from the host rocks plot in the magnesio-hastingsite field.

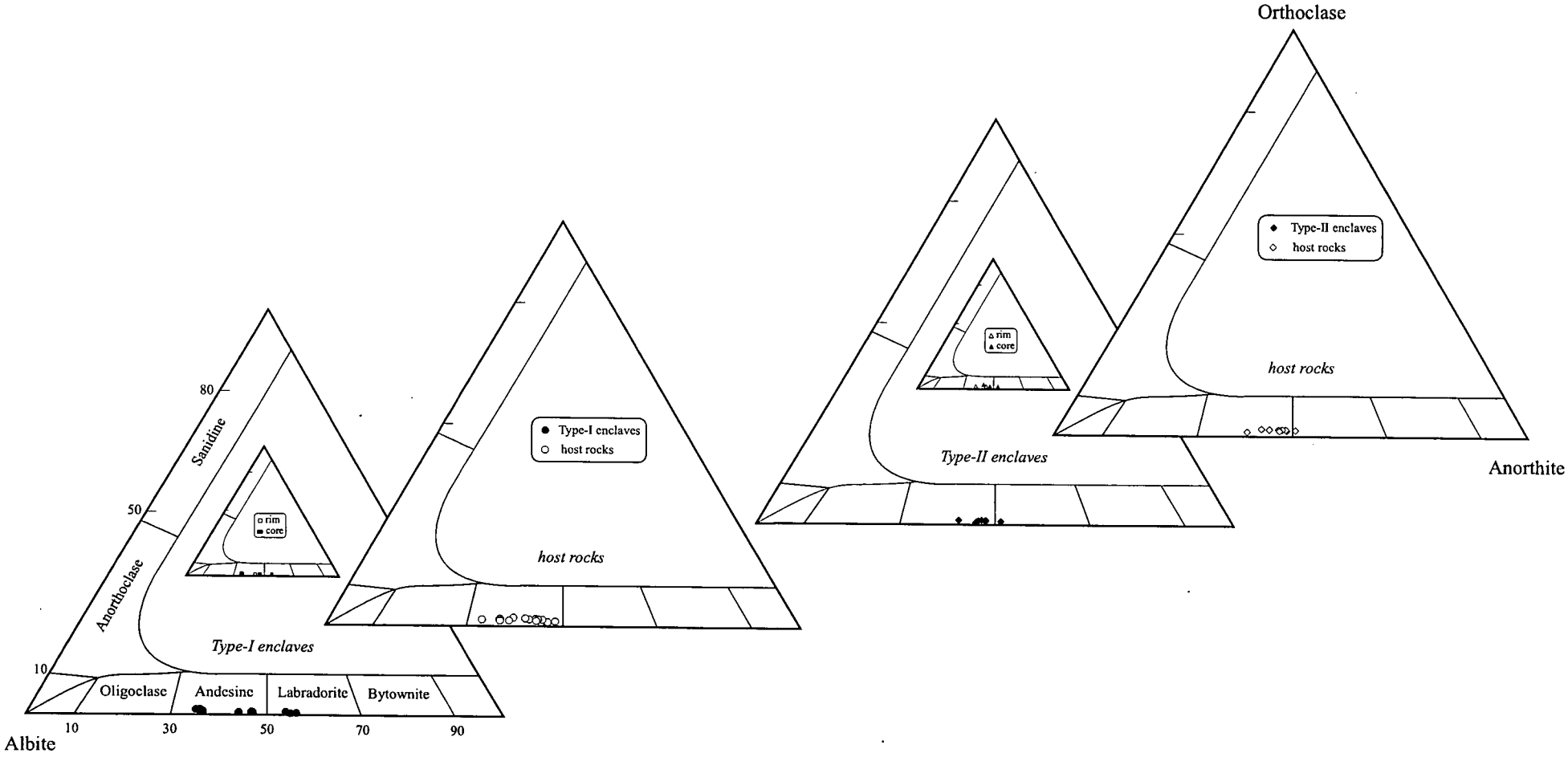

Figure 6.2. Compositions of plagioclase feldspars in the enclaves and their host rocks.

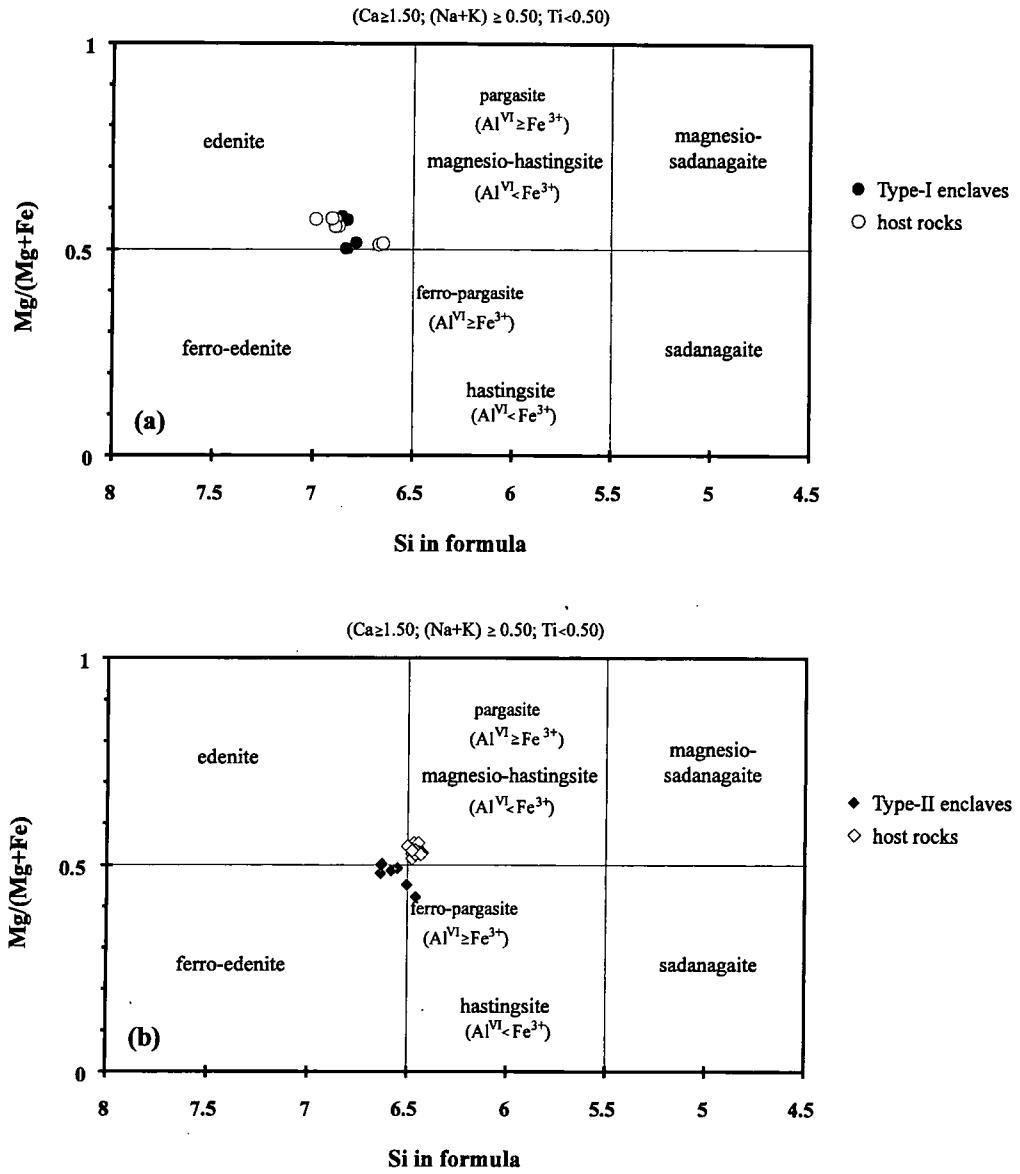

Figure 6.3. (a) Amphibole crystals from the Type-I enclaves and host rocks plotted on the classification diagram of Leake et al. (1997) on the basis of (Na+K) ≥ 0.50; and (b) amphiboles from the Type-II enclaves and host rocks.

6.3.3. Clinoproxenes and biotites

Clinopyroxene is a more common mafic phase in the Type-I enclaves than in the Type-II enclaves. On the other hand, biotite is a more common mafic phase in the Type-II enclaves compared to the Type-I enclaves.

Clinopyroxenes from *the Type-I enclaves* have a TiO_2 content of 0.92 to 3.70 wt.% and an Al_2O_3 content of 0.15 to 0.56 wt.%. Clinopyroxenes from the host rocks have a lower TiO_2 (0.02 to 0.17 wt.%), but they have a slightly higher Al_2O_3 (0.45 to 1.07 wt.%) than the enclaves. Clinopyroxenes in the host rocks have a slightly

limited range in a mg# (Mg/Mg+Fe) ratio (0.57-0.68) than those in the enclaves (0.63-0.76). Clinopyroxenes in the enclaves and host rocks are salite in composition (Figure 6.4).

Clinopyroxenes from *the Type-II enclaves* have a TiO_2 content of 0.76 to 0.83 wt.% and an Al_2O_3 content of 0.05-0.12 wt.%. Clinopyroxenes from the host rocks have a lower TiO_2 (0.00 to 0.12 wt.%), but they have a higher Al_2O_3 (0.33 to 0.96 wt.%) than the enclaves. Clinopyroxenes in the enclaves have a slightly higher mg# (Mg/Mg+Fe) ratio (0.67-0.71) than those in the host rocks (0.62-0.65). Clinopyroxenes in the enclaves and host rocks are salite in composition (Figure 6.4).

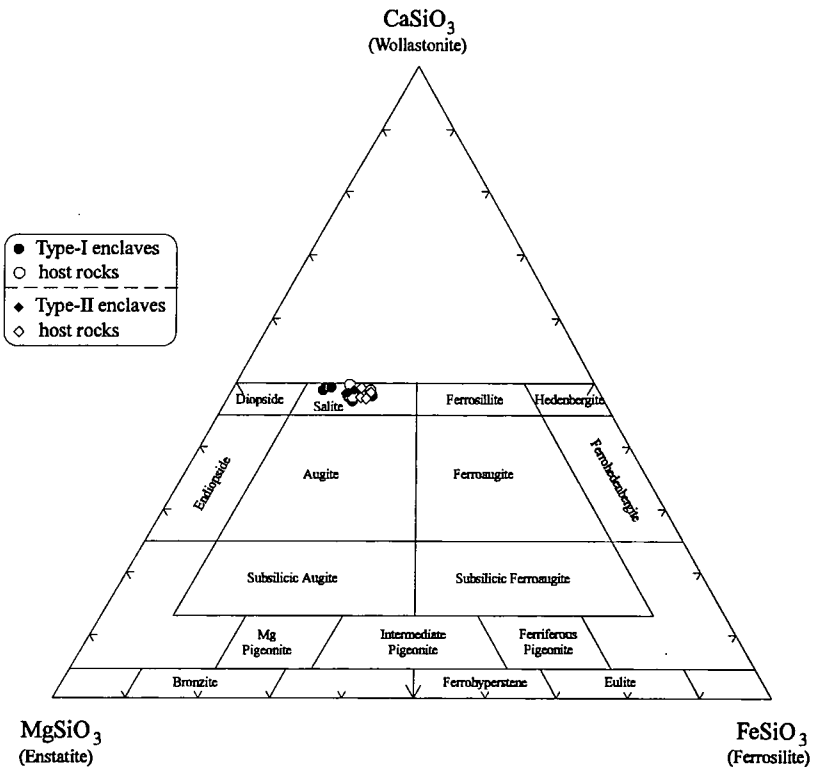

Figure 6.4. Distribution of the composition of clinopyroxenes from the enclaves and their host rocks.

In *the Type-II enclaves* and host rocks, biotites are generally enriched in Fe (FeO_{tot} >19 wt.%) and Ti (TiO_2 > 2.8 wt.%). The enclaves are characterised by a mg# (Mg/Mg+Fe) ratio between 0.42 and 0.45. On the other hand, biotites in the host rocks are slightly more magnesian (mg# = 0.45-0.51) than those in the Type-II enclaves.

6.4. Chemical constraints

A total of 37 enclave samples were analysed to investigate chemical differences between the enclaves and the BCC (Behrekdag, Cefalikdag, Celebi) plutonic rocks. There is broad range of silica contents of the enclaves, from 42 to 66 wt.% (Figure 6.5). The Type-I enclaves are more silicic (55-66 wt.%) than the Type-II enclaves (42-59 wt.%).

On Harker diagrams of SiO_2 against other major oxides (Figure 6.5), the enclaves and the BCC plutonic rocks generally display linear correlations. TiO_2, Fe_2O_3 (total), MnO, MgO, CaO and P_2O_5 show negative correlations with silica for the BCC plutonic rocks and both types of enclave.

Al_2O_3 decreases slightly until ~58 wt.% SiO_2 and then decreases sharply for the BCC plutonic rocks. It describes a more scattered trend for both types of enclave.

Na_2O, however, remains constant until about 68 wt.% SiO_2 and then decreases for the BCC intrusive rocks. It increases until ~50 wt.% SiO_2 and then remains almost constant for the Type-II enclaves, and it decreases for the Type-I enclaves. K_2O (Figure 6.5i) displays a positive correlation with silica for the BCC plutonic rocks and both types of enclave.

The concentrations of TiO_2, Fe_2O_3, MnO, MgO, CaO and P_2O_5 are, in general, higher in the Type-II enclaves, compared to the BCC plutonic rocks and Type-I enclaves. The concentrations of TiO_2, Fe_2O_3, MgO, CaO and P_2O_5 in the Type-I enclaves are similar to the BCC plutonic rocks. However, the Type-I enclaves have higher K_2O contents than the Type-II enclaves.

On Harker diagrams of SiO_2 against trace elements (Figure 6.6), Sc, V, Co, Ni, Zn and Ga have a negative correlation with silica in the BCC plutonic rocks and both types of enclave. Cr and Cu decrease for the BCC plutonic rocks, whereas they display no significant correlation for the enclaves.

The most distinctive feature of the ferromagnesian trace elements (Sc, V, Cr, Ni, Cu and Zn) in the enclaves is the low abundance of Ni and Cr. Two Type-II enclave samples have Ni around 61 ppm. All the remaining enclave samples have Ni less than 31 ppm. Apart from two Type-II enclave samples, all enclave samples have Cr less than 68 ppm, with the majority having less than 30 ppm.

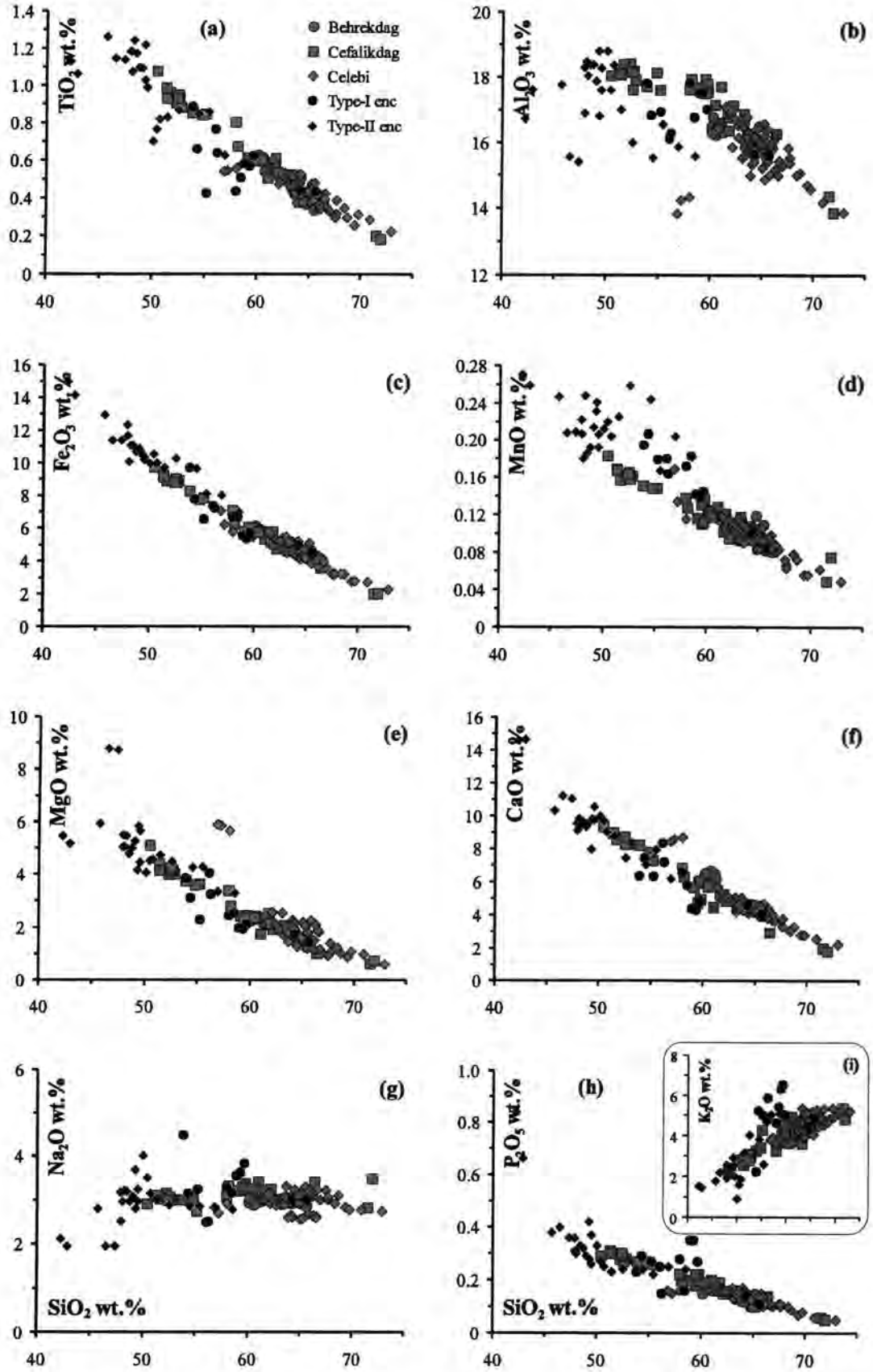

Figure 6.5. Harker variation diagrams of the BCC (Behrekdag, Cefalikdag, Celebi) intrusive rocks and enclaves from the Massif. Abbreviation: enc-enclave.

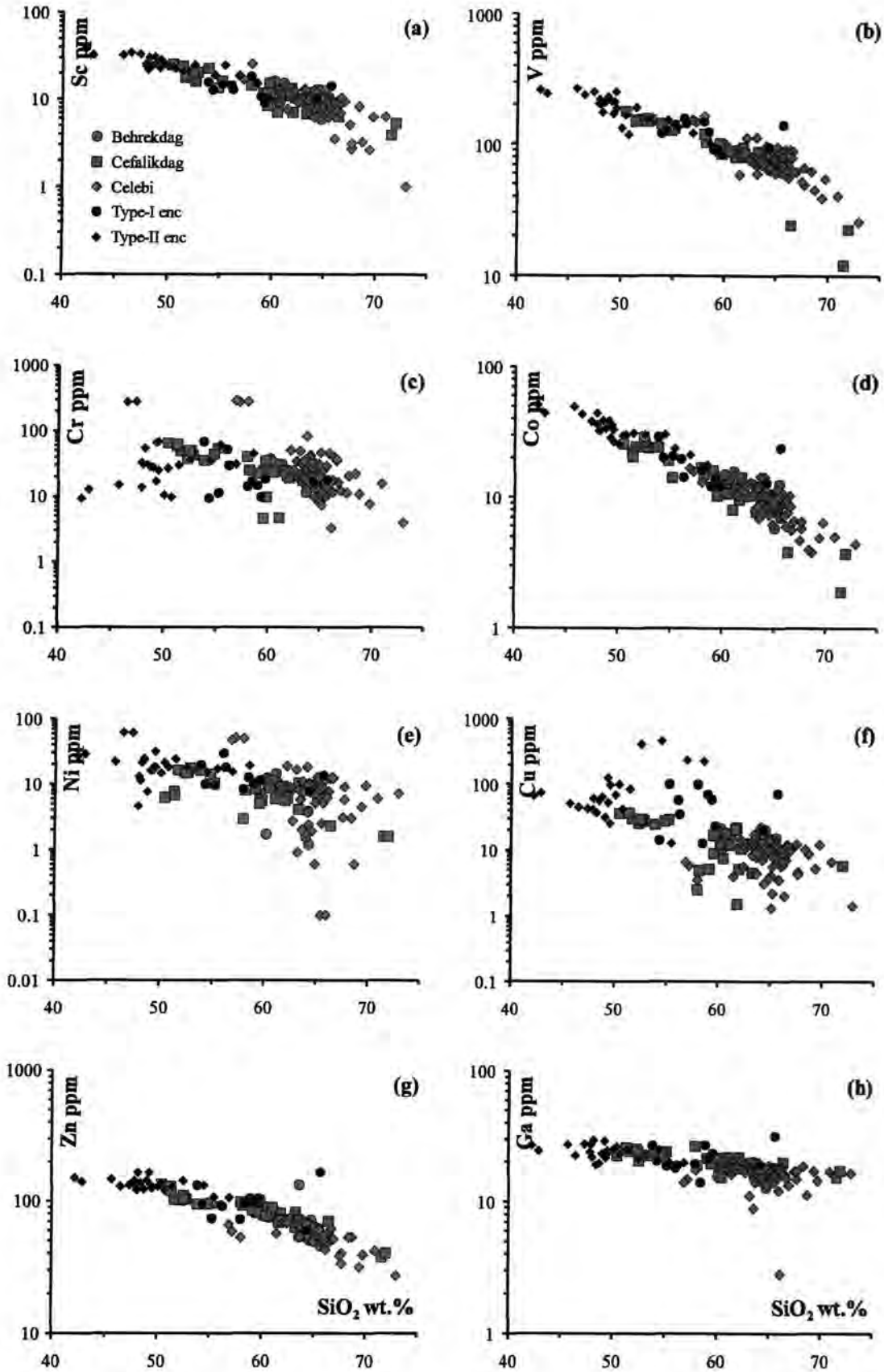

Figure 6.6. Log-normal plots of Sc, V, Cr, Co, Ni, Cu, Zn, Ga, Rb, Sr, Y, Zr, Nb, Ba, La, Ce, Nd, Pb, Th and U against silica displaying differences between the BCC (Behrekdag, Cefalikdag, Celebi) intrusive rocks and enclaves. Abbreviation: enc-enclave.

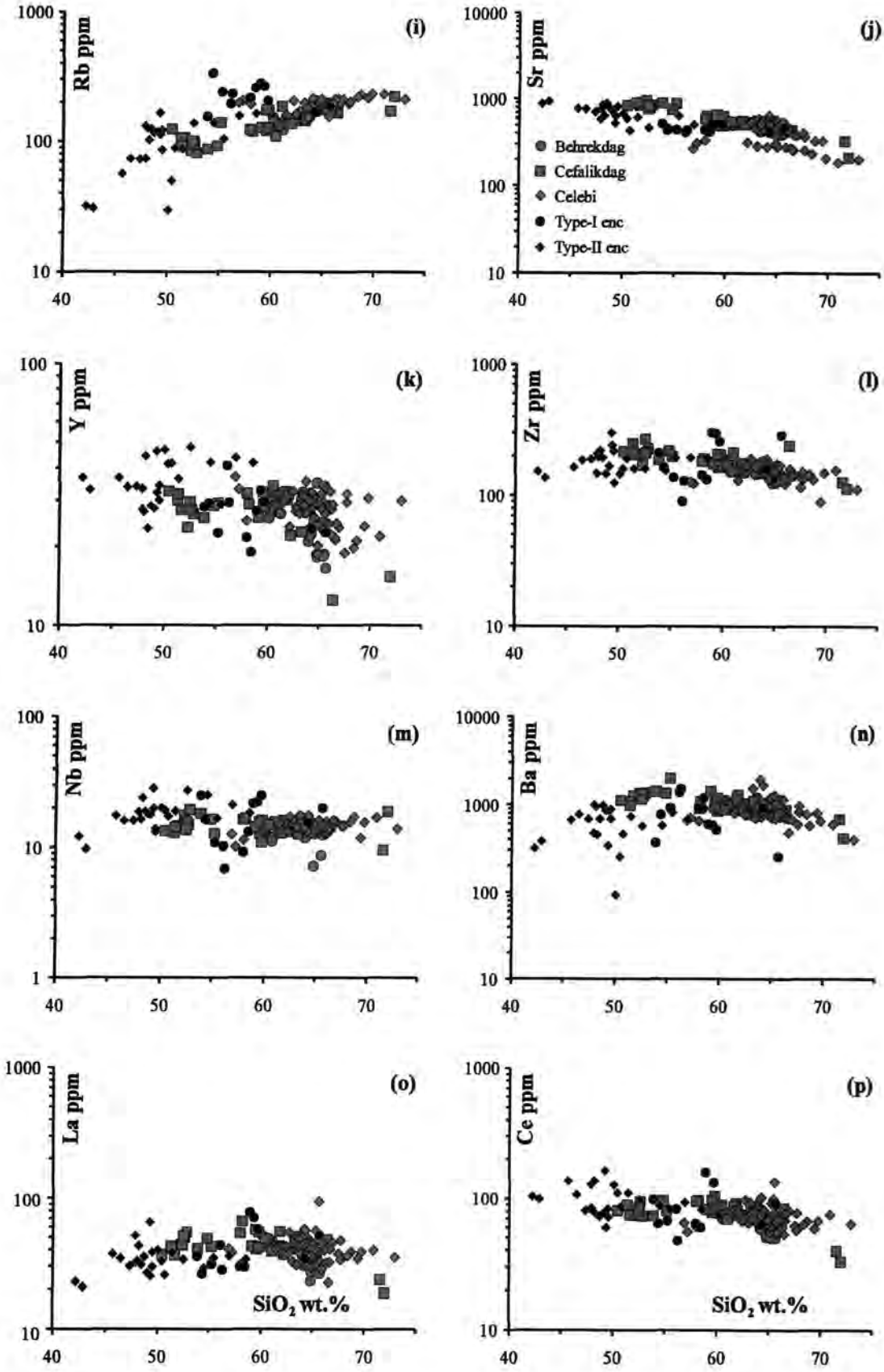

Figure 6.6. (continued).

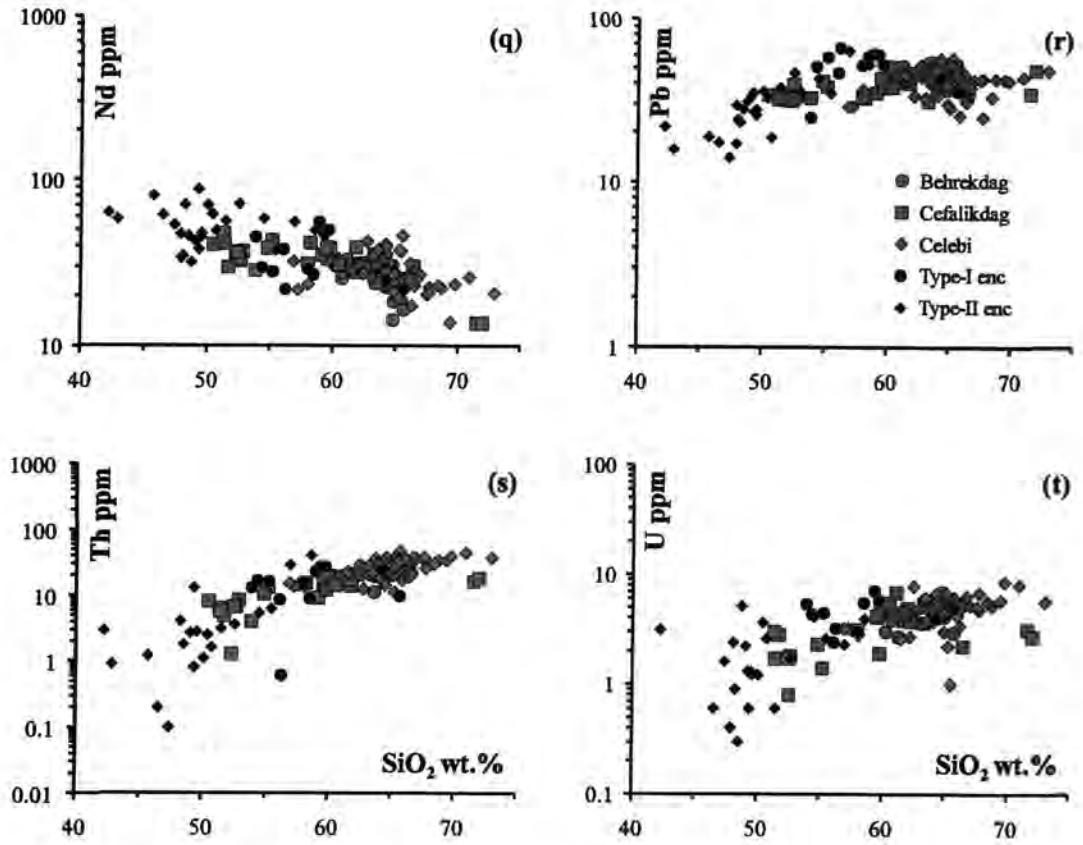

Figure 6.6. (continued).

Rb shows a positive correlation with silica for the BCC intrusive rocks and Type-II enclave. However, it increases until ~58 wt.% SiO_2 and then rather ambiguous for the Type-I enclaves.

Sr remains constant until ~55 wt.% SiO_2 and then decreases for the BCC plutonic rocks, whereas it remains almost constant for the Type-I enclaves. It decreases for the Type-II enclaves.

Y increases slightly until ~62 wt.% SiO_2 and then decreases for the BCC plutonic rocks. It decreases for the Type-I enclaves but it increases for the Type-II enclaves.

Zr demonstrates a constant decrease for the BCC intrusive rocks. It increases until ~50 wt.% SiO_2 and then remains constant for the Type-II enclaves, whereas it decreases for the Type-I enclaves.

Nb remains constant for the BCC plutonic rocks. It increases until ~50 wt.% SiO_2 and then remains constant for the Type-II enclaves. It increases for the Type-I enclaves.

Ba increases slightly with silica until ~55 wt.% SiO_2 and decreases for the BCC plutonic rocks. It increases until ~50 wt.% SiO_2 and then decreases for the Type-II enclaves. It increases until ~56 wt.% SiO_2 and then decreases for the Type-I enclaves.

La, Ce and Nd decrease slightly for the BCC intrusive rocks. However, they decrease for both types of enclave.

Pb, Th and U have positive correlations with silica for the BCC plutonic rocks and Type-II enclaves. However, Pb, Th and U increase until ~58 wt.% SiO_2 and then decrease for the Type-I enclaves.

In Figure 6.6, the Type-II enclaves are, in general, enriched in Sc, V, Co, Cu compared to the BCC plutonic rocks and Type-I enclaves. However, most of the Type-I enclave samples are enriched in Cu compared to the BCC plutonic rocks. In addition, the Type-I enclaves have higher Rb, Th and U contents than the Type-II enclaves.

The rare earth element patterns of the enclaves are characterised by enrichment in the LREE (La_N/Yb_N=7.51-25.82) relative to the MREE and HREE, with small to moderate Eu anomalies (Eu/Eu*=0.45-0.75) (Figure 6.7). Except for sample N139, the Type-I enclaves all exhibit similar REE patterns (Figure 6.7a). Except for sample N226, the Type-II enclaves all display similar REE patterns (Figure 6.7b).

The Type-II enclaves are slightly more enriched in HREE compared to the Type-I enclaves. The Type-II enclaves have smaller Eu anomalies (Eu/Eu*=0.57-0.74) than the Type-I enclaves (Eu/Eu*=0.45-0.75). As can be seen from Figure 6.7a, the REE patterns of the Type-I enclaves are, in general, similar to those of the BCC plutonic rocks. On the other hand, the Type-II enclaves are slightly enriched in LREE (e.g. Pr, Nd) MREE and HREE compared to the BCC plutonic rocks (Figure 6.7b).

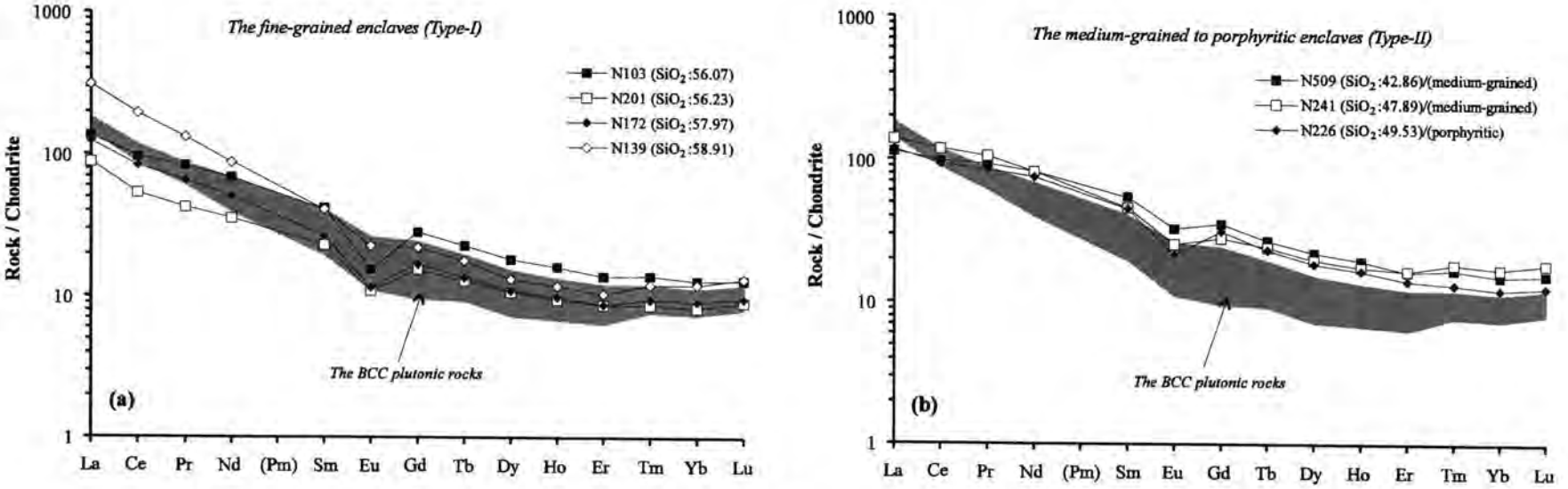

Figure 6.7. Chondrite-normalised REE patterns for the representative enclave samples from the Central Anatolian Massif. Normalisation factors are taken from Boynton, 1984. Abbreviations: BCC-Behrekdag, Cefalikdag and Celebi plutons.

The Type-I enclaves are generally characterised by enrichments in LILEs (e.g. Rb, Ba, Th, U, K) relative to HFSEs (Ta, Nb, Hf, Zr, Y, Yb) (Figure 6.8a). As shown in Figure 6.8a, the multi-element patterns of the Type-I enclaves are generally similar to those of the BCC plutonic rocks.

The Type-II enclaves are only slightly enriched in LILEs compared to HFSEs (Figure 6.8b). As can be seen from Figure 6.8, the Type-I enclaves are slightly more enriched in LILEs and more depleted in HFSEs than the Type-II enclaves. However, the Type-II enclaves are more depleted in LILEs (Rb, Ba, Th, U, K) relative to the BCC plutonic rocks (Figure 6.8b).

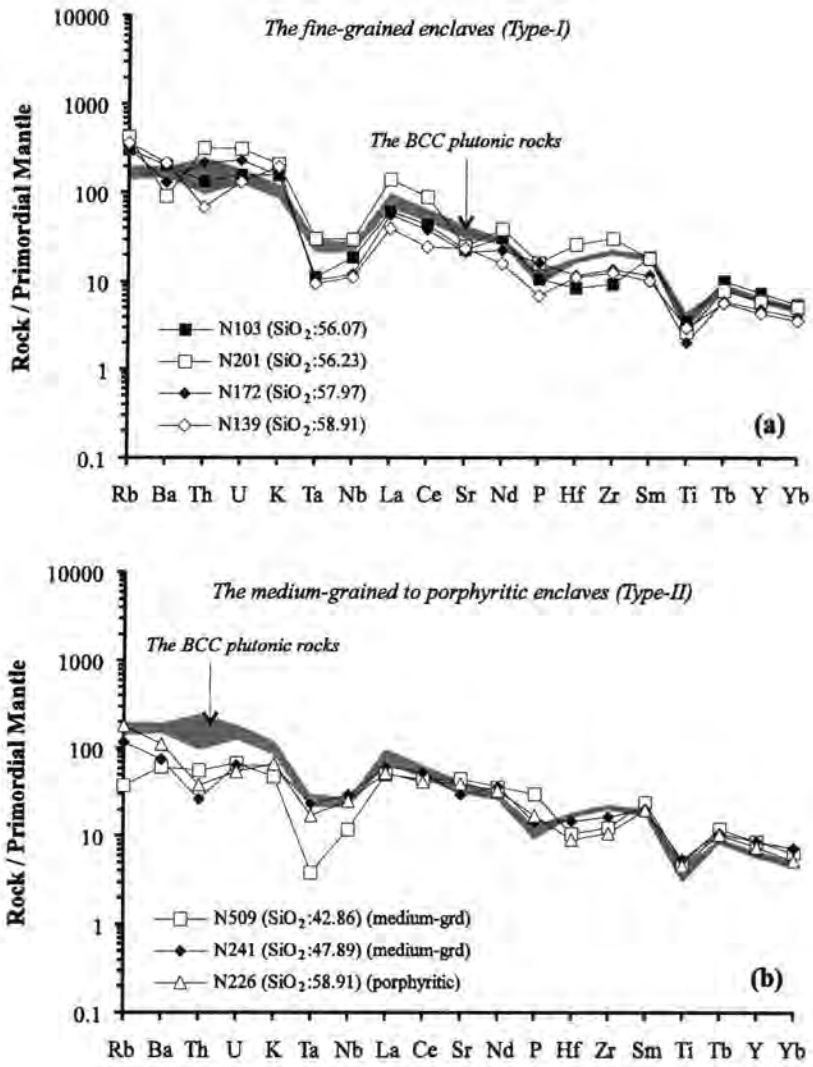

Figure 6.8. Primordial mantle-normalised multi-element diagrams for the enclaves from the Massif Normalisation factors are taken from Sun and McDonough (1989). Abbreviations: BCC-Behrekdag, Cefalikdag, Celebi plutons and grd-grained.

6.5. Origin of the enclaves

The various models and hypotheses that have been proposed to account for the origin of enclaves will now be discussed. In each case, the possible application of models to the enclaves from the BCC (Behrekdag, Cefalikdag, Celebi) plutonic rocks will be assessed.

WALL-ROCK FRAGMENTS (XENOLITHS)

Xenoliths could be originated from assimilation of sedimentary, metamorphic or igneous country rocks by magmas during emplacement of the latter (Didier, 1973; Maury and Didier, 1991). Xenoliths are generally reworked by chemical and mechanical action of the enveloping magma and are partially digested and recrystallised (Nockolds, 1932; Loomis, 1961; Bateman et al., 1963; Link, 1970).

The general characteristics of xenoliths are compared to the enclaves of the BCC plutonic rocks in Table 6.2.

Xenoliths	*Type-I enclaves*	*Type-II enclaves*
show textural evidence of thermal metamorphism and recrystallisation (e.g. granoblastic texture)	igneous textures; and no recrystallisation textures	igneous textures; and no recrystallisation textures
concentrated in the proximity of the margins of plutons	evenly distributed	evenly distributed

Table 6.2. Comparison of xenoliths with the enclaves from the Central Anatolian Massif (e.g. Maury and Didier, 1991).

The following features of ***the enclaves*** in the BCC plutonic rocks are inconsistent with xenoliths:

(i) Neither type of enclave shows any recrystallisation textures (see Section 6.2).

(ii) If the enclaves are fragments of country rocks, they are unlikely to be evenly distributed; most probably they will be more concentrated in the proximity of the margins of the BCC plutons. However, both types of enclave in these plutons are, as mentioned above, widely distributed (see Section 6.1).

(iii) No igneous rocks that could be regarded as the parental materials of the enclaves are found in the country rocks of the BCC plutonic rocks at the present level of exposure.

On the basis of these arguments, it can be concluded that the enclaves are unlikely to be fragments of country rocks (xenoliths).

CUMULATES

Palm (1957) (see also Didier, 1973, pp. 295-297; Didier, 1984) proposed a cumulate hypothesis to explain the origin of the enclaves that he studied. According to his hypothesis, the enclaves could be aggregates of earlier minerals (e.g. calcic plagioclase, hornblende, biotite) that crystallised from a magma parental to both host granites and enclaves.

The knowledge of cumulate enclaves in granitic plutons is very poor (Didier and Barbarin, 1991). Such enclaves have been studied only in some special cases such as in several plutons of the Sierra Nevada batholith (Frost and Mahood, 1987; Dorais et al., 1990; Barbarin, 1991; Reid et al., 1993). Cumulate enclaves provide insights about differentiation histories and magma chamber processes (e.g. Varekamp, 1983; Tait, 1988; Tait et al., 1989; Giannettti and Luhr, 1990; Turbeville, 1992).

The general characteristics of cumulates are compared to the enclaves of the BCC plutonic rocks in Table 6.3.

cumulates	*Type-I enclaves*	*Type-II enclaves*
medium-grained	fine-grained	medium-grained to porphyritic
cumulate textures	no cumulate textures; hypidiomorphic, granular textures	cumulate to hypidiomorphic, granular textures
mineral phases similar to host rocks	mineral phases similar to the BCC plutonic rocks	mineral phases similar to the BCC plutonic rocks
they lie on extrapolation of granite compositions to more mafic values	most of the samples have major and trace element contents similar to the BCC plutonic rocks	most of the samples lie on the extensions of the BCC plutonic rock trends

Table 6.3. Comparison of the general characteristics of cumulates with the enclaves from the BCC plutonic rocks (e.g. Didier, 1973; Didier and Barbarin, 1991).

The following features of ***the Type-I enclaves*** in the BCC plutonic rocks are inconsistent with cumulates:

(i) They are fine-grained rather than medium-grained.

(ii) If they are cumulates, they are likely to have cumulate textures. However, they have a hypidiomorphic, granular texture.

(iii) If they are cumulates, they should lie on the extensions of the BCC plutonic rock trends in the major and trace element variation diagrams (Figures 6.5, 6.6). However, in these diagrams, the Type-I enclaves do not lie on the extrapolation of the BCC plutonic rocks to more mafic values. Most of the samples have major and trace element contents similar to the BCC plutonic rocks (e.g. Figures 6.5c, e, g, h; Figures 6.6a, b, d, e, g, h).

(iv) They have too high total alkalis (Na_2O+K_2O) (6.69-10.16 wt.%) and some incompatible trace element abundances (e.g. Rb, Pb, Th, U) (Figures 6.6i, r, s, t) to be cumulates. The higher Rb, Pb, Th and U contents in the enclaves could result from extensive crystal accumulation (~50 %) if the Type-I enclaves are accumulates of early precipitating phases from granitoid magmas. However, such large amounts of accumulation are not consistent with the similar Fe_2O_3, MgO, CaO, Sc and V (Figures 6.5c, e, f; Figures 6.6a, b) contents in the Type-I enclaves and BCC plutonic rocks.

The Type-I enclaves have mineral phases and mineral compositions similar to the BCC plutonic rocks. For example, plagioclase crystals from both the Type-I enclaves and host rocks are mainly andesine in composition (Figure 6.2). In addition, amphiboles from the Type-I enclaves and host rocks are classified as edenite on the IMA classification scheme (Figure 6.3) (for more explanation see Section 6.3). Furthermore, clinopyroxenes from both the enclaves and host rocks are salite in composition (Figure 6.4).

On the basis of these arguments, it can be concluded that the Type-I enclaves are unlikely to be cumulates.

On the other hand, the following features of ***the Type-II enclaves*** in the BCC plutonic rocks are consistent with cumulates:

(i) They are medium-grained to porphyritic.

(ii) They show cumulate to hypidiomorphic, granular textures.

(iii) They also have mineral phases and mineral compositions similar to those of the BCC plutonic rocks. For example, these enclaves and host rocks are made up of plagioclase, amphibole, biotite, clinopyroxene, alkali feldspar and quartz. However, the enclaves are more enriched in mafic minerals than the host rocks. In addition, plagioclases from both the Type-II enclaves and host rocks are, in general, andesine in composition (Figure 6.2).

(iv) They lie on the extensions of the BCC plutonic rock trends in the major and trace element variation diagrams (Figures 6.5, 6.6). For example, in most of the major element versus silica diagrams (Figures 6.5a, c, e-i), the Type-II enclaves lie on the extrapolation of the BCC plutonic rocks to more mafic values.

Some major elements are plotted against silica to demonstrate that the Type-II enclaves formed as early crystal cumulates of minerals from granitoid magmas (Figure 6.9). Electron microprobe data of clinopyroxene, amphibole, biotite and plagioclase minerals from these enclaves and their host rocks are also plotted on these diagrams.

As can be seen from Figure 6.9, most of the enclaves plot within clinopyroxene, amphibole, biotite, plagioclase space. In Figures 6.9a, b, linear trends of Fe_2O_3 and MgO in plots against silica for the Type-II enclaves and BCC plutonic rocks may indicate that these enclaves formed as early crystal cumulates (clinopyroxene, plagioclase, amphibole and biotite) which precipitated from the granitoid magmas. In Figures 6.9a, b, most of the Type-II enclaves contain more Fe_2O_3 and MgO than the BCC plutonic rocks. In Figures 6.9a, b, amphibole and biotite minerals with high contents of Fe_2O_3 and MgO plot above the extension of the Type-II enclaves and BCC plutonic rock trends, indicating accumulation of amphibole, biotite and to a lesser extent clinopyroxene, plagioclase in the enclaves. However, magnetite as well as amphibole, biotite, clinopyroxene and plagioclase may have accumulated from the granitoid magmas.

In Figure 6.9c, although most of the Type-II enclaves have Al_2O_3 contents similar to the least acidic BCC plutonic rocks, more of these enclaves lie below than the extension of the BCC plutonic rock trend. In Figure 6.9c, plagioclase minerals with a high content of Al_2O_3 plot above the extension of the Type-II enclaves and

BCC plutonic rock trends. On the other hand, amphibole and biotite minerals with low contents of Al_2O_3 plot below the extension of the Type-II enclaves and BCC plutonic rock trends, indicating accumulation of amphibole, biotite and plagioclase in the enclaves.

In Figure 6.9d, most of the Type-II enclaves lie on the extrapolation of the BCC plutonic rocks to more mafic values. Amphiboles from the Type-II enclaves and host rocks plot close to the Type-II enclave trends. On the other hand, plagioclase from the Type-II enclaves and host rocks falls above the BCC plutonic rock trend. In Figure 6.9d, clinopyroxenes are more enriched in CaO compared to plagioclase and amphibole minerals indicating accumulation of clinopyroxene, amphibole, plagioclase and biotite in the enclaves.

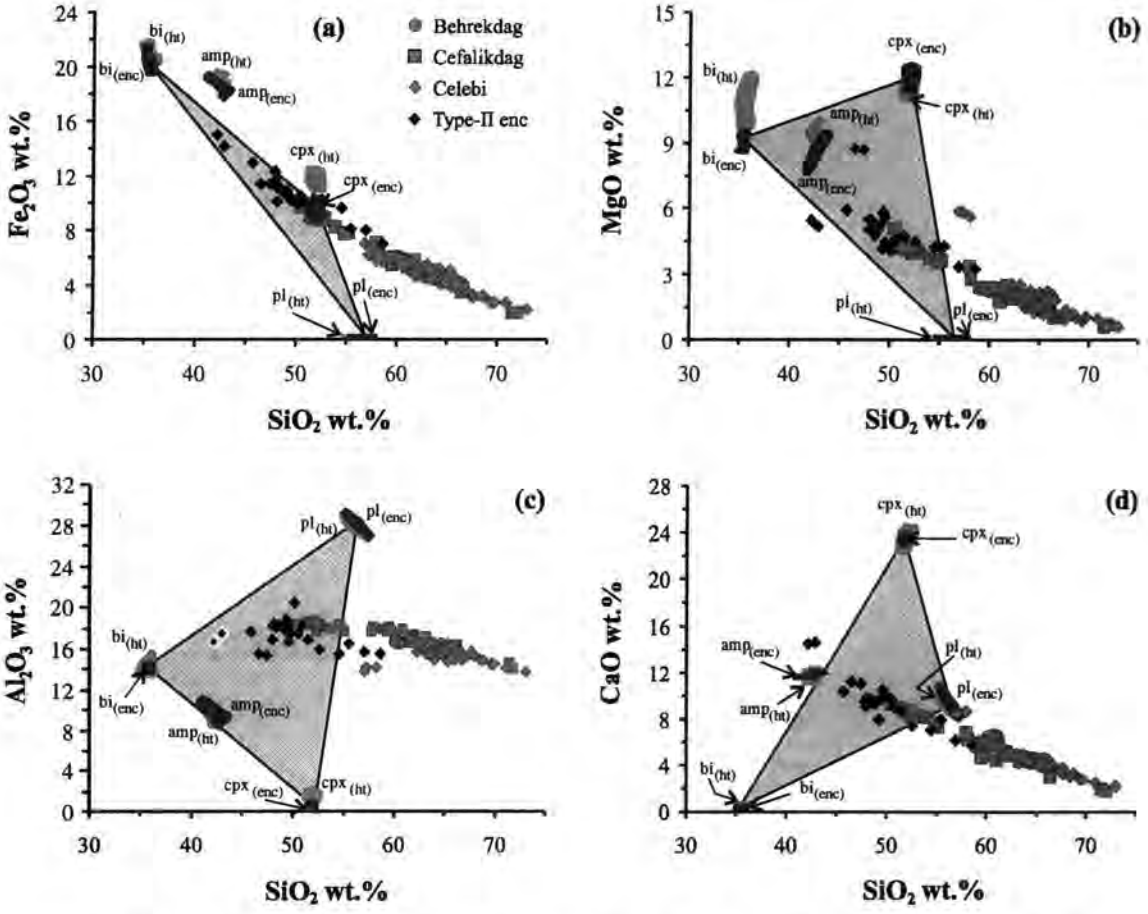

Figure 6.9. Fe_2O_3, MgO, Al_2O_3 and CaO versus silica diagrams for the Type-II enclaves and BCC plutonic rocks. Abbreviations: amp-amphibole, bi-biotite, cpx-clinopyroxene, pl-plagioclase, ht-host and enc-enclave.

On the basis of these arguments, it can be concluded that the Type-II enclaves can reasonably be interpreted as cumulates of early-crystallised minerals (clinopyroxene, plagioclase, amphibole and biotite) from the granitoid magmas.

RESTITES

Bateman et al. (1963, p.17) suggested that the enclaves in some Sierra Nevada granites could be 'refractory material that was not melted when the magma was formed'. Chappell (1966) argued that enclaves in certain granites of the Moonbi district in eastern Australia could also be material residual from the partial melting event. This proposal was developed by later workers (White and Chappell, 1977; Chappell, 1978; Griffin et al., 1978; Hine et al., 1978). Chappell et al. (1987) and Chappell and White (1991) describe the term "restite" to refer to any solid material in a plutonic or volcanic rock that is residual from the partial melting of a source.

There are two types of restite in granitoids. The first, mainly enclosed in S-type granitoids, contains Al-rich minerals and has a clear metamorphic texture. The second, mainly enclosed in I-type granitoids, has an igneous texture.

Pyroxene- and amphibole-bearing clots, and/or clinopyroxene rimmed by amphibole, are common in I-type granitoids. For these, a restite or re-equilibrated restite origin has been put forward by Presnall and Bateman (1973), White and Chappell (1977) and Chappell et al. (1987). However, Wall et al. (1987) argued that mafic clots (which commonly contain plagioclase) in I-type granitoids may represent accumulations of relatively early-crystallised magmatic material. Wall et al. (1987) further argued that clinopyroxene rimmed by amphibole could represent material crystallised from melt at high temperature and lower f_{H2O} which has partially reacted with magma later in its crystallisation history. In addition, some authors have shown that clinopyroxenes have broad P-T-f_{H2O} stability fields in intermediate to silicic magmas (e.g. Rutherford et al., 1985; Clemens et al., 1986).

White and Chappell (1977) argued that complexly zoned and twinned plagioclase is characteristic of modified restite in granitoids. They further argued irregular, patchily zoned, often corroded, calcic cores to be definitive origin of restite. However, Hibbard (1981), Tsuchiyama (1985) and Cocirta (1986) have shown that magma mixing/mingling can also lead to complex resorption and zoning patterns.

The general characteristics of restites are compared to the enclaves of the BCC plutonic rocks in Table 6.4.

restites	*Type-I enclaves*	*Type-II enclaves*
fine-grained to porphyritic	fine-grained	medium-grained to porphyritic
hypidiomorphic, granular textures	hypidiomorphic, granular textures	cumulate to hypidiomorphic, granular textures
show linear correlations for major and trace elements, they should lie on extrapolation of granite compositions to lower silica values	have major and trace element contents similar to the BCC plutonic rocks	generally show linear trends in the major and trace element diagrams, most of the samples lie on the extensions of the BCC plutonic rock trends

Table 6.4. The general characteristics of restites comparison with the enclaves from the BCC plutonic rocks (e.g. Chappell et al., 1987).

The following petrographic features of ***the Type-I enclaves*** in the BCC plutonic rocks are consistent with restites:

(i) They are fine-grained.

(ii) They have a hypidiomorphic, granular texture.

The following features of *the Type-I enclaves* in the BCC plutonic rocks are inconsistent with restites:

(i) They occasionally show fine-grained margins, indicating rapid cooling of mafic magma against granitic host magma (e.g. Vernon, 1983).

(ii) They have acicular minerals, such as apatite, indicating rapid cooling of mafic magma (e.g. Vernon, 1983).

(iii) If they are restites, they should lie on the extensions of the BCC plutonic rock trends in the major and trace element variation diagrams (Figures 6.5, 6.6). However, in these diagrams, the Type-I enclaves do not lie on the extrapolation of the BCC plutonic rocks to more mafic values. Instead, they generally have major and trace element contents similar to the BCC plutonic rocks (e.g. Figures 6.5c, e, g, h; Figures 6.6a, b, d, e, g, h).

On the basis of these arguments, it can be concluded that the Type-I enclaves are unlikely to be restites.

The following geochemical characteristic of ***the Type-II enclaves*** in the BCC plutonic rocks is consistent with restites:

They generally show linear trends on major and trace element diagrams (Figures 6.5, 6.6). Most of the samples lie on the extensions of the BCC plutonic rock trends in Figures 6.5, 6.6. However, if they are aggregates of early-crystallised minerals (see *Cumulates*), they also would lie on the extrapolation of the BCC plutonic rocks to more mafic values. Therefore, their geochemical characteristics may not be conclusive. In addition, Wall et al. (1987) argued that restite unmixing could result in linear trends if all restite fragments are chemically homogeneous. If not, large and/or mafic restite will unmix more readily than small and/or felsic restite, resulting in non-linear trends on Harker variation diagrams.

However, the following characteristics of *the Type-II enclaves* in the BCC plutonic rocks are inconsistent with restites:

(i) They are medium-grained to porphyritic.

(ii) If they are restites they are unlikely to have cumulate textures; most probably they will have hypidiomorphic, granular textures. However, the enclaves generally show cumulate textures.

Although their geochemical characteristics are similar to restites (e.g. linear trends in Harker variation diagrams), on the basis of their grain size (e.g. medium-grained) and textures (e.g. cumulate), the restite model can be excluded for the Type-II enclaves.

MAGMA MIXING (AND/OR MINGLING)

Barbarin (1988) defined the terms "mixing" and "mingling" as follows: the former is restricted to interactions that produce "hybrid rocks" in which the identities of the original magmas are obscured; the latter indicates interactions in which the original magmas retain their identities in the mixture.

Field and petrographic studies (Pitcher and Berger, 1972; Eichelberger, 1975, 1980; Furman and Spera, 1985; Reid and Hamilton, 1987; Hydnman and Foster, 1988) together with fluid dynamic modelling (Sparks et al., 1977, 1984) have

provided evidence that enclaves may result from injection of mafic magma (e.g. as dykes) into more silicic magma.

The general characteristics of magma mixing/mingling are compared to the enclaves of the BCC plutonic rocks in Table 6.5.

Magma mixing/mingling	***Type-I enclaves***	***Type-II enclaves***
fine-grained margins	occasionally fine-grained margins	no fine-grained margins
fine-grained to porphyritic	fine-grained	medium-grained to porphyritic
hypidiomorphic, granular textures	hypidiomorphic, granular textures	cumulate to hypidiomorphic, granular textures
mineral phases similar to host rocks	mineral phases similar to the BCC plutonic rocks	mineral phases similar to the BCC plutonic rocks
the presence of acicular minerals, such as apatite, indicating rapid cooling of mafic magma	acicular apatite	no acicular apatite
show linear correlations for major and trace elements, they should lie on extrapolation of granite compositions to lower silica values	have major and trace element contents similar to the BCC plutonic rocks	generally show linear trends in the major and trace element diagrams, most of the samples lie on the extensions of the BCC plutonic rock trends

Table 6.5. The general characteristics of magma mixing/mingling comparison with the enclaves from the Massif (e.g. Vernon, 1983).

The following features of ***the Type-I enclaves*** in the BCC plutonic rocks are consistent with magma mixing/mingling:

(i) They occasionally have fine-grained margins, indicating rapid cooling of mafic magma against granitic host magma (e.g. Didier, 1973; Vernon, 1983).

(ii) They are fine-grained, reflecting rapid crystallisation and quenching of hot mafic magma as it mingled with relatively cooler felsic magma (e.g. Fernandez and Barbarin, 1991).

(iii) They have a hypidiomorphic, granular texture.

(iv) They have mineral phases similar to the BCC plutonic rocks. For example, these enclaves and host rocks are made up of plagioclase, alkali feldspar, clinopyroxene, amphibole, biotite and quartz. However, the enclaves are more enriched in mafic minerals (e.g. amphibole, biotite, clinopyroxene) than the host rocks (Appendix C-I).

(v) They have acicular apatites, indicating rapid cooling of mafic magma (Didier, 1973, 1987; Reid et al., 1983).

(vi) Most of the samples have major and trace element contents similar to the BCC plutonic rocks (e.g. Figures 6.5c, e, g, h; Figures 6.6a, b, d, e, g, h). In addition, the Type-I enclaves have high silica value similar to the host rocks. Zorpi et al. (1991) argued that high silica contents of enclaves result from a migration of silica from host rocks. They further argued that migration of silica from the host rocks would be related to silica contents of host rocks.

(vii) Most of the samples are enriched in some elements, such as K, Rb and Pb, compared to the host rocks (Figures 6.5i; 6.6i, r). These enrichments were also observed by Zorpi et al. (1989, 1991) for the calc-alkaline plutons of Sardinia and Corsica. They argued that volatile migration between the magmas, from the acid to the mafic component, could result in enrichments in certain elements, such as K, P, Rb, Cs and Zr in enclaves. Furthermore, most of the Type-I enclaves (including Type-II enclaves) are enriched in MnO and Cu (Figures 6.5d; 6.6f) compared to the host rocks. These enrichments may indicate hydrothermal alteration of the enclaves, although this has not been observed macroscopically or microscopically.

(viii) The REE and multi-element patterns of the Type-I enclaves are generally similar to those of the BCC plutonic rocks (Figures 6.7a; 6.8a). Some authors argued that this could be due to re-equilibration of REE, LILE and HFSE between enclaves and their host rocks (e.g. Holden et al., 1987; Allen, 1991; Barbarin, 1991).

The following feature of *the Type-I enclaves* is inconsistent with magma mixing/mingling:

Their mineral compositions are similar to the BCC plutonic rocks. For example, plagioclase crystals from both the Type-I enclaves and host rocks are mainly andesine in composition (Figure 6.2). In addition, amphiboles from these enclaves and host rocks are edenite (Figure 6.3). Furthermore, clinopyroxenes from both the enclaves and host rocks are salite in composition (Figure 6.4). This compositional similarity has been also observed by Reid et

al. (1983), Vernon (1983, 1991), Didier (1987). Vernon (1991) argued that during the cooling stage of enclaves, diffusion in the melt could cause the exchange of elements between enclaves and host rocks. This would induce reaction between crystals and melt in enclaves, which may account for the compositional similarity of minerals in enclaves and host rocks. On the other hand, Van der Laan and Wyllie (1993) argued that partly crystallised enclaves can approach chemical equilibrium with silicic host magma although still retaining higher modal amounts of mafic minerals. They further argued that if the mafic minerals are in equilibrium with the melt in the mafic domain, and if the melts in both mafic and silicic domains are almost mutually equilibrated, then the minerals in enclaves should be also close to equilibrium with the melt in the silicic domain. Therefore, they should be similar to the mafic minerals that precipitated from the silicic host magma.

On the basis of these arguments, it can be concluded that the Type-I enclaves originated by magma mixing/mingling.

The following features of ***the Type-II enclaves*** in the BCC plutonic rocks are consistent with magma mixing/mingling:

(i) They have mineral phases similar to the BCC plutonic rocks. For example, these enclaves and host rocks are made up of amphibole, plagioclase, clinopyroxene, biotite, alkali feldspar and quartz. However, the enclaves are more enriched in mafic minerals (e.g. amphibole, biotite) and depleted in silicic minerals (e.g. alkali feldspar, quartz) than the host rocks (Appendix C-I).

(ii) They show linear trends in most of the major and trace element diagrams (e.g. Figures 6.5c, d, f, i; Figures 6.6a, b, d, g, h). Most of the samples lie on the extensions of the BCC plutonic rock trends in Figures 6.5, 6.6.

The following features of *the Type-II enclaves* are inconsistent with magma mixing/mingling:

(i) They do not have fine-grained margins, reflecting rapid cooling of mafic magma against host acidic magma.

(ii) They are medium-grained to porphyritic.

(iii) They show cumulate to hypidiomorphic, granular textures.

(iv) Their mineral compositions are similar to the BCC plutonic rocks. For example, plagioclase crystals from both the Type-II enclaves and host rocks are generally andesine in composition (see Section 6.3).

(v) They do not have acicular minerals to indicate rapid cooling of a mafic magma.

On the basis of these arguments, it can be concluded that the Type-II enclaves did not originate from magma mixing/mingling.

6.6. Summary

Two types of igneous enclave have been recognised in the BCC (Behrekdag, Cefalikdag, Celebi) plutonic rocks: (i) fine-grained (Type-I); and (ii) medium-grained to porphyritic with feldspar megacrysts (Type-II).

The Type-I enclaves have been interpreted as magma mixing/mingling products resulted from injection of mafic magma into a more acidic magma. This is evident from their fine-grained margins which indicates rapid cooling of mafic magma against more acidic magma. In addition, they are fine-grained which reflects rapid crystallisation and quenching of hot mafic magma against relatively cooler acidic magma. Moreover, they have acicular apatites, indicating rapid cooling of mafic magma. The Type-I enclaves are generally enriched in K, Rb and Pb, compared to the host rocks. These enrichments have been explained by volatile migration between the magmas, from the acid to the mafic component. The Type-I enclaves and host rocks show similar REE and multi-element patterns. This has been explained by re-equilibration of REE, LILE and HFSE between the enclaves and their host rocks.

The Type-II enclaves have been interpreted as cumulates of early-crystallised minerals from the granitoid magmas. This is well supported by their grain size (medium-grained and porphyritic) and textures (cumulate to hypidiomorphic, granular). The close similarity in mineral phases and mineral compositions between the enclaves and the BCC plutonic rocks also indicates that the enclaves are accumulates of early precipitating phases from the granitoid magmas. In the major and trace element variation diagrams, they lie on the extensions of the BCC plutonic

rock trends, supporting the cumulate origin for the Type-II enclaves. Some major elements (Fe_2O_3, MgO, Al_2O_3 and CaO) on Harker diagrams show that they formed as early crystal cumulates of minerals (clinopyroxene, plagioclase, amphibole and biotite) from the granitoid magmas.

The general features of the Type-I and Type-II enclaves have been summarised in Table 6.6.

Enclave	*Type-I (fine-grained varieties)*	*Type-II (medium to porphyritic varieties)*
Rock unit	quartz diorite, quartz monzodiorite	gabbro (1), quartz diorite (2)
Shape	rounded to ellipsoidal	rounded to ellipsoidal
Contact	sharp	sharp
Grain size	fine-grained	medium-grained (1) and porphyritic (2)
Texture	hypidiomorphic, granular	cumulate (1); hypidiomorphic, granular (2)
Mafic phase	cpx, amp, bi	amp, cpx, bi (1); cpx, amp, bi (2)
Origin	magma mixing/ mingling	cumulate
Host	monzodiorite to granite	

Table 6.6. The macroscopic and microscopic characteristics of the enclaves from Central Anatolian Massif. Abbreviations: cpx-clinopyroxene, amp-amphibole and bi-biotite.

Chapter 7
PETROGENESIS

Introduction

The objective of this Chapter is to produce a petrogenetic model that will explain the observed compositional variations within and between the Central Anatolian plutonic rocks. This Chapter also presents new Sr and Nd isotopic data for the plutonic rocks.

7.1. Sr and Nd isotope geochemistry

Sr and Nd isotope ratios, both initial measured, and Rb, Sr, Sm and Nd concentrations of the Central Anatolian plutonic rocks are listed in Table 7.1. As can be seen from this Table, the plutonic rocks have high initial $^{87}Sr/^{86}Sr$ and low initial $^{143}Nd/^{144}Nd$ ratios.

Initial $^{143}Nd/^{144}Nd$ ratios are plotted against initial $^{87}Sr/^{86}Sr$ ratios for the plutonic rocks in Figure 7.1, together with published data for mantle reservoirs (DePaolo, 1988). Unfortunately, there are insufficient isotope data to define crustal end-member compositions of the Central Anatolian Massif, so the metasedimentary rock data (Palaeozoic-270 Ma) from Central Europe (Voshage et al., 1990) have been used as the crustal contaminants.

As can be seen from Figure 7.1, the Central Anatolian plutonic rocks fall within a narrow range for both initial $^{87}Sr/^{86}Sr$ (0.70804 to 0.70964) and $^{143}Nd/^{144}Nd$ (0.512206 to 0.512303) ratios. They plot in the high $^{87}Sr/^{86}Sr$ and low $^{143}Nd/^{144}Nd$ quadrant, in the range characteristic of continental crustal sources or mantle sources with large continental crustal components.

Initial $^{87}Sr/^{86}Sr$ ratios range between 0.70896 and 0.70964 for the BCC (Behrekdag, Cefalikdag, Celebi) rock samples and 0.70822 and 0.70838 for the H (Hamit) rock samples. The sample from the B (Baranadag) pluton has the lowest value (0.70804) of analysed samples for the Central Anatolian plutonic rocks.

Table 7.1. Isotopic analysis of the intrusive samples from the Central Anatolian Massif. Abbreviations: qmz-quartz monzonite, mzdi-monzodiorite, gr-granite, nemzsy-nepheline monzosyenite and qsy- quartz syenite.

Pluton	Sample no	Rock type	Age (Ma)	SiO_2 wt.%	Rb ppm	Sr ppm	$^{87}Rb/^{86}Sr$	$^{87}Sr/^{86}Sr_{(meas)}$	$^{87}Sr/^{86}Sr_i$	εSr	Sm ppm	Nd ppm	$^{147}Sm/^{144}Nd$	$^{143}Nd/^{144}Nd_{(meas)}$	$^{143}Nd/^{144}Nd_i$	εNd
Behrekdag	N2	qmz	79.5	60.11	136	546	0.7194	0.71004±11	0.70923	68.5	5.84	35.59	0.09885	0.512263±4	0.512212	-6.3
Cefalikdag	N78	mzdi	66.6	53.86	93	891	0.3024	0.70972±09	0.70943	71.0	7.20	38.40	0.11290	0.512256±5	0.512207	-6.7
	N20	qmz	66.6	61.82	143	508	0.8166	0.71002±08	0.70924	68.4	7.14	42.19	0.10182	0.512295±5	0.512251	-5.9
	N395	gr	66.6	71.53	160	356	1.2994	0.71087±19	0.70964	74.0	2.50	16.50	0.09113	0.512300±5	0.512260	-5.7
Celebi	N75	gr	70.0	65.07	187	462	1.1695	0.71028±35	0.70896	64.7	6.04	36.35	0.10003	0.512298±5	0.512253	-5.5
Baranadag	N26	mz	76.4	58.44	192	882	0.6286	0.70873±11	0.70804	51.6	9.90	60.12	0.09913	0.512324±5	0.512274	-5.2
Hamit	N33	nemzsy	70.0	53.32	213	1253	0.4915	0.70875±12	0.70826	54.6	13.35	79.18	0.10145	0.512349±5	0.512303	-4.8
	N285	nemzsy	70.0	56.09	241	1300	0.5374	0.70876±11	0.70822	54.0	10.36	63.48	0.09824	0.512348±5	0.512303	-4.8
	N290	qsy	70.0	66.78	365	240	4.3936	0.71275±09	0.70838	56.3	6.33	43.61	0.08740	0.512307±5	0.512267	-5.5

[$\lambda\ ^{87}Rb=1.42*10^{-11}\ yr^{-1}$
$(^{87}Rb/^{86}Sr)_{UR}=0.0816$; $(^{87}Sr/^{86}Sr)_{UR}=0.7045$ (DePaolo, 1988);
$\lambda\ ^{147}Sm=6.54*10^{-12}\ yr^{-1}$
$(^{147}Sm/^{144}Nd)_{CHUR}=0.1967$; $(^{143}Nd/^{144}Nd)_{CHUR}=0.512638$ (Jacobsen and Wasserburg, 1984)].

Initial $^{143}Nd/^{144}Nd$ ratios range from 0.512206 to 0.512252 for the BCC rock samples, and from 0.512216 to 0.512303 for the H rock samples. The sample from the B intrusion has a value of 0.512227.

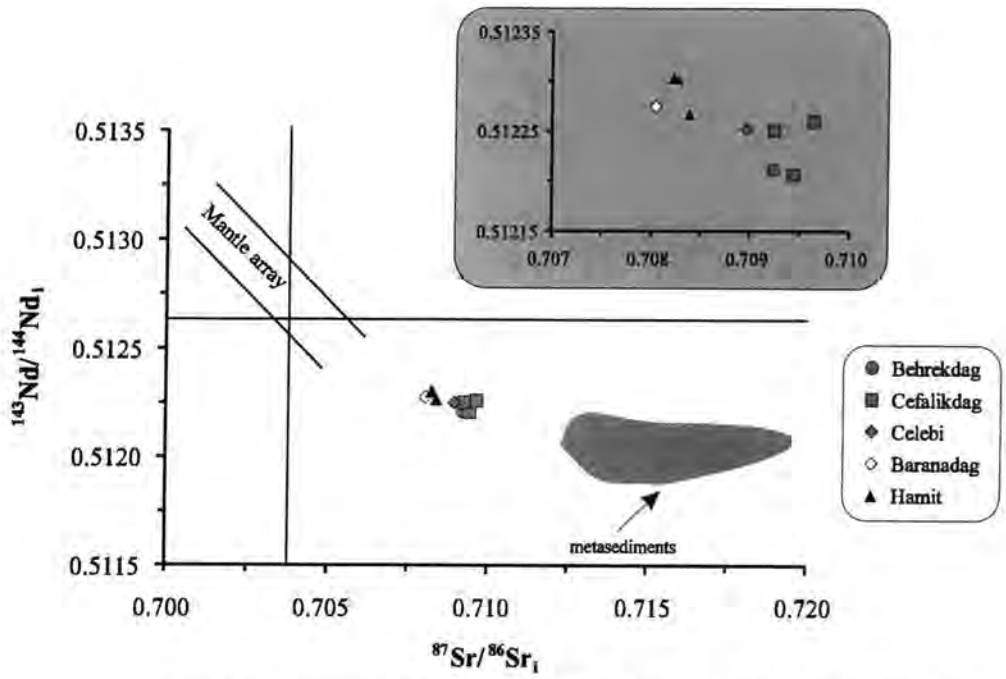

Figure 7.1. Initial $^{143}Nd/^{144}Nd$ ratios versus initial $^{87}Sr/^{86}Sr$ ratios diagram for the Central Anatolian plutonic rocks. The mantle array is after DePaolo (1988). The metasedimentary rock data are taken from Voshage et al. (1990). The inset graph shows the Central Anatolian plutonic rock data in detail.

7.1.1. Interpretation of the Sr and Nd data

The isotopic ratios shown in Figure 7.1 provide a good framework for addressing several petrogenetic aspects for the Central Anatolian plutonic rocks. As can be seen from Figure 7.1, the main problem to be solved is whether the distinctive trace element and isotopic characteristics can be related to mantle source enrichment by recycling of crustal material (e.g. Gill, 1981; Sun and McDonough, 1989), or to fractional crystallisation combined with crustal assimilation (AFC) (e.g. Hildreth and Moorbath, 1988).

Mantle source enrichment as used here describes the process of contamination of mantle source by recycling of crustal material during subduction. Subduction of sediment and/or altered oceanic crust releases aqueous fluids and/or siliceous melts into the overlying mantle wedge via a series of dehydration reactions of the hydrous phases. This process results in enrichment in large ion lithophile elements (LILE) in the mantle wedge. The introduction of aqueous fluids

and/or siliceous melts lowers the solidus of the peridotites, initiating melting. The mixture of fluids and melts and mantle undergoes partial melting to produce magmas enriched in LILEs.

Mantle source enrichment is well documented in many subduction-related settings (e.g. Gill, 1981; White and Dupré, 1986; McDermott et al., 1993). It is also supported by ^{10}Be anomalies (e.g. Brown et al., 1982; Tera et al., 1986) and high $^{207}Pb/^{204}Pb$ ratios in modern volcanic arc basalts (e.g. Kay et al., 1978; White and Dupré, 1986). However, it is rarely discussed in connection with plutonic rocks (e.g. Hill et al., 1986; Von Blanckburg et al., 1992; Tommasini et al., 1995).

Mantle source enrichment is difficult to identify by major and trace element geochemistry in plutonic rocks because all intrusive members, and thus their elemental concentrations, are usually modified by fractional crystallisation. Nevertheless, a combination of sensitive isotopic indicators, such as Sr and Nd, which have high contaminant/mantle concentration ratios, with an abundant element such as O (oxygen) which has approximately equal concentrations in mantle and contaminant, often enables a distinction to be made between source contamination and other processes (e.g. James, 1981).

Mantle source enrichment can be modelled by mixing of two components. A general mixing model first presented by Langmuir et al. (1978) was subsequently adapted by DePaolo and Wasserburg (1979) for use with the epsilon notation of Nd and Sr. The two-component mixing equation based on the work of Langmuir et al. (1978) is as follows:

$$\varepsilon_m^x = \left[\frac{\varepsilon_a^x X_a F + \varepsilon_b^x X_b (1-F)}{X_a F + X_b (1-F)} \right] \qquad \text{(Eq. 7.1)}$$

where;

ε_a^x : *isotopic parameter of element X in crust*
ε_b^x : *isotopic parameter of element X in mantle*
X_a : *concentration of element X in crust*
X_b : *concentration of element X in mantle*
F : *mass fraction of crust in mixture*

AFC process was first considered by Bowen (1928). He emphasised that assimilation is not a simple mixing process but has a minimum of three end-members, namely the magma, the country rocks and the cumulates.

It is defined as the contamination by assimilation of wall-rock coupled to concurrent fractional crystallisation. It was modelled by DePaolo (1981). He derived the equations for both trace element and isotopic variations (Equations 7.2-7.7). He proved that the tenet of the simple mixing model, that the concentration in the magma would change in the direction of that in the wall-rock, was not necessarily true if fractional crystallisation was also operating.

(a) General equations applicable to most of the cases:

$$C_m / C_m^0 = F^{-z} + \left(\frac{r}{r-1}\right)\frac{C_a}{zC_m^0}\left(1 - F^{-z}\right) \qquad \text{(not applicable for } r=1\text{)} \qquad \text{(Eq. 7.2)}$$

$$C_m / C_m^0 = 1 + \left(\frac{r}{r-1}\right)\frac{C_a}{C_m^0}\ln F^{-z} \qquad \text{(special case } r+D=1 \text{ and } z=0\text{)} \qquad \text{(Eq. 7.3)}$$

(b) For the isotopic ratio (ε):

$$\frac{\varepsilon_m - \varepsilon_m^0}{\varepsilon_a - \varepsilon_m^0} = 1 - (C_m^0 / C_m)F^{-z} \qquad \text{(Eq. 7.4)}$$

where;

M_m : *mass of magma*
M_m^o : *mass of original magma*
M_c : *crystallisation rate (mass/unit time)*
M_a : *assimilation rate (mass/unit time)*
C_a : *elemental concentration in wall-rock*
C_m : *elemental concentration in the contaminated magma*
C_m^o : *elemental concentration in the original magma*
D : *bulk solid/liquid partition coefficient for the element between the fractionating crystalline phases and the magma*
DC_m : *elemental concentration in crystallising phases*
ε_m : *isotopic ratio in the contaminated magma*
ε_m^o : *isotopic ratio in the original magma*
ε_a : *isotopic ratio in wall-rock*

$$F = \frac{M_m}{M_m^o} \qquad \textit{(the ratio of magma mass to original magma mass)} \qquad \text{(Eq. 7.5)}$$

$$r = \frac{M_a}{M_c} \qquad \textit{(the ratio of the rate of assimilation to fractional crystallisation)} \qquad \text{(Eq. 7.6)}$$

$$z = \frac{r + D - 1}{r - 1} \qquad \text{(Eq. 7.7)}$$

7.1.1.1. Mantle source enrichment or fractional crystallisation combined with crustal assimilation

In order to assess the relative importance of source enrichment processes in the origin of the Central Anatolian plutonic rocks, the plot of initial $^{143}Nd/^{144}Nd$ ratios against initial $^{87}Sr/^{86}Sr$ ratios for the plutonic rocks is re-examined (Figure 7.2).

In Figure 7.2, the mantle source enrichment process has been modelled using the mixing equation of Langmuir et al. (1978) (Equation 7.1). In the modelling, depleted mantle (from Zindler and Hart, 1986) and melt from depleted mantle (from Hawkesworth et al., 1991) are used as a "mantle" end-member, and, an average of metasedimentary rocks (from Voshage et al., 1990) is used as a "crustal" end-member (Table 7.2). The mixing curve in Figure 7.2 has been marked off in increments of the weight fraction (*F*) of the crustal component.

A mixing curve representing contamination of depleted mantle with crust is shown in Figure 7.2a. A mixing curve between melt from depleted mantle and crust is demonstrated in Figure 7.2b.

	Depleted mantle[a]	***Melt from depleted mantle[b]***	***Contaminant (C)[c]***	
				average
$^{87}Sr/^{86}Sr_i$	0.7027	0.7028	0.71514-0.71924	0.71553
$^{143}Nd/^{144}Nd_i$	0.5131	0.5130	0.51192-0.51213	0.51202
Sr ppm	13.3	54	137-296	229
Nd ppm	0.8	4.4	31-59	39

Table 7.2. Composition of end-members used to assess source enrichment processes in the origin of the Central Anatolian plutonic rocks. Data sources are: (a) Zindler and Hart (1986); (b) Hawkesworth et al. (1991); and (c) Voshage et al. (1990).

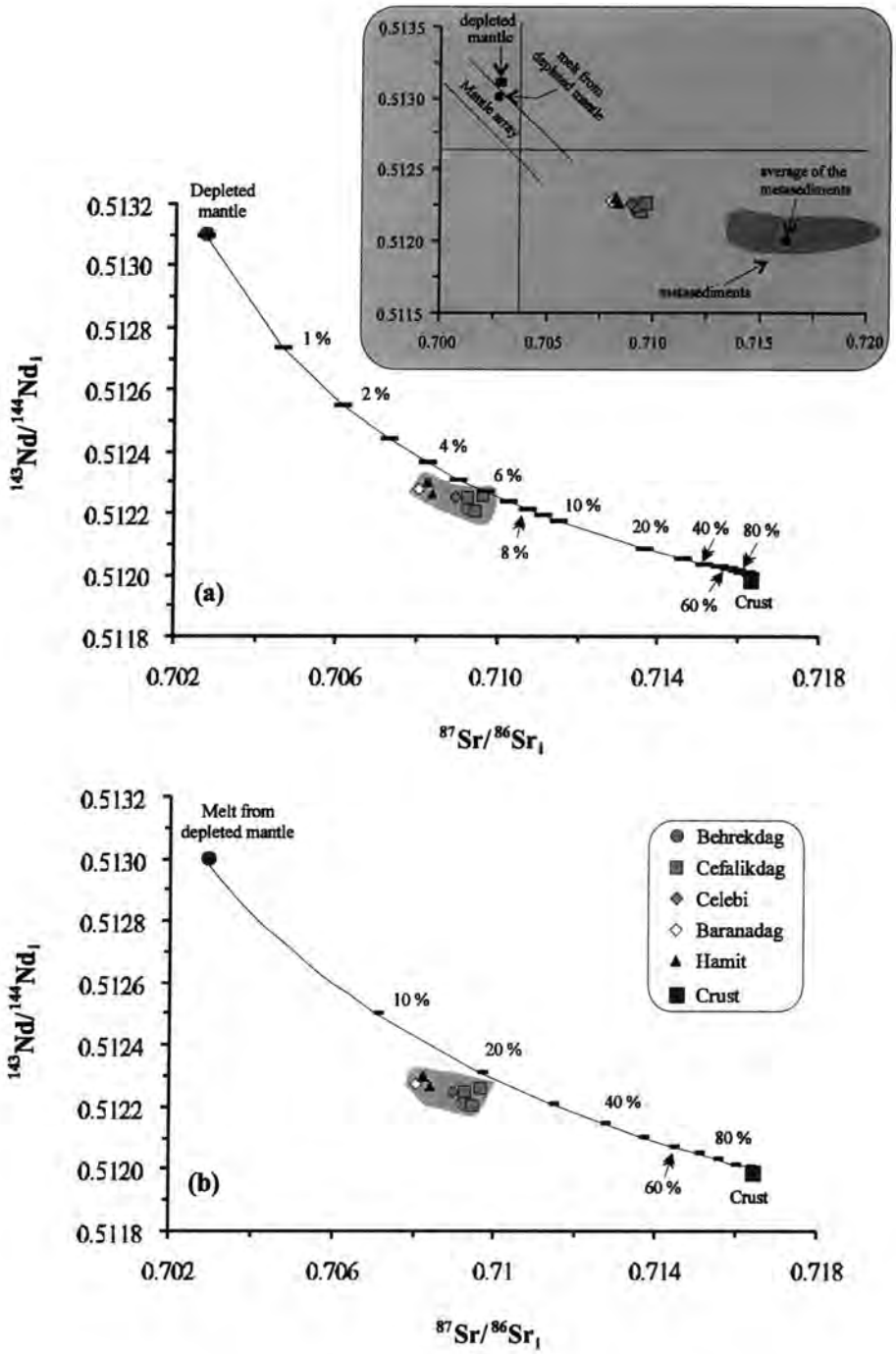

Figure 7.2. Mantle source mixing model to explain Sr and Nd isotope variations in the Central Anatolian plutonic rocks. Mixing curves are calculated for (a) mantle + crust, and (b) melt from depleted mantle + crust. Depleted mantle is from Zindler and Hart (1986), melt from depleted mantle is taken from Hawkesworth et al. (1991) and average composition of metasedimentary rocks is taken from Central Europe (Voshage et al., 1990). Tick marks on the mixing curves show the percentage of crust added. The inset graph shows depleted mantle, melt from depleted mantle and metasedimentary rocks in relation to the plutonic rocks.

In Figure 7.2, the mixing curves pass close to the Central Anatolian plutonic rocks. As shown in Figure 7.2a, the sediment contribution to depleted mantle is between 4% and 6%. However, the addition of sediment component to melt from depleted mantle is much greater (~15-20%) (Figure 7.2b). These large amounts are inconsistent with the amount of sediment commonly believed to be added to a subduction zone mantle source (e.g. Whitford et al., 1981; Vroon et al., 1993). Therefore, the actual sediment contribution to depleted mantle produce source(s) for the Central Anatolian plutonic rocks is likely to be closer to 4-6% than to 15-20%.

Initial $^{87}Sr/^{86}Sr$ and $^{143}Nd/^{144}Nd$ ratios of the Central Anatolian plutonic rocks are plotted against SiO_2 (Figure 7.3) to further assess AFC or source enrichment processes in the origin of these rock types.

In Figure 7.3, estimation of the compositions of possible parental magma(s) and also crustal component(s) for the Central Anatolian plutonic rocks is a very difficult problem, as there are no rock samples that can be taken as representative of parental magmas. All Anatolian plutonic rock types have high initial $^{87}Sr/^{86}Sr$ and low initial $^{143}Nd/^{144}Nd$ ratios. The chosen values for parental magmas are similar to those of the least acidic samples for the BCC, B and H intrusive rocks though.

In Figure 7.3, the least acidic sample (N78- from the Cefalikdag pluton) in the BCC plutonic rocks is a cumulate (see section 7.2.1 for more explanation). It appears only as a subordinate border facies. Therefore, it is not regarded as parental magma for the BCC intrusive rocks. On the other hand, parental magma chosen for the BCC intrusive rocks (source I-S_I) has initial $^{87}Sr/^{86}Sr$ and $^{143}Nd/^{144}Nd$ ratios of 0.70940 and 0.51220 (Table 7.3). The least acidic sample (N31- from the Hamit pluton) chosen as parental magma for the B and H intrusive rocks (source II-S_{II}) has initial $^{87}Sr/^{86}Sr$ and $^{143}Nd/^{144}Nd$ ratios of 0.70826 and 0.51230.

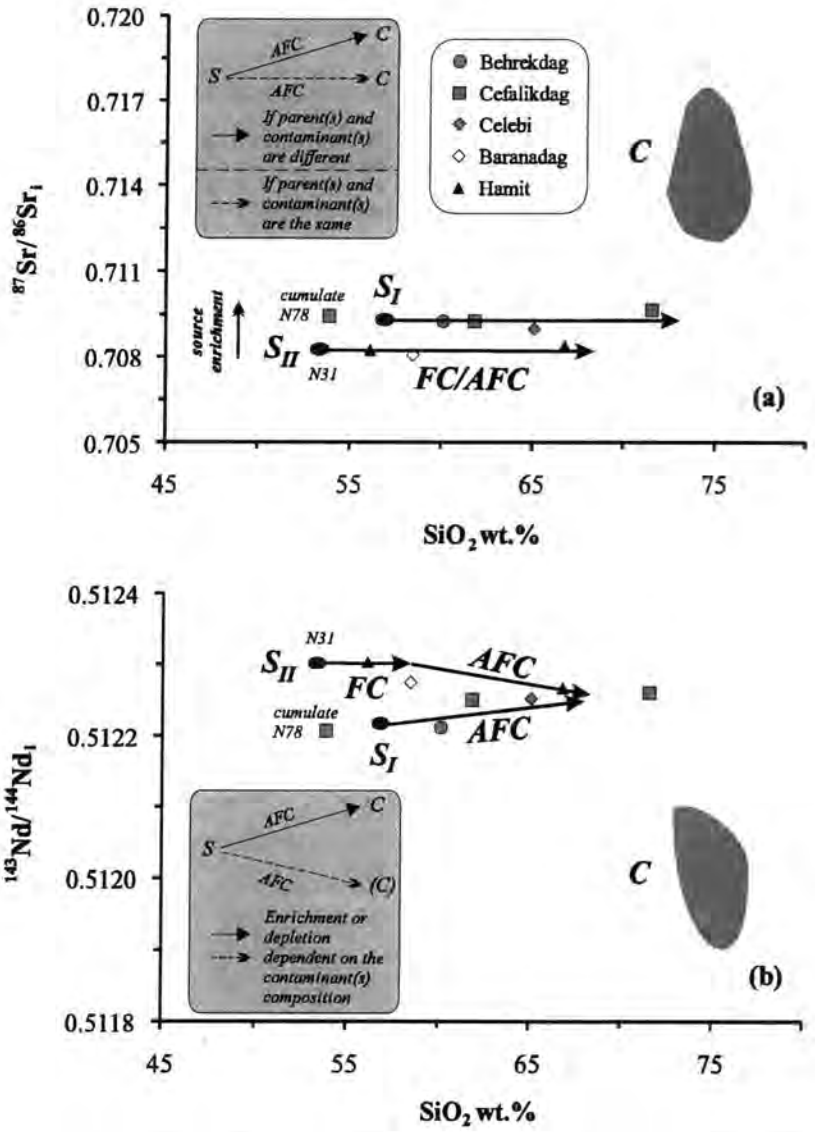

Figure 7.3. (a) Initial $^{87}Sr/^{86}Sr$ ratios versus silica; and (b) initial $^{143}Nd/^{144}Nd$ ratios versus silica diagrams for the Central Anatolian plutonic rocks. The metasedimentary rock data are taken from Voshage et al. (1990). Abbreviations: S- source, FC- fractional crystallisation, AFC- coupled fractional crystallisation and crustal assimilation and C- crust.

	Source I (S_I) for the BCC (Behrekdag, Cefalikdag, Celebi) plutonic rocks	***Source II (S_{II}) for the B (Baranadag) and H (Hamit) plutonic rocks (N31- from the H pluton)***	***Contaminant (C)$^{\#}$***
SiO_2 wt.%	56	52	73-78*
$^{87}Sr/^{86}Sr_i$	0.70940	0.70826	0.71514-0.71924
$^{143}Nd/^{144}Nd_i$	0.51220	0.51230	0.51192-0.51213

*Table 7.3. Table showing possible parental magmas and contaminant for the Central Anatolian plutonic rocks (see text for more explanation). $^{\#}$- Metasedimentary rock data are taken from Central Europe (Voshage et al., 1990), and *- estimated values from published data.*

In Figure 7.3, radiogenic isotope ratios do not show well-defined correlations against silica. If parent(s) and contaminant(s) are different, combined assimilation and fractional crystallisation (AFC) causes enrichment in initial $^{87}Sr/^{86}Sr$ ratios with increasing silica. If not, AFC causes no change in initial $^{87}Sr/^{86}Sr$ ratios with increasing silica.

Two contrasting groups can be seen in Figures 7.3a and b: (i) the BCC rock samples; and (ii) the H rock samples (including the B rock sample). Figure 7.3a shows that the BCC rock samples (derived from source I-S_I) have slightly higher initial $^{87}Sr/^{86}Sr$ ratios than the H rock samples, including the B sample (derived from source II-S_{II}). However, the BCC and H rock samples (including the B sample) generally show no correlation with silica, indicating that the contaminant and parental magmas of the BCC, B and H rock samples have similar initial $^{87}Sr/^{86}Sr$ ratios.

In Figure 7.3, the metasedimentary rocks from Central Europe have higher initial $^{87}Sr/^{86}Sr$ and lower initial $^{143}Nd/^{144}Nd$ ratios than the BCC, B and H rock samples. This may indicate that the crustal rock compositions in the Central Anatolian Massif are less radiogenic in terms of Sr, and more radiogenic in terms of Nd, compared to the metasedimentary rocks from Central Europe (Voshage et al., 1990).

Figure 7.3b demonstrates that the BCC rock samples (derived from source I-S_I) have relatively low initial $^{143}Nd/^{144}Nd$ ratios that increase with increasing silica, indicating the importance of a combined assimilation and fractional crystallisation process in the origin of these rock types.

On the other hand, the H rock samples together with the B rock sample (derived from source II-S_{II}) mostly have high initial $^{143}Nd/^{144}Nd$ ratios, which remain almost constant until ~56 wt.% SiO_2 and then decrease with increasing silica (on limited data). This may indicate that combined assimilation and fractional crystallisation was an important process in the origin of these rock types. The rock samples from the BCC and H plutons converge at about ~66 wt.% SiO_2. This may indicate that the parental magmas (sources I and II-S_{I-II}) of these rock types assimilated the same contaminant.

As can be seen from Figures 7.3a and b, source I (S_I) has higher initial $^{87}Sr/^{86}Sr$ and lower initial $^{143}Nd/^{144}Nd$ ratios than source II (S_{II}). This may be explained by either a greater subduction component in source I or more crustal contamination during uprise through continental crust compared to source II, or that source II is more mantle-enriched and less crustal contaminated than source I.

7.1.1.1.1. Trace element evidence for source enrichment or fractional crystallisation combined with crustal assimilation processes

The main variations shown by the initial isotope ratio data (Sr, Nd) (Figures 7.1-7.3) for the Central Anatolian plutonic rocks can also be seen in a plot of Th/Yb against Ta/Yb (Figure 7.5). However, first, the Th/Yb and Ta/Yb ratios of the plutonic rocks from the Central Anatolian Massif are plotted against silica in Figure 7.4 to assess the sensitivity of these ratios to AFC.

Yb is used as the normalising factor to minimise variations created by partial melting and fractional crystallisation provided that olivine, pyroxenes and feldspars are the dominant crystallising or residual phases (Pearce, 1982). Pearce (1982) demonstrated that the greater mobility of Th in subduction components results in an increase in Th relative to Ta which results in a shift to higher Th/Yb ratios in the mantle wedge above the subduction zone. Assimilation of crust has a similar effect, although assimilation of granulitic crust, which has low Th contents, can cause a shift in the opposite direction (Pearce et al., 1990). Garnet residues from partial melting will lower Ta/Yb and Th/Yb ratios by similar amounts, and amphibole residues will lower Ta/Yb slightly more than Th/Yb; crystallisation of these phases will have the reverse effect (Pearce et al., 1990), because the partition coefficient of Ta for amphibole in basic compositions (0.25) is five times higher

than that of Th (0.05) and the partition coefficients of both Ta and Th are lower than Yb (0.80).

Figure 7.4a shows that the Th/Yb ratio increases with silica for the BCC (Behrekdag, Cefalikdag, Celebi) intrusive rocks. However, it is rather ambiguous for the B (Baranadag) and H (Hamit) plutonic rocks.

In Figure 7.4b, the Ta/Yb ratio increases slightly with silica for the BCC intrusive rocks, whereas it remains almost constant for the B plutonic rocks. In contrast, this ratio increases until ~57 wt.% SiO_2 and then is rather ambiguous for the H intrusive rocks.

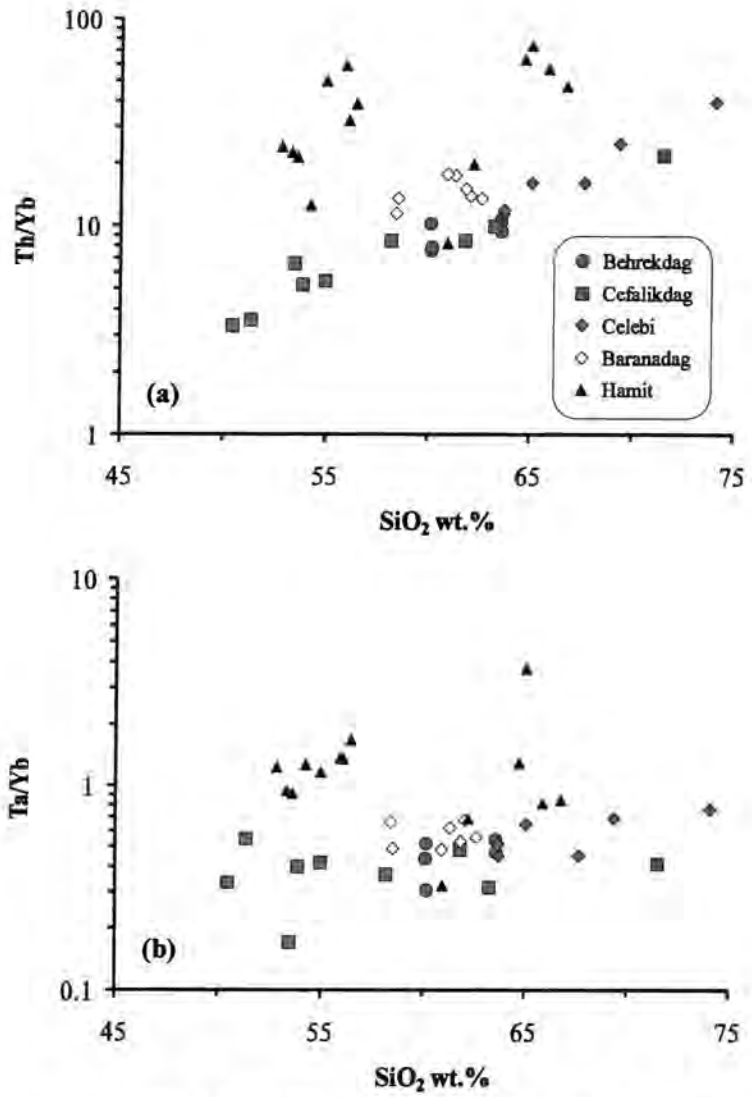

Figure 7.4. Th/Yb (a) and Ta/Yb (b) versus silica diagrams for the Central Anatolian plutonic rocks.

The Th/Yb ratio of the Central Anatolian plutonic rocks is plotted against their Ta/Yb ratio (Figure 7.5). The plutonic rocks up to 63 wt.% SiO_2 are plotted, because trends for these ratios in the plutonic rocks are generally constant up to this value (see Figures 7.4a, b). In Figure 7.5, a greywacke sample (quartz-rich; sample no: N490; Appendix C) (crust I- C_I) collected near the H pluton and a pelite sample (sample no: C2; Appendix C) (crust II- C_{II}) of the Central Anatolian Massif have been also plotted as the crustal contaminants.

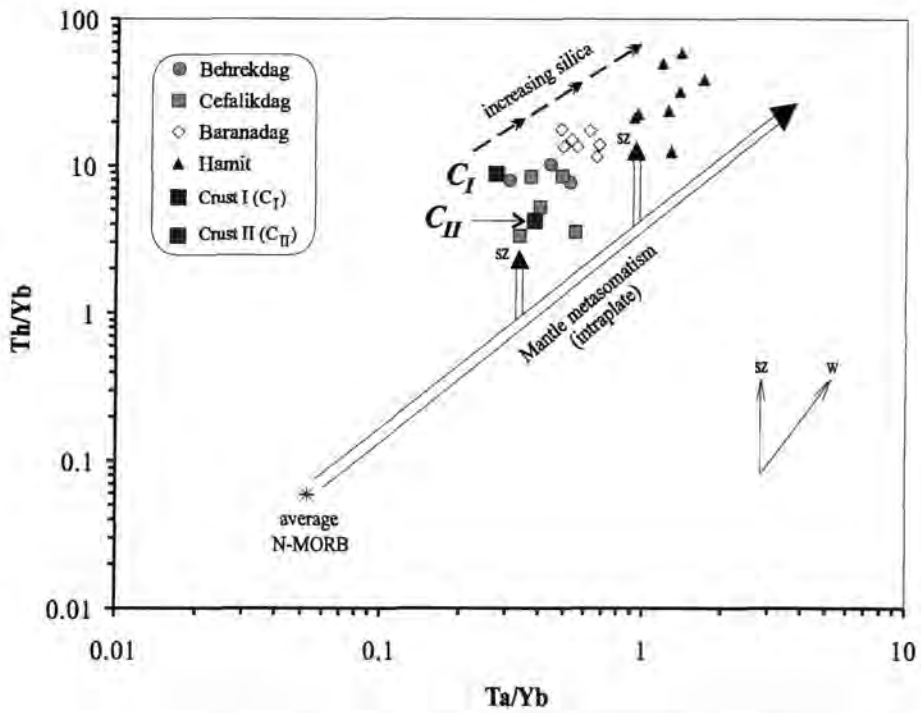

Figure 7.5. Th/Yb versus Ta/Yb diagram (after Pearce, 1983) for the Central Anatolian plutonic rocks (up to 63 wt.% SiO_2). N-type MORB values from Sun and McDonough (1989). Crust I (C_I) : a greywacke sample (quartz-rich; sample no: N490) collected near the H pluton; and crust II (C_{II}): a pelite sample (sample no: C2) of the Central Anatolian Massif. Abbreviations: sz-subduction zone enrichment, w-within plate enrichment and C-crust.

Figure 7.5 shows that all intrusive rocks from the Central Anatolian Massif form trends that run parallel to the mantle metasomatism array but are displaced towards higher Th/Yb ratios, suggesting either derivation from an enriched mantle source to which a subduction component had been added, or coupled crustal contamination with fractional crystallisation or both. In addition, both ratios increase from the Behrekdag and Cefalikdag through the B to the H intrusive rocks. The high Ta/Yb ratio of the H intrusive rocks could be explained by derivation from a more enriched-mantle source than that of the Behrekdag and Cefalikdag plutonic rocks.

As can be seen from Figure 7.5, the Central Anatolian plutonic rocks do not form trends from the mantle array to crust I (C_I) or II (C_{II}), so AFC is not likely the only process for the generation of the plutonic rocks. As in the isotope plot (Figure 7.3), the parental magmas for the plutonic rocks must be enriched in Th as well as Sr and Nd isotope ratios. Figure 7.5 also shows that the Hamit plutonic rocks are more enriched in a within-plate component than the Behrekdag, Cefalikdag and Baranadag plutonic rocks.

The variations shown by the Behrekdag and Cefalikdag plutonic rocks might indicate that these rocks are derived from a mantle source containing large subduction components, and have experienced assimilation and fractional crystallisation during uprise through continental crust. In contrast, the B and H intrusive rocks might be derived from a more enriched-mantle source with less coupled crustal assimilation-fractionation compared to the Behrekdag and Cefalikdag plutonic rocks.

7.2. Interpretation of LILE fractionation trends for the Central Anatolian plutonic rocks

The isotope and trace element geochemical variations between and within the Central Anatolian plutonic rocks have been explained by the mantle source enrichment and AFC processes (as discussed above). However, in this Section the discussion is expanded to determine which phases, if removed from the melt, could cause the observed evolution from the least acidic to the most acidic compositions.

Some authors (e.g. McCarthy and Groves, 1979; Tindle and Pearce, 1981) argued that granites cannot be treated as either pure 'melts' or pure 'cumulates', but should instead be thought of as "crystal mushes". As such, it is unlikely that perfect (Rayleigh) fractional crystallisation would apply to granite crystallisation. Instead, since cumulus crystals trap interstitial melt, granite crystallisation lies somewhere between the extremes of equilibrium crystallisation and perfect fractional crystallisation.

In spite of these arguments, most authors favour perfect (Rayleigh) fractional crystallisation (e.g. McCarthy and Groves, 1979; Tindle and Pearce, 1981) because crystals are commonly removed from the site of formation after crystallisation and

the distribution of trace elements is not an equilibrium process. At best, surface equilibrium may be attained. Thus, crystallisation is better described by the Rayleigh Law for the Central Anatolian plutonic rocks (Equation 7.8).

In theory, two basic equations describe the extremes of behaviour of trace elements during crystallisation:

$$C_L / C_0 = F^{(D-1)} \qquad \text{(Eq. 7.8)}$$

for perfect (Rayleigh) fractional crystallisation (where only the surface of the crystals is in equilibrium with the melt):

$$C_L / C_0 = 1/[F + D(1-F)] \qquad \text{(Eq. 7.9)}$$

for equilibrium crystallisation (where the whole of each solid phase remains at all times in equilibrium with the melt).

where;

C_0: the weight concentration of a trace element in the parental liquid

C_L: the weight concentration of a trace element in the residual liquid

F : the weight fraction of melt remaining

D: bulk distribution coefficient of the fractionation assemblage during crystallisation $\left(D = \sum_i^n K_d^i X_i \right)$

where;

K_d^i: partition coefficient of a trace element for phase i

X_i: the weight fraction of phase i

Several attempts at petrogenetic modelling of granite systems have been based on the LILEs (Ba, Rb and Sr) (e.g. McCarthy and Hasty, 1976; McCarthy and Groves, 1979; Tindle and Pearce, 1981). These elements are useful because they occur only in the major silicate minerals, thus avoiding problems in estimating accessory mineral abundances and behaviour.

Changes in LIL element concentrations during fractionation can be examined and modelled more quantitatively by comparing observed and theoretical fractionation vectors on log-log bivariate plots. Therefore, the LILE data of the Central Anatolian plutonic rocks are presented as logarithmic plots of Ba against Rb and Ba against Sr (Figure 7.6).

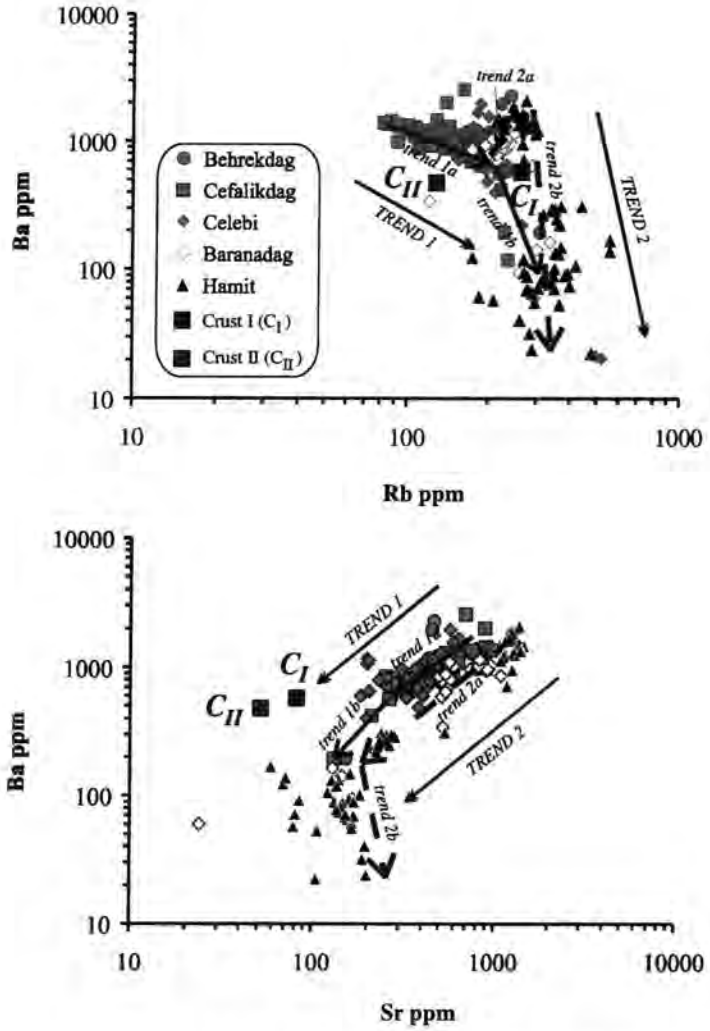

Figure 7.6. Ba-Rb and Ba-Sr co-variation diagrams for the plutonic rocks. Crust I (C_I) is an average of greywacke samples (N490-N491) collected near the H pluton. Crust II (C_{II}) is an average of pelite samples (C1-C2) of the Massif. Abbreviation: C-crust.

In Figure 7.6, two main trends are observed for the Central Anatolian plutonic rocks: trend 1 for the BCC (Behrekdag, Cefalikdag and Celebi) plutonic rocks and trend 2 for the B (Baranadag), H (Hamit) intrusive rocks. Therefore, in order to show differences in detail between the BCC (Behrekdag, Cefalikdag, Celebi) and the B (Baranadag), H (Hamit) plutonic rocks, the LILE data for these plutonic rocks are plotted separately in Figures 7.7, 7.8. In the following paragraphs, the BCC and B, H plutonic rocks will be discussed separately.

In Figure 7.6, an average of greywacke samples (quartz-rich; sample nos: N490-N491; Appendix C) (crust I- C_I) collected near the H pluton and an average of

pelite samples (sample nos: C1-C2; Appendix C) (crust II- C_{II}) of the Central Anatolian Massif have been also plotted as the crustal contaminants.

Figures 7.7b, 7.8b attemp to explain Figure 7.6 by explaining the theoretical effects on melt composition of crystallising mineral phases. In these Figures, theoretical vectors are modelled for 30% crystallisation (with 5% interval) of single phases involving clinopyroxene, plagioclase, hornblende, biotite and alkali feldspar. In Figures 7.7b, 7.8b, the vectors can be moved to any presumed parental compositions, so the starting composition is not crucial.

For the vectors shown in Figures 7.7 and 7.8, mineral/melt partition coefficients have been gathered from published compilations of partition coefficients (Table 7.4). Figures 7.7c, 7.8c display how the observed LILE variations may be modelled graphically.

Element	*Mineral*				
	cpx	*pl*	*hbl*	*bi*	*ksp*
Rb	0.032	0.048	0.014	4.200	0.487
Sr	0.516	2.840	0.022	0.120	3.870
Ba	0.131	0.360	0.044	6.360	6.120

Table 7.4. Mineral/liquid partition coefficients derived from Arth (1976), Mahood and Hildreth (1983) and Nash and Crecraft (1985). Abbreviations: cpx- clinopyroxene, pl- plagioclase, hbl- hornblende, bi- biotite and ksp- alkali feldspar.

7.2.1. The BCC (Behrekdag, Cefalikdag and Celebi) plutonic rocks

In detail, two sub-trends show up in Figures 7.6, 7.7 for the BCC plutonic rocks: trend 1a (followed by a majority of samples) in which Rb increases while Ba and Sr decrease; and trend 1b (followed by the most acidic samples) in which Ba decreases rapidly, Sr decreases and Rb increases.

In Figure 7.7, plagioclase, hornblende, alkali feldspar and biotite could control trend 1a for the BCC plutonic rocks. These minerals are chosen because they are observed in these rock types. As shown in Table 7.4, Ba is strongly partitioned into alkali feldspar and biotite, whereas Sr is strongly partitioned into plagioclase and alkali feldspar. Therefore, fractional crystallisation of these minerals results in decrease in Ba and Sr. On the other hand, Rb, Sr and Ba are weakly partitioned into hornblende. Thus, fractionation of this mineral causes enrichment in these elements.

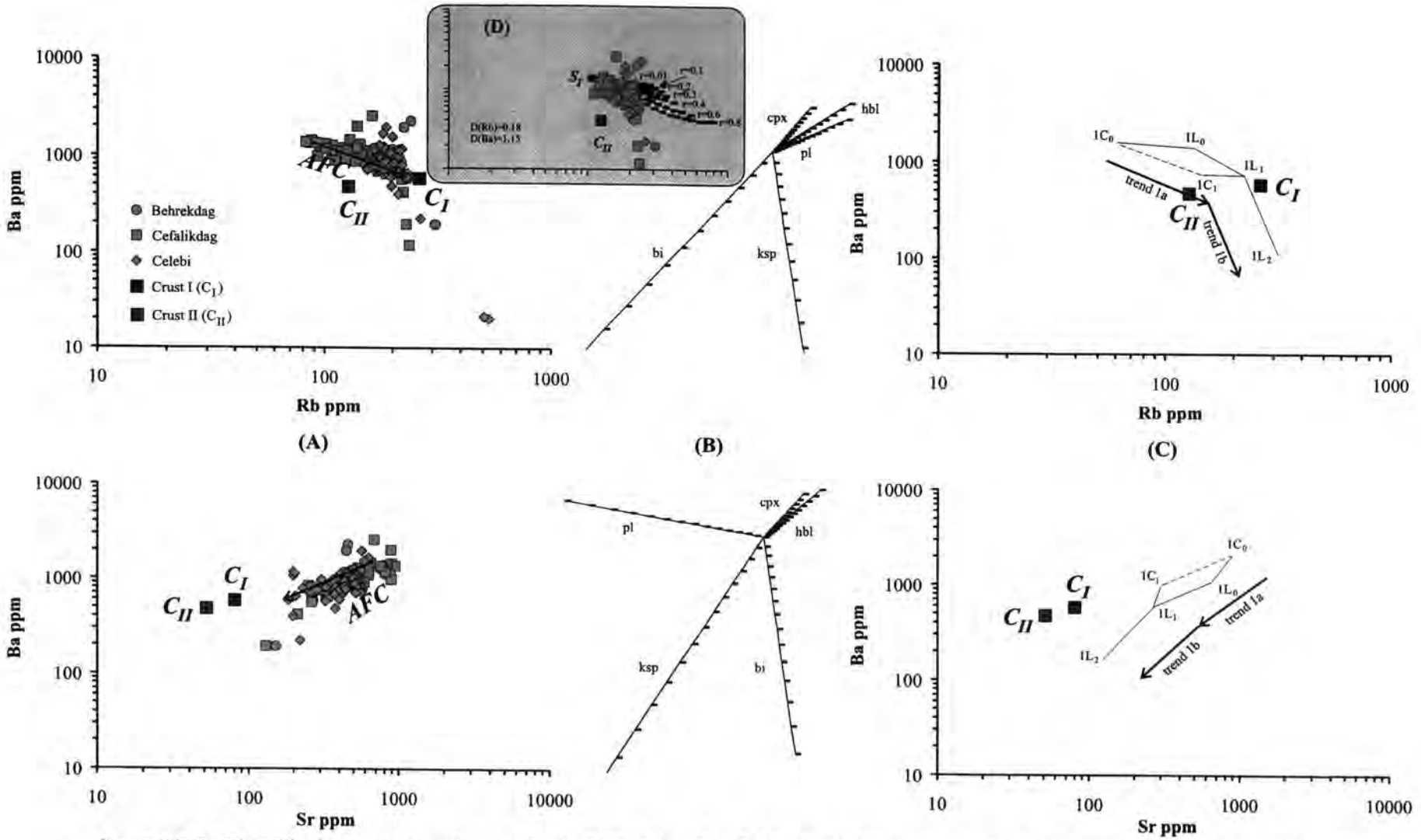

Figure 7.7. Ba-Rb and Ba-Sr co-variation diagrams for the BCC (Behrekdag, Cefalikdag, Celebi) intrusive rocks. (A) shows the distribution of data points; (B) displays the theoretical effects on melt composition of crystallising single mineral phases; (C) presents the modelled variations which combined the effects of certain minerals as discussed in the text. (D) (the inset graph) shows combined fractionation and assimilation processes in the BCC plutonic rocks. The vectors are marked with values for F, the relative amount of melt remaining. Bulk partition coefficients were calculated from Table 7.4. Abbreviations: AFC- combined fractionation and assimilation, C- crust, S- source, D- bulk partition coefficient, cpx- clinopyroxene, hbl- hornblende, pl- plagioclase, bi- biotite and ksp- alkali feldspar. Crust I (C_I) is an average of greywacke samples (N490-N491) collected near the H (Hamit) pluton. Crust II (C_{II}) is an average of pelite samples (C1-C2) from the Central Anatolian Massif.

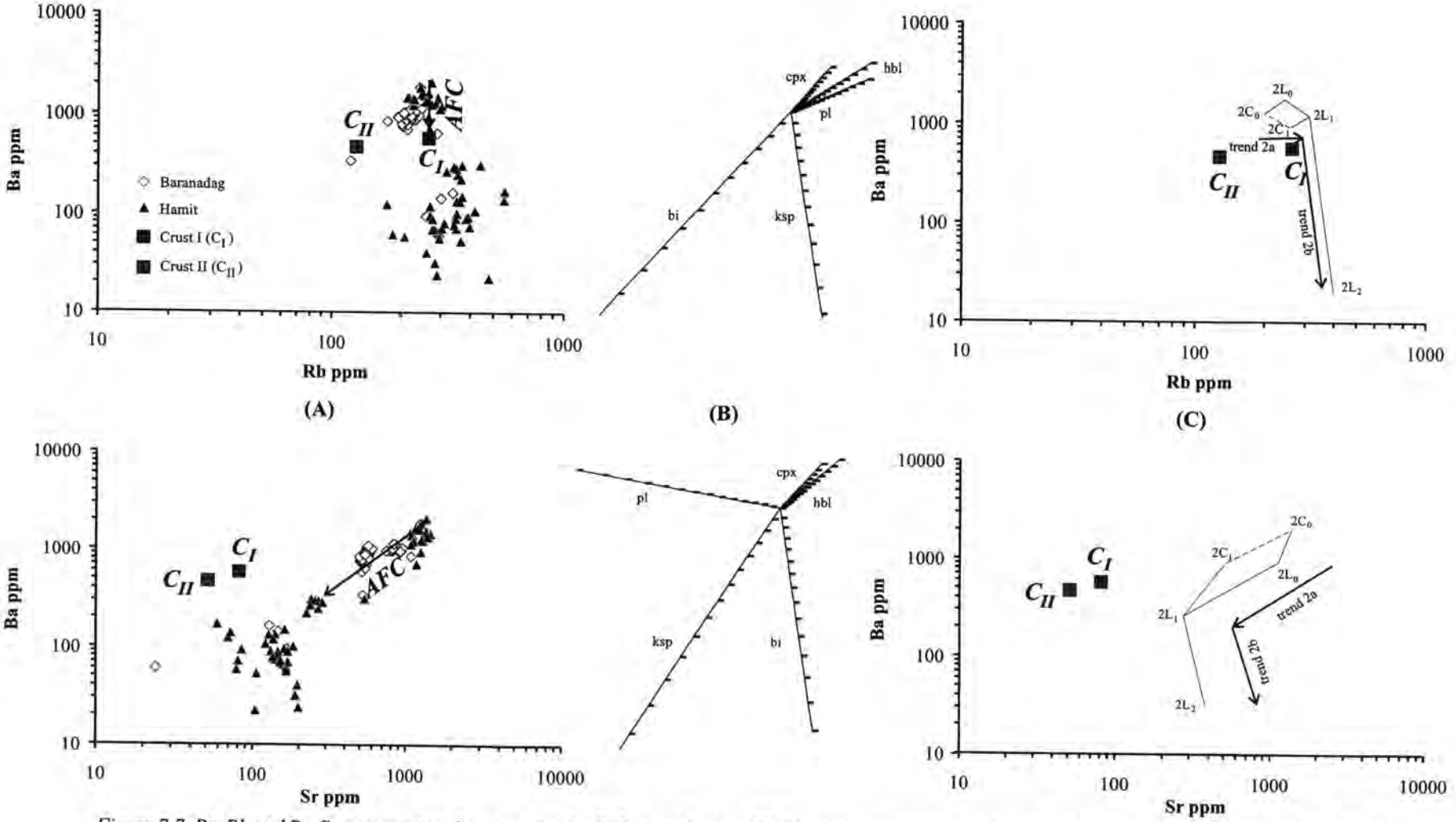

Figure 7.7. Ba-Rb and Ba-Sr co-variation diagrams for the B (Baranadag) and H (Hamit) intrusive rocks. (A) shows the distribution of data points; (B) displays the theoretical effects on melt composition of crystallising single mineral phases; and (C) presents the modelled variations which combined the effects of certain minerals as discussed in the text. The vectors are marked with values for F, the relative amount of melt remaining. Bulk partition coeffients were derived from Table 7.4. Abbreviations: AFC- combined fractionation and assimilation, C- crust, cpx- clinopyroxene, hbl- hornblende, pl- plagioclase, bi- biotite and ksp- alkali feldspar. Crust I (C_I) is an average of greywacke samples (N490-N491) collected near the H (Hamit) pluton. Crust II (C_{II}) is an average of pelite samples (C1-C2) from the Central Anatolian Massif

In Figure 7.7, alkali feldspar is a possible candidate in addition to plagioclase and biotite for the most silicic BCC plutonic rocks (trend 1b). As shown in Table 7.4, Ba is strongly partitioned into biotite and alkali feldspar. Thus, fractional crystallisation of these minerals causes sharp decrease in Ba. On the other hand, Rb is strongly partitioned into biotite. Therefore, fractionation of biotite results in decrease in Rb, whereas Rb is weakly partitioned into plagioclase and alkali feldspar (Table 7.4). Thus, fractionation of these minerals causes enrichment in Rb. However, Sr is strongly partitioned into plagioclase and alkali feldspar. Therefore, fractional crystallisation of these minerals results in decrease in Ba and Sr.

In Figure 7.7c, the mineral assemblages of the plutonic rocks were estimated from their modal analyses. The vectors were then drawn for these mineral assemblages (Table 7.5). In Figure 7.7c, the main problem is to locate the compositions of the parental magmas for the plutonic rocks. In theory, they must lie between the bulk compositions of the cumulate phases and the melts. It is assumed that the least acidic rock types (monzodiorite/quartz monzodiorite) in the Cefalikdag pluton appear only as a subordinate border facies and that these are cumulates (C_0) (Figure 7.7c). It is assumed that magma such as $1L_0$ (initial liquid composition) for the BCC plutonic rocks evolved to composition $1L_1$ by loss of plagioclase, hornblende, alkali feldspar and biotite whose average bulk composition was $1C_0$ (initial cumulate composition). Mushes belonging to this trend (trend 1a) would fall within the parallelograms $1L_1$-$1L_0$-$1C_0$-$1C_1$. The second trend (1b) is restricted to the aplites of the BCC plutons.

As Figure 7.7c shows, predicted trends produce a very close fit to observed trends.

Pluton	***Observed trend and rock unit***	***Mineral***				
		cpx	***pl***	***hbl***	***bi***	***ksp***
	trend 1					
BCC (Behrekdag, Cefalikdag, Celebi)	*trend 1a* (followed by majority of samples)		45	34	2	19
	trend 1b (followed by the most acidic samples)		35		5	60

Table 7.5. Results of the LILE modelling for the BCC plutonic rocks (values in percent). Abbreviations: cpx-clinopyroxene, pl-plagioclase, hbl-hornblende, bi-biotite and ksp-alkali feldspar.

The trends observed in Figure 7.7 can be also controlled by the coupled crustal assimilation and fractional crystallisation (AFC) process. The inset graph in Figure 7.7 shows a diagram of Ba against Rb for the BCC plutonic rocks, upon which has been superimposed theoretical curves to illustrate the evaluation of the BCC parental magma composition by crustal assimilation and fractional crystallisation. The AFC equations of DePaolo (1981) presented in Section 7.1.1 have been used for the modelling of LILEs (Ba, Rb) from the BCC plutonic rocks. Theoretical AFC curves were calculated for different values of r (the ratio of assimilation rate to crystallisation rate). The ratio of remaining magma mass to original magma mass (F) is marked on each curve at 5% intervals.

In the modelling, an average of pelite samples from the Massif (Crust II-C_{II}) is used as the crustal contaminant. Parental magma chosen (S_I) for the BCC plutonic rocks has initial Rb and Ba contents of 120 ppm and 1400 ppm. Bulk partition coefficients (D) were calculated using the values from Table 7.4.

In the inset graph (Figure 7.7), the BCC plutonic rocks (cumulates and dykes are excluded) plot between r=0.01 and r=0.8. However, most of the samples plot between the curves for r=0.3 and r=0.8, indicating great crustal assimilation from the crust. It should be noted that the precise values of r are not meaningful, because of likely variations in end-member compositions and also variations in the bulk partition coefficients (D) of elements during fractional crystallisation.

Unfortunately, as can be seen from Figure 7.7, the least acidic rock samples and the contaminants from the Massif have similar compositions of Sr and Ba. Therefore, the AFC modelling does not give useful information on the plutonic rocks on these projections. On the other hand, fractional crystallisation of mineral assemblages given in Table 7.5 coupled with crustal assimilation could result in decrease in Sr and Ba for the BCC plutonic rocks.

7.2.2. The B (Baranadag) and H (Hamit) plutonic rocks

Two sub-trends also show up for the B and H plutonic rocks (Figure 7.8): trend 2a (followed by the mainly least acidic samples) in which Rb increases, Ba increases and Sr decreases; and trend 2b, which is like trend 1b (followed by the most acidic samples), in which Ba and Sr decrease while Rb increases. In Figure 7.8, there is a noticeable compositional gap between trends 2a and 2b.

Plagioclase, clinopyroxene and alkali feldspar could control trend 2a for the least acidic H and B rocks (Figure 7.8), although the trends for these rock types are not so clear. These minerals are chosen because they are observed in these rock types. As can be seen from Table 7.4, Rb, Sr and Ba are weakly partitioned into clinopyroxene. Therefore, fractional crystallisation of this mineral results in enrichment in these elements. The partition coefficients of plagioclase and alkali feldspar for Ba, Sr and Rb are as mentioned in Section 7.2.1.

Alkali feldspar and plagioclase could control trend 2b for the most acidic B and H rocks, even though the trends for these rock types are not so clear. The partition coefficients of plagioclase and alkali feldspar for Ba, Sr and Rb are discussed in Section 7.2.1.

In Figure 7.8c, the mineral assemblages of the plutonic rocks were estimated from their modal analyses. The vectors were then drawn for these mineral assemblages (Table 7.6). In Figure 7.8c, magma such as $2L_0$ (initial liquid composition) for the B and H plutonic rocks evolved to composition $2L_1$ by loss of plagioclase, clinopyroxene and alkali feldspar whose average bulk composition was $2C_0$ (initial cumulate composition). Mushes belonging to this trend (trend 2a) would fall within the parallelograms $2L_1$-$2L_0$-$2C_0$-$2C_1$. The second trend (2b) is restricted to the aplites of the B pluton and alkali feldspar syenite and quartz syenite for the H pluton. Alkali feldspar is a possible candidate in addition to plagioclase for the most silicic B and H plutonic rocks.

Pluton	***Observed trend and rock unit***	***Mineral***				
		cpx	***pl***	***hbl***	***bi***	***ksp***
	trend 2					
B (Baranadag) and H (Hamit)	***trend 2a*** (followed by the least acidic samples)	30	50			20
	trend 2b (followed by the most acidic samples)		30			70

Table 7.6. Results of the LILE modelling for the B and H plutonic rocks (values in percent). Abbreviations: cpx-clinopyroxene, hbl-hornblende, pl-plagioclase, bi-biotite and ksp-alkali feldspar.

The trends observed in Figure 7.8 could be also controlled by the coupled crustal assimilation and fractional crystallisation (AFC) processes. The least acidic

rock samples and the contaminants from the Massif have similar compositions of Rb and Ba, therefore the AFC modelling does not give useful information on the plutonic rocks on these projections. However, fractional crystallisation of mineral assemblages given in Table 7.6 coupled with crustal assimilation could result in increase in Rb and decrease in Ba for the B and H plutonic rocks.

7.3. Evalution of Rb, Nb and Y for the Central Anatolian plutonic rocks as indicators of source and tectonic setting

The discriminant diagram of Rb versus (Y+Nb) (Pearce et al., 1984) (Figure 7.10) is used to assess the petrological evolution of the Central Anatolian plutonic rocks. In this diagram, two parameters are not known: (i) parental compositions, and (ii) AFC trends. Therefore, in order to find out these parameters, first the data are plotted on diagrams of Rb, Nb and Y versus silica (Figure 7.9).

As mentioned in Section 7.2.1, the least acidic samples of the BCC plutonic rocks are cumulates. Therefore, considering the entire data set for Figures 7.9a-c, the parental magma chosen for the BCC intrusive rocks (source I-S_I) has silica, Rb, Nb and Y contents of 56 wt.%, 120 ppm, 18 ppm and 30 ppm (see also Table 7.7).

The least acidic sample (N31- from the Hamit pluton) chosen as parental magma for the B and H intrusive rocks (source II-S_{II}) has silica, Rb, Nb and Y contents of 52 wt.%, 210 ppm, 30 ppm and 40 ppm respectively.

In Figures 7.9, 7.10, an average of greywacke samples (sample nos: N490-N491) (crust I-C_I) collected near the H pluton and an average of pelite samples (sample nos: C1-C2) (crust II-C_{II}) of the Central Anatolian Massif are used as the contaminants. The greywacke samples have Nb and Y values similar to those for the pelite samples, although the former is more enriched in Rb.

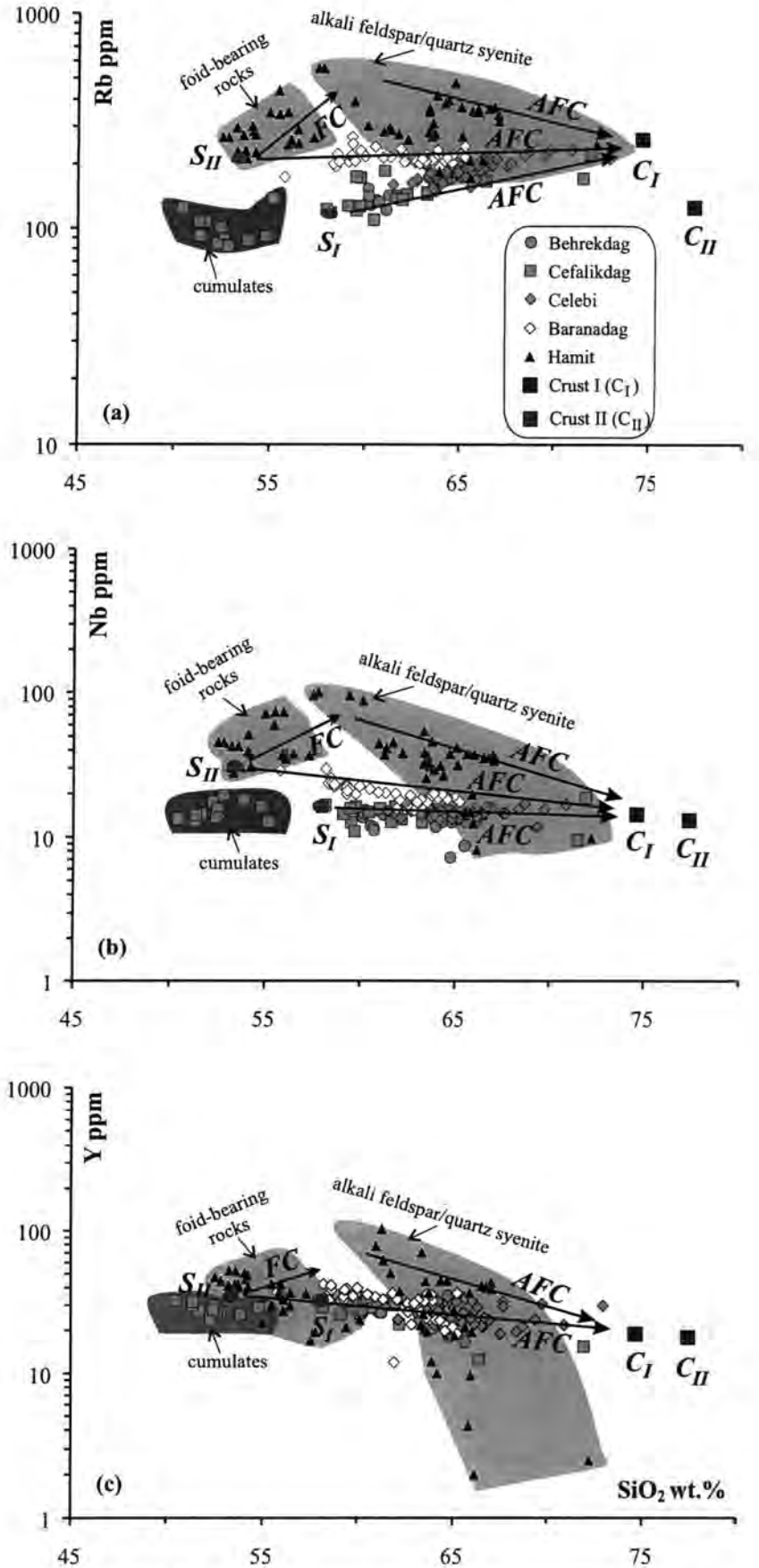

Figure 7.9. Rb, Nb and Y versus silica diagrams showing the AFC effects on the genesis of the Central Anatolian plutonic rocks. Abbreviations: FC- fractional crystallisation, AFC- combined fractionation-assimilation, S- source and C-crust.

	Source I (S_I) for the BCC (Behrekdag, Cefalikdag, Celebi) plutonic rocks	*Source II (S_{II}) for the B (Baranadag) and H (Hamit) plutonic rocks (N31- from the H pluton)*	*Contaminants (C)* C_I	C_{II}
SiO_2 wt.%	56	52	75	77
Rb ppm	120	210	261	126
Nb ppm	18	30	14	13
Y ppm	30	40	19	18
(Y+Nb) ppm	48	70	33	31

Table 7.7. Table showing possible parental magmas and contaminants for the Central Anatolian plutonic rocks (see text for more explanation). C_I - (crust I): an average of greywacke samples (N490-N491) and C_{II} - (crust II): an average of pelite samples of the Massif.

As can be seen from Figure 7.9a, the BCC intrusive rocks (derived from source I-S_I) have the lowest Rb contents. Rb increases with silica for these intrusive rocks. However, Rb remains almost constant with increasing silica for the B plutonic rocks. The H intrusive rocks from the Massif have the highest Rb contents. The Rb abundance increases until ~58 wt.% SiO_2 in the foid-bearing rocks and then decreases in the alkali feldspar syenite and quartz syenite.

The enrichment in Rb for the BCC plutonic rocks can be explained by fractional crystallisation of hornblende, plagioclase, clinopyroxene and/or alkali feldspar, because as can be seen from Table 7.4, Rb is weakly partitioned into these minerals. As shown in Figure 7.7, fractionation of these minerals coupled with crustal assimilation could result in enrichment.

The constant Rb content with silica for the B intrusive rocks could be produced by fractional crystallisation of hornblende, plagioclase, clinopyroxene and/or alkali feldspar coupled with crustal assimilation (depending on the crustal composition), because the parental magma for the B plutonic rocks (source II) and the crustal contaminants have similar Rb values (Figure 7.9a).

The enrichment in Rb for the foid-bearing Hamit rocks could be explained by fractional crystallisation of foid minerals (e.g. nepheline), clinopyroxene, hornblende and/or alkali feldspar, because Rb is weakly partitioned into these minerals. The partition coefficient of Rb for nepheline is 0.44 for intermediate compositions (Larsen, 1979) and those for other minerals are given in Table 7.4.

On the other hand, the depletion in Rb for the alkali feldspar syenite and quartz syenite could be produced by fractional crystallisation of biotite, because Rb

is strongly partitioned into this mineral. Biotite is in minor amounts in these rock types though. The partition coefficient of Rb in biotite is 4.2 for acidic compositions (see Table 7.4). The depletion in Rb for these rock types could be also produced by fractional crystallisation of biotite coupled with crustal assimilation depending on the crustal composition, because the parental rocks (the most siliceous foid-bearing rocks) for the alkali feldspar syenite and quartz syenite have higher Rb contents than the crustal contaminants.

In Figure 7.9b, Nb increases slightly with silica for the BCC plutonic rocks. However, it decreases slightly with silica for the B plutonic rocks. On the other hand, Nb increases to about 58 wt.% SiO_2 for the foid-bearing rocks and then decreases for the alkali-feldspar syenite and quartz syenite.

The enrichment in Nb for the BCC intrusive rocks can be explained by fractional crystallisation of clinopyroxene and/or plagioclase, as the partition coefficients of Nb for clinopyroxene and plagioclase are 0.80 and 0.06 for acidic compositions (Arth, 1976). Fractional crystallisation of these minerals coupled with crustal assimilation could also cause enrichment in Nb (depending on the crustal composition). As can be seen from Figure 7.9b, the parental magma for the BCC plutonic rocks (source I) has slightly higher Nb content than the crustal contaminants, leading to enrichment in Nb for these rock types during combined crustal assimilation and fractional crystallisation.

On the other hand, the depletion in Nb for the B plutonic rocks can be produced by fractional crystallisation of clinopyroxene and/or plagioclase and crustal assimilation, because as can be seen from Figure 7.9b, the parental magma for the B plutonic rocks (source II) has slightly higher Nb content than the crustal contaminants. Thus, AFC may cause depletion in Nb for the B intrusive rocks.

The enrichment in Nb for the foid-bearing rocks could be explained by fractional crystallisation of foid minerals (e.g. leucite, nepheline), clinopyroxene and/or plagioclase, because Nb is weakly partitioned into these minerals. The partition coefficients of Nb for leucite and nepheline are 0.020 and 0.011 for intermediate compositions (Caroff et al., 1993; Larsen, 1979). On the other hand, the depletion in Nb for the alkali feldspar syenite and quartz syenite can be produced by fractionation of hornblende, biotite, magnetite and/or ilmenite, because Nb is strongly partitioned into these minerals. The partition coefficients of Nb for

hornblende, biotite, magnetite and ilmenite are 4.0, 6.4, 2.5 and 6.3 for intermediate and acidic compositions (Arth, 1976; Pearce and Norry, 1979; Nash and Crecraft, 1985; Green and Pearson, 1986). Fractional crystallisation of these minerals coupled with crustal assimilation could also cause depletion in Nb depending on the crustal composition. As can be seen from Figure 7.9b, the parental rocks (the most acidic foid-bearing rocks) for the alkali feldspar syenite and quartz syenite plutonic rocks have higher Nb contents than the crustal contaminants.

In Figure 7.9c, Y remains almost constant with increasing silica for the BCC plutonic rocks. However, it decreases with silica in the B intrusive rocks. Y behaviour is rather ambiguous for the H plutonic rocks. It decreases with silica for the foid-bearing rocks, whereas it is rather scattered for the alkali feldspar syenite/quartz syenite.

The constant Y contents with silica for the BCC intrusive rocks could be produced by fractional crystallisation of hornblende, clinopyroxene, biotite, magnetite and/or apatite and coupled with crustal assimilation depending on the crustal composition. Y is strongly partitioned into these minerals for intermediate and acidic compositions. The partition coefficients of Y for hornblende, clinopyroxene, biotite, magnetite and apatite are 6.0, 4.0, 1.2, 2.0 and 40 (Arth, 1976; Nash and Crecraft, 1985). As can be seen from Figure 7.9c, the parental magma for the BCC plutonic rocks (source I) and the crustal contaminants have broadly similar Y values.

On the other hand, the depletion in Y for the B plutonic rocks could be explained by fractional crystallisation of hornblende, clinopyroxene, biotite, magnetite and/or apatite. The partition coefficients of Y for these minerals are as listed above. The depletion in Y for these plutonic rocks could also be caused by fractional crystallisation of hornblende, clinopyroxene, biotite, magnetite and/or apatite and coupled with crustal assimilation (depending on the crustal composition). As shown in Figure 7.9c, the parental magma for the B plutonic rocks (source II) has slightly higher Y values the crustal contaminants. This could cause depletion in Y for the B intrusive rocks.

The depletion in Y for the H plutonic rocks could be explained by fractional crystallisation of hornblende, clinopyroxene, biotite, magnetite, apatite and/or garnet. The partition coefficient of Y for garnet is 35 for acidic compositions (Arth, 1976).

The partition coefficients of Y for hornblende, clinopyroxene, biotite, magnetite and apatite are 6.0, 4.0, 1.2, 2.0 and 40 (Arth, 1976; Nash and Crecraft, 1985). The depletion in Y could be also produced by fractionation of these minerals and coupled with crustal assimilation, since the parental magma for the H intrusive rocks (source II-S_{II}) has slightly higher Y contents than the crustal contaminants (Figure 7.9c).

The data are plotted on the Rb versus (Y+Nb) diagram (Pearce et al., 1984) (Figure 7.10) to show the petrogenetic pathways for the Central Anatolian plutonic rocks on the discriminant diagram.

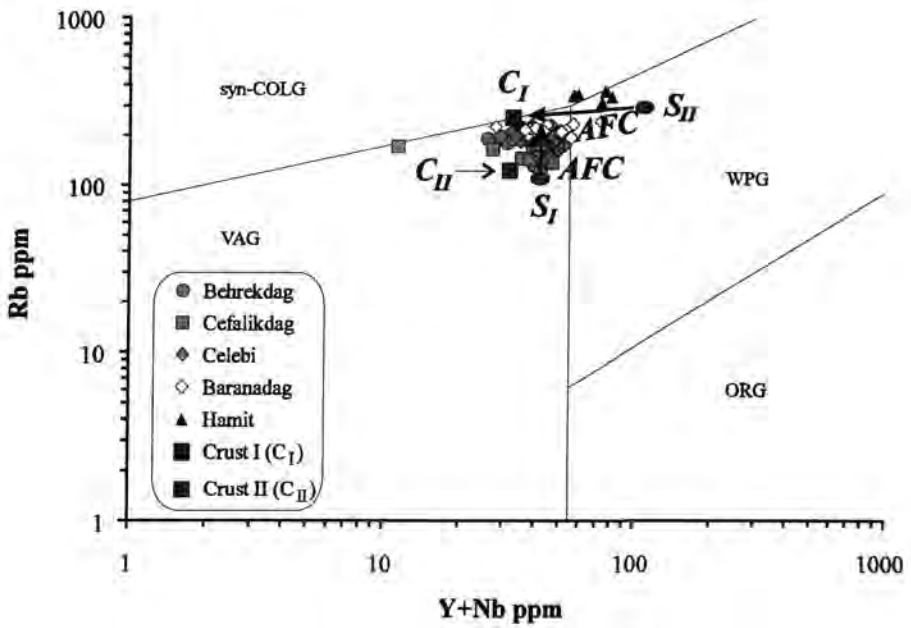

Figure 7.10. Rb versus (Y+Nb) discriminant diagram showing the AFC effects on the genesis of the Central Anatolian plutonic rocks (>5% modal quartz) (after Pearce et al., 1984). Abbreviations: AFC-combined fractionation-assimilation, S-source and C-crust. S_I-source for the BCC (Behrekdag, Cefalikdag, Celebi) and S_{II}-source for the B (Baranadag) and H (Hamit) intrusive rocks. Crust I (C_I) : an average of greywacke samples (N490-N491) collected near the H pluton; and crust II (C_{II}): an average of pelite samples (C1-C2) of the Massif.

The Rb versus (Y+Nb) diagram has been used to discriminate tectonic setting (Pearce et al., 1984) for granites. This plot is also an indicator of protolith and process, which are partly functions of tectonic setting (Arculus, 1987; Twist and Harmer, 1987).

As can be seen from Figure 7.10, the parental magma for the B and H intrusive rocks (S_{II}) is more enriched in (Y+Nb) and Rb than the parental magma for the BCC plutonic rocks (S_I). The former plots in the WPG field, whereas the latter falls in the VAG field. This indicates that the parental magma for the BCC plutonic rocks may have formed in a volcanic-arc setting, while the parental magma for the B, H plutonic rocks may have formed in a within-plate setting.

The BCC plutonic rocks follow a vertical evolution trend of increasing Rb with constant (Y+Nb). Rb remains constant and (Y+Nb) decreases for the B and H intrusive rocks. In Figure 7.10, the contaminant (crust I-C_I) has higher Rb and lower (Y+Nb) contents than the parental magma (source I-S_I) for the BCC plutonic rocks, whereas it has slightly lower Rb and lower (Y+Nb) contents than the parental magma for the B, H plutonic rocks (source II-S_{II}).

As Figures 7.9a-c show, the Rb, Nb and Y characteristics of the Central Anatolian plutonic rocks cannot solely be accounted for fractional crystallisation. However, fractional crystallisation coupled with crustal assimilation could result in the observed trends for the BCC, B and H plutonic rocks (Figure 7.10). As can be seen from Figure 7.10, the AFC process has been affected to take the B, H plutonic rocks from the WPG field to the VAG field and syn-COLG field. On the other hand, for the BCC plutonic rocks the AFC process has caused no change in (Y+Nb) but enrichment in Rb. Therefore, the BCC plutonic rocks have remained in the VAG field.

7.4. The petrological model for the collision-related plutonic rocks of the Central Anatolian Massif

The plutonic rocks from the Central Anatolian Massif have been shown to: (i) vary from calc-alkaline (BCC-Behrekdag, Cefalikdag, Celebi) through transitional (B-Baranadag) to alkaline (H-Hamit) (see Chapter 5: Section 5.1.1.1); (ii) range from monzodiorite through monzonite to granite/syenite (see Chapter 2: Section 2.1); (iii) have hydrous crystallising assemblages (see Chapter 3); (iv) have trace element and isotope ratios which indicate mantle sources (sources I and II: S_I and S_{II}) with large crustal (subduction) components (see Section 7.1); and (v) have experienced significant crustal assimilation (see Section 7.1).

In the following Sections, the mechanism for these enriched geochemical characteristics for the Central Anatolian plutonic rocks will first be discussed; and a model for source and evolution for the plutonic rocks will then be presented. Lastly, a model for magma generation in the Massif will be given.

7.4.1. Mechanism for the enriched isotopic and trace element characteristics of the Central Anatolian plutonic rocks

LILE enrichment in subduction zone magmas can be explained by three main mechanisms: (i) contamination of mantle-derived magmas in the lower crust (melting, assimilation, storage, homogenisation - MASH) (e.g. Hildreth and Moorbath, 1988); (ii) addition of crustal lithospheric components to the mantle wedge (e.g. Saunders et al., 1980; Gill, 1981; Pearce, 1983); and (iii) crustal assimilation coupled with fractional crystallisation (e.g. DePaolo, 1981).

(i) Hildreth and Moorbath (1988) proposed that there is a zone of extensive ***melting, assimilation, storage and homogenisation (MASH)*** beneath each large magmatic centre in the Andes. This zone is located, in general, in the lowermost crust or mantle-crust transition. Magmas reaching this zone induce local melting, assimilate the wall-rocks and mix with each other. It is also a zone where fractionation takes place before re-establishment of buoyant ascent of these magmas. This fractionation has a critical importance in the establishment of the magma system, without which the magma would not rise to or near the surface in a situation of perfect gravitational equilibrium (Fyfe, 1992). According to Hildreth and Moorbath (1988), magmas ascending from these zones may range from evolved basalts to dacites but all will have a base-level isotopic and trace element signatures characteristic of that particular MASH domain. They argued that the MASH process is not simple contamination of basalt but true magma generation in the lower crust or uppermost part of the mantle.

The MASH process can be excluded for the generation of the Central Anatolian plutonic rocks. As shown in Figure 7.2b, if the MASH process is primarily responsible for the enriched isotope signature of the plutonic rocks, the sediment contribution to a melt from depleted mantle should not be quite large (~15-20%). Such high proportions of sediment contribution to mantle are inconsistent with the amount of sediment added to a subduction zone mantle source.

(ii) The alternative to a MASH model is the addition of a subduction component to a mantle source ***(source enrichment).*** The subduction component (sediment and altered oceanic crust) varies according to the composition and temperature of the subducted lithosphere (Pearce and Peate, 1995).

The enriched trace element [Figure 5.12 (see Chapter 5)] and isotopic characteristics (Figures 7.1, 7.3) of the plutonic rocks in the Central Anatolian Massif can be explained by mantle source enrichment by recycling of crustal material during subduction. This has been supported by the two component mixing model (Figure 7.2a). Figure 7.2a shows that small additions of sediment (4% to 6%) to depleted mantle could produce contaminated mantle source(s) for the Central Anatolian plutonic rocks.

(iii) ***Crustal assimilation and fractional crystallisation (AFC)*** plays an important role in the evolution of continental margin magmas (e.g. Hildreth and Moorbath, 1988) and some continental tholeiites (e.g. Cox and Hawkesworth, 1985; Petrini et al., 1987).

The Central Anatolian plutonic rocks have been affected by crustal assimilation coupled with fractional crystallisation (AFC). Although this has been supported by Rb, Nb and Y versus SiO_2 and Rb versus (Y+Nb) diagrams, this process cannot be solely responsible for the enriched trace element and isotope signature of the plutonic rocks. A combination of both trace element and isotope data allows the identification of several components contributing to the genesis of the plutonic rocks.

In a first stage, the mantle source was contaminated by a subduction component. This source contamination process may have predated the generation of partial mantle melts. Hydration of the mantle wedge by a slab-derived fluid component provides both a trigger to partial melting (by lowering the solidus of the mantle wedge peridotite) and the chemical modification of the mantle wedge to produce the characteristic subduction zone chemical signature of high LILE/HFSE ratios.

In a second stage, which took place in a post-collisional setting, partial melts from the contaminated mantle have been affected by crustal assimilation and fractional crystallisation (AFC) during uprise through the crust.

A similar interference of source and crustal contamination processes was described by James and Murcia (1984) for the northern Andean volcanics and Von Blanckenburg et al. (1992) for the Bergell intrusives.

7.4.2. Model for the source and evolution of the Central Anatolian plutonic rocks

A possible model for the origin of the plutonic rocks should explain the coexistence of calc-alkaline and alkaline magmatism in the same tectonic setting. Recently, the genesis of this association has been the subject of debate (e.g. Bonin, 1990; Pearce et al., 1990).

Bonin (1990) carried out some work on the intrusive rocks in the Alps, where magmatism changed from calc-alkaline to alkaline around the end of Permian. He pointed out the role played by water in the genesis of these intrusive rocks. He argued that the source was roughly similar, and the change from calc-alkaline to alkaline magmatism was caused by decreasing water contents. He argued that, during the early Permian, subduction of oceanic crust and sediment released volatiles which transported LIL elements into the mantle wedge of the over-riding plate. The melting of LILE-enriched mantle produced the calc-alkaline magmas in the Alps. Around the end of the Permian, the subduction process ceased and collision started. This implied that no new hydrous material was transported to depth. Therefore, there was not a continuous influx of water into the melting zones. He pointed out that such an evolution in water flux, possibly combined with changes in tectonic conditions (from orogenic to anorogenic), could cause the switch from calc-alkaline to alkaline magmatism.

This argument can mainly be excluded for the origin of the Central Anatolian plutonic rocks, because the BCC (Behrekdag, Cefalikdag, Celebi) and B (Baranadag) and H (Hamit) plutonic rocks formed at roughly the same time (Chapter 2; Sections 2.3, 2.4). In addition, these rock types were generated in a similar environment (post-collisional). Moreover, both the BCC and B, H plutonic rocks have subduction components in their sources (Figures 7.1-7.3), even though the parental magma for the B, H plutonic rocks (source II- S_{II}) is more enriched in within-plate mantle components than the parental magma for the BCC plutonic rocks (source I- S_I).

Pearce et al. (1990) worked on the collision-related volcanic rocks in Eastern Anatolia. They argued that derivation from mantle above an earlier subduction zone gives a calc-alkaline character and derivation from the lithosphere beneath the passive margin gives an alkaline character.

In order to assess the argument proposed by Pearce et al. (1990) for the Central Anatolian plutonic rocks, the least acidic intrusive rock samples are normalised to primordial mantle (Figure 7.11a-c). The alkaline volcanic rocks from the Eastern Anatolian Volcanic Province are also plotted for comparison (Figure 7.11d). As can be seen from Figure 7.11, this model can be also excluded for the plutonic rocks, because like the least acidic rocks of the BCC plutons, those of the H pluton have subduction components in their compositions (Figure 7.11). On the other hand, the alkaline volcanic rocks from Eastern Anatolia have no (sample no: 1912) or little (sample nos: 2114, 2111, 3111) subduction components in their compositions (Figure 7.11d). According to the argument proposed by Pearce et al. (1990), if the H plutonic rocks originated from the passive margin, they should not contain subduction components.

The coexistence of calc-alkaline and alkaline magmatism in the Central Anatolian Massif can be attributed to mantle source heterogeneity before collision. As mentioned in previous Sections, the Central Anatolian plutonic rocks have high Sr and low Nd isotope ratios (Figures 7.1-7.3). However, the BCC plutonic rocks in the Massif show higher degrees of HFSE depletion (e.g. Ta and Nb) (Figure 7.11a), higher initial $^{87}Sr/^{86}Sr$ ratios and lower initial $^{143}Nd/^{144}Nd$ ratios (Figure 7.3) than the B, H plutonic rocks. This may indicate that the source for the BCC plutonic rocks has a greater subduction component than the source for the B, H plutonic rocks. The geochemical differences between the calc-alkaline (BCC) and alkaline (H) plutonic rocks in the Massif may also reflect differences in their mantle source regions (Figure 7.12). The source region beneath the B, H plutonic rocks is more enriched in within-plate mantle components than the source region beneath the BCC plutonic rocks (Figure 7.5).

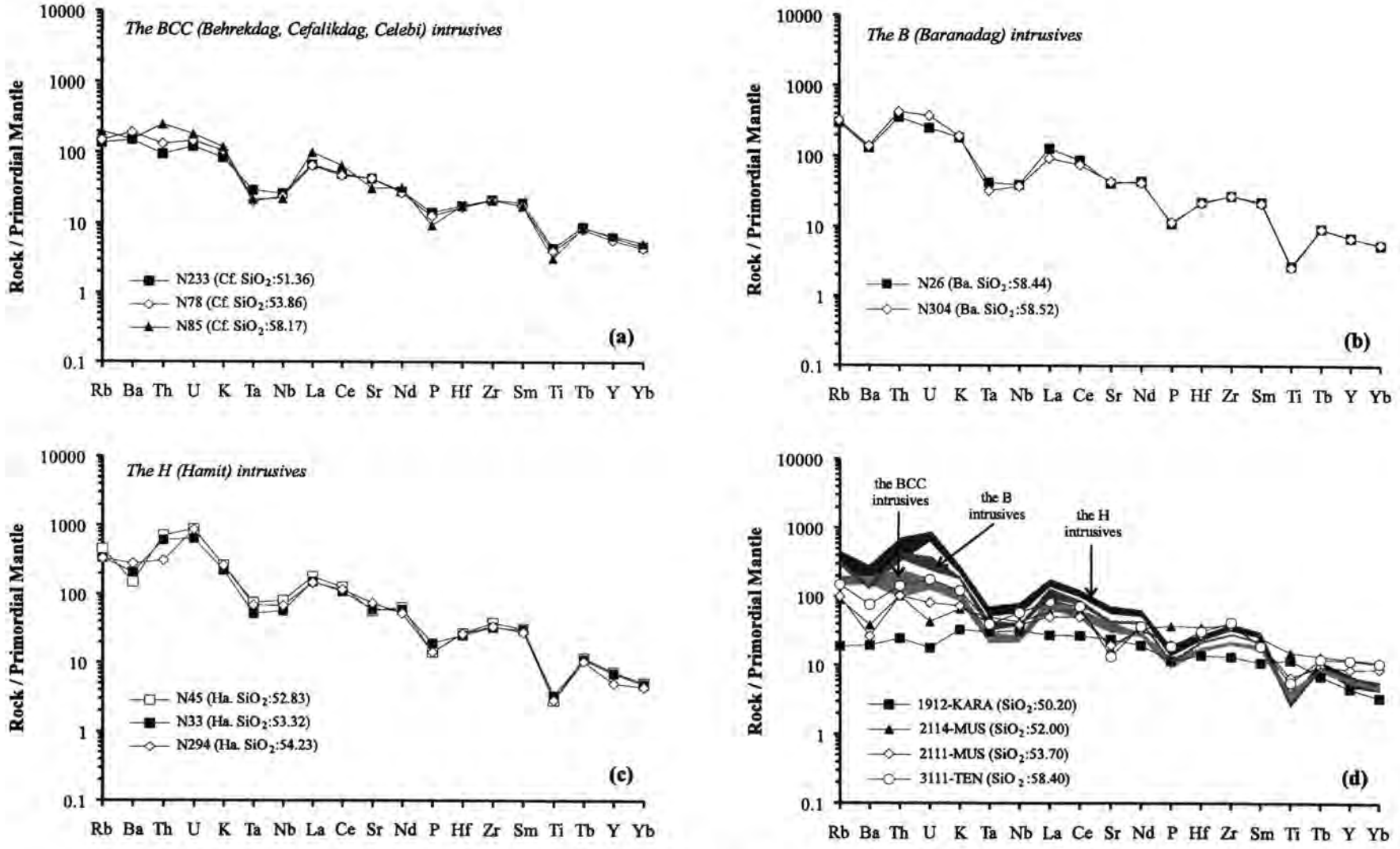

Figure 7.11. Primordial mantle-normalised trace element variation diagrams for: (a) the BBC (Behrekdag, Cefalikdag, Celebi); (b) the B (Baranadag), (c) the H (Hamit) intrusive rocks; and (d) the volcanic rocks from the Eastern Anatolian Collision Zone are also given for comparison (Pearce et al., 1990). Abbreviations: Cf-Cefalikdag, Ba-Baranadag, H-Hamit, KARA-Karacalidag (mildly alkaline), MUS-Mus (mildly alkaline) and TEN-Tendurek (strongly alkaline). Normalisation factors are taken from Sun and McDonough (1989).

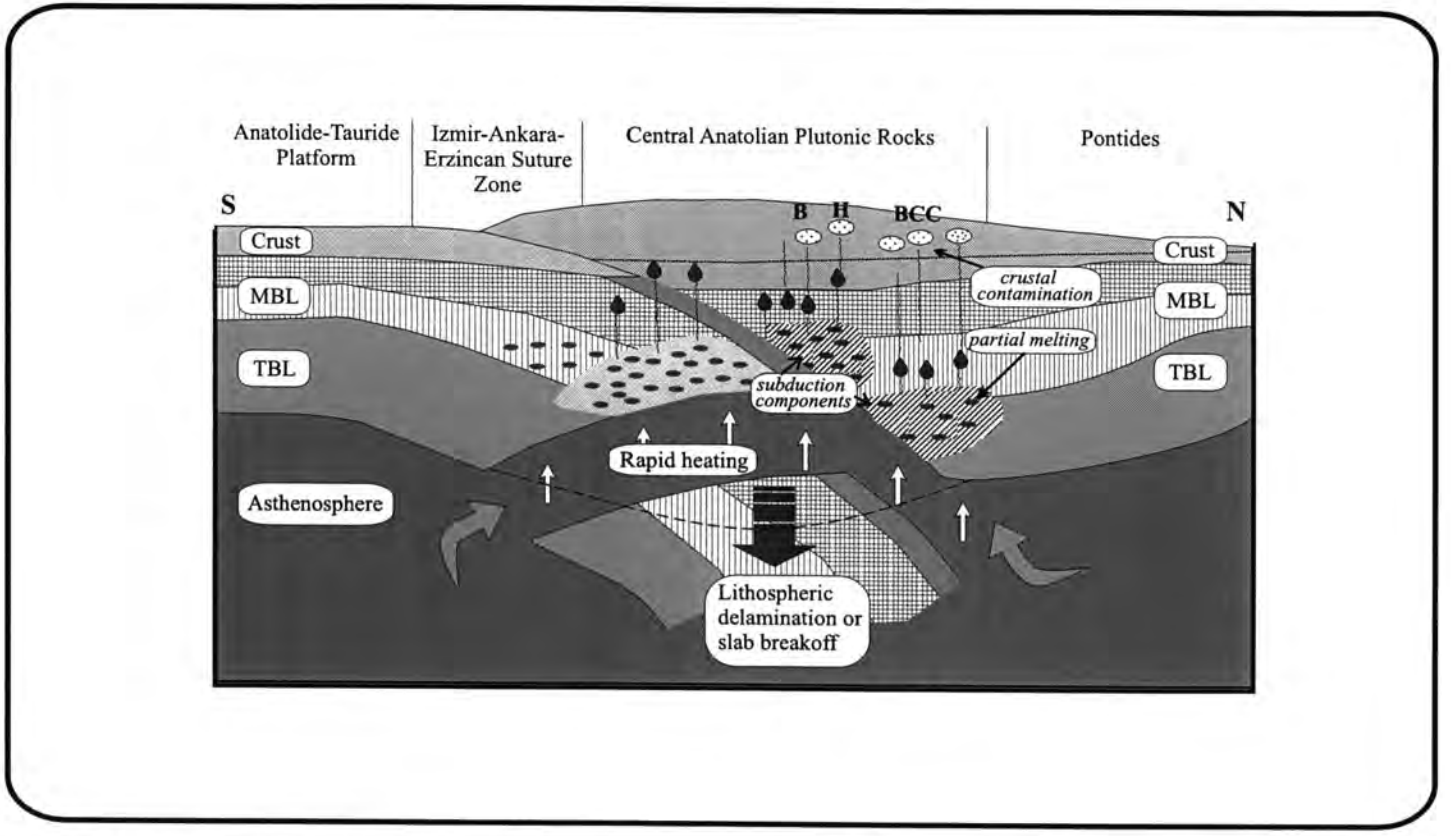

Figure 7.12. Systematic model showing the possible origin of coexisting calc-alkaline (BCC) and alkaline (H) magmas in the Central Anatolian Massif. Abbreviations: MBL-mechanical boundary layer, TBL-thermal boundary layer, BCC-Behrekdag, Cefalikdag, Celebi plutons, B-Baranadag pluton and H-Hamit pluton.

7.4.3. Model for magma generation

The heat source generating post-collisional Central Anatolian plutonic rocks in the Massif could be provided by the lithospheric delamination of the thickened thermal boundary layer, or by the removal of a subducted plate (Figure 7.12).

The original concept of ***delamination*** was developed by Bird (1978, 1979), Bird and Baumgardner (1981) and Houseman et al. (1981). Recent geophysical research undertaken on active and fossil collision zones strengthened the idea that the lithospheric delamination is both common and fundamentally important for collision settings (Nelson, 1992).

It has been argued that the thickened thermal boundary layer (TBL), being colder and denser than its surroundings, could be convectively replaced by asthenosphere (Houseman et al., 1981; England and Houseman, 1988; Platt and England, 1993; England, 1993), causing asthenosphere to rise close to the metasomatised lithosphere. This close contact leads to extensive partial melting of the metasomatised lithosphere.

A lithospheric delamination model for magma genesis in the Eastern Anatolian Collision Zone was constructed by Pearce et al. (1990). They argued that because of the thermal constraints in melting the convecting upper mantle, and the weight of evidence against a mantle plume origin, volcanism across the Eastern Anatolian Collision Zone were derived from delamination of the thermal boundary layer, or localised extension, or both.

The original concept of ***a removal of a subducted plate (slab breakoff)*** was proposed by Davies and Blackenburg (1995). Continental collisions are preceded by subduction of dense oceanic lithosphere, and followed by attempted subduction of buoyant continental lithosphere. The situation of opposing buoyancy forces leads to extensional deformation in the subducted slab. A narrow rifting mode of deformation will result if there is strain localisation. Slab breakoff results. As a result of the rifting during breakoff, the asthenosphere upwells into the narrow rift. The resulting conducted thermal perturbation leads to melting of the metasomatised overriding mantle lithosphere.

Unfortunately, the mechanism to generate melt in the Central Anatolian Massif is not clear and there is not any structural evidence for the localised extension in the Massif. Therefore, either the delamination of the TBL or slab breakoff may

have generated the primary magmas for the Central Anatolian plutonic rocks. Delamination of the TBL or slab breakoff have increased the thermal gradient in the Massif, and thus weakened the lithosphere. This may have assisted or initiated orogenic collapse that followed collision and uplift.

7.5. Summary

The major and trace element and mainly isotope data have revealed a number of important features of the Central Anatolian plutonic rocks.

The Central Anatolian plutonic rocks show isotopic and trace element evidence of containing a significant crustal component. That crustal component is comprised of two parts, one of which (source enrichment) is associated with a subduction zone, and the other of which (crustal contamination) took place via assimilation during magmatic ascent through the thickened Central Anatolian crust.

In the Central Anatolian Massif, first, the mantle source is contaminated by a material containing radiogenic Sr and unradiogenic Nd. Subduction of sediment and/or altered oceanic crust released fluids into the mantle. A small amount of continental material (4% to 6%) has been contributed to the source contamination process.

In a post-collisional setting, partial melts from this metasomatised mantle have been affected by crustal assimilation and fractional crystallisation (AFC) during uprise through the crust.

Initial $^{87}Sr/^{86}Sr$ and $^{143}Nd/^{144}Nd$ ratios versus silica diagrams show that the parental magma for the BCC plutonic rocks (source I-S_I) has higher initial $^{87}Sr/^{86}Sr$ and lower initial $^{143}Nd/^{144}Nd$ ratios than the parental magma for the B, H plutonic rocks (source II-S_{II}). This has been explained by either a greater subduction component in source I or more crustal contamination during uprise through continental crust compared to source II. These explanations have been supported by the Th/Yb versus Ta/Yb plot.

On diagrams of Ba against Rb and Ba against Sr (Chapter 7), two main trends are distinguished for the BCC (trend 1a) and B, H plutonic rocks (trend 2a). In addition, two sub-trends are identified for the BCC (trend 1b) and B, H plutonic rocks (trend 2b). The Ba against Rb and Ba against Sr diagrams show that trend 1a was controlled by plagioclase, hornblende, alkali feldspar and biotite crystallisation,

whereas trend 1b was controlled by alkali feldspar, plagioclase and biotite crystallisation. On the other hand, trend 2a was controlled by plagioclase, clinopyroxene and alkali feldspar crystallisation, whereas trend 2b was controlled by alkali feldspar and plagioclase crystallisation.

In the Rb versus (Y+Nb) diagram, the parental magma for the BCC plutonic rocks plots in the VAG field, whereas the parental magma for the B, H plutonic rocks falls in the WPG field. Coupled crustal assimilation and fractional crystallisation of the parental magma for the BCC plutonic rocks could cause enrichment in Rb and consistency in (Y+Nb) for these plutonic rocks. Therefore, all rock compositions from the BCC plutons remain in the VAG field. On the other hand, coupled crustal assimilation and fractional crystallisation of the parental magma for the B, H plutonic rocks could result in depletion in Rb and (Y+Nb). Crustal assimilation coupled with fractional crystallisation has been invoked to take the B, H plutonic rocks from the WPG field to the VAG field.

Coexistence of calc-alkaline and alkaline magmatism in the Central Anatolian Massif has been explained by differences in their mantle source regions and mantle heterogeneity pre-collision. The source region beneath the BCC plutonic rocks is more enriched in Sr isotope ratios and more depleted in Nd isotope ratios than the source region for the B, H plutonic rocks. The Th/Yb versus Ta/Yb diagram shows that the H plutonic rocks are more enriched in a within-plate mantle component than the BCC and B plutonic rocks.

Because of the lack of evidence for localised extension, initiation of post-collisional magmatism in the Central Anatolian Massif has been explained by either a delamination of the thickened thermal boundary layer (TBL), or a removal of a subducted plate (slab breakoff). Either of these mechanisms can cause the hot asthenosphere to rise close to the metasomatised lithosphere, initiating melting.

Chapter 8
CONCLUSIONS

Introduction

This chapter summarises the general characteristics of the Central Anatolian plutonic rocks, as presented in previous chapters.

8.1. General characteristics of the Central Anatolian plutonic rocks

The intrusive rocks of the Central Anatolian Massif can be divided into three main groups on the basis of their major-trace element and isotopic characteristics. These are: (i) calc-alkaline (Behrekdag, Cefalikdag, Celebi-BCC); (ii) transitional between calc-alkaline and alkaline (Baranadag-B); and (ii) alkaline (Hamit-H).

8.1.1. The BCC (Behrekdag, Cefalikdag, Celebi) plutonic rocks

These plutonic rocks cover a broad petrological range from monzodiorite to granite, mainly monzonite (Chapter 2). The Behrekdag and Celebi plutonic rocks are quartz monzonite and granite in composition. The Cefalikdag intrusive rocks range from monzodiorite (Savciliebeyit monzodiorite) through quartz monzonite (Kucukcurtepe quartz monzonite) to granite (Kaletepe granite). These rock types are generally coarse-grained to porphyritic with feldspar megacrysts. The BCC plutonic rocks are, in general, cut by aplitic and pegmatitic dykes. Enclaves are common throughout these plutons.

The Behrekdag and Celebi plutonic rocks comprise plagioclase, alkali feldspar, quartz, amphibole, biotite, and clinopyroxene (Chapter 3). The Savciliebeyit monzodiorite and Kucukcurtepe quartz monzonite are made up of similar mineral compositions. However, the former is more enriched in mafic minerals such as amphibole, biotite and clinopyroxene compared to the latter. The Kaletepe granite comprises alkali feldspar, plagioclase, quartz and biotite.

Plagioclases from the Behrekdag and Celebi plutons are mainly andesine, whereas plagioclases from the Cefalikdag plutons are labradorite to oligoclase in composition (Chapter 4). On the classification diagram of Leake et al. (1997),

amphiboles from the BCC plutons plot into the edenite and magnesio-hornblende fields. On the Quad diagrams, clinopyroxenes from the BCC plutons plot in the salite field. The BCC plutonic rocks have pressures between 2.6 and 5.2 kbar (using the Schmidt's calibration, 1992). They have crystallisation temperatures ranging from 716 to 858 °C (using the Blundy and Holland's calibration, 1990).

These rock types are generally calc-alkaline, metaluminous and I-type (Chapter 5). The BCC plutonic rocks have LREE-enriched patterns with small to moderate negative Eu anomalies (Chapter 5). In the tectonic discrimination diagrams of Pearce et al. (1984), they plot in the volcanic arc granite (VAG) and syn-COLG granite fields.

8.1.1.1. The enclaves

Two types of igneous enclave have been recognised in the BCC plutonic rocks (Chapter 6); (i) fine-grained (Type-I); and (ii) medium-grained to porphyritic with feldspar megacrysts (Type-II).

(i) Fine-grained varieties (Type-I)

They are quartz diorite and quartz monzodiorite, which are made up of plagioclase, alkali feldspar, clinopyroxene, amphibole, biotite and quartz. They are finer-grained and darker than the host. Contacts with host rocks are generally sharp and, occasionally, have crenulated fine-grained margins. They show a hypidiomorphic, granular texture.

Plagioclase from the Type-I enclaves is mainly andesine in composition. On the IMA classification scheme (Leake et al., 1997), amphiboles from the enclaves are classified as edenite. Clinopyroxenes in the Type-I enclaves are salite in composition.

The rare earth element patterns of the Type-I enclaves are characterised by enrichment in the LREE relative to the MREE and HREE, with small to moderate Eu anomalies. The Type-I enclaves are generally characterised by enrichments in LILEs relative to HFSEs.

(ii) Medium-grained to porphyritic varieties (Type-II)

They are darker than the host rocks and contacts are sharp. They are quartz diorite and gabbro, comprising plagioclase, amphibole, biotite, clinopyroxene, alkali feldspar and quartz. They are medium-grained and show generally cumulate textures.

Plagioclase from the Type-II enclaves is mainly andesine in composition. On the IMA classification scheme (Leake et al., 1997), amphiboles from the Type-II enclaves predominantly fall in the ferro-edenite field. Clinopyroxenes in the Type-II enclaves are salite in composition.

The Type-II enclaves have LREE-enriched patterns with small to moderate Eu anomalies. They are slightly more enriched in HREE compared to the Type-I enclaves. The Type-II enclaves have smaller Eu anomalies than the Type-I enclaves. The Type-II enclaves show enrichment in LILEs relative to HFSEs.

The Type-I enclaves have been interpreted as magma mixing/mingling products originated from injection of mafic magma into more silicic magma. This is evident from their textural features (fine-grained margins), grain size (fine-grained), petrographic characteristics (hypidiomorphic granular texture; acicular apatite), and geochemical characteristics (most of the samples show similar major and trace element contents to the host rocks).

However, the Type-II enclaves have been interpreted as cumulates of early-crystallised minerals (clinopyroxene, plagioclase, amphibole and biotite) from the granitoid magmas. This is evident from their grain size (medium-grained), petrographic characteristics (cumulate textures; similar mineral phases to the host rocks), mineralogical features (similar mineral compositions to the host rocks) and geochemical characteristics (e.g. most of the samples lie on the extensions of the BCC plutonic rock trends).

Origin and evolution of enclaves are strongly linked to those of their host rocks. For example, mafic to intermediate Type-I enclaves (originated from magma mixing/mingling) in the BCC plutonic rocks indicate existence of some interaction between silicic magmas and mantle-derived melts. On the other hand, mafic Type-II enclaves (formed as cumulates of early crystallised minerals) give an information about the early crystallised minerals in the parental magma of the plutonic rocks.

8.1.2. The B (Baranadag) plutonic rocks

They are monzonite and quartz monzonite, which comprise alkali feldspar, plagioclase, quartz, amphibole, clinopyroxene, and biotite. These rock types are generally coarse-grained to porphyritic with feldspar megacrysts. The B plutonic rocks are cut by aplitic, pegmatitic and microsyenitic dykes. Enclaves are common throughout this pluton.

Plagioclase from the B pluton is mainly andesine and oligoclase (Chapter 4). On the classification diagram of Leake et al. (1997), amphiboles from the B pluton fall in both the edenite and magnesio-hastingsite fields. On the Quad diagrams, clinopyroxenes from the B pluton fall in the salite field. The B plutonic rocks have pressures between 4.1 and 5.3 kbar. They have crystallisation temperatures ranging from 750 to 783 ^{o}C.

They are calc-alkaline, metaluminous and I-type (Chapter 5). The B plutonic rocks have steeper LREE-enriched patterns than the BCC plutonic rocks but they have similar small to moderate negative Eu anomalies (Chapter 5). In the tectonic discrimination diagrams of Pearce et al. (1984), they fall between the volcanic arc granite and syn-COLG granite and the within-plate granite (WPG) fields.

8.1.3. The H (Hamit) plutonic rocks

They range from nepheline monzosyenite/pseudoleucite monzosyenite through alkali feldspar syenite to quartz syenite (Chapter 2). The nepheline monzosyenite is medium-grained and occasionally porphyritic with alkali feldspar megacrysts. The pseudoleucite monzosyenite is porphyritic with alkali feldspar and pseudoleucite megacrysts. The alkali feldspar syenite and quartz syenite are generally medium-grained. The nepheline monzosyenite and pseudoleucite monzosyenite are cut by foid-bearing micro-syenitic rocks. However, the alkali feldspar syenite and quartz syenite are cut by aplitic and silicic dykes.

The foid-bearing rocks are mainly composed of alkali feldspar, plagioclase, (±) pseudoleucite, clinopyroxene, nepheline, garnet, amphibole and biotite (Chapter 3). The foid-bearing rocks have a higher proportion of mafic minerals (e.g. clinopyroxene, amphibole, biotite) than the alkali feldspar syenite and the quartz syenite. The alkali feldspar syenite and quartz syenite are mainly made up of alkali feldspar, plagioclase and (±) quartz.

Plagioclase from the nepheline monzosyenite plots in the labradorite, andesine and oligoclase fields (Chapter 4). Plagioclase from the pseudoleucite monzosyenite is mainly labradorite, whereas plagioclase from the alkali feldspar syenite is mainly albite. However, plagioclase in the quartz syenite is albite and oligoclase. On the classification diagram of Leake et al. (1997), amphiboles from the nepheline monzosyenite and pseudoleucite monzosyenite fall in the hastingsite field, however those from the alkali feldspar syenite and quartz syenite plot in the edenite field. On the Quad diagrams, clinopyroxenes from the H pluton fall in the salite field. The quartz syenite from the H pluton has pressures ranging from 3.4 to 3.9 kbar and its crystallisation temperatures ranging from 736 to 751 °C.

They are alkaline-potassic. The nepheline monzosyenite and pseudoleucite monzosyenite are metaluminous but the alkali feldspar syenite and quartz syenite are generally peralkaline and A-type (Chapter 5). The H plutonic rocks have higher abundances of LREE and MREE than the BCC and B plutonic rocks (Chapter 5). In the tectonic discrimination diagrams of Pearce et al. (1984), the alkali feldspar syenite and quartz syenite plot in the WPG field.

8.2. Magmatic evolution of the Central Anatolian plutonic rocks

After consideration of all available data from this work, an evolution model of the Central Anatolian plutonic rocks has emerged as follows:

(i) The parental magmas for the BCC and B, H plutonic rocks were generated from mantle sources which were modified by a subduction component before collision. The initial Sr versus Nd isotope ratios diagram shows that the addition of a subduction component into a mantle source was primarily responsible for the enriched isotope characteristics of the plutonic rocks. In addition, in the multi-element diagrams, the plutonic rocks have enrichments in LILE and LREE relative to HFSE (defined by negative Ta and Nb anomalies), indicating subduction components in their sources. Furthermore, in the Th/Yb versus Ta/Yb plot the plutonic rocks form trends that run parallel to the mantle metasomatism array but are displaced towards higher Th/Yb ratios, reflecting derivation from an enriched mantle source to which a subduction component had been added. This diagram also shows that the H

plutonic rocks are more enriched in a within-plate mantle component compared to the BCC and B plutonic rocks. In keeping with the behaviour of the trace elements, the isotopic characteristics for the H plutonic rocks also reveal a subduction modified, less radiogenic mantle source characterised by lower initial $^{87}Sr/^{86}Sr$ but higher initial $^{143}Nd/^{144}Nd$ ratios compared to the BCC plutonic rocks.

(ii) The magmas have experienced coupled crustal assimilation and fractional crystallisation during uprise through the Central Anatolian crust. Rb, Nb, Y versus silica diagrams and the tectonic discrimination diagram of Rb versus (Y+Nb) show that the BCC and B, H plutonic rocks have been affected by assimilation combined with fractional crystallisation processes.

(iii) The magmas evolved by fractional crystallisation. The least acidic rocks of the BCC plutons were predominantly controlled by plagioclase, hornblende and alkali feldspar crystallisation. However, the more acidic rocks of the BCC plutons were controlled by alkali feldspar, plagioclase and biotite crystallisation. On the other hand, the least acidic rocks of the B, H plutons were controlled by plagioclase, clinopyroxene and alkali feldspar crystallisation, whereas the more acidic rocks of the B, H plutons were controlled by alkali feldspar and plagioclase crystallisation.

(iv) Coexistence of calc-alkaline and alkaline magmatism in the Central Anatolian Massif has been attributed to compositional differences in their mantle sources and mantle source heterogeneity before collision.

(v) Because of the lack of evidence for localised extension, initiation of magmatism in the Massif has been ascribed to have been caused by either a delamination of the thickened thermal boundary layer (TBL), or a removal of a subducted plate (slab breakoff).

REFERENCES

Akiman, O., Erler, A., Göncüoglu, M.C., Gülec, N., Geven, A., Türeli, T.K. and Kadioglu, Y.K., 1993. Geochemical characteristics of granitoids along the western margin of the Central Anatolian Crystalline Complex and their implications. *Geological Journal,* v. 28, pp. 371-382.

Allégre, C.J., Provost, A. and Jaupart, C., 1987. A discussion of PIXAN and PIXANPC – the AAEC PIXE analysis computer packages. *Nuclear Instruments and Methods,* v. B22, pp. 64-67.

Allen, C.M., 1991. Local equilibrium of mafic enclaves and granitoids of the Turtle pluton, southeast California: mineral, chemical, and isotopic evidence. *American Mineralogist,* v. 76, pp. 574-588.

Anderson, J.L., 1983. Proterozoic anorogenic granite plutonism of North America. *Geological Society of America Memoir,* v. 161, pp. 133-152.

Anderson, J.L., 1996. Status of thermobarometry in granitic batholiths. *Transactions of the Royal Society of Edinburgh,* v. 87, pp. 125-138.

Anderson, J.L. and Smith, D.R., 1995. The effects of temperature and fO_2 on the Al-in-hornblende barometer. *American Mineralogist,* v. 80, pp. 549-559.

Arculus, R.J., 1987. The significance of source versus process in the tectonic controls of magma genesis. *Journal of Volcanology and Geothermal Research,* v. 32, pp. 1-12.

Arculus, R.J. and Willis, K.J.A., 1980. The petrology of plutonic blocks and inclusions from the Lesser Antilles island arc. *Journal of Petrology,* v. 21, pp. 743-799.

Arth, J.G., 1976. Behavior of trace elements during magmatic processes-a summary of theoretical models and their applications. *Jour. Research U.S. Geol. Survey,* v. 4, pp. 41-47.

Ataman, G., 1972. Ankara'nin güneydogusundaki granodiyoritik kütlelerden Cefalik Daginin radyometrik yasi hakkinda ön calisma. *Hacettepe Fen ve Mühendislik Bilimleri Dergisi,* v. 2, pp. 44-49.

Ayan, M., 1963. Contribution a l'etude petrographique et geologique de la region situee au Nord-Est de Kaman. *Maden Tetkik ve Arama Enstitüsü Yayini,* v. 115, pp. 1-332.

Bacon, C.R., 1986. Magmatic inclusions in silicic and intermediate volcanic rocks. *Journal of Geophysical Research,* v. 91, pp. 6091-6112.

Barbarin, B., 1988. Field evidence for successive mixing and mingling between the Piolard diorite and the Saint-Julien-la-Vêtre monzogranite (Nord-Forez, Massif Central, France). *Canadian Journal of Earth Sciences,* v. 25, pp. 49-59.

Barbarin, B., 1991. Enclaves of the Mesozoic calc-alkaline granitoids of the Sierra Nevada batholith, California. In: Didier, J. and Barbarin, B. (eds), *Granites and Their Enclaves: The Bearing of Enclaves on the Origin of Granites.* Developments in Petrology, 3. Elsevier, Amsterdam, pp. 135-153.

Barth, T.F.W., 1951. The feldspar geologic thermometers. *Neues Jachrbuch fur Mineralogie, Abhandlungen,* v. 82, pp. 143-154.

Barth, A.P., Wooden, J.L, Tosdal, R.M. and Morrison, J., 1995. Crustal contamination in the petrogenesis of a calc-alkalic rock series: Josephine Mountain intrusion, California. *Bulletin of Geological Society of America,* v. 107, pp. 201-212.

Bateman, P.C., Clark, L.D., Huber, N.K., Moore, J.G. and Rinehart, C.D., 1963: The Sierra Nevada batholith- a synthesis of recent work across the central part. *U.S. Geol. Surv., Prof. Pap.,* 414: D1-D46.

Bayhan, H., 1984. Kesikköprü skarn kusaginin (Bala-Ankara) mineralojisi ve petrolojisi. *Yerbilimleri,* v. 11, pp. 45-57.

Bayhan, H., 1986. Ic Anadolu granitoyid kusagindaki Celebi sokulumunun jeokimyasi ve kökensel yorumu. *Jeoloji Mühendisligi Dergisi,* v. 29, pp. 27-36.

Bayhan, H., 1987. Cefalikdag ve Baranadag plutonlarinin (Kaman) petrografik ve kimyasal-mineralojik özellikleri. *Jeoloji Mühendisligi Dergisi,* v. 30-31, pp. 11-16.

Bayhan, H., 1989. Keskin sokulumunun (Ankara) petrografik ve kimyasal-mineralojik ozellikleri. *Yerbilimleri,* v. 15, pp. 29-36.

Bingöl, E., 1989. Geological map of Turkey, 1:2 000 000. *Mineral Research and Technical Institute,* Ankara.

Bird, P., 1978. Initiation of intracontinental subduction in the Himalaya. *Journal of Geophysical Research,* v. 83, pp. 4975-4987.

Bird, P., 1979. Continental delamination and the Colorado Plateau. *Journal of Geophysical Research,* v. 84, pp. 7561-7571.

Bird, P. and Baumgardner, J., 1981. Steady propagation of delamination events. *Journal of Geophysical Research,* v. 86, pp. 4891-4903.

Blundy, J.D. and Holland, T.J.B., 1990. Calcic amphibole equilibria and a new amphibole-plagioclase thermometer. *Contributions to Mineralogy and Petrology,* v. 104, pp. 208-224.

Bonin, B., 1990. From orogenic to anorogenic settings: evolution of granitoid suites after a major orogenesis. *Geological Journal,* v. 25, pp. 261-270.

Bowen, N.L., 1928. *The Evolution of the Igneous Rocks.* Princeton University Press, 332 pp.

Boynton, W.V., 1984. Geochemistry of the rare earth elements: meteorite studies. In: Henderson, P. (ed), *Rare Earth Element Geochemistry.* Elsevier, pp. 63-114.

Brown, L., Klein, J., Middleton, R, Sacks, I.S. and Tera, F., 1982. ^{10}Be in island-arc volcanoes and implications for subduction. *Nature,* v. 299, pp. 718-720

Brown, W.L. and Parsons, I., 1981. Towards a more practical two feldspar geothermometer. *Contributions to Mineralogy and Petrology,* v. 76, pp. 369-377.

Buddington, A.F. and Lindsley, D.H., 1964. Iron-titanium oxide minerals and synthetic equivalents. *Journal of Petrology,* v. 54, pp. 310-357.

Carroff, M., Maurey, R.C., Leterrier, J., Joron, J.L., Cotten, J. and Guille, G., 1993. Trace element behavior in the alkali basalt-comenditic trachyte series from Mururoa Atoll, French Polynesia. *Lithos,* v. 30, pp. 1-22.

Carmichael, I.S.E., 1991. The redox states of basic and silicic magmas: a reflection of their source regions? *Contributions to Mineralogy and Petrology,* v. 106, pp. 129-141.

Castro, A., Moreno-Ventas, I. and De la Rosa, J.D., 1990. Microgranular enclaves as indicators of hybridization processes in granitoid rocks, Hercynian belt, Spain. *Geological Journal,* v. 25, pp. 391-404.

Cawthorn, R.G. and Collerson, K.D, 1974. The recalculation of pyroxene end-member parameters and the estimation of ferrous and ferric iron content from electron microprobe analyses. *American Mineralogist,* v. 59, pp. 1203-1208.

Chappell, B.W., 1966. Petrogenesis of the Granites at Moonbi, New South Wales. Ph.D. Thesis, The Australian National University (unpublished).

Chappell, B.W., 1978. Granitoids from the Moonbi district, New England batholith, eastern Australia. *Journal of Geological Society, Australia,* v. 25, pp. 267-283.

Chappell, B.W. and White, A.J.R., 1974. Two contrasting granite types. *Pacific Geology,* v. 8, pp. 173-179.

Chappell, B.W., White, A.J.R. and Wyborn, D., 1987. The importance of residual source material (restite) in granite petrogenesis. *Journal of Petrology,* v. 28, pp. 1111-1138.

Chappell, B.W. and White, A.J.R, 1991. Restite enclaves and the restite model. In: Didier, J. and Barbarin, B. (eds), *Granites and Their Enclaves: The Bearing of*

Enclaves on the Origin of Granites. Developments in Petrology, 3. Elsevier, Amsterdam, pp. 375-381.

Clemens, J.D., Holloway, J.R. and White, A.J.R., 1986. Origin of A-type granite: experimental constraints. *American Mineralogist,* v. 71, pp. 317-324.

Cocirta, C., 1986. Les enclaves microgrenues sombre du massif de Bono (Sardaigne septentrionale). Signification pétrogénétique des plagioclases complex et de leur inclusions. *C. R. Acad. Sc. Paris,* v. 302, pp. 441-446.

Collins, W.J., Beams, S.D., White, A.J.R. and Chappell, B.W., 1982. Nature and origin of A-type granites with particular reference to southeastern Australia. *Contributions to Mineralogy and Petrology,* v. 80, pp. 189-200.

Cox, K.G. and Hawkesworth, C.J., 1985. Geochemical stratigraphy of the Deccan Traps, at Mahabaleshwar, western Ghats, India, with implications for open system magmatic processes. *Journal of Petrology,* v. 26, pp. 355-377.

Currie, K.L., 1991. A simple quantitative calculation of mol fractions of amphibole end-members. *Canadian Mineralogist,* v. 29, pp. 287-299.

Czamanske, G.K. and Wones, D.R., 1973. Oxidation during magmatic differentiation, Finnmarka complex, Oslo area, Norway: Part 2, the mafic silicates. *Journal of Petrology,* v. 14, pp. 349-380.

Czamanske, G.K., Ishihara, S. and Atkin, S.A., 1981. Chemistry of rock-forming minerals of the Cretaceous-Paleocene batholith in southwestern Japan and implications for magma genesis. *Journal of Geophysical Research,* v. 86, pp. 10431-10469.

Davies, J.H. and Von Blanckenburg, F., 1995. Slab breakoff: a model of lithosphere detachment and its test in the magmatism and deformation of collisional orogens. *Earth and Planetary Science Letters,* v. 129, pp. 85-102.

DePaolo, D.J., 1981. A Nd and Sr isotopic study of the Mesozoic calc-alkaline granitic batholiths of the Sierra Nevada and Peninsula ranges, California. *Journal of Geophysical Research,* v. 86, pp. 10470-10488.

DePaolo, D.J., 1988. *Neodymium Isotope Geochemistry: An Introduction.* Minerals and Rocks 20, Springer-Verlag, New York, 187 pp.

DePaolo, D.J. and Wasserburg, G.J., 1979. Petrogenetic mixing models and Nd-Sr isotopic patterns. *Geochimica et Cosmochima Acta,* v. 43, pp. 615-627.

Didier, J., 1973. *Granites and Their Enclaves: The Bearing of Enclaves on the Origin of Granites.* Developments in Petrology, 3. Elsevier, Amsterdam, 393 pp.

Didier, J., 1984. The problem of enclaves in granitic rocks, a review of recent ideas on their origin. In: Xu, K. and Tu, G. (eds), *Geology of Granites and Their Metallogenic Relations*. Beijing, Science Press, pp. 137-144.

Didier, J., 1987. Contribution of enclave studies to the understanding of origin and evolution of granitic magmas. *Geologische Rundschau,* v.76, pp. 41-50.

Didier, J. and Barbarin, B., 1991. The different type of enclaves in granites-nomenclature. In: Didier, J. and Barbarin, B. (eds), *Granites and Their Enclaves: The Bearing of Enclaves on the Origin of Granites.* Developments in Petrology, 3. Elsevier, Amsterdam, pp. 19-21.

Dietrich, H. and Petrakakis, K., 1986. A linear algebraic method for the calculation of pyroxene end-member components. *Tschermaks Mineralogische und Petrographische Mitteilungen,* v. 35, pp. 275-282.

Dollase, W. and Newman, W., 1984. Statistically most probable stoichiometric formulae. *American Mineralogist,* v. 69, pp. 553-556.

Dorais, M.J., Whitney, J.A. and Redon, M.F., 1990. Origin of mafic enclaves in the Dinkey Creek pluton, central Sierra Nevada batholith, California. *Journal of Petrology*, v. 31, pp. 853-881.

Dudas, M.J., Schmidt, R.A. and Harward, M.E., 1971. Trace element partitioning between volcanic plagioclase and dacitic pyroclastic matrix. *Earth and Planetary Science Letters,* v. 11, pp. 440-446.

Eichelberger, J.C., 1975. Origin of andesite and dacite: evidence of mixing at Lass Mountain in California and other circum-Pacific volcanoes. *Bulletin of Geological Society of America,* v. 86, pp. 1381-1391.

Eichelberger, J.C., 1980. Vesiculation of mafic magma during replenishment of silicic magma reservoirs. *Nature,* v. 288, pp. 446-450.

Elkins, L.T. and Grove, T.L., 1990. Ternary feldspar experiments and thermodynamic models. *American Mineralogist,* v. 75, pp. 544-559.

Emslie, R.F. and Stirling, J.A.R., 1993. Rapakivi and related granitoids of the Nain plutonic suite: geochemistry, mineral assemblages and fluid equilibria. *Canadian Mineralogist,* v. 31, pp. 821-847.

England, P., 1993. Convective removal of thermal boundary layer of thickened continental lithosphere: a brief summary of causes and consequences with special reference to the Cenozoic tectonics of the Tibetan Plateau and surrounding regions. *Tectonophysics,* v. 223, pp. 67-73.

England, P.C. and Houseman, G.A., 1988. The mechanics of the Tibetan Plateau. *Philosophical Transactions of Royal Society of London,* v. 326, pp. 523-532.

Erkan, Y., 1976. Kirsehir cevresindeki rejyonal metamorfik bölgede saptanan izogradlar ve bunlarin petrolojik yorumlamalari. *Yerbilimleri,* v. 1, pp. 213-218.

Erkan, Y., 1981. Orta Anadolu Masifinin metamorfizmasi üzerine yapilmis calismalarda varilan sonuclar. In: Akkök, R., Oygur, V. and Terlemez, I. (eds), *Ic Anadolu'nun Jeolojisi Sempozyumu.* Türkiye Jeoloji Kurumu, pp. 9-11.

Erkan, Y. and Ataman, G., 1981. Orta Anadolu Masifi (Kirsehir yöresi) metamorfizma yasi üzerine K-Ar yöntemi ile bir inceleme. *Yerbilimleri,* v. 8. pp. 27-30.

Erler, A., Akiman, O., Unan, C., Dalkilic, B., Geven, A. and Onen, P., 1991. Kaman (Kirsehir) ve Yozgat yörelerinde Kirsehir Masifi magmatik kayaclarinin petrolojisi ve jeokimyasi. *Doga-Türk Yerbilimleri Dergisi,* v. 15, pp. 76-100.

Ewart, A., 1982. The mineralogy and petrology of Tertiary-Recent orogenic volcanic rocks: with special reference to the andesitic-basaltic compositional range. In: Thorpe, R.S. (ed), *Andesites: Orogenic Andesites and Related Rocks.* Allen and Urwin, London, pp. 25.87.

Ewart, A., Hildreth, W. and Carmichael, I.S.E., 1975. Quaternary acid magmas in New Zealand. *Contributions to Mineralogy and Petrology,* v. 51, pp. 1-27.

Faure, G., 1986. *Principles of Isotope Geology.* John Wiley and Sons, New York 589 pp.

Fernandez, A.N. and Barbarin, B., 1991. Relative rheology of coeval mafic magmas: nature of resulting interaction processes. Shape and mineral fabrics of mafic microgranular enclaves. In: Didier, J. and Barbarin, B. (eds), *Granites and Their Enclaves: The Bearing of Enclaves on the Origin of Granites.* Developments in Petrology, 3. Elsevier, Amsterdam, pp. 263-275.

Frost, T.P. and Mahood, G.A., 1987. Field, chemical and physical constraints on mafic-felsic magma interaction in the Lamarck granodiorite, Sierra Nevada, California. *Bulletin of Geological Society of America,* v. 99, pp. 272-291.

Fuhrman, M.L. and Lindsley, D.H., 1988. Ternary-feldspar modelling and thermometry. *American Mineralogist,* v. 73, pp. 201-215.

Furman, T. and Spera, F.J., 1985. Co-mingling of acid and basic magma with implications for the origin of mafic I-type xenoliths: field and petro-chemical relations of an unusual dike complex at Eagle Lake, Sequoia National Park, California, USA. *Journal of Volcanology and Petrology,* v. 24, pp. 151-178.

Fyfe, W.S., 1992. Magma underplating of continental crust. *Journal of Volcanology and Petrology,* v. 50, pp. 33-40.

Geven, A., 1992. Mineralogy, Petrography and Geochemistry of Cefalikdag Plutonic Rocks (Kaman Region-Central Anatolia). Ph.D. Thesis, Middle East Tehnical University, 165 pp. (unpublished).

Ghiorso, M.S., 1984. Activity/composition relations in the ternary feldspars. *Contributions to Mineralogy and Petrology,* v. 87, pp. 201-215.

Giannetti, B. and Luhr, J.F., 1990. Phologopite-clinopyroxene nodules from high-K magmas, Roccamonfina volcano, Italy: evidence for a low pressure metasomatic origin. *Earth and Planetary Science Letters,* v. 101, pp. 404-424.

Gill, J.B., 1981. *Orogenic Andesites and Plate Tectonics.* Springer-Verlag, Berlin, 390 pp.

Gòmez, J.M.C., 1990. PX: a program for pyroxene classification and calculation of end-members. *American Mineralogist,* v. 75, pp. 1426-1427.

Göncüoglu, M.C., 1977. Geologie des westlichen Nigde Massivs. Ph.D. Thesis, University of Bonn, 181 pp. (unpublished).

Göncüoglu, M.C., 1986. Orta Anadolu Masifinin güney ucundan jeokronolojik yas bulgulari. *Maden Tetkik ve Arama Enstitüsü Dergisi,* v. 105-106, pp. 111-124.

Göncüoglu, M.C., 1990. Subophilitic metamorphics at the Kütahya-Bolkardag Belt: northern margin of the Menderes Massif, NW Anatolia. *Ofioliti,* v. 15, pp. 340-345.

Göncüoglu, M.C., Erler, A., Toprak, V., Yaliniz, K., Olgun, E. and Rojay, B., 1991. Orta Anadolu Masinin Bati Kesiminin Jeolojisi, Bölüm I: Güney Kesim. *Türkiye Petrolleri Anonim Ortakligi Raporu.* Rapor No:2909, 134 pp.

Göncüoglu, M.C., Erler, A., Toprak, V., Yaliniz, K., Olgun, E. and Rojay, B., 1992a. Orta Anadolu Masinin Bati Kesiminin Jeolojisi, Bölüm II: Orta Kesim. *Türkiye Petrolleri Anonim Ortakligi Raporu.* Rapor No:3155, 766 pp.

Görür, N., Oktay, F.Y., Seymen, I. and Sengör, A.M.C., 1984. Paleotectonic evolution of the Tuzgolu basin complex, central Anatolia (Turkey): sedimentary record of a Neo-Tethyan closure. In: Dixon, J.E. and Robertson, A.H.F. (eds), *The Geological Evolution of the Eastern Mediterranean.* Geological Society of London Special Publication No: 17. Blackwell Scientific Publications, Oxford, pp. 467-482.

Green, N.L. and Usdansky, S.I., 1986. Ternary-feldspar mixing relations and thermobarometry. *American Mineralogist,* v. 71, pp. 110-1108.

Green, T.H. and Pearson, N.J., 1986. Rare-earth element partitioning between sphene and coexisting silicate liquid at high pressure and temperature. *Chemical Geology,* v. 55, pp. 105-119.

Griffin, T.J., White, A.J.R. and Chappell, B.W., 1978. The Moruya batholith and geochemical contrasts between the Moruya and Jindabyne Suites. *Journal of Geological Society, Australia,* v. 25, pp. 235-247.

Gromet, L.P. and Silver, L.T., 1983. Rare earth element distributions among minerals in a granodiorite and their petrogenetic implications. *Geochimica et Cosmochimica Acta,* v. 47, pp. 925-9391.

Gülec, N., 1994. Rb-Sr isotope data from the Agacoren granitoid (east of Tuz Golu): geochronological and genetical implications. *Turki sh Journal of Earth Sciences,* v. 3, pp. 39-43.

Gündogdu, N., Bros, R., Kuruc, A. and Bayhan, H., 1988. Bayindir feldispatoyidli siyenitlerinin Rb-Sr tüm kayac sistematigi (Kaman-Kirsehir). *Hacettepe Universitesi Yerbilimlerinin 20. Yili Sempozyumu,* Bildiri Ozetleri, p. 55.

Guiraud, M., 1986. Application des méthods d'inversion stochastique au calcul des formules structurales des minéraux. *Bulletin de Minéralogie,* v. 109, pp. 289-299.

Haggerty, S.E., 1976. Opaque Mineral Oxides in Terrestrial Igneous Rocks. *Mineralogical Society of America Short Course Notes,* 3, Hg101-Hg300.

Hammerstrom, J.M. and Zen, E-an., 1986. Aluminum in hornblende: an empirical igneous geobarometer. *American Mineralogist,* v. 71, pp. 1297-1313.

Hammerstrom, J.M. and Zen, E-an., 1992. Discussion of Blundy and Holland's (1990) "calcic amphibole equilibria and a new amphibole-plagioclase geothermometer". *Contributions to Mineralogy and Petrology,* v. 111, pp. 264-266.

Harris, N.B.W., Kelley, S. and Okay, A.I., 1994. Post-collision magmatism and tectonics in northwest Anatolia. *Contributions to Mineralogy and Petrology,* v. 117, pp. 241-252.

Haselton, H.T.Jr., Hovis, G.L., Hemingway, B.S. and Robie, R.A., 1983. Calorimetric investigation of the excess entropy of mixing in albite-sanidine solid solutions: lack of evidence for Na, K short-range order and implications for two-feldspar thermometry. *American Mineralogist,* v. 68, pp. 398-413.

Hawkesworth, C.J., Hergt, J.M., Ellam, R.M. and McDermontt., F., 1991. Element fluxes associated with subduction related magmatism. *Philosophical Transactions of the Royal Society, London,* v. 335, pp. 158-170.

Hibbard, M.J., 1981. The magma mixing origin of mantled feldspars. *Contributions to Mineralogy and Petrology,* v. 76, pp. 158-170.

Hildreth, W. and Moorbath, S., 1988. Crustal contribution to arc magmatism in the Andes of southern Chile. *Contributions to Mineralogy and Petrology,* v. 98, pp. 455-489.

Hill, R.R., Silver, I.T. and Taylor, H.P.Jr., 1986. Coupled Sr-O isotope variations as an indicator of source heterogeneity for the Northern Peninsular Ranges batholith. *Contributions to Mineralogy and Petrology,* v. 92, pp. 351-361.

Hine, R., Williams, I.S., Chappell, B.W. and White, A.J.R., 1978. Contrasts between I- and S-type granitoids of the Kosciusko batholith. *Journal of Geological Society, Australia,* v. 25, pp. 219-234.

Holden, P., Halliday, A.N. and Stephens, W.E., 1987. Neodymium and strontium isotope content of microdiorite enclaves points to mantle input to granitoid production. *Nature,* v. 330, pp. 53-57.

Hollister, L.S., Grissom, G.C., Peters, E.K., Stowell, H.H. and Sisson, V., 1987. Confirmation of the empirical correlation of Al in hornblende with pressure of solidification of calc-alkaline plutons. *American Mineralogist,* v. 72, pp. 231-239.

Houseman, G.A., McKenzie, D.P. and Molnar, P., 1981. Convective instability of a thickened boundary layer and its relevance for the thermal evolution of continental convergent belts. *Journal of Geophysical Research,* v. 86, No:B7, pp. 6115-6132.

Hydmann, D.W. and Foster, D.A., 1988. The role of tonalites and mafic dikes in the generation of the Idaho batholith. *Journal of Geology,* v. 96, pp. 31-46.

Ilbeyli, N. and Pearce, J.A., 1997. Petrogenesis of the Collision-Related Central Anatolian Granitoids, Turkey. *Terra Abstracts,* v. 9, p. 502.

Ilbeyli, N., Pearce, J.A., Thirlwall, M.F. and Mitchell, J.G., (in prep). Genesis of Collision-Related Plutonic Rocks, Central Anatolia (Turkey).

Irvine, T.N. and Baragar, W.R.A., 1971. A guide to the chemical classification of the common volcanic rocks. *Canadian Journal of Earth Sciences,* v. 8, pp. 523-548.

Ishihara, S., 1977. The magnetite-series and ilmenite-series granitic rocks. *Mining Geology,* v. 27, pp. 293-305.

Jacobsen, S.B. and Wasserburg, G.J., 1984. Sm-Nd isotopic evolution of chondrites and achondrites. *Earth and Planetary Science Letters,* v. 67, pp. 137-150.

James, D.E., 1981. The combined use of oxygen and radiogenic isotopes as indicators of crustal contamination. *Earth and Planetary Science Letters,* v. 9, pp. 311-344.

James, D.E. and Murcia, L.A., 1984. Crustal assimilation in northern Andean volcanics. *Journal of Geological Society, London,* v. 141, pp. 823-830.

Jamtveit, B., Wogelius, R.A. and Fraser, D.G., 1993. Zonation patterns of skarn garnets: records of hydrothermal system evolution Geology, v. 21, pp. 113-116.

Johnson, M.C. and Rutherford, M.J., 1989. Experimental calibration of the aluminum-in-hornblende geobarometer with application to Long Valley caldera (California) volcanic rocks. *Geology,* v. 17, pp. 837-841.

Kara, H. and Dönmez, M., 1990. 1:100 000 Olcekli Acinsama Nitelikli Türkiye Jeoloji Haritalari Serisi, Kirsehir-G17 Paftasi, No:34. *Maden Tetkik ve Arama Enstitüsü Yayini,* Ankara, 17 pp.

Kay, R.W., Sun, S.S. and Lee Hu, C.N., 1978. Pb and Sr isotopes in volcanic rocks from the Aleutian islands and Pribilof islands, Alaska. *Geochimica et Cosmochimica Acta,* v. 42, pp. 263-278.

Ketin I., 1955. Yozgat bölgesinin jeolojisi ve Orta Anadolu Masifinin tectonic durumu. *Türkiye Jeoloji Kurumu Bülteni,* v. VI, pp. 1-28.

Ketin, I., 1963. 1:500 000 Olcekli Türkiye Jeoloji Haritasi, Kayseri Paftasi. *Maden Tetkik ve Arama Enstitüsü Yayini,* 90 pp.

Kushiro, I., 1962. Clinopyroxene solid solutions. Part I. The $CaAl_2SiO_6$ component. *Japan Journal of Geology and Geography,* v. 33, pp. 213-220.

Langmuir, C.H., Vocke, R.D., Hanson, G.N. and Hart, S.N., 1978. A general mixing equation with applications to Icelandic basalts. *Earth and Planetary Science Letters,* v. 37, 380-392.

Larsen, L.M., 1979. Distribution of REE and other trace elements between phenocrysts and peralkaline undersaturated magmas, exemplified by rocks from Gardar igneous province, south Greenland. *Lithos,* v. 12, pp. 303-315.

Leake, B.E., 1978. Nomenclature of amphiboles. *American Mineralogist,* v. 63, pp. 1023-1052.

Leake, B.E., 1997. Nomenclature of amphiboles: report of the subcommittee on Amphiboles of the International Mineralogical Association Commission on new minerals and mineral names. *Mineralogical Magazine,* v. 61, pp. 295-321.

Leeman, W.P. and Phelps, D.W. 1981. Partitioning rare earths and other trace elements between sanidine and coexisting volcanic glass. *Journal of Geophysical Research,* v. 86, pp. 10193-10199.

L'Heureux, I. And Fowler, A.D., 1994. A nonlinear dynamic model of oscillatory zoning in plagioclase. *American Mineralogist,* v. 79, pp. 885-891.

Le Maitre, R.W. (ed) with Bateman, P., Dubek, A., Keller, J., Lameyre, J., Le Bas, M.J., Sabine, P.A., Schmid, R., Sorensen, H., Streckeisen, A., Wooley, A.R. and Zanettin, B., 1989. *A Classification of Igneous Rocks and Glossary of Terms: Recommendations of the International Union of Geological Sciences Subcommision on the Systematics of Igneous Rocks.* Blackwell, Oxford, 193 pp.

Lindsley, D.H., 1986. Discussion of a linear algebraic method for the calculation of pyroxene end-member components, Dietrich and Petrakakis. *Tschermaks Mineralogische und Petrographische Mitteilungen,* v. 35, pp. 283-285.

Lindsley, D.H. and Anderson, D.J., 1983. A two pyroxene thermometer: Proceedings of the Thirteenth Lunar and Planetary Science Conference, Part 2. *Journal of Geophysical Research,* Supplement, v. 88, pp. A887-A906.

Link, A.J., 1970. Inclusions in the Half Dome Quartz Monzonite, Yosemite National Park, California. Ph.D. Thesis, Northwestern University, 113 pp. (unpublished).

Loisella, M.C. and Wones, D.R., 1979. Characteristics and origin of anorogenic granites. *Geological Society of America Abstracts with Programs,* v. 7, p. 568.

Loomis, A., 1961. Pètrology of the Fallen Leaf Lake area, California. Ph.D. Thesis, Stanford University, Stanford, California, 121 pp. (unpublished).

Luhr, J.F., Carmichael, I.S.E. and Varekamp, J.C., 1984. The 1982 eruptions of El Chichon volcano, Chiapas, Mexico: mineralogy and petrology of the anhyrite-bearing pumices. *Journal of Volcanology and Geothermal Research,* v. 23, pp. 69-108.

Lünel, A.T. 1985. An approach to the naming, origin and age of Baranadag monzonite of the Kirsehir intrusive suite. Middle Eastern Technical University, *Journal of Pure and Applied Science*, v. 18, pp. 385-404.

Mahood, G. and Hildreth, W., 1983. Large partition coefficients for trace elements in high-silica rhyolites. *Geochimica et Cosmochima Acta,* v. 47, pp. 11-30.

Maury, R.C. and Didier, J., 1991. Xenoliths and the role of assimilation. In: Didier, J. and Barbarin, B. (eds), *Granites and Their Enclaves: The Bearing of Enclaves on the Origin of Granites*. Developments in Petrology, 3. Elsevier, Amsterdam, pp. 529-542.

McCarthy, T.S. and Hasty, R.A., 1976. Trace element distribution patterns and their relationship to crystallization of granitic melts. *Geochimica et Cosmochimica Acta,* v. 40, pp. 1351-1358.

McCarthy, T.S. and Groves, D.I., 1979. The Blue Tier batholith, northeastern Tasmania. A cumulate-like product of fractional crystallization. *Contributions to Mineralogy and Petrology,* v. 71, pp. 193-209.

McDermott, F., Defant, M.J., Hawkesworth, C.J., Maury, R.C. and Joron, J.L., 1993. Isotopic and trace element evidence for three component mixing in the genesis of the North Luzon, arc lavas. *Contributions to Mineralogy and Petrology,* v. 113, pp. 9-23.

McHone, J.G., 1987. PCX: an APL program for calculating pyroxene structural formulae and end-members. *Computers and Geosciences,* v. 13, pp. 89-91.

Middlemost, E.A.K., 1994. Naming materials in the magma/igneous rock system. *Earth-Science Reviews,* v. 37, pp. 215-224.

Miller, C.F. and Mittlefehldt, D.W., 1982. Depletion of light rare-earth elements in felsic magmas. *Geology,* v. 10, pp. 129-133.

Morimoto, N., 1989. Nomenclature of pyroxenes. *Canadian Mineralogist,* v. 27, pp. 143-156.

Morimoto, N. and Kitamura, M., 1983. Q-J diagram for classification of pyroxenes. *Journal of Japanese Association of Mineralogy, Petrology and Economical Geology,* v. 78, pp. 141.

Nabelek, C.R. and Lindsley, D.H., 1985. Tetrahedral Al in amphibole: a potential thermometer for some mafic rocks. *Geological Society of America, Abstracts with Program,* v. 17, p. 673.

Nagasawa, H. and Schnetzler, C.C., 1971. Partitioning of rare earth, alkali and alkaline earth elements between phenocrysts and acidic igneous magma. *Geochimica et Cosmochimica Acta,* v. 35, pp. 953-968.

Nash, W.P. and Crecraft, H.R., 1985. Partition coefficients for trace elements in silicic magmas. *Geochimica et Cosmochimica Acta,* v. 49, pp. 2309-2322.

Nekvasil, H. and Burnham, C.W., 1987. The calculated individual effects of pressure and water content on phase equilibria in the granite system. In: Mysen, B.O. (ed), *Magmatic Processes: Physicochemical Principles.* The Geological Society, University Park, PA, pp. 433-445.

Nelson, D.R., 1992. Isotopic characteristics of potassic rocks: evidence for the involvement of subducted sediments in magma genesis. *Lithos,* v. 28, pp. 403-420.

Nockolds, S.R., 1932. The contaminated granite of Bibette Head, Alderney. *Geological Magazine,* v. 69, pp. 433-452.

Okay, A.I., 1984a. Distribution and characteristics of the northwest Turkish blueschists. In: Dixon, J.E. and Robertson, A.H.F. (eds), *The Geological Evolution of the Eastern Mediterranean.* Geological Society of London Special Publication No: 17. Blackwell Scientific Publications, Oxford, pp. 455-466.

Onen, A.P. and Hall, R., 1993. Ophiolites and related metamorphic rocks from the Kütahya region, north-west Turkey. *Geological Journal,* v. 28, pp. 399-412.

Ozcan, A., Göncüoglu, M.C. and Turhan, N., 1989. Kütahya-Cifteler-Bayat-Issaniye Yöresinin Temel Jeolojisi. *Maden Tetkik ve Arama Enstitüsü Raporu.* Rapor No: 8118, 142 pp.

Pabst, A., 1928. Observations on inclusions in the granitic rocks of the Sierra Nevada. *Univ. Calif. Publ. Geol. Sci.,* v. 17, pp. 325-386.

Palm, Q.A., 1957. Les roches cristallines des Cévennes médianes à hauter de Laugentière, Ardèche, France. Storm, Utrect, 121 pp.

Peacock, M.A., 1931. Classification of igneous rock series. *Journal of Geology,* v. 39, pp. 54-67.

Pearce, J.A., 1982. Trace element characteristics of lavas from destructive plate boundaries. In: Thorpe, R.S. (ed), *Andesites: Orogenic Andesites and Related Rocks.* John Wiley, New York, pp. 525-548.

Pearce, J.A., 1983. Role of the sub-continental lithosphere in magma genesis at active continental margins. In: C.J. Hawkesworth and M.J. Norry (eds), *Continental Basalts and Mantle Xenoliths,* Shiva, U.K, pp. 230-249.

Pearce, J.A., 1996. Sources and settings of granitic rocks. *Episodes,* v. 19, pp. 120-125.

Pearce, J.A. and Norry, M.J., 1979. Petrogenetic implications of Ti, Zr, Y and Nb variations in volcanic rocks. *Contributions to Mineralogy and Petrology,* v. 69, pp. 33-47.

Pearce, J.A., Harris, N.B.W. and Tindle, A.G., 1984. Trace element discrimination diagrams for the tectonic interpretation of granitic rocks. *Journal of Petrology,* v. 25, pp. 956-983.

Pearce, J.A., Bender, J.F., De Long, S.E., Kidd, W.S.F., Low, P.J., Güner, Y., Saroglu, F., Yilmaz, Y., Moorbath, S. and Mitchell, J.G., 1990. Genesis of collision volcanism in eastern Anatolia, Turkey. *Journal of Volcanology and Geothermal Research,* v. 44, pp. 189-229.

Pearce, J.A. and Peate, D.W., 1995. Tectonic implications of the composition of volcanic arc magmas. *Annual Reviews in Earth and Planetary Sciences,* v. 23, pp. 251-285.

Petrini, R., Civetta, L., Piccerillo, E.M., Bellini, G., Comin-Chiraramonti, P., Marques, L.S. and Melfi, A.J., 1987. Mantle heterogeneity and crustal contamination in the genesis of low-Ti continental flood basalts from the Parana Plateau (Brazil): Sr-Nd isotope and geochemical evidence. *Journal of Petrology,* v. 28, pp. 701-726.

Pitcher, W.S. and Berger, A.R., 1972. *The Geology of Donegal. A Study of Granite Emplacement and Unroofing.* John Wiley, New York, 435 pp.

Platt, J.P. and England, P.C., 1993. Convective removal of lithosphere beneath mountain belts: thermal and mechanical consequences. *American Journal of Science,* v. 293, pp. 307-336.

Poli, S. and Schmidt, M.W., 1992. A comment on 'calcic amphibole equilibria and a new amphibole-plagioclase geothermeter'. *Contributions to Mineralogy and Petrology,* v. 111, pp. 273-282.

Powell, M. and Powell, R., 1977. Plagioclase-alkali feldspar geothermometry revisited. *Mineralogical Magazine,* v. 41, pp. 253-256.

Presnall, D.C. and Bateman, P.C., 1973. Fusion relations in the system $NaAlSi_3O_8$ - $CaAl_2Si_2O_8$ - $KAlSi_3O_8$ - SiO_2 - H_2O and generation of granitic magmas in the Sierra Nevada batholith. *Bulletin of Geological Society of America,* v. 84, pp. 3182-3202.

Reid, J.B.Jr., Evans, O.C. and Fates, D.G., 1983. Magma mixing in granitic rocks of the central Sierra Nevada, California. *Earth and Planetary Science Letters,* v. 66, pp. 243-261.

Reid, J.B.Jr. and Hamilton, M.A., 1987. Origin of Sierra Nevada granite: evidence from small scale composite dikes. *Contributions to Mineralogy and Petrology,* v. 96, pp. 441-454.

Reid, J.B.Jr., Murray, D.P., Hermes, O.D. and Steig, E.J., 1993. Fractional crystallization in granites of the Sierra Nevada: how important is it? *Geology,* v. 21, pp. 587-590.

Richard, L.R. and Clarke, D.B., 1990. AMPHIBOL: a program for calculating structural formulae and for classifying and plotting chemical analyses of amphiboles. *American Mineralogist,* v. 75, pp. 421-423.

Rock, N.M.S. and Leake, B.E., 1984. The International Mineralogical Association amphibole nomenclature scheme: computerization and its consequences. *Mineralogical Magazine,* v. 48, pp. 211-227.

Rutherford, M.J., Sigurdsson, H., Carey, S. and Davis, A., 1985. The May 18, 1980 eruption of Mount St. Helens 1. Melt composition and experimental phase equilibria: *Journal of Geophysical Research,* v. 90, pp. 2929-2947.

Rutherford, M.J. and Johnson, M.C., 1992. Comment on Blundy and Holland's (1990) "calcic amphibole equilibria and a new amphibole-plagioclase geothermometer". *Contributions to Mineralogy and Petrology,* v. 111, pp. 266-268.

Saunders, A.D., Tarney, J. and Weaver, S.D., 1980. Transverse geochemical variations across the Antarctic peninsula: implications for the genesis of calc-alkaline magmas. *Earth and Planetary Science Letters,* v. 46, pp. 344-360.

Sawka, W.N., 1988. REE and trace element variations in accessory minerals and hornblende from the strongly zoned McMurry Meadows pluton, California. *Transactions of the Royal Society of Edinburgh,* v. 79, pp. 157-168.

Schmidt, M. W., 1992. Amphibole composition in tonalite as a function of pressure: an experimental calibration of the Al-in-hornblende barometer. *Contributions to Mineralogy and Petrology,* v. 110, pp. 304-310.

Sengör, A.M.C. and Yilmaz, Y. 1981. Tethyan evolution of Turkey: a plate tectonic approach. *Tectonophysics,* v. 75, pp. 181-241.

Sengör, A.M.C., Yilmaz, Y. and Ketin, I., 1982. Remnants of a pre-Late Jurassic ocean in northern Turkey: fragments of Permian-Triassic Paleo-Tethys?; Reply. *Bulletin of Geological Society of America,* v. 93, pp. 932-936.

Sengör, A.M.C., Satir, M. and Akkök, R., 1984. Timing of tectonic events in the Menderes Massif, western Turkey: implications for tectonic evolution and evidence for Pan-African basement in Turkey. *Tectonics,* v. 3, pp. 693-707.

Seymen, I., 1975. Kelkit Vadisi Kesiminde Kuzey Anadolu Fay Zonunun Tektonik Ozelligi. Doktora Tezi, Istanbul Teknik Universitesi, Maden Fakültesi, 164 pp. (yayinlanmamis).

Seymen, I., 1981. Kaman (Kirsehir) dolayinda Kirsehir Masifi'nin metamorfizmasi. *Türkiye Jeoloji Kurumu 35. Bilimsel ve Teknik Kurultayi, Ic Anadolu'nun Jeolojisi Sempozyumu,* pp. 12-15.

Seymen, I., 1982. Kaman Dolayinda Kirsehir Masifi'nin Jeolojisi. Docentlik Tezi, Istanbul Teknik Universitesi, Maden Fakültesi, 164 pp. (yayinlanmamis).

Seymen, I., 1983. Tamadag (Kaman-Kirsehir) cevresinde Kaman grubunun ve onunla sinirdas olusuklarin karsilastirilmali tektonik ozellikleri. *Türkiye Jeoloji Kurumu Bülteni,* v. 26, pp. 89-98.

Seymen, I., 1985. Kirsehir Masifi metamorfitlerinin jeolojik evrimi. *Türkiye Jeoloji Kurumu, Ketin Sempozyumu,* pp. 133-148.

Shand, S.J., 1951. *Eruptive Rocks.* John Wiley, New York, 444 pp.

Shore, M. and Fowler, A.D., 1996. Oscillatory zoning in minerals: a common phenomenon. *Canadian Mineralogist,* v. 34, pp. 1111-1126.

Sparks, R.S.J., Sigurdsson, H. and Wilson, L., 1977. Magma mixing: a mechanism for triggering acid explosive eruptions. *Nature,* v. 267, pp. 315-318.

Sparks, R.S.J., Huppert, H.E. and Turner, J.S., 1984. The fluid dynamics of evolving magma chambers. *Philosophical Transactions of the Royal Society, London,* v. 301, pp. 381-399.

Spear, F.S., 1980. NaSi:CaAl exchange equilibrium between plagioclase and amphibole, an empirical model. *Contributions to Mineralogy and Petrology,* v. 72, pp. 33-41.

Spear, F.S., 1981. Amphibole-plagioclase equilibria: an empirical model for the reaction albite+tremolite=edenite+4 quartz. *Contributions to Mineralogy and Petrology,* v. 77, pp. 355-364.

Speer, J.A., 1987. Evolution of magmatic AFM mineral assemblages in granitoid rocks: the hornblende+melt=biotite reaction in the Liberty Hill pluton, south Carolina. *American Mineralogist,* v. 72, pp. 863-878.

Stormer, J.C., 1975. A practical two-feldspar geothermometer. *American Mineralogist,* v. 60, pp. 667-674.

Streckeisen, A., 1976. To each plutonic rock its proper name. *Earth-Science Reviews,* v. 12, pp. 1-33.

Sun, S.S. and McDonough, W.F., 1989. Chemical and isotopic systematics of oceanic basalts: implications for mantle composition and processes: In: Saunders, A.D. and Norry, M.J. (eds), *Magmatism in the Ocean Basins.* Geological Society Special Publications No:42, pp. 313-345.

Tait, S.R., 1988. Samples from the crystallizing boundary layer of a zoned magma chamber. *Contributions to Mineralogy and Petrology,* v. 100, pp. 470-480.

Tait, S.R., Worner, G., Van den Bogaard, P. and Schemincke, U., 1989. Cumulate nodules as evidence for convective fractionation in a phonolitic magma chamber. *Journal of Volcanology and Geothermal Research,* v. 37, pp. 31-37.

Takahashi, M., Aramaki, S. and Ishihara, S., 1980. Magnetite series/ilmenite series vs. I-type/S-type granitoids. In: Ishihara, S. and Takenouchi, S. (eds), *Granitic Magmatism and Related Mineralization.* Mining Mineralogy Special Issue No. 8. The Society of Mining Mineralogists of Japan, Tokyo, pp. 13-38.

Taner, A., 1974. Geologische untersuchung von Keskin und Umbebung. *Ankara Universitesi Fen Fakültesi Tebligler Dergisi,* Ankara.

Tera, B., Brown, L., Morris, J., Sacks, I.S., Klein, J. and Middleton, R., 1986. Sediment incorporation in island arc magmas: inferences from ^{10}Be. *Geochimica et Cosmochimica Acta,* v. 50, pp. 535-550.

Thirlwall, M.F., 1991a. Long-term reproducibility of multicollector Sr and Nd ratio analysis. *Chemical Geology,* v. 94, pp. 85-104.

Thirlwall, M.F., 1991b. High precision multicollector isotope analysis of low levels of Nd as oxide. *Chemical Geology,* v. 94, pp. 13-22.

Tindle, A.G. and Pearce, J.A., 1981. Petrogenetic modeling of insitu fractional crystallization in the zoned Loch Doon pluton, Scotland. *Contributions to Mineralogy and Petrology,* v. 78, pp. 196-207.

Tindle, A.G. and Pearce, J.A., 1983. Assimilation and partial melting of continental crust: evidence from the mineralogy and geochemistry of autoliths and xenoliths. *Lithos,* v. 16, pp. 185-202.

Tommasini, S., Poli, G. and Halliday, A.N., 1995. The role of sediment subduction and crustal growth in Hercynian plutonism: isotopic and trace element evidence from the Sardinia-Corsica batholith. *Journal of Petrology,* v. 36, pp. 1305-1332.

Tsuchiyama, A., 1985. Dissolution kinetics of plagioclase in the melt of the system: diopside - albite - anorthite, and the origin of dusty plagioclase in andesites. *Contributions to Mineralogy and Petrology,* v. 89, pp. 1-16.

Turbeville, B.N., 1992. Relationships between chamber margin accumulates and pore liquids: evidence from arrested in situ processes in ejecta, Latera caldera, Italy. *Contributions to Mineralogy and Petrology,* v. 110, pp. 429-441.

Twist, D. and Harmer, R.E.J., 1987. Geochemistry of contrasting siliceous magmatic suites in the Bushveld complex: genetic aspects and the implications for tectonic discrimination diagrams. *Journal of Volcanology and Geothermal Research,* v. 32, pp. 83-98.

Van der Laan, S.R. and Wyllie, P.J., 1993. Experimental interaction of granitic and basaltic magmas and implications for mafic enclaves. *Journal of Petrology,* v. 34, pp. 491-517.

Varekamp, J.C., 1983. The significance of mafic nodules in ultrapotassic rocks from central Italy-discussion. *Journal of Volcanology and Geothermal Research,* v. 16, pp. 161-172.

Verhoogen, J., 1962. Distribution of titanium between silicates and oxides in igneous rocks. *Journal of Geology,* v. 70, pp. 168-181.

Vernon, R.H., 1983. Restite, xenoliths and microgranitod enclaves in granites. *Journal and Proceedings, Royal Society of New South Wales,* v. 116, pp. 77-103.

Vernon, R.H., 1991. Interpretation of microstructures of microgranitoid enclaves. In: Didier, J. and Barbarin, B. (eds), *Granites and Their Enclaves: The Bearing of Enclaves on the Origin of Granites.* Developments in Petrology, 3. Elsevier, Amsterdam, pp. 277-292.

Von Blanckenburg, F., Fruh-Green, G., Diethelm, K. and Stille, P., 1992. Nd-, Sr- and O- isotopic and chemical evidence for a two-stage contamination history of mantle magma in the Central Alpine Bergell intrusion. *Contributions to Mineralogy and Petrology,* v. 110, pp. 33-45.

Voshage, H., Hofmann, A.W., Mazzucchelli, M., Rivalenti, G., Sinigoi, S., Raczek, I. and Demarchi, G., 1990. Isotopic evidence from the Ivrea zone for a hybrid lower crust formed by magmatic underplating. *Nature,* v. 347, pp. 731-736.

Wall, V.J., Clemens, J.D. and Clarke, D.B., 1987. Models for granitoid evolution and source compositions. *Journal of Geology,* v. 95, pp. 731-749.

Wand, Y. and Merino, E., 1992. Dynamic model of oscillatory zoning of trace elements in calcite: double layer, inhibition, and self-organization. *Geochimica et Cosmochimica Acta,* v. 56, pp. 587-596.

Wen, S. and Nekvasil, H., 1994. SOLVCALC: an interactive graphics program package for calculating the ternary feldspar solvus and for two-feldspar geothermometry. *Computers and Geosciences*, v. 20, pp. 1025-1040.

Whalen, J.B., Currie, K.L. and Chappell, B.W., 1987. A-type granites: geochemical characteristics, discrimination and petrogenesis. *Contributions to Mineralogy and Petrology*, v. 95, pp. 407-419.

White, A.J.R. and Chappell, B.W., 1977. Ultrametamorphism and granitoid genesis. *Tectonophysics,* v. 43, pp. 7-22.

White, A.J.R. and Chappell, B.W., 1983. Granitoid types and their distribution in the Lachlan Fold Belt, southeastern Australia. In: Roddick, J.A. (ed), *Circum-Pacific Plutonic Terranes*. Geological Society America Memoir No:159, pp. 21-34.

White, W.M. and Dupré, B., 1986. Sediment subduction and magma genesis in the Lesser Antilles: isotopic and trace element constraints. *Journal of Geophysical Research,* v. 91, pp. 5927-5941.

Whitford, D.J., White, W.M. and Jezek, P.A., 1981. Neodymium isotopic composition of Quaternary arc lavas from Indonesia. *Geochimica et Cosmochimica Acta,* v. 45, pp. 989-995.

Whitney, J.A. and Stormer, J.C., 1977. Two-feldspar geothermometry, geobarometry in mesozonal granitic intrusions: three examples from the Piedmont of Georgia. *Contributions to Mineralogy and Petrology,* v. 63, pp. 51-64.

Wones, D.R., 1981. Mafic silicates as indicators of intensive variables in granitic magmas. *Mining Geology (Japan),* v. 31, pp. 191-212.

Wones, D.R., 1989. Significance of the assemblage titanite+magnetite+quartz in granitic rocks. *American Mineralogist,* v. 74, pp. 744-749.

Yadete, H.M., 1990. Rock Geochemical Exploration in Intrusive Rocks of the Behrekdag Area (Celebi-Kirikkale). MSc. Thesis, Middle East Technical University, 120 pp. (unpublished).

Yaliniz, M.K., Floyd, P.A. and Göncüoglu, M.C., 1996. Supra-subduction zone ophiolites of central Anatolia: geochemical evidence from the Sarikaraman Ophiolite, Aksaray, Turkey. *Mineralogical Magazine,* v. 60, pp. 697-710.

Yardley, B.W.D., Rochella, C.A., Barnicoat, A.C. and Lloyd, G.E., 1991. Oscillatory zoning in metamorphic minerals: an indicator of infiltration metasomatism. *Mineralogical Magazine,* v. 55, pp. 357-365.

Zeck, H.P. and Unlü, T., 1987. Parallel whole-rock isochrons from a composite, monzonitic pluton, Alpine belt, central Anatolia, Turkey. *Neues Jahrbuch fur Mineralogie, Abchandlungen,* v. 5, pp. 193-204.

Zindler, A. and Hart, S., 1986. Chemical geodynamics. *Annual Reviews in Earth and Planetary Sciences,* v. 14, pp. 493-571.

Zorpi, M.J., Coulon, C., Orsini, J.B. and Cocirta, C., 1989. Magma mingling, zoning and emplacement in calc-alkaline granitoid plutons. *Tectonophysics,* v. 157, pp. 315-329.

Zorpi, M.J., Coulon, C., and Orsini, J.B., 1991. Hybridization between felsic and mafic magmas in calc-alkaline granitoids-a case study in northern Sardinia, Italy. *Chemical Geology,* v. 92, pp. 45-86.

APPENDICES

APPENDIX A- Analytical technique

I. MODAL ANALYSIS

The modal proportions of minerals in 162 samples (intrusive rocks and enclaves) are presented in Appendix C (I). The data were collected using a Swift Model F automatic point counter fitted with an automated stage. Samples were either normal thin sections or polished that had been prepared for microprobe analysis. A total of 1200 points were counted on each specimen in such a way that the whole surface of thin section was covered.

Both major phases and the more common minor phases are presented in the tables. Where "tr" appears in the tables it implies that the mineral was observed, but not point counted. The data for a given rock type are arranged in order of increasing silica content.

II. XRF ANALYSIS

II.1. Sample preparation

Wherever possible, the freshest available samples were collected. Samples first cut into slices by a diamond-saw. After this stage, samples were split into small pieces about 3 cm using a hydraulic splitter and then crush into pieces of less than 0.5 cm cubed using a jaw crusher. To avoid contamination in these two stages, after each sample the hydraulic splitter and jaw crusher were cleaned by wire brush and alcohol. After being quartered, approximately 100 grams of the crushed rock were powdered to less than 200 mesh using an agate-ball grinding mill. After each sample, agate bowls and balls were cleaned by water, alcohol and also quartz sand. Samples are ready now to make pressed powder pellets and fused glass discs for X-ray fluorescence spectrometry (XRF).

II.1.1. Preparation of pressed powder pellets

Previously dried about 8 grams of powdered samples were thoroughly mixed with a binder (Movoil) until the uniformity is succeeded. After that they were pressed in stainless steel mould between a pair of steel discs using a hydraulic pellet press. Pellets were then labelled and placed into an oven for dryness about 100 °C prior to analysis. After that, these pellets were analysed for major and trace elements using X-ray fluorescence spectrometry (XRF).

II.1.2. Determination of loss on ignition

About 4-5 grams of each sample powder was placed into in a glass vial and labelled. These powder samples were then oven-dried at 110 °C for over 1 hour to remove surface water. They are then stored in a desiccator to avoid sample loss through spillage and surface water, which might be gained from the atmosphere.

About 4 grams from each sample was weighted and put into the porcelain crucibles. Ignitions were performed at about 900 °C for two-three hours. After allowing samples to cool in a dessicator they were reweighted and eventually their loss on ignition was calculated from the difference in the weight.

II.1.3. Preparation of fused glass discs

Before making fusion discs, the flux (lithium tetraborate and lithium metaborate) was dried in the furnace overnight at 600 °C to remove any absorbed water or any other volatiles taken up from the atmosphere. Dried flux was stored in a desiccator during fused disc preparations.

Previously ignited samples were dried at 110 °C for about 24 hours. They were taken out from furnace and put them in dessicator for cooling. After that 0.45 grams of sample and 2.25 grams of flux was mixed using an agate-ball grinding mill and these mixtures then were transferred into platinum crucibles. After that they were placed into furnace at 1050 °C for 20 minutes.

After taking them out, samples were poured into the graphite moulds to give a shape. After cooling on a cooling block, they were labelled and put into dessicator until they were analysed by X-ray fluorescence spectrometry (XRF).

II.2. Analytical work

Major and trace elements were analysed by X-ray fluorescence spectrometry (XRF) using an automated Philips PW 1400 spectrometer with a Rh anode tube and automatic loader at the University of Durham. X-ray fluorescence analyses were carried out on about 303 samples from the Central Anatolian Massif. Major elements (SiO_2, TiO_2, Al_2O_3, Fe_2O_3, MnO, MgO, CaO, Na_2O, K_2O and P_2O_5) were analysed by both on pressed powder elements and fused glass discs and trace elements on pressed powder pellets (Sc, V, Cr, Co, Ni, Cu, Zn, Ga, Rb, Sr, Y, Zr, Nb, Ba, La, Ce, Nd, Pb, Th and U). The XRF spectrometer was calibrated using a suite of analysed

standards selected from approximately 30 international standards to cover the compositional range from basalt to granite. Some of these standards and samples were run repeatedly to monitor machine drift. Analytical accuracy and precision were then calculated using international standards and these samples (Appendix B).

III. ICP-MS ANALYSIS

III.1. Sample preparation for whole-rocks

To ensure dissolution, fused discs were used rather than powdered samples. Fused discs were prepared as mentioned in Sections II.1.2 and II.1.3. After that, these fused disc samples were powdered using a hand agate grinder.

Small amount of powdered samples was put into the labelled glass vials in an oven at 105 °C overnight to dry. Previously dishwasher-cleaned teflon containers were filled with 2 ml of Analar Nitric acid and left on a hot plate at 130-150 °C for at least 24 hours. After that teflon containers were washed with de-ionised water and placed them in the oven at 105 °C until they were dried. Previously overnight-dried powder samples were then weighed about 0.1±0.001 gram using anti-static gun and transferred into labelled teflon containers. In addition to the samples, at least 6 international standards and two blanks were prepared.

After that, 1 ml of Aristar HNO_3 and 4 ml of Aristar HF were added into these teflon containers and placed on the hot plate at about 130 °C for about 24 hours for complete digestion. At the end of this period, samples were evaporated on the hot plate to dryness in order to remove HF acid from the system and to allow the formation of nitrate salts. After completing evaporation, 1 ml of Aristar HNO_3 was added to teflon containers and evaporated again. This procedure was repeated twice. Then 2.5 ml of Aristar HNO_3 and 10-15 ml of de-ionised water were put into the teflons and replaced on the hot plate for 30 minutes to dissolve nitrate salts. The solutions were allowed to cool and spiked with 1.25 ml of internal standard. The internal standard was made up of 2 ppm Bi, Re and Rh. After this stage, they were transferred into the 50 ml volumetric flasks and made up accurately to 50 ml with de-ionised water.

III.2. Sample preparation for minerals

Representative rock samples collected from different plutons were studied microscopically to select minerals which are both fresh and have no mineral inclusions or zoning. These whole-rock samples were crushed into small pieces by a jaw crusher. To avoid contamination the jaw crusher was cleaned by wire brush and alcohol prior to each session of crushing. Minerals were then separated from these samples by hand-picking under binocular microscope. These separated minerals were cleaned in reagent grade acetone and de-ionised water.

After that minerals were put into the labelled glass vials in an oven at 105 °C overnight to dry. These minerals were then powdered using a hand agate grinder. Small amount of powdered minerals was put into the labelled glass vials in an oven at 105 °C overnight to dry. Previously dishwasher-cleaned teflon containers were filled with 2 ml of Analar Nitric acid and left on a hot plate at 130-150 °C for at least 24 hours. After that teflon containers were washed with de-ionised water and placed them in the oven at 105 °C until they were dried. Previously overnight-dried powder minerals were then weighed about 0.1±0.001 gram using anti-static gun and transferred into labelled teflon containers. In addition to minerals, at least 6 international whole-rock and mineral standards and two blanks were prepared.

After that, 1 ml of Aristar HNO_3 and 4 ml of Aristar HF were added into these teflon containers and placed on the hot plate at about 130 °C for about 24 hours for complete digestion. At the end of this period, the samples were evaporated on the hot plate for dryness. After completing evaporation, 2 ml of Aristar HNO_3 was added to the teflon containers and evaporated again. After completing evaporation, 2 ml of Aristar HCl was added to the teflon containers and evaporated again. This procedure repeated twice. 2.5 ml of Aristar HNO_3 and 10-15 ml of de-ionised water were then put into the teflons and replaced on the hot plate for 30 minutes to dissolve nitrate salts. The solutions were allowed to cool and spiked with 1.25 ml of 2 ppm Bi, Re and Rh internal standard. After this stage, they were transferred into the 50 ml volumetric flasks and made up accurately to 50 ml with de-ionised water.

III.3. Analytical work

A subset of trace (Rb, Sr, Y, Zr, Nb, Cs, Ba) and rare earth elements (La, Ce, Pr, Nd, Sm, Eu, Gd, Tb, Dy, Ho, Er, Tm, Yb, Lu) were analysed by Inductively Coupled Plasma Mass Spectrometry (ICP-MS) at the University of Durham.

IV. K-Ar DATING

The three representative biotite and hornblende minerals were chosen for the dating. The preparation for the dating was the same as in Section III.2. K values were determined at the University of Durham by Atomic Absorption Spectrophotometry (AAS). K-Ar age determinations of three samples were carried out by Dr. J.G. Mitchell at the Department of Physics, Newcastle University.

V. ELECTRON MICROPROBE ANALYSIS

Before the analysis, polished thin sections were coated in carbon to provide a conductive layer and to minimise charge build-up under the electron beam.

Electron microprobe analysis was carried out using a Cameca CAMEBAX instrument at the University of Edinburgh. Run conditions were ~20 KV accelerating voltage, ~2/nA beam current, 30s. pk count, 15s. background count, 1mm^2 spot size and 25 mm^2 retard beam size.

VI. ISOTOPE ANALYSIS

Sr and Nd analyses were determined using the automated VG 354 multicollector thermal ionisation mass spectrometer at the Department of Geology, Royal Halloway, University of London. Sr and Nd were extracted on the same solution from 200±20 mg of rock powder. Samples were dissolved using the dissolved using approximately 1 ml of HNO_3 and 3-5 ml of HF. After the dissolution, the solution was evaporated to dryness. It was then converted to nitrate by the addition of 2 ml of HNO_3, followed by evaporation and dryness. The residue was converted to chloride using 2.5M HCl.

The separation of Rb and Sr and the preliminary separation of Sm-Nd were performed on a cation exchange resin column eluted with 2.5M HCl. Before separation of the samples, the column resin was cleaned by passing sequential

volumes of 50% acid and water. A small volume of the sample solution was loaded into the column, washed into the resin bed carefully with eluent, and then washed through with more eluent until fraction was collected when the desired element was released from the resin. This was evaporated to dryness, ready to load onto a single Ta filament with silica gel. Following the chemical mineral acid separation, Sr and Nd were determined multidynamically with Nd, as NdO (Thirlwall, 1991a, b).

During the period of analysis, the NBS SRM 987 standard gave an $^{87}Sr/^{86}Sr$ mean value of 0.71025±21 (2σ) (n=58), and the internal Aldrich Nd standard gave a $^{143}Nd/^{144}Nd$ mean value of 0.71025±8 (2σ) (n=28). Blanks were around 1 ng and 200 pg for Sr and Nd respectively. Age corrections for $^{87}Sr/^{86}Sr$ and $^{143}Nd/^{144}Nd$ were estimated from Sr, Sm and Nd values determined by ICP-MS.

APPENDIX B- Accuracy and precision of analytical data

APPENDIX B (I)- Error calculations of XRF major element data

		W-2	G-2	MRG-1	DR-N	SY-2	BHVO-1	G-1	AGV-1	± standard error
SiO_2	*recommended*	**52.44**	**69.94**	**39.12**	**52.85**	**60.11**	**49.94**	**72.46**	**59.25**	*0.63*
	1st run	52.42	69.05	39.83	54.17	61.12	49.87	72.86	60.09	
	2nd	52.32	69.07	39.82	54.03	60.71	50.07	73.09		
	3rd	52.25	68.94	39.87	53.83	60.30	49.82			
	4th	52.21	69.46	39.80	53.89	60.24	49.94			
	5th	52.67	69.17	39.88	53.76					
	6th	52.42	69.14	39.90	53.85					
	7th	52.46								
	8th	52.41								
	9th	52.35								
	10th	52.21								
	standard dev.	*0.14*	*0.18*	*0.04*	*0.15*	*0.41*	*0.11*	*0.16*		
TiO_2	*recommended*	**1.06**	**0.49**	**3.77**	**1.09**	**0.15**	**2.71**	**0.25**	**1.06**	*0.02*
	1st run	1.05	0.48	3.83	1.08	0.15	2.73	0.26	1.08	
	2nd	1.06	0.49	3.83	1.08	0.14	2.72	0.26		
	3rd	1.05	0.49	3.87	1.08	0.15	2.71			
	4th	1.06	0.48	3.85	1.08	0.14	2.72			
	5th	1.05	0.49	3.85	1.08					
	6th	1.07	0.49	3.82	1.09					
	7th	1.06								
	8th	1.07								
	9th	1.07								
	10th	1.06								
	standard dev.	*0.01*	*0.00*	*0.02*	*0.00*	*0.00*	*0.01*	*0.00*		
Al_2O_3	*recommended*	**15.35**	**15.14**	**8.47**	**17.52**	**12.04**	**13.8**	**14.23**	**17.15**	*0.16*
	1st run	15.53	15.42	8.56	18.07	12.37	13.71	14.41	17.44	
	2nd	15.36	15.35	8.44	18.17	12.10	13.66	14.46		
	3rd	15.33	15.50	8.61	18.02	12.10	13.78			
	4th	15.40	15.58	8.61	18.00	12.12	13.81			
	5th	15.10	15.44	8.67	17.94					
	6th	15.44	15.36	8.60	17.77					
	7th	15.29								
	8th	15.40								
	9th	15.25								
	10th	15.37								
	standard dev.	*0.12*	*0.09*	*0.08*	*0.13*	*0.13*	*0.07*	*0.04*		
Fe_2O_3	*recommended*	**10.74**	**2.67**	**17.98**	**9.70**	**6.31**	**12.23**	**1.94**	**6.76**	*0.08*
	1st run	10.80	2.62	17.98	9.86	6.22	12.19	1.86	6.93	
	2nd	10.80	2.65	17.98	9.70	6.22	12.18	1.84		
	3rd	10.58	2.64	18.06	9.80	6.31	12.26			
	4th	10.87	2.58	18.21	9.96	6.40	12.29			
	5th	10.73	2.59	18.24	9.90					
	6th	10.71	2.69	18.09	9.74					
	7th	10.70								
	8th	10.80								
	9th	10.88								
	10th	10.98								
	standard dev.	*0.11*	*0.04*	*0.11*	*0.10*	*0.09*	*0.05*	*0.01*		
MnO	*recommended*	**0.16**	**0.03**	**0.17**	**0.22**	**0.32**	**0.17**	**0.03**	**0.10**	*0.00*
	1st run	0.16	0.03	0.17	0.22	0.31	0.17	0.03	0.10	
	2nd	0.17	0.03	0.17	0.22	0.31	0.17	0.03		
	3rd	0.16	0.03	0.17	0.22	0.31	0.17			
	4th	0.17	0.03	0.18	0.22	0.32	0.17			
	5th	0.16	0.03	0.18	0.22					
	6th	0.17	0.03	0.17	0.23					
	7th	0.16								
	8th	0.16								
	9th	0.17								
	10th	0.17								
	standard dev.	*0.00*	*0.00*	*0.00*	*0.01*	*0.00*	*0.00*	*0.00*		

		W-2	G-2	MRG-1	DR-N	SY-2	BHVO-1	G-1	AGV-1	± standard error
MgO	*recommended*	**6.37**	**0.76**	**13.55**	**4.40**	**2.69**	**7.23**	**0.39**	**1.53**	*0.09*
	1st run	6.43	0.73	13.53	4.48	2.65	7.25	0.45	1.75	
	2nd	6.43	0.72	14.13	4.48	2.73	7.20	0.44		
	3rd	6.45	0.75	13.93	4.47	2.70	7.45			
	4th	6.51	0.75	13.91	4.44	2.72	7.25			
	5th	6.24	0.77	13.93	4.43					
	6th	6.57	0.71	13.73	4.56					
	7th	6.62								
	8th	6.42								
	9th	6.39								
	10th	6.44								
	standard dev.	*0.10*	*0.02*	*0.21*	*0.05*	*0.04*	*0.11*	*0.01*		
CaO	*recommended*	**10.87**	**1.97**	**14.70**	**7.05**	**7.96**	**11.4**	**1.38**	**4.94**	*0.11*
	1st run	10.93	1.93	15.18	7.18	8.02	11.42	1.28	5.11	
	2nd	10.91	1.91	15.12	7.15	8.00	11.38	1.28		
	3rd	10.89	1.92	14.98	7.17	8.00	11.38			
	4th	10.90	1.92	15.04	7.11	7.94	11.40			
	5th	10.94	1.92	14.93	7.12					
	6th	10.93	1.92	14.98	7.28					
	7th	10.98								
	8th	11.03								
	9th	10.93								
	10th	10.93								
	standard dev.	*0.04*	*0.01*	*0.10*	*0.06*	*0.03*	*0.02*	*0.00*		
Na_2O	*recommended*	**2.14**	**4.07**	**0.74**	**2.99**	**4.31**	**2.26**	**3.33**	**4.25**	*0.06*
	1st run	2.22	4.04	0.73	2.96	4.16	2.29	3.44	4.18	
	2nd	2.19	4.04	0.85	2.99	4.25	2.22	3.45		
	3rd	2.24	4.13	0.82	3.10	4.25	2.36			
	4th	2.30	3.98	0.78	3.09	4.37	2.25			
	5th	2.13	4.10	0.80	3.18					
	6th	2.21	4.01	0.92	3.04					
	7th	2.16								
	8th	2.21								
	9th	2.20								
	10th	2.25								
	standard dev.	*0.05*	*0.06*	*0.06*	*0.08*	*0.09*	*0.06*	*0.01*		
K_2O	*recommended*	**0.63**	**4.49**	**0.18**	**1.70**	**4.45**	**0.52**	**5.48**	**2.90**	*0.03*
	1st run	0.63	4.45	0.18	1.75	4.52	0.52	5.57	2.95	
	2nd	0.63	4.44	0.18	1.74	4.51	0.52	5.56		
	3rd	0.63	4.47	0.19	1.75	4.53	0.52			
	4th	0.63	4.47	0.19	1.76	4.49	0.52			
	5th	0.62	4.48	0.19	1.76					
	6th	0.63	4.50	0.19	1.74					
	7th	0.63								
	8th	0.63								
	9th	0.63								
	10th	0.63								
	standard dev.	*0.00*	*0.02*	*0.00*	*0.01*	*0.02*	*0.00*	*0.01*		
P_2O_5	*recommended*	**0.13**	**0.14**	**0.08**	**0.25**	**0.43**	**0.27**	**0.09**	**0.48**	*0.01*
	1st run	0.14	0.12	0.09	0.25	0.43	0.27	0.07	0.51	
	2nd	0.12	0.13	0.10	0.25	0.44	0.28	0.07		
	3rd	0.14	0.14	0.11	0.24	0.43	0.28			
	4th	0.12	0.14	0.08	0.23	0.44	0.27			
	5th	0.14	0.13	0.07	0.22					
	6th	0.14	0.14	0.08	0.24					
	7th	0.14								
	8th	0.14								
	9th	0.12								
	10th	0.13								
	standard dev.	*0.01*	*0.01*	*0.01*	*0.01*	*0.01*	*0.01*	*0.00*		

APPENDIX B (II)- Error calculations of XRF trace element data

		G-2	MRG-1	DR-N	W-2	DNC-1	BE-N	GS-N	BHVO-1	± standard error
Sc	***recommend***	**3.5**	**55**	**28**	**35.39**	**31**	**22**	**7.3**	**31.8**	***1.29***
	1st run	3.8	49.7	25.7	36.2	32.6	22.7	8.0	31.0	
	2nd	4.2	55.1	26.3	38.9	32.0				
	3rd	4.3	54.0	26.3	34.5					
	4th	3.7	53.4							
	5th	4.2								
	standard dev	*0.27*	*2.34*	*0.35*	*2.22*	*0.42*				
V	***recommend***	**36**	**526**	**220**	**264.14**	**148**	**235**	**65**	**317**	***3.03***
	1st run	37.5	522.0	218.4	262.2	152.7	233.1	62.6	311.1	
	2nd	36.1	528.6	224.3	263.6	148.2				
	3rd	38.6	528.0	220.0	260.9					
	4th	36.0	532.9							
	5th	37.4								
	standard dev	*1.08*	*4.48*	*3.05*	*1.35*	*3.18*				
Cr	***recommend***	**9**	**430**	**42**	**99.5**	**285**	**360**	**55**	**289**	***6.11***
	1st run	5.1	431.5	41.5	94.8	292.9	363.7	65.8	283.0	
	2nd	11.3	432.2	41.9	97.5	287.0				
	3rd	4.9	430.1	42.9	88.3					
	4th	6.4	430.4							
	5th	8.6								
	standard dev	*2.70*	*0.97*	*0.72*	*4.73*	*4.17*				
Co	***recommend***	**4.6**	**87**	**35**	**45.47**	**54.7**	**61**	**65**	**45**	***6.67***
	1st run	4.6	84.5	42.4	44.1	53.0	45.9	63.0	42.0	
	2nd	4.4	92.0	43.2	46.9	53.3				
	3rd	4.6	87.0	39.9	47.5					
	4th	4.2	86.6							
	5th	4.5								
	standard dev	*0.17*	*3.18*	*1.72*	*1.81*	*0.21*				
Ni	***recommend***	**4.9**	**193**	**15**	**97.53**	**247**	**267**	**34**	**121**	***2.91***
	1st run	5.7	191.3	14.2	92.2	241.2	270.2	33.0	122.0	
	2nd	5.6	195.4	16.0	96.3	242.4				
	3rd	8.8	195.0	16.5						
	4th	6.8	193.3							
	5th	2.5								
	standard dev	*2.29*	*1.87*	*1.21*	*2.90*	*0.85*				
Cu	***recommend***	**11**	**134**	**50**	**105.74**	**96**	**72**	**20**	**136**	***1.36***
	1st run	12.3	133.5	49.6	107.2	90.9	73.0	21.4	135.0	
	2nd	10.1	132.7	50.8	106.9	95.0				
	3rd	11.7	133.5	50.7	103.8					
	4th	10.7	135.2							
	5th	8.5								
	standard dev	*1.48*	*1.05*	*0.67*	*1.88*	*2.90*				
Zn	***recommend***	**85**	**191**	**145**	**77.27**	**66**	**120**	**48**	**105**	***1.48***
	1st run	81.4	191.4	144.5	78.7	68.5	121.0	50.0	107.0	
	2nd	85.6	193.5	144.4	80.8	67.6				
	3rd	86.2	193.8	144.3	74.3					
	4th	82.9	193.4							
	5th	81.4								
	standard dev	*2.28*	*1.10*	*0.10*	*3.32*	*0.64*				
Ga	***recommend***	**22**	**17**	**22**	**17.53**	**15**	**17**	**22**	**21**	***2.73***
	1st run	22.7	15.4	21.7	20.1	13.7	3.3	21.2	7.5	
	2nd	23.5	16.3	23.0	17.0	14.7				
	3rd	23.5	17.9	23.2	18.9					
	4th	20.7	17.8							
	5th	24.1								
	standard dev	*1.33*	*1.21*	*0.81*	*1.56*	*0.71*				

		G-2	MRG-1	DR-N	W-2	DNC-1	BE-N	GS-N	BHVO-1	± standard error
Rb	*recommend*	**170**	**8.5**	**73**	**20.36**	**4.5**	**47**	**185**	**11**	***0.95***
	1st run	167.8	9.1	73.0	20.8	5.2	46.0	181.6	9.2	
	2nd	171.6	9.7	73.0	20.4	4.5				
	3rd	168.4	7.6	72.7	20.1					
	4th	166.7	9.0							
	5th	166.8								
	standard dev	*2.00*	*0.89*	*0.17*	*0.35*	*0.49*				
Sr	*recommend*	**478**	**266**	**400**	**193.31**	**145**	**1370**	**570**	**403**	***3.74***
	1st run	479.3	267.8	397.4	196.5	144.7	1389.4	593.2	402.0	
	2nd	475.8	269.0	395.7	196.0	144.8				
	3rd	479.7	269.3	395.8	193.0					
	4th	472.9	269.8							
	standard dev	*3.20*	*0.85*	*0.95*	*1.89*	*0.07*				
Y	*recommend*	**11.4**	**14**	**28**	**21.36**	**18**	**30**	**19**	**27.6**	***1.46***
	1st run	12.1	14.7	26.8	21.7	16.7	31.7	21.0	25.6	
	2nd	11.8	14.7	28.9	21.8	18.1				
	3rd	8.3	14.5	26.9	23.6					
	4th	9.5	14.6							
	5th	11.4								
	standard dev	*1.65*	*0.10*	*1.18*	*1.07*	*0.99*				
Zr	*recommend*	**300**	**108**	**125**	**92.87**	**41**	**265**	**235**	**179**	***4.04***
	1st run	297.5	105.3	120.3	91.5	38.2	267.1	224.6	177.5	
	2nd	292.7	106.0	121.3	91.9					
	3rd	290.2	102.9	124.9	92.5					
	4th	289.5	103.0							
	5th	294.5								
	standard dev	*3.26*	*1.59*	*2.42*	*0.50*					
Nb	*recommend*	**13**	**20**	**8**	**7.76**	**3**	**100**	**21**	**19**	***0.94***
	1st run	13.0	20.7	8.8	7.7	3.0	96.5	20.8	17.8	
	2nd	14.3	20.7	8.7	7.6	1.8				
	3rd	13.5	20.9	8.7	8.0					
	4th	14.0	22.2							
	5th	14.3								
	standard dev	*0.56*	*0.72*	*0.06*	*0.21*	*0.85*				
Ba	*recommend*	**1880**	**61**	**385**	**167.08**	**114**	**1025**	**1400**	**139**	***2.43***
	1st run	1867.5	58.3	388.7	167.3	114.6	1021.0	1390.0	140.0	
	2nd	1857.9	64.2	389.6	170.5	116.1				
	3rd	1869.9	54.2	381.8	169.8					
	4th	1859.0								
	5th	1865.7								
	standard dev	*5.30*	*5.03*	*4.27*	*1.68*	*1.06*				
La	*recommend*	**86**	**9.8**	**21**	**10.61**	**3.8**	**82**	**75**	**15.8**	***1.30***
	1st run	85.4	8.9	23.6	10.5	5.9	81.3	68.1	16.3	
	2nd	87.5	9.8	21.2	12.4	5.1				
	3rd	89.9	10.8	22.9	9.8					
	4th	89.5	9.4							
	5th	90.2								
	standard dev	*2.03*	*0.81*	*1.23*	*1.35*	*0.57*				
Ce	*recommend*	**159**	**26**	**46**	**23.03**	**10.6**	**152**	**135**	**39**	***3.98***
	1st run	163.8	23.5	58.4	28.3	8.6	151.0	133.1	40.4	
	2nd	158.6	29.9	57.4	37.2	9.7				
	3rd	160.7	28.9	49.0	24.9					
	4th	156.5	33.0							
	5th	162.9								
	standard dev	*3.01*	*3.96*	*5.16*	*6.35*	*0.78*				

		G-2	MRG-1	DR-N	W-2	DNC-1	BE-N	GS-N	BHVO-1 ± standard error
Nd	*recommend*	**53**	**19.2**	**23**	**13.22**	**4.9**	**70**	**50**	**25.2**	***1.33***
	1st run	57.3	21.7	24.7	15.7	5.7	68.4	49.7	26.4	
	2nd	51.9	21.7	27.1	15.3	5.1				
	3rd	52.7	19.3	26.2						
	4th	56.7	22.0							
	5th	55.4								
	standard dev	*2.40*	*1.26*	*1.21*	*0.28*	*0.42*				
Pb	*recommend*	**31**	**10**	**55**	**7.81**	**6.3**	**4**	**53**	**2.6**	***2.71***
	1st run	28.5	8.9	53.7	5.7	7.4	7.6	45.4		
	2nd	27.7	9.6	53.6	8.1	7.2				
	3rd	32.2	10.6	52.8	8.2					
	4th	30.9	8.3							
	5th	32.1								
	standard dev	*2.07*	*0.99*	*0.49*	*1.42*	*0.14*				
Th	*recommend*	**24.6**	**0.93**	**5**	**2.04**	**0.2**	**11**	**42**	**1.08**	***1.55***
	1st run	26.7	1.3	5.7	0.9			40.0	1.0	
	2nd	27.7	1.3	5.7	0.8	0.3				
	3rd	27.1	1.0	4.8	3.5					
	4th	24.8	1.6							
	5th	30.9								
	standard dev	*2.22*	*0.24*	*0.52*	*1.53*					
U	*recommend*	**1.3**		**1.5**	**1.7**	**0.1**				***0.83***
	1st run	1.3		1.9	0.6	0.2				
	2nd	2		2.1	0.8					
	3rd	1.4			0.5					
	standard dev	*0.34*		*0.31*	*0.55*	*0.07*				

APPENDIX B (III)- Error calculations of ICP-MS rare earth element data

		AGV-1	W-2	BHV0-1	X-108	AL-1	BCR-1	G-2	± standard error
Cs	***recommended***	**1.26**	**0.87**	**0.13**	**0.65**	**0.34**	**0.96**	**1.33**	***0.03***
	1st run	1.23	0.86	0.10	0.70	0.35	0.96	1.33	
	2nd	1.23	0.83	0.12	0.73	0.36	0.96	1.30	
	3rd	1.26	0.86	0.11	0.70	0.35	0.95		
	4th	1.25	0.82	0.09	0.67				
	5th	1.27	0.80	0.09					
	standard dev.	*0.02*	*0.02*	*0.01*	*0.02*	*0.01*	*0.00*	*0.02*	
La	***recommended***	**38**	**10.61**	**15.8**	**0.93**	**9.9**	**24.9**	**86**	***0.50***
	1st run	37.97	10.48	15.47	0.90	9.56	25.21	86.38	
	2nd	38.80	10.01	14.62	1.49	9.45	25.64	86.66	
	3rd	38.16	9.54	15.38	1.53	9.53	25.12		
	4th	38.11	9.63	15.06	1.33				
	5th	38.19	9.67	15.39					
	standard dev.	*0.32*	*0.39*	*0.35*	*0.29*	*0.06*	*0.28*	*0.20*	
Ce	***recommended***	**66**	**23.03**	**39**	**1.73**	**21**	**53.7**	**159**	***1.63***
	1st run	67.80	22.77	37.59	1.68	21.24	52.63	157.12	
	2nd	67.72	21.71	36.62	1.89	22.68	53.73		
	3rd	67.20	22.13	36.95	2.04	22.48	52.69		
	4th	67.49	20.59	36.44	1.88				
	5th	68.18		37.48					
	standard dev.	*0.36*	*0.91*	*0.51*	*0.15*	*0.78*	*0.62*		
Pr	***recommended***	**6.5**	**2.94**	**5.7**	**0.25**	**2.73**	**6.8**	**19**	***1.22***
	1st run	8.45	2.99	5.49	0.28	2.51	6.95	17.22	
	2nd	8.80	2.92	5.60	0.34	2.51	7.09	16.96	
	3rd	8.86	3.12	5.70	0.34	2.50	6.99		
	4th	8.82	2.82	5.61	0.32				
	5th	8.57	2.82	5.48					
	standard dev.	*0.18*	*0.13*	*0.09*	*0.03*	*0.00*	*0.07*	*0.18*	
Nd	***recommended***	**34**	**13.22**	**25.2**	**1.14**	**10**	**28.8**	**53**	***0.94***
	1st run	33.55	13.16	25.53	1.31	10.15	30.01	55.83	
	2nd	33.32	12.85	25.49	1.55	10.08	29.67	55.56	
	3rd	33.63	13.77	26.01	1.53	10.03			
	4th	33.11		25.60	1.46				
	5th								
	standard dev.	*0.24*	*0.47*	*0.24*	*0.11*	*0.06*	*0.24*	*0.19*	
Sm	***recommended***	**5.9**	**3.36**	**6.2**	**0.38**	**2.74**	**6.59**	**7.2**	***0.09***
	1st run	5.76	3.30	6.21	0.37	2.76	6.74	7.43	
	2nd	5.85	3.17	6.25	0.39	2.69	6.82	7.33	
	3rd	5.85	3.35	6.25	0.40	2.68	6.66		
	4th	6.16	3.19	6.37	0.41				
	5th	5.92	3.13	6.21					
	standard dev.	*0.15*	*0.09*	*0.07*	*0.02*	*0.04*	*0.08*	*0.07*	
Eu	***recommended***	**1.66**	**1.12**	**2.06**	**0.12**	**0.19**	**1.95**	**1.41**	***0.07***
	1st run	1.69	1.07	2.02	0.12	0.20	1.99	1.51	
	2nd	1.74	1.03	2.01	0.12	0.20	2.03	1.50	
	3rd	1.74	1.09	1.99	0.13	0.20	1.98		
	4th	1.75	1.00	2.00	0.12				
	5th	1.74	1.00	2.02					
	standard dev.	*0.02*	*0.04*	*0.01*	*0.01*	*0.00*	*0.02*	*0.01*	
Gd	***recommended***	**5.2**	**3.63**	**6.4**	**0.44**	**1.9**	**6.68**	**4.1**	***0.29***
	1st run	5.43	3.57	6.11	0.45	1.95	6.81	3.53	
	2nd	4.92	3.64	6.52	0.54	1.99	6.99	3.56	
	3rd	4.80	3.82	6.72	0.47	2.02	7.01		
	4th	4.85	3.53	6.47	0.48				
	5th	4.77	3.68	6.39					
	standard dev.	*0.27*	*0.11*	*0.22*	*0.04*	*0.03*	*0.11*	*0.02*	
Tb	***recommended***	**0.71**	**0.62**	**0.96**	**0.08**	**0.6**	**1.05**	**0.48**	***0.11***
	1st run	0.66	0.62	0.96	0.08	0.30	1.08	0.49	
	2nd	0.68	0.60	0.98	0.08	0.30	1.11	0.47	
	3rd	0.71	0.62	0.96	0.09	0.30	1.08		
	4th	0.67	0.57	0.98	0.09				
	5th	0.67	0.59	0.96					
	standard dev.	*0.02*	*0.02*	*0.01*	*0.01*	*0.00*	*0.01*	*0.02*	

		AGV-1	W-2	BHV0-1	X-108	AL-1	BCR-1	G-2	± standard error
Ho	***recommended***	**0.73**	**0.74**	**0.99**	**0.12**	**0.2**	**1.26**	**0.37**	***0.03***
	1st run	0.67	0.77	0.99	0.14	0.20	1.28	0.36	
	2nd	0.69	0.75	0.98	0.15	0.20	1.30	0.39	
	3rd	0.70	0.79	1.01	0.17	0.21	1.29		
	4th	0.71	0.72	1.05	0.14				
	5th	0.67	0.74	0.98					
	standard dev.	*0.02*	*0.03*	*0.03*	*0.01*	*0.00*	*0.01*	*0.02*	
Dy	***recommended***	**3.8**	**3.71**	**5.2**	**0.59**	**1.4**	**6.34**	**2.5**	***0.17***
	1st run	3.48	3.78	5.33	0.60	1.31	6.38	2.06	
	2nd	3.50	3.70	5.27	0.56	1.28	6.50	2.19	
	3rd	3.74	3.91	5.25	0.66	1.31	6.39		
	4th	3.61	3.63	5.34	0.63				
	5th	3.57	3.63	5.31					
	standard dev.	*0.10*	*0.12*	*0.04*	*0.04*	*0.02*	*0.07*	*0.10*	
Er	***recommended***	**1.61**	**2.23**	**2.4**	**0.48**	**0.59**	**3.63**	**1.2**	***0.19***
	1st run	1.78	2.14	2.49	0.45	0.59	3.56	0.82	
	2nd	1.82	2.10	2.37	0.43	0.61	3.60	0.85	
	3rd	1.75	2.12	2.31	0.49	0.60	3.59		
	4th	1.88	1.94	2.36	0.42				
	5th	1.81	1.98	2.46					
	standard dev.	*0.05*	*0.09*	*0.07*	*0.03*	*0.01*	*0.02*	*0.02*	
Tm	***recommended***	**0.32**	**0.34**	**0.33**	**0.09**		**0.56**	**0.17**	***0.03***
	1st run	0.28	0.34	0.37	0.09		0.56	0.13	
	2nd	0.28	0.34	0.37	0.09		0.58	0.13	
	3rd	0.29	0.34	0.35	0.10		0.56		
	4th	0.28	0.31	0.36	0.08				
	5th	0.28	0.32	0.36					
	standard dev.	*0.01*	*0.01*	*0.01*	*0.01*		*0.01*	*0.00*	
Yb	***recommended***	**1.67**	**2.03**	**2.02**	**0.68**	**0.78**	**3.38**	**0.78**	***0.04***
	1st run	1.66	2.04	2.05	0.63	0.68	3.37	0.77	
	2nd	1.71	2.00	1.97	0.59	0.70	3.42	0.76	
	3rd	1.75	2.06	1.97	0.73	0.69	3.40		
	4th	1.73	1.95	2.01	0.63				
	5th	1.67	1.93	2.03					
	standard dev.	*0.04*	*0.06*	*0.04*	*0.06*	*0.01*	*0.02*	*0.00*	
Lu	***recommended***	**0.28**	**0.33**	**0.291**	**0.11**	**0.11**	**0.51**	**0.113**	***0.01***
	1st run	0.26	0.32	0.29	0.11	0.11	0.53	0.11	
	2nd	0.28	0.31	0.30	0.12	0.11	0.54	0.11	
	3rd	0.26	0.33	0.30	0.14	0.11	0.53		
	4th	0.28	0.31	0.32	0.11				
	5th	0.26	0.32	0.29					
	standard dev.	*0.01*	*0.01*	*0.01*	*0.01*	*0.00*	*0.00*	*0.00*	
Hf	***recommended***	**5.1**	**2.49**	**4.38**	**0.69**	**2.6**	**4.95**	**7.9**	***0.09***
	1st run	5.10	2.39	4.45	0.60	2.37	4.95	7.79	
	2nd	5.16	2.34	4.28	0.68	2.40	4.93	7.83	
	3rd	5.12	2.54	4.37	0.69	2.38	4.93		
	4th	5.08	2.27	4.31	0.65				
	5th	5.16	2.26	4.44					
	standard dev.	*0.04*	*0.11*	*0.07*	*0.04*	*0.01*	*0.01*	*0.03*	
Ta	***recommended***	**0.92**	**0.54**	**1.23**	**0.052**	**1.85**	**0.81**	**0.88**	***0.11***
	1st run	0.90	0.49	1.26	0.04	1.92	0.82	0.75	
	2nd	0.91	0.48	1.26		1.93	0.82	0.58	
	3rd	1.05	0.48	1.14		1.93	0.83		
	4th	1.08	0.10	0.92					
	5th	0.92	0.14	1.25					
	standard dev.	*0.08*	*0.20*	*0.15*		*0.00*	*0.01*	*0.13*	
Pb	***recommended***	**36**	**7.81**	**2.6**	**1.62**	**4.5**	**13.6**	**31**	***0.99***
	1st run	35.88	7.76	2.08	2.02	2.36	13.99	29.16	
	2nd	36.10	7.79	2.28	1.71	2.35	13.97	29.96	
	3rd	36.09	7.45	1.51	1.53	2.36	13.88		
	4th	36.51	6.37	1.61	1.84				
	5th	35.93	6.56	1.96					
	standard dev.	*0.25*	*0.67*	*0.32*	*0.21*	*0.00*	*0.06*	*0.57*	

		AGV-1	W-2	BHV0-1	X-108	AL-1	BCR-1	G-2	± standard error
Th	***recommended***	**6.5**	**2.04**	**1.08**	**0.13**	**9.5**	**5.98**	**24.6**	***0.46***
	1st run	6.38	2.17	1.28	0.13	11.13	6.04	25.94	
	2nd	6.44	2.18	1.26	0.19	11.03	6.09	26.37	
	3rd	6.48	2.16	1.27	0.21	10.98	5.98		
	4th	6.56	2.08	1.32	0.19				
	5th	6.44	2.07	1.23					
	standard dev.	*0.07*	*0.05*	*0.03*	*0.03*	*0.08*	*0.05*	*0.30*	
U	***recommended***	**1.89**	**0.5**	**0.42**	**0.16**	**5.8**	**1.75**	**2.04**	***0.19***
	1st run	1.93	0.50	0.44	0.12	7.35	1.71	2.07	
	2nd	1.91	0.50	0.39	0.14	7.25	1.71	2.06	
	3rd	1.89	0.47	0.43	0.14	7.37	1.70		
	4th	1.92	0.48	0.43	0.14				
	5th	1.94	0.48	0.42					
	standard dev.	*0.02*	*0.01*	*0.02*	*0.01*	*0.06*	*0.01*	*0.01*	

APPENDIX C- Analytical data

ABBREVIATIONS

enc: enclave
grd: grained
wr: whole-rock
bear: bearing

gb: gabbro
mzgb: monzogabbro
gb: diorite
qdi: quartz diorite
ton: tonalite
mzdi: monzodiorite
qmzdi: quartz monzodiorite
qmz: quartz monzonite
mz: monzonite
grd: granodiorite
gr: granite
sy: syenite
fgb: foid gabbro
fmzsy: foid monzosyenite
nemzsy: nepheline monzosyenite
pdmzsy: pseudoleucite monzosyenite
fsy: foid syenite
kspsy: alkali feldspar syenite
qsy: quartz syenite
pho: phonolite

amp: amphibole
bi: biotite
pl: plagioclase
ksp: alkali feldspar

APPENDIX C (I)- Modal analyses data

APPENDIX C (I)

Modal analyses (based on 1200 points per sample arranged in order of increasing silica content). Values are in percent.

Pluton	Behrekdag	Behrekdag	Behrekdag	Behrekdag	Behrekdag	Behrekdag	Behrekdag	Behrekdag	Behrekdag	Behrekdag	Behrekdag	Behrekdag	Behrekdag	Behrekdag
Sample no	**N2**	**N99**	**N107**	**N1**	**N10**	**N102**	**N105**	**N3**	**N104**	**N184**	**N5**	**N6**	**N180**	**N160**
SiO_2 wt.% of the host rock	60.11	60.15	60.20	60.27	60.57	60.70	60.73	61.10	61.25	63.37	63.58	63.61	63.97	64.16
Quartz	13.3	16.0	13.0	11.9	15.0	10.2	8.6	9.0	9.8	12.1	13.2	15.1	18.1	21.0
Alkali feldspar	31.3	39.0	36.2	25.2	37.3	35.5	29.8	33.8	28.0	37.2	35.5	32.2	33.0	38.1
Plagioclase	29.6	34.2	39.4	41.7	31.3	33.0	40.3	32.6	42.6	31.3	29.6	27.3	29.0	32.2
Amphibole	23.6	9.0	10.2	19.2	13.4	20.4	18.3	20.1	14.3	16.2	18.1	22.1	15.4	7.2
Biotite	0.7	tr	tr	0.6	1.2	0.2	1.6	1.3	2.1	1.7	1.1	1.2	2.3	1.1
Clinopyroxene	0.6	0.1	0.1	0.6	0.3	0.2	tr	1.2	1.5	tr	1.4	1.3	0.9	0.1
Titanite	0.5	0.2	0.4	0.4	0.2	0.3	0.2	0.5	0.4	0.3	0.5	0.5	0.3	0.2
Apatite	tr	tr	tr	0.1	0.1	tr	-	tr	-	-	tr	tr	tr	tr
Zircon	0.1	tr	tr	0.1	-	tr	-	tr	-	-	tr	tr	tr	tr
Epidote	-	-	-	-	-	-	-	-	-	-	-	-	-	-
Allanite	-	-	-	-	-	-	-	-	-	-	-	-	-	-
Opaques	0.4	1.5	0.6	0.2	1.2	0.2	1.1	1.4	1.2	1.1	0.6	0.4	1.1	0.2
Others														

Pluton	Behrekdag	Behrekdag	Behrekdag	Behrekdag	Behrekdag	Behrekdag	Behrekdag	Behrekdag	Behrekdag	Behrekdag	Behrekdag	Cefalikdag	Cefalikdag	Cefalikdag
Sample no	**N165**	**N171**	**N164**	**N182**	**N7**	**N161**	**N183**	**N163**	**N185**	**N9**	**N166**	**N225**	**N226**	**N233**
SiO_2 wt.% of the host rock	64.25	64.28	64.48	64.74	64.78	64.83	65.06	65.43	65.48	65.52	65.66	50.45	51.33	51.36
Quartz	20.8	19.7	20.0	22.8	17.2	23.0	19.6	21.1	26.0	18.6	23.0	0.2	2.1	1.3
Alkali feldspar	42.1	38.6	41.0	42.1	37.1	38.2	41.3	37.0	38.0	42.2	40.0	18.0	16.2	20.7
Plagioclase	28.8	31.8	29.0	28.0	32.1	31.9	33.0	29.0	30.0	33.5	34.0	52.0	41.3	40.8
Amphibole	4.5	6.8	5.7	4.2	9.7	5.6	4.1	11.2	4.0	3.4	2.0	19.7	26.3	23.8
Biotite	1.9	2.7	4.1	2.3	3.7	1.0	1.8	1.1	1.4	1.3	0.8	5.5	8.9	10.1
Clinopyroxene	0.1	tr	tr	tr	tr	0.1	tr	0.2	tr	0.2	tr	3.3	4.3	2.3
Titanite	0.2	0.1	0.1	0.1	0.1	0.1	0.2	0.3	0.1	0.4	0.2	0.1	0.2	0.3
Apatite	tr	0.1	0.1	0.1	tr	tr	tr	tr	0.2	0.2	tr	0.2	0.3	tr
Zircon	tr	0.1	-	0.1	-	-	-	-	tr	tr	-	-	-	-
Epidote	-	-	-	-	-	-	-	-	-	-	-	-	-	-
Allanite	-	-	-	-	-	-	-	-	-	-	-	-	-	-
Opaques	1.7	0.2	0.1	0.4	0.2	0.2	0.1	0.2	0.4	0.3	0.1	1.1	0.4	0.6
Others														

APPENDIX C (I)

Modal analyses (based on 1200 points per sample arranged in order of increasing silica content). Values are in percent.

Pluton	Cefalikdag	Cefalikdag	Cefalikdag	Cefalikdag	Cefalikdag	Cefalikdag	Cefalikdag	Cefalikdag	Cefalikdag	Cefalikdag	Cefalikdag	Cefalikdag	Cefalikdag	Cefalikdag
Sample no	**N224**	**N80**	**N235**	**N232**	**N231**	**N81**	**N78**	**N237**	**N236**	**N316**	**N85**	**N83**	**N319**	**N82**
SiO_2 wt.% of the host rock	51.67	52.28	52.44	52.51	52.62	52.81	53.86	54.80	55.16	57.98	58.17	59.10	59.50	59.53
Quartz	1.0	2.4	1.2	3.1	2.4	3.3	4.4	6.7	7.8	11.8	7.4	8.5	13.0	16.7
Alkali feldspar	8.0	17.1	20.2	16.2	21.1	16.3	20.0	21.0	20.5	20.8	21.7	7.9	22.0	25.0
Plagioclase	57.4	48.1	53.5	45.0	46.9	45.6	39.3	44.4	52.0	49.0	41.3	53.5	48.1	44.6
Amphibole	24.5	24.8	18.7	21.2	17.3	17.6	29.0	13.5	14.0	13.1	22.5	18.9	12.8	12.0
Biotite	7.0	6.6	4.6	12.0	7.8	4.5	2.9	10.1	4.5	5.0	6.5	9.3	3.4	1.3
Clinopyroxene	1.4	0.2	1.1	2.0	4.2	0.2	1.2	3.4	0.8	0.1	0.3	0.2	0.1	0.2
Titanite	0.1	0.3	0.2	0.2	0.1	0.7	1.7	0.5	0.2	0.1	0.1	0.9	0.3	0.1
Apatite	tr	0.1	0.3	0.2	tr	tr	tr	0.1	0.1	tr	0.1	tr	tr	-
Zircon	tr	-	-	-	-	-	-	0.1	-	-	tr	-	-	-
Epidote	-	-	-	-	-	-	-	-	-	-	-	-	-	-
Allanite	-	-	-	-	-	-	-	-	-	-	-	-	-	-
Opaques	0.4	0.4	0.3	0.2	0.3	0.5	0.3	0.2	0.2	0.1	0.2	0.5	0.2	0.1
Others	0.3					5.6	1.3					0.2		

Pluton	Cefalikdag	Cefalikdag	Cefalikdag	Cefalikdag	Cefalikdag	Cefalikdag	Cefalikdag	Cefalikdag	Cefalikdag	Cefalikdag	Cefalikdag	Cefalikdag	Cefalikdag	Cefalikdag
Sample no	**N84**	**N318**	**N327**	**N317**	**N324**	**N322**	**N20**	**N325**	**N323**	**N310**	**N321**	**N394**	**N395**	**N404**
SiO_2 wt.% of the host rock	59.71	59.76	60.46	61.02	61.64	61.75	61.82	61.96	62.20	63.27	63.27	66.39	71.53	71.95
Quartz	10.1	13.5	12.0	15.9	13.4	12.3	16.1	15.4	15.9	17.1	15.3	20.3	22.1	23.2
Alkali feldspar	31.1	32.3	28.3	28.2	31.7	30.3	31.7	31.7	28.1	33.2	33.2	41.5	44.2	44.5
Plagioclase	42.9	43.0	51.2	44.3	38.7	43.5	34.7	40.3	48.2	37.0	38.2	32.3	30.3	25.9
Amphibole	12.1	9.0	4.5	8.8	10.9	8.3	9.6	7.8	5.2	10.1	8.9	-	-	-
Biotite	2.4	2.0	3.6	2.1	4.9	5.2	7.0	4.7	2.2	2.1	4.0	5.5	3.3	6.3
Clinopyroxene	1.1	0.1	0.1	tr	tr	tr	0.3	tr	0.1	tr	tr	-	-	-
Titanite	0.2	-	0.1	0.4	0.2	0.2	0.2	0.1	0.2	0.3	0.2	0.2	0.1	0.1
Apatite	tr	-	tr	0.1	tr	tr	0.1	tr	tr	0.1	tr	0.1	-	-
Zircon	tr	-	tr	0.1	tr	tr	tr	tr	tr	tr	tr	tr	tr	tr
Epidote	-	-	-	-	-	-	-	-	-	-	-	-	-	-
Allanite	-	-	-	-	-	-	-	-	-	-	-	0.1	tr	tr
Opaques	0.2	0.1	0.3	0.2	0.2	0.2	0.1	0.1	0.1	0.1	0.3	0.1	tr	tr
Others														

APPENDIX C (I)

Modal analyses (based on 1200 points per sample arranged in order of increasing silica content). Values are in percent.

Pluton	Celebi	Celebi	Celebi	Celebi	Celebi	Celebi	Celebi	Celebi	Celebi	Celebi	Celebi	Celebi	Celebi	Celebi
Sample no	**N339**	**N116**	**N344**	**N23**	**N338**	**N115**	**N343**	**N25**	**N349**	**N345**	**N76**	**N66**	**N24**	**N71**
SiO_2 wt.% of the host rock	61.45	62.14	62.44	62.70	62.74	63.08	63.19	63.32	63.44	63.58	63.67	63.70	63.71	63.72
Quartz	10.9	12.6	14.1	11.7	13.0	13.5	14.0	12.3	15.0	11.9	17.0	15.0	16.8	12.1
Alkali feldspar	35.6	32.2	34.0	37.6	36.3	34.5	36.1	38.1	39.7	42.0	41.9	39.3	38.7	41.1
Plagioclase	37.6	36.7	39.1	38.2	41.2	40.0	39.2	32.5	35.5	31.7	33.3	35.6	37.6	29.5
Amphibole	11.0	11.7	9.2	9.3	8.0	7.0	8.8	12.8	8.1	10.0	7.6	6.6	4.9	12.3
Biotite	4.5	6.7	3.4	1.2	1.2	5.0	1.3	1.9	1.3	4.0	0.2	2.9	1.3	2.1
Clinopyroxene	0.1	tr	tr	tr	0.1	tr	0.1	tr	tr	0.1	tr	tr	0.2	2.2
Titanite	0.2	0.1	0.1	0.4	0.1	tr	0.2	0.3	0.2	0.1	tr	0.2	0.1	0.5
Apatite	tr	-	-	0.1	-	-	0.1	tr	-	-	-	-	-	tr
Zircon	tr	-	-	tr	-	-	-	tr	-	-	-	-	-	tr
Epidote	tr	-	-	-	-	-	-	-	-	-	-	-	-	-
Allanite	-	-	-	-	-	-	-	-	-	-	-	-	-	-
Opaques	0.2	0.1	0.2	1.6	0.2	0.1	0.3	2.1	0.3	0.2	0.1	0.4	0.3	0.2
Others														

Pluton	Celebi	Celebi	Celebi	Celebi	Celebi	Celebi	Celebi	Celebi	Celebi	Celebi	Celebi	Celebi	Celebi	Celebi
Sample no	**N112**	**N77**	**N72**	**N201**	**N218**	**N215**	**N111**	**N75**	**N74**	**N202**	**N203**	**N208**	**N73**	**N109**
SiO_2 wt.% of the host rock	64.05	64.40	64.47	64.53	64.85	64.88	65.06	65.07	65.20	65.22	65.43	65.51	65.64	65.84
Quartz	14.5	12.5	16.1	14.9	15.6	12.7	17.0	17.7	21.2	22.0	23.4	21.3	19.8	21.0
Alkali feldspar	40.9	45.3	43.1	41.0	43.2	35.0	42.0	41.5	42.0	41.0	36.8	39.7	36.4	40.0
Plagioclase	28.8	25.3	30.1	33.2	35.6	40.4	32.1	25.1	29.6	30.5	31.0	32.0	30.0	27.3
Amphibole	11.0	11.1	9.3	7.2	4.3	9.8	6.7	11.8	5.6	6.0	7.9	6.7	11.0	9.8
Biotite	4.5	0.4	0.2	2.3	1.2	0.4	1.8	1.4	1.1	0.2	0.7	0.2	2.3	1.4
Clinopyroxene	0.2	0.1	tr	1.2	tr	tr	tr	0.3	tr	tr	tr	tr	0.1	0.2
Titanite	0.1	0.7	0.2	0.1	0.1	0.2	0.1	0.4	0.1	0.1	tr	0.1	0.2	0.1
Apatite	tr	tr	-	tr	-	tr	0.1	0.1	tr	-	-	-	-	tr
Zircon	tr	tr	-	tr	-	tr	tr	tr	-	-	-	-	-	-
Epidote	tr	3.2	0.8	tr	-	-	0.1	1.3	0.1	tr	tr	tr	tr	0.2
Allanite	-	-	-	-	-	-	-	-	-	-	-	-	-	-
Opaques	0.1	0.9	0.2	0.2	0.1	1.5	0.2	0.3	0.2	0.1	0.2	0.1	0.2	0.1
Others		0.5	0.1					0.2						

APPENDIX C (I)

Modal analyses (based on 1200 points per sample arranged in order of increasing silica content). Values are in percent.

Pluton	Celebi	Celebi	Celebi	Celebi	Celebi	Celebi	Celebi	Celebi	Celebi	Celebi	Celebi	Celebi	Baranadag	Baranadag
Sample no	**N210**	**N204**	**N209**	**N70**	**N110**	**N114**	**N113**	**N205**	**N211**	**N213**	**N214**	**N212**	**N13**	**N27**
SiO_2 wt.% of the host rock	65.97	66.04	66.16	66.18	66.32	66.52	66.60	66.69	67.52	68.70	69.39	72.95	55.78	58.33
Quartz	23.6	22.1	19.9	21.2	23.0	24.2	23.2	24.0	25.1	26	25.3	25.9	2.3	2.6
Alkali feldspar	38.0	40.0	37.5	39.0	39.8	40.3	42.0	44.6	43.2	39.1	45.4	46.3	39.7	38.6
Plagioclase	30.0	30.7	32.4	33.0	30.2	27.7	26.3	24.3	21.8	24.5	23.1	23.8	32.2	36.6
Amphibole	7.0	6.3	8.9	6.0	5.6	6.4	7.4	5.7	8.0	10.1	5.3	2.4	14.0	12.3
Biotite	1.2	0.6	0.2	0.2	1.0	1.2	0.3	0.1	1.3	0.2	0.4	1.2	0.2	1.4
Clinopyroxene	tr	tr	0.3	0.1	tr	tr	tr	tr	tr	tr	0.2	0.2	8.0	7.4
Titanite	0.2	0.1	0.2	0.1	0.3	0.1	0.2	0.1	0.2	tr	0.1	0.1	1.1	0.3
Apatite	tr	-	tr	-	-	-	0.1	tr	-	-	-	0.1	0.7	0.3
Zircon	tr	-	tr	-	-	-	tr	tr	-	-	0.1	-	-	-
Epidote	-	-	0.4	0.1	-	-	0.1	-	0.1	-	-	-	-	-
Allanite	-	-	-	-	-	-	-	-	-	-	-	-	-	-
Opaques	0.1	0.2	0.3	0.2	0.1	0.2	0.2	0.6	0.2	0.1	0.2	0.1	1.7	0.5
Others							0.2	0.5						

Pluton	Baranadag	Baranadag	Baranadag	Baranadag	Baranadag	Baranadag	Baranadag	Baranadag	Baranadag	Baranadag	Baranadag	Baranadag	Baranadag	Baranadag
Sample no	**N26**	**N304**	**N297**	**N28**	**N309**	**N299**	**N301**	**N298**	**N19**	**N18**	**N15**	**N16**	**N159**	**N132**
SiO_2 wt.% of the host rock	58.44	52.52	58.64	59.11	59.32	59.76	59.98	60.51	60.93	61.33	62.07	62.62	62.99	63.25
Quartz	2.1	2.8	3.0	3.4	4.2	4.1	4.2	3.9	3.4	5.0	8.0	10.4	12.0	11.2
Alkali feldspar	40.1	41.6	42.0	42.2	42.7	40.7	43.6	45.0	44.2	45.6	44.8	39.5	41.2	43.1
Plagioclase	39.2	35.2	34.4	35.8	38.9	38.6	37.8	39.1	38.6	36.8	35.2	38.2	39.1	35.2
Amphibole	8.8	10.5	15.0	13.0	9.8	10.7	9.7	8.6	12.1	8.7	9.5	11.0	6.0	9.3
Biotite	1.1	3.4	0.6	0.2	0.4	0.9	1.1	0.7	0.5	1.5	0.8	0.2	1.1	0.4
Clinopyroxene	6.6	5.8	4.0	4.2	3.4	4.5	3.4	2.1	0.6	0.9	0.3	0.2	0.4	0.1
Titanite	1.2	0.3	0.6	0.9	0.4	0.2	0.1	0.2	0.2	0.4	0.4	0.1	0.1	0.2
Apatite	0.2	0.1	0.2	0.1	tr	tr	0.1	0.1	0.1	0.5	0.6	0.1	tr	0.1
Zircon	-		tr	tr	-	-	-	tr	tr	tr	-	-	-	-
Epidote	-	-	-	-	-	-	-	-	-	-	-	-	-	-
Allanite	-	-	-	-	-	-	-	-	-	-	tr	tr	tr	tr
Opaques	0.6	0.2	0.2	0.3	0.2	0.2	0.1	0.2	0.3	0.5	0.5	0.3	0.2	0.5
Others														

APPENDIX C (I)

Modal analyses (based on 1200 points per sample arranged in order of increasing silica content). Values are in percent.

Pluton	Baranadag	Baranadag	Baranadag	Baranadag	Baranadag
Sample no	**N138**	**N158**	**N143**	**N144**	**N135**
SiO_2 wt.% of the host rock	63.62	63.88	64.10	64.58	65.24
Quartz	13.4	14.1	16.2	17.2	15.8
Alkali feldspar	42.6	42.4	45.6	46.0	39.3
Plagioclase	36.8	38.3	33.9	31.2	34.9
Amphibole	5.4	4.1	3.4	5.1	7.3
Biotite	1.0	0.8	0.5	0.2	1.9
Clinopyroxene	0.4	0.2	0.2	tr	0.1
Titanite	0.1	0.1	0.1	0.1	0.2
Apatite	0.1	tr	tr	tr	0.2
Zircon	tr	-	-	-	-
Epidote	-	-	-	-	-
Allanite	tr	tr	tr	tr	0.1
Opaques	0.2	0.1	0.1	0.3	0.2
Others					0.1

Others include alteration minerals (e.g. sericite, chlorite, carbonate).

APPENDIX C (I)

Modal analyses (based on 1200 points per sample arranged in order of increasing silica content). Values are in percent.

Pluton	Hamit	Hamit	Hamit	Hamit	Hamit	Hamit	Hamit	Hamit	Hamit	Hamit	Hamit	Hamit	Hamit	Hamit	Hamit	Hamit
Sample no	**N46**	**N45**	**N31**	**N255**	**N32**	**N293**	**N256**	**N253**	**N295**	**HAMID-II**	**N294**	**N283**	**N281**	**N43**	**N50**	**N282**
SiO_2 wt.% of the host rock	52.52	52.83	53.19	53.25	53.37	53.60	53.70	53.77	54.06	54.11	54.25	55.89	55.93	56.00	56.45	56.48
Nepheline	11.4	14.4	12.8	8.4	8.6	15.2	8.9	9.1	14.2	16.3	13.0	8.6	9.5	8.8	10.3	10.1
Alkali feldspar	41.3	43.0	40.8	52.1	44.9	39.2	45.2	42.0	36.0	36.7	42.1	42.4	44.2	43.0	43.0	47.8
Plagioclase	20.6	21.0	22.9	17.6	16.3	22.1	29.7	28.0	20.3	22.6	21.0	27.2	25.3	30.0	27.2	28.0
Clinopyroxene	10.1	9.3	10.6	13.2	11.9	9.0	7.0	12.2	8.6	6.7	6.1	10.2	11.1	9.8	8.3	8.0
Amphibole	3.1	1.3	8.6	5.4	7.8	2.3	5.1	4.8	2.1	1.1	0.2	6.4	5.8	4.4	1.2	3.3
Biotite	0.3	0.1	0.4	0.2	1.0	tr	1.1	1.8	tr	tr	tr	0.2	3.3	0.3	tr	1.2
Pseudoleucite	7.1	5.0	-	-	-	6.7	-	-	7.8	8.1	6.6	-	-	-	-	-
Nosean	1.2	0.8	-	-	-	1.8	-	-	2.2	2.5	3.4	-	-	-	-	-
Garnet	2.2	3.4	-	-	-	2.5	-	-	5.6	5.8	4.2	-	-	-	6.5	-
Cancrinite	2.2	1.2	3.2	2.5	9.0	0.8	2.4	1.6	2.8	0.2	3.0	4.5	0.7	3.2	3.2	1.4
Titanite	0.1	0.1	0.2	0.1	0.1	tr	0.1	0.2	0.1	tr	tr	0.2	0.1	0.2	0.1	0.1
Apatite	0.2	0.1	0.3	0.1	0.2	0.1	0.2	0.1	tr	tr	0.1	0.1	tr	0.1	0.1	tr
Opaques	0.2	0.3	0.1	0.3	0.2	0.2	0.3	0.1	0.2	0.1	0.2	0.1	0.1	0.2	0.1	0.1

Pluton	Hamit
Sample no	**N280**
SiO_2 wt.% of the host rock	57.30
Nepheline	9.7
Alkali feldspar	42.7
Plagioclase	26.5
Clinopyroxene	11.3
Amphibole	5.6
Biotite	0.1
Pseudoleucite	-
Nosean	-
Garnet	-
Cancrinite	3.7
Titanite	0.1
Apatite	0.2
Opaques	0.2

Other minerals present in these rocks are:

Fluorite: all samples
Zircon: all samples

APPENDIX C (I)

Modal analyses (based on 1200 points per sample arranged in order of increasing silica content). Values are in percent.

Pluton	Hamit	Hamit	Hamit	Hamit	Hamit	Hamit	Hamit	Hamit	Hamit	Hamit	Hamit	Hamit	Hamit	Hamit
Sample no	**N37**	**N36**	**N44**	**N34**	**N40**	**N246**	**N48**	**N47**	**N49**	**N291**	**N290**	**N289**	**N292**	**N265**
SiO_2 wt.% of the host rock	62.23	63.46	63.76	64.37	64.72	65.56	65.64	65.88	66.00	66.53	66.78	67.02	67.06	72.34
quartz	1.2	2.1	3.0	0.7	1.8	2.2	13.8	15.9	14.2	11.1	14.0	13.9	14.8	23.0
alkali feldspar	87.8	90.0	86.3	89.2	86.6	90.2	55.2	49.8	58.0	62.1	56.8	70.2	67.5	65.0
plagioclase	9.3	6.6	9.5	7.7	9.6	6.9	23.7	26.2	22.3	26.2	22.4	15.1	16.8	11.6
amphibole	1.0	1.1	0.8	2.0	1.7	0.2	6.7	7.8	5.0	0.2	4.7	tr	0.3	-
biotite	0.2	tr	0.1	0.2	0.1	tr	0.2	0.1	-	0.1	tr	0.1	0.2	0.3
clinopyroxene	0.1	tr	tr	0.1	tr	tr	0.1	-	0.2	tr	1.2	tr	tr	-
titanite	0.1	0.1	0.2	tr	tr	0.1	0.2	0.1	0.1	0.2	0.4	0.3	0.2	0.1
apatite	0.1	-	-	-	-	-	-	0.1	-	-	-	-	-	-
zircon	tr	-	-	-	-	-	-	-	-	-	-	-	-	-
allanite	0.1	-	0.1	-	0.1	0.2	-	-	-	-	-	-	-	-
opaques	0.1	0.2	0.1	0.2	0.1	0.2	0.1	0.1	0.1	0.2	0.4	0.4	0.2	0.1

Pluton	Cefalikdag	Cefalikdag	Cefalikdag	Cefalikdag	Cefalikdag	Cefalikdag	Celebi	Behrekdag	Behrekdag	Behrekdag	Behrekdag	Behrekdag	Behrekdag
Characteristic	*medium-grd enc.*	*medium-grd enc.*	*medium-grd enc.*	*medium-grd enc.*	*medium-grd enc.*	*medium-grd enc.*	*fine-grd enc.*	*fine-grd enc.*	*fine-grd enc.*	*fine-grd enc.*	*fine-grd enc.*	*fine-grd enc.*	*fine-grd enc.*
Sample no	**N509**	**N379**	**N241a**	**N80**	**N226a**	**N389**	**N478**	**N173**	**N103**	**N172**	**N174**	**N140**	**N158**
SiO_2 wt.% of the host rock	42.86	45.70	47.89	48.47	49.53	51.44	54.32	55.22	56.07	57.97	58.44	59.29	65.44
Quartz	tr	tr	tr	5.0	11.6	14.2	10.0	9.7	12.8	7.8	10.8	13.1	16.7
Alkali feldspar	tr	tr	tr	0.6	1.5	0.3	3.0	11.2	16.0	4.8	14.5	5.3	2.6
Plagioclase	57.2	64.2	60.2	66.8	65.0	62.0	56.1	54.0	47.2	55.0	53.4	54.4	52.1
Amphibole	30.0	21.1	22.0	10.4	8.7	9.6	-	12.0	9.0	12.1	8.7	1.4	17.6
Biotite	2.0	8.9	14.5	2.3	1.2	7.5	10.1	3.7	1.9	3.4	2.3	8.7	3.0
Clinopyroxene	8.0	3.4	1.4	13.2	10.3	5.4	19.5	8.7	12.3	16.5	9.5	16.7	7.6
Titanite	-	-	tr	0.1	0.1	0.2	0.2	0.1	0.2	0.1	0.1	0.1	0.1
Apatite	-	-	tr	0.2	0.1	-	0.6	0.2	0.3	0.2	0.2	0.2	0.3
Zircon	-	-	tr	-	0.1	-	0.1	-	-	tr	0.1	-	tr
Opaques	2.9	2.4	2.0	1.4	1.5	0.9	0.4	0.4	0.3	0.1	0.4	0.2	0.1

APPENDIX C (II)- K-Ar dating data

Table showing K-Ar dating results of the intrusive samples from the Central Anatolian Massif.

Sample no	Pluton	Rock composition	Mineral	K_2O (wt.%)	Radiogenic ^{40}Ar (x10^^{3} mm^3 g-1)	% Atmosphere	Age (Ma±1σ)
N6	Behrekdag	granite	hornblende	0.82±0.01	2.15±0.04	37.1	79.5±1.7
N20	Cefalikdag	quartz monzonite	biotite	7.02±0.07	0.154±0.018	9.30	66.6±1.1
N26	Baranadag	monzonite	hornblende	1.31±0.01	3.30±0.05	27.4	76.4±1.3

[λ_e=0.581 x 10^{-10} a^{-1}
λ_b=4.962 x 10^{-10} a^{-1}
$^{40}K/K$=1.167±10^{-2} atom%].

APPENDIX C (III)- XRF whole-rock major and trace element dataset

APPENDIX C (III)

XRF analyses of the samples from the Central Anatolian Massif.

Pluton	*Behrekdag*	*Behrekdag*	*Behrekdag*	*Behrekdag*	*Behrekdag*	*Behrekdag*	*Behrekdag*	*Behrekdag*	*Behrekdag*
Sample no	**N2**	**N99**	**N107**	**N1**	**N100**	**N102**	**N105**	**N3**	**N104**
Rock type	*qmz*	*qmz*	*qmz*	*qmz*	*qmz*	*qmz*	*qmz*	*qmz*	*qmz*
Geochemical description	*mz*	*mz*	*mz*	*mz*	*mz*	*mz*	*mz*	*mz*	*mz*
SiO_2	60.11	60.15	60.20	60.27	60.57	60.70	60.73	61.10	61.25
TiO_2	0.61	0.63	0.61	0.59	0.61	0.60	0.54	0.58	0.58
Al_2O_3	16.49	16.38	16.29	16.77	16.22	16.47	16.43	16.60	16.30
Fe_2O_3	6.04	6.11	5.87	5.81	5.91	5.84	5.72	5.77	5.66
MnO	0.12	0.12	0.12	0.12	0.13	0.12	0.12	0.12	0.12
MgO	2.42	2.26	2.33	2.34	2.40	2.43	2.31	2.28	2.16
CaO	6.38	6.21	6.50	6.43	6.58	6.68	6.45	6.49	6.18
Na_2O	2.94	2.92	3.03	2.95	2.88	2.95	2.90	3.02	2.95
K_2O	3.89	4.22	4.04	3.87	4.03	3.87	3.89	3.66	4.00
P_2O_5	0.18	0.18	0.15	0.17	0.17	0.17	0.17	0.16	0.16
L.O.I	0.37	0.55	0.57	0.37	0.49	0.37	0.51	0.35	0.73
TOTAL (L.O.I. free)	99.18	99.19	99.15	99.32	99.50	99.83	99.26	99.77	99.35
Sc	15.4	14.9	16.2	13.6	9.1	9.2	12.1	15.3	13.4
V	91.4	93.1	94.5	89.2	88.7	86.2	86.2	86.1	90.7
Cr	28.3	37.2	34.8	30.1	31.2	26.9	30.9	26.2	30.7
Co	13.4	11.2	14.9	15.0	13.0	13.8	10.8	15.8	11.9
Ni	11.7	1.7	10.0	12.1	11.1	8.6	11.2	14.3	10.4
Cu	12.0	21.6	12.1	10.1	18.2	18.3	17.5	12.7	17.3
Zn	77.5	91.9	91.5	76.9	77.5	75.2	78.4	76.2	84.5
Ga	15.5	21.3	21.5	17.0	16.7	20.4	16.9	17.4	20.8
Rb	131.5	153.2	142.1	128.9	136.1	133.7	133.0	122.0	143.0
Sr	547.6	531.3	539.3	556.9	503.8	501.5	502.4	549.2	530.9
Y	25.6	31.8	27.5	26.6	29.9	28.9	28.7	26.9	26.7
Zr	177.0	189.7	179.8	178.0	158.0	154.4	151.7	152.0	172.4
Nb	13.8	13.8	14.4	15.3	12.0	11.7	11.1	14.9	14.3
Ba	1042.2	1068.5	1108.0	1032.7	1145.5	1034.8	1031.1	931.4	1056.9
La	51.4	42.2	41.9	50.1	45.5	46.7	48.5	45.9	40.8
Ce	76.6	89.3	81.6	86.7	70.5	71.5	77.9	78.2	71.9
Nd	31.1	33.8	31.7	30.3	32.3	25.4	27.6	33.2	29.8
Pb	43.3	50.5	51.3	42.4	45.9	43.9	50.6	40.9	51.4
Th	19.1	18.4	16.8	19.5	17.6	18.5	18.7	14.8	20.3
U		4.4	3.0		4.6	4.4	3.8		2.7
cipw									
%AN	45	44	42	46	44	45	45	45	44
Q	10	9	9	10	10	10	11	11	11
or	23	25	24	23	24	23	23	22	24
ab	25	25	26	25	24	25	25	26	25
an	20	19	19	21	19	20	20	21	19
ne									
C									
di	9	9	10	8	10	10	9	9	9
hy	10	10	9	10	9	10	10	10	9
wo									
ol									
mt	1	1	1	1	1	1	1	1	1
il	1	1	1	1	1	1	1	1	1
ap									

APPENDIX C (III)

XRF analyses of the samples from the Central Anatolian Massif.

Pluton	*Behrekdag*	*Behrekdag*	*Behrekdag*	*Behrekdag*	*Behrekdag*	*Behrekdag*	*Behrekdag*	*Behrekdag*	*Behrekdag*
Sample no	**N184**	**N5**	**N6**	**N180**	**N160**	**N165**	**N171**	**N164**	**N182**
Rock type	*qmz*	*qmz*	*qmz*	*qmz*	*gr*	*gr*	*gr*	*gr*	*gr*
Geochemical description	*qmz*	*qmz*	*qmz*	*qmz*	*qmz*	*qmz*	*qmz*	*qmz*	*qmz*
SiO_2	63.37	63.58	63.61	63.97	64.16	64.25	64.28	64.48	64.74
TiO_2	0.45	0.45	0.42	0.37	0.40	0.44	0.39	0.42	0.42
Al_2O_3	15.87	16.19	16.29	16.09	16.07	15.65	15.61	15.97	16.48
Fe_2O_3	4.95	4.93	4.68	4.44	4.58	4.97	4.60	4.62	4.32
MnO	0.11	0.10	0.10	0.10	0.10	0.10	0.11	0.10	0.12
MgO	1.83	1.83	1.69	1.57	1.63	1.76	1.62	1.68	1.65
CaO	4.81	4.72	4.79	4.48	4.48	4.61	4.47	4.65	4.62
Na_2O	3.03	2.93	3.05	2.93	2.96	3.02	2.91	3.07	2.95
K_2O	4.39	4.89	4.51	4.79	4.83	4.46	4.61	4.47	4.77
P_2O_5	0.13	0.14	0.13	0.12	0.14	0.14	0.12	0.12	0.11
L.O.I	0.63	0.51	0.54	0.43	0.32	1.12	0.45	0.76	0.85
TOTAL (L.O.I. free)	98.94	99.77	99.27	98.87	99.35	99.40	98.71	99.58	100.18
Sc	10.3	10.2	11.8	11.3	9.8	10.1	12.9	12.9	5.8
V	83.5	81.2	79.4	81.7	79.0	94.7	83.4	81.9	73.5
Cr	17.0	15.2	11.3	22.0	21.3	16.3	24.1	13.3	8.8
Co	12.1	10.1	10.8	7.8	10.0	12.8	8.5	10.3	9.7
Ni	9.1	8.6	8.7	1.6	3.8	7.6	1.2	7.7	9.6
Cu	12.4	12.2	16.9	19.1	20.1	19.9	17.5	20.5	15.6
Zn	65.1	132.4	53.2	60.4	65.1	59.6	68.6	52.3	72.2
Ga	19.4	20.1	15.4	17.7	16.3	18.8	14.9	17.9	14.6
Rb	173.8	172.6	164.4	197.7	205.8	168.5	186.9	170.6	182.9
Sr	424.7	486.7	492.1	442.7	439.6	432.5	421.0	413.1	407.3
Y	32.2	27.5	26.9	20.9	22.1	23.4	22.4	25.2	35.0
Zr	146.4	149.0	146.8	149.7	154.6	158.0	148.3	150.0	131.1
Nb	14.2	14.6	14.8	11.8	12.5	15.4	12.7	15.6	15.2
Ba	970.3	1223.0	1184.0	1067.5	939.9	931.6	865.4	870.7	1059.1
La	47.7	50.8	44.4	36.1	30.2	34.1	35.1	32.1	39.4
Ce	83.2	74.6	77.3	66.0	59.4	63.4	58.4	69.3	69.5
Nd	23.7	33.0	33.3	23.3	23.6	24.7	22.5	25.7	30.7
Pb	45.2	40.9	54.7	36.1	37.4	43.4	40.4	42.8	47.9
Th	21.0	19.1	11.0	18.9	27.2	24.7	21.9	20.2	23.4
U	5.8			4.6	5.4	3.9	4.5	5.5	6.9
cipw									
%AN	39	40	40	40	39	38	39	39	41
Q	14	13	14	15	15	15	16	16	15
or	26	29	27	28	29	26	27	26	28
ab	26	25	26	25	25	26	25	26	25
an	17	17	17	17	16	16	16	17	18
ne									
C									
di	5	5	5	4	4	5	5	5	4
hy	9	9	9	8	9	9	8	9	9
wo									
ol									
mt	1	1	1	1	1	1	1	1	1
il	1	1	1	1	1	1	1	1	1
ap									

APPENDIX C (III)

XRF analyses of the samples from the Central Anatolian Massif.

Pluton	*Behrekdag*	*Behrekdag*	*Behrekdag*	*Behrekdag*	*Behrekdag*	*Behrekdag*	*Behrekdag*	*Cefalikdag*	*Cefalikdag*
Sample no	**N7**	**N161**	**N183**	**N163**	**N185**	**N9**	**N166**	**N225**	**N226**
Rock type	*qmz*	*gr*	*gr*	*gr*	*gr*	*qmz*	*gr*	*mzdi*	*mzdi*
Geochemical description	*qmz*	*qmz*	*qmz*	*qmz*	*qmz*	*qmz*	*qmz*	*mzgb*	*mzdi*
SiO_2	64.78	64.83	65.06	65.43	65.48	65.52	65.66	50.45	51.33
TiO_2	0.38	0.36	0.38	0.41	0.41	0.33	0.38	1.08	0.99
Al_2O_3	16.08	16.02	15.71	15.54	15.75	15.76	15.82	18.04	18.10
Fe_2O_3	4.40	4.25	4.27	4.26	4.63	4.20	3.96	9.71	9.22
MnO	0.10	0.08	0.10	0.09	0.11	0.09	0.08	0.18	0.17
MgO	1.50	1.41	1.55	1.46	1.76	1.42	1.37	5.09	4.40
CaO	4.50	4.32	4.36	4.24	4.56	3.96	3.95	9.34	8.96
Na_2O	3.10	3.04	2.97	2.95	2.95	2.90	2.85	2.90	3.07
K_2O	4.51	4.66	4.60	4.63	4.55	4.96	5.12	2.80	2.82
P_2O_5	0.12	0.10	0.10	0.10	0.12	0.12	0.11	0.29	0.31
L.O.I	0.50	0.98	0.59	0.77	0.75	0.37	0.95	0.49	0.85
TOTAL (L.O.I. free)	99.47	99.08	99.10	99.11	100.31	99.27	99.30	99.88	99.36
Sc	11.3	11.7	6.8	10.5	6.8	8.9	8.7	25.4	24.1
V	64.0	74.8	70.3	81.6	76.9	66.5	72.8	177.1	152.7
Cr	10.6	14.3	9.1	12.8	10.3	11.0	12.1	64.7	57.7
Co	8.1	9.7	5.8	7.5	12.5	9.2	7.0	25.5	21.9
Ni	8.1	8.0	5.9	6.7	5.9	8.3	6.1	6.2	7.7
Cu	9.9	9.8	9.8	11.9	10.6	15.2	7.7	36.0	36.8
Zn	50.1	53.7	49.6	51.4	62.2	50.4	45.9	133.8	129.0
Ga	12.8	15.9	16.2	16.1	18.0	18.0	15.6	22.3	25.7
Rb	190.5	179.8	193.2	189.1	174.3	181.2	197.8	124.5	106.9
Sr	451.1	445.5	381.3	415.5	388.3	444.4	435.2	845.2	886.7
Y	18.6	18.2	30.3	18.4	34.1	18.7	16.5	32.5	30.0
Zr	124.3	150.3	127.3	140.6	141.3	132.1	137.8	216.0	250.1
Nb	7.2	12.7	13.9	14.2	14.9	8.7	12.5	13.4	12.9
Ba	1014.9	1034.6	791.1	800.9	899.2	901.8	1164.0	1134.5	1098.0
La	23.2	27.1	36.2	29.5	38.2	29.2	26.5	36.9	41.1
Ce	50.4	52.6	59.0	58.7	64.5	56.0	49.7	81.0	88.3
Nd	14.3	18.4	21.0	21.8	25.3	18.4	16.4	41.0	47.6
Pb	44.9	36.8	38.8	41.8	51.4	52.6	44.8	34.3	31.9
Th	20.3	22.4	22.8	37.2	24.2	29.5	26.5	8.2	6.3
U		4.1	4.9	5.4	6.1		2.9		3.0
cipw									
%AN	39	39	39	38	39	38	39	57	52
Q	16	16	17	18	17	17	17		
or	27	28	27	27	27	29	30	17	17
ab	26	26	25	25	25	25	24	21	25
an	17	16	16	15	16	15	15	28	27
ne								2	
C									
di	4	4	4	4	5	3	3	14	13
hy	8	8	8	8	9	8	8		
wo									
ol								15	13
mt	1	1	1	1	1	1	1	1	1
il	1	1	1	1	1	1	1	2	2
ap								1	1

APPENDIX C (III)

XRF analyses of the samples from the Central Anatolian Massif.

Pluton	*Cefalikdag*	*Cefalikdag*	*Cefalikdag*	*Cefalikdag*	*Cefalikdag*	*Cefalikdag*	*Cefalikdag*	*Cefalikdag*	*Cefalikdag*
Sample no	**N233**	**N224**	**N80**	**N235**	**N232**	**N231**	**N81**	**N78**	**N237**
Rock type	*mzdi*	*mzdi*	*mzdi*	*mzdi*	*mzdi*	*mzdi*	*mzdi*	*mzdi*	*mzdi*
Geochemical description	*mzdi*	*mzdi*	*mzdi*	*mzdi*	*mzdi*	*mzdi*	*mzdi*	*mzdi*	*mzdi*
SiO_2	51.36	51.67	52.28	52.44	52.51	52.62	52.81	53.86	54.80
TiO_2	0.93	0.96	0.90	0.93	0.95	0.94	0.88	0.85	0.84
Al_2O_3	18.08	18.39	18.41	18.15	17.60	18.18	17.91	17.70	18.13
Fe_2O_3	9.08	8.84	8.84	8.74	8.99	8.76	8.87	8.22	7.70
MnO	0.17	0.16	0.16	0.16	0.17	0.16	0.16	0.15	0.15
MgO	4.15	4.18	3.98	4.23	4.17	4.15	4.00	3.74	3.59
CaO	8.94	8.57	8.71	8.71	8.28	8.26	8.28	8.22	7.77
Na_2O	3.10	3.02	3.15	2.98	2.97	3.05	2.99	2.99	3.02
K_2O	2.56	2.88	2.83	2.77	3.02	3.06	2.98	3.23	3.40
P_2O_5	0.30	0.30	0.28	0.30	0.29	0.27	0.28	0.27	0.27
L.O.I	0.66	0.76	0.84	0.86	0.82	0.75	0.80	0.78	1.05
TOTAL (L.O.I. free)	98.67	98.97	99.54	99.41	98.94	99.44	99.16	99.24	99.66
Sc	24.0	17.8	20.7	19.6	17.6	16.0	20.4	22.5	13.3
V	148.4	150.6	153.5	148.0	156.9	148.2	151.8	143.7	126.6
Cr	62.5	48.3	36.9	49.3	48.4	49.4	42.1	35.2	43.6
Co	20.4	24.7	24.4	28.8	26.8	24.4	23.9	24.1	19.1
Ni	6.8	16.1	15.6	14.6	15.1	15.1	17.3	15.8	14.0
Cu	37.0	30.2	25.8	29.6	29.1	29.6	27.6	24.3	27.7
Zn	119.2	102.8	101.4	104.3	110.6	105.7	103.5	95.1	95.2
Ga	25.4	24.2	25.2	24.2	20.5	22.3	22.8	22.6	22.6
Rb	92.2	107.1	85.0	100.5	100.2	94.2	82.1	87.3	91.9
Sr	895.8	845.3	953.0	817.6	770.1	787.6	850.2	902.7	756.8
Y	31.8	27.6	23.7	27.6	29.7	27.7	26.7	25.7	28.6
Zr	218.0	204.5	170.1	207.6	266.4	212.0	226.1	186.9	217.1
Nb	14.3	14.6	17.7	13.6	15.7	14.9	19.6	18.2	16.4
Ba	981.6	1276.8	1359.8	1171.0	1327.7	1276.3	1382.1	1434.6	1350.2
La	42.3	36.5	43.7	43.2	51.0	49.5	54.4	40.5	48.8
Ce	89.2	75.1	74.2	81.7	86.3	94.8	73.6	73.9	96.9
Nd	41.3	29.9	35.7	36.4	37.0	32.6	37.2	28.5	39.0
Pb	33.1	32.4	31.2	32.5	39.8	35.2	33.8	32.6	41.5
Th	5.7	4.9	1.3	6.6	6.6	6.8	8.5	4.0	10.4
U	1.7	2.8		1.7	0.8	1.8			2.3
cipw									
%AN	52	52	51	53	51	51	51	50	50
Q									
or	15	17	17	16	18	18	18	19	20
ab	26	26	27	25	25	26	25	25	26
an	28	28	28	28	26	27	27	25	26
ne									
C									
di	12	10	11	11	11	10	11	11	9
hy	3	4	3	8	8	6	10	13	15
wo									
ol	11	11	10	7	7	8	6	2	
mt	1	1	1	1	1	1	1	1	1
il	2	2	2	2	2	2	2	2	2
ap	1	1	1	1	1	1	1	1	1

APPENDIX C (III)

XRF analyses of the samples from the Central Anatolian Massif.

Pluton	*Cefalikdag*	*Cefalikdag*	*Cefalikdag*	*Cefalikdag*	*Cefalikdag*	*Cefalikdag*	*Cefalikdag*	*Cefalikdag*	*Cefalikdag*
Sample no	**N236**	**N316**	**N85**	**N83**	**N319**	**N82**	**N84**	**N318**	**N327**
Rock type	*mzdi*	*qmzdi*	*qmzdi*	*qmzdi*	*qmzdi*	*qmz*	*qmzd*	*qmzd*	*qmzd*
Geochemical description	*mzdi*	*mz*	*mz*	*mz*	*mz*	*mz*	*mz*	*mz*	*mz*
SiO_2	55.16	57.98	58.17	59.10	59.50	59.53	59.71	59.76	60.46
TiO_2	0.84	0.80	0.67	0.61	0.60	0.61	0.61	0.60	0.60
Al_2O_3	17.59	17.61	17.94	17.69	17.49	17.94	17.80	17.54	17.14
Fe_2O_3	7.82	7.07	6.27	5.77	6.03	5.51	5.64	6.05	5.72
MnO	0.15	0.14	0.13	0.12	0.13	0.11	0.11	0.14	0.12
MgO	3.63	3.38	2.80	2.43	2.35	2.44	2.44	2.36	2.37
CaO	7.29	6.82	6.30	5.68	4.73	5.96	6.04	4.92	5.72
Na_2O	2.74	3.08	3.31	3.20	3.28	3.26	3.23	3.36	3.25
K_2O	4.25	3.25	3.62	4.22	4.57	4.06	4.09	4.36	3.61
P_2O_5	0.26	0.22	0.20	0.20	0.22	0.18	0.20	0.22	0.19
L.O.I	0.55	0.72	0.90	0.75	1.17	0.77	0.66	1.00	0.73
TOTAL (L.O.I. free)	99.73	100.35	99.41	99.02	98.89	99.60	99.87	99.31	99.18
Sc	15.9	14.3	15.1	11.6	11.7	8.3	15.4	11.4	7.0
V	131.7	119.3	102.7	93.7	101.5	88.0	84.4	99.1	88.8
Cr	54.3	40.1	24.7	22.1	4.5	24.0	34.7	9.5	23.1
Co	14.2	17.0	15.0	16.0	10.2	12.8	10.9	11.2	10.6
Ni	10.1	2.9	7.9	8.3	5.0	7.0		5.5	8.5
Cu	29.1	2.5	4.9	5.1	17.1	8.9	16.7	18.8	7.5
Zn	96.4	98.4	93.5	85.5	100.7	82.5	81.8	101.7	77.1
Ga	23.9	26.5	18.8	21.4	19.5	19.4	20.6	21.6	15.3
Rb	138.2	122.9	118.9	128.0	175.1	120.8	126.7	172.8	109.9
Sr	890.5	596.5	632.1	657.4	493.3	604.3	635.2	490.5	547.0
Y	29.2	32.0	29.0	25.7	32.2	29.0	28.4	32.2	34.1
Zr	198.5	182.2	191.1	174.5	206.9	163.8	186.4	205.1	170.4
Nb	12.8	16.3	16.7	14.4	15.8	12.7	10.9	16.2	14.9
Ba	2013.0	916.7	1094.9	1460.5	939.3	1204.9	1199.3	848.6	891.6
La	42.1	53.4	66.3	42.3	57.1	40.3	41.7	54.3	48.5
Ce	80.3	95.3	97.2	82.6	98.2	78.6	85.7	105.3	89.4
Nd	43.4	31.4	41.8	35.3	39.1	33.4	38.8	37.7	30.9
Pb	38.3	33.3	32.6	35.2	43.5	41.2	37.6	41.0	37.9
Th	13.1	14.6	15.5	9.0	21.7	12.7	12.2	18.8	14.1
U	1.4	3.1			4.2	4.1	1.9	5.4	5.5
cipw									
%AN	50	49	46	44	41	45	45	41	44
Q		6	5	7	6	7	7	7	10
or	25	19	21	25	27	24	24	26	21
ab	23	26	28	27	28	28	27	28	28
an	23	25	23	21	20	22	22	20	22
ne									
C									
di	9	6	5	5	2	5	6	3	5
hy	16	15	13	12	14	11	11	13	12
wo									
ol									
mt	1	1	1	1	1	1	1	1	1
il	2	2	1	1	1	1	1	1	1
ap	1	1			1			1	

APPENDIX C (III)

XRF analyses of the samples from the Central Anatolian Massif.

Pluton	*Cefalikdag*	*Cefalikdag*	*Cefalikdag*	*Cefalikdag*	*Cefalikdag*	*Cefalikdag*	*Cefalikdag*	*Cefalikdag*	*Cefalikdag*
Sample no	**N317**	**N324**	**N322**	**N20**	**N325**	**N323**	**N310**	**N321**	**N394**
Rock type	*qmz*	*qmz*	*qmz*	*qmz*	*qmz*	*qmz*	*qmz*	*qmz*	*gr*
Geochemical description	*mz*	*mz*	*mz*	*mz*	*mz*	*mz*	*qmz*	*qmz*	*qmz*
SiO_2	61.02	61.64	61.75	61.82	61.96	62.20	63.27	63.27	66.39
TiO_2	0.51	0.57	0.56	0.61	0.54	0.52	0.52	0.50	0.36
Al_2O_3	17.71	16.88	16.77	16.36	16.95	17.12	16.87	16.69	16.27
Fe_2O_3	5.34	5.14	5.17	5.77	5.01	4.73	4.94	4.59	3.53
MnO	0.13	0.10	0.10	0.12	0.11	0.10	0.12	0.09	0.08
MgO	1.75	2.21	2.24	2.52	2.14	1.92	2.06	1.94	1.00
CaO	4.46	5.24	5.07	5.14	5.23	4.88	4.42	4.58	2.96
Na_2O	3.40	3.15	3.04	2.99	3.15	3.24	3.61	3.01	3.40
K_2O	4.93	4.32	4.50	4.19	4.10	4.32	3.58	4.65	4.99
P_2O_5	0.20	0.17	0.16	0.19	0.16	0.15	0.15	0.16	0.14
L.O.I	0.89	0.62	0.67	0.51	0.63	0.74	1.06	0.68	0.99
TOTAL (L.O.I. free)	99.44	99.42	99.36	99.71	99.34	99.18	99.54	99.48	99.12
Sc	11.1	11.7	10.8	13.4	7.0	10.1	9.1	6.7	6.3
V	79.7	81.9	82.1	93.2	84.7	80.1	88.0	71.7	24.0
Cr	4.6	24.0	20.3	22.0	18.8	21.1	20.8	17.2	
Co	8.0	9.6	11.6	14.2	11.5	10.2	10.4	7.7	3.8
Ni	6.0	8.5	9.1	8.7	5.5	6.1	4.1	10.1	2.3
Cu	11.8	20.7	21.8	1.5	5.1	10.5	4.5	12.6	7.8
Zn	90.3	68.7	70.2	80.5	71.5	72.7	82.1	63.1	70.9
Ga	21.8	19.0	19.3	20.2	17.9	21.7	19.8	18.2	19.9
Rb	185.4	138.5	142.6	141.7	136.9	145.0	144.1	148.4	166.4
Sr	511.0	556.9	538.2	509.6	512.0	539.9	475.9	496.5	433.8
Y	32.1	30.7	32.4	30.2	31.6	22.0	22.7	29.8	12.5
Zr	211.4	157.2	149.7	176.1	151.4	158.1	161.2	149.8	238.9
Nb	15.8	12.8	13.5	16.2	14.9	13.2	15.5	12.7	14.5
Ba	985.7	1195.4	1297.3	961.4	868.0	1044.2	1091.3	1115.7	874.0
La	39.0	42.3	42.3	55.0	41.5	36.9	40.5	45.7	47.5
Ce	69.5	88.0	82.9	91.9	81.1	75.4	82.2	85.4	85.1
Nd	30.2	30.5	27.7	39.1	29.8	31.5	35.7	29.6	30.3
Pb	44.4	43.1	40.2	43.9	46.5	46.4	30.9	48.7	33.9
Th	17.7	17.1	13.9	19.8	20.9	20.7	23.1	23.1	23.8
U	6.8	4.5	3.8		4.9	3.7	3.6	5.1	2.2
cipw									
%AN	39	42	42	43	43	41	39	42	32
Q	8	11	11	12	12	12	14	13	18
or	29	26	27	25	24	26	21	27	29
ab	29	27	26	25	27	27	31	25	29
an	19	19	19	19	20	19	19	18	14
ne									
C									
di	2	5	4	5	4	3	1	3	
hy	11	10	11	12	10	10	12	10	8
wo									
ol									
mt	1	1	1	1	1	1	1	1	1
il	1	1	1	1	1	1	1	1	1
ap									1

APPENDIX C (III)

XRF analyses of the samples from the Central Anatolian Massif.

Pluton	*Cefalikdag*	*Cefalikdag*	*Celebi*	*Celebi*	*Celebi*	*Celebi*	*Celebi*	*Celebi*	*Celebi*
Sample no	**N395**	**N404**	**N339**	**N116**	**N344**	**N23**	**N338**	**N115**	**N343**
Rock type	*gr*	*gr*	*qmz*	*qmz*	*qmz*	*qmz*	*qmz*	*qmz*	*qmz*
Geochemical description	*gr*	*gr*	*mz*	*mz*	*mz*	*mz*	*mz*	*qmz*	*qmz*
SiO_2	71.53	71.95	61.45	62.14	62.44	62.70	62.74	63.08	63.19
TiO_2	0.20	0.18	0.60	0.47	0.54	0.51	0.53	0.47	0.46
Al_2O_3	14.37	13.87	17.09	15.85	16.70	16.52	16.14	15.53	16.49
Fe_2O_3	1.98	1.99	5.69	5.30	5.20	5.37	5.17	5.45	4.49
MnO	0.05	0.08	0.12	0.12	0.11	0.11	0.10	0.12	0.09
MgO	0.61	0.73	2.42	2.57	2.12	1.95	1.91	2.54	1.73
CaO	1.97	1.79	5.72	5.14	5.05	4.92	4.81	5.04	4.21
Na_2O	2.82	3.48	3.24	2.91	3.02	2.99	2.87	2.99	2.88
K_2O	5.37	4.82	3.62	4.09	4.20	4.33	4.27	3.93	5.36
P_2O_5	0.06	0.05	0.18	0.16	0.16	0.15	0.16	0.17	0.13
L.O.I	0.79	0.80	0.87	0.88	1.42	0.33	0.60	0.70	0.49
TOTAL (L.O.I. free)	98.96	98.94	100.12	98.75	99.53	99.55	98.70	99.31	99.03
Sc	3.9	5.3	7.6	12.3	9.0	10.3	10.1	13.0	12.5
V	12.1	22.5	58.4	110.7	75.4	78.3	73.7	111.9	59.5
Cr			21.0	50.0	24.5	19.3	33.7	48.8	30.9
Co	1.9	3.7	10.3	12.7	12.3	13.0	12.9	12.6	8.0
Ni	1.6	1.6	9.3	18.6	8.9	8.2	2.7	16.5	0.9
Cu		5.8	4.0	14.5	5.6	11.2	12.9	12.6	13.8
Zn	37.7	40.6	56.8	69.9	68.1	73.4	74.1	71.9	68.6
Ga	15.2	17.1	16.1	18.7	20.4	17.6	16.7	17.4	11.1
Rb	171.0	221.1	160.1	205.7	163.2	166.0	170.0	211.6	198.3
Sr	331.0	213.0	563.0	315.8	540.6	473.6	579.7	287.6	594.1
Y	1.9	15.3	29.4	23.8	32.4	27.3	28.4	26.8	29.2
Zr	126.9	113.2	130.3	148.4	171.1	160.9	190.9	145.1	163.7
Nb	9.5	18.8	15.2	13.5	17.2	15.1	16.3	15.9	14.3
Ba	686.2	416.8	803.7	873.5	781.0	853.6	767.0	757.5	1552.9
La	23.7	18.9	40.6	36.3	41.9	37.8	54.4	32.3	43.8
Ce	39.9	33.1	78.8	78.5	67.4	75.8	97.9	65.1	93.7
Nd	13.6	13.6	28.6	31.1	27.2	30.4	42.4	25.8	34.7
Pb	34.5	48.5	45.0	33.7	46.2	52.1	44.4	32.6	54.3
Th	16.2	18.2	22.3	22.0	28.9	12.4	26.2	20.5	27.9
U	3.1	2.7	2.6	2.7	7.8		4.8	3.5	5.9
cipw									
%AN	28	21	44	42	43	43	43	41	40
Q	28	27	11	13	13	13	15	14	13
or	32	28	21	24	25	26	25	23	32
ab	24	29	27	25	26	25	24	25	24
an	9	8	21	18	20	19	19	17	16
ne									
C									
di			5	5	4	4	4	5	3
hy	4	5	12	12	11	11	10	12	9
wo									
ol									
mt			1	1	1	1	1	1	1
il			1	1	1	1	1	1	1
ap									

APPENDIX C (III)

XRF analyses of the samples from the Central Anatolian Massif.

Pluton	*Celebi*	*Celebi*	*Celebi*	*Celebi*	*Celebi*	*Celebi*	*Celebi*	*Celebi*	*Celebi*
Sample no	**N25**	**N349**	**N345**	**N76**	**N66**	**N24**	**N71**	**N342**	**N112**
Rock type	*qmz*	*qmz*	*qmz*	*qmz*	*qmz*	*qmz*	*qmz*	*qmz*	*qmz*
Geochemical description	*qmz*	*qmz*	*qmz*	*qmz*	*qmz*	*qmz*	*qmz*	*qmz*	*qmz*
SiO_2	63.32	63.44	63.58	63.67	63.70	63.71	63.72	63.91	64.05
TiO_2	0.47	0.52	0.47	0.43	0.52	0.47	0.42	0.47	0.44
Al_2O_3	16.03	15.60	16.77	16.15	15.73	16.32	16.04	14.99	15.33
Fe_2O_3	4.98	5.12	4.60	4.77	5.15	4.79	4.65	4.93	4.87
MnO	0.11	0.11	0.09	0.10	0.10	0.10	0.10	0.11	0.10
MgO	1.88	2.00	1.82	1.46	2.02	1.85	1.60	2.05	2.28
CaO	4.77	4.62	4.93	4.51	4.81	5.01	4.51	4.28	4.60
Na_2O	2.96	2.89	3.08	3.08	2.92	3.01	3.31	2.60	2.91
K_2O	4.37	4.56	4.24	4.67	3.96	3.91	4.54	5.45	4.51
P_2O_5	0.14	0.15	0.14	0.13	0.16	0.14	0.14	0.15	0.17
L.O.I	0.29	0.56	0.63	1.05	0.69	0.39	0.49	0.44	0.82
TOTAL (L.O.I. free)	99.03	99.00	99.71	98.96	99.07	99.31	99.02	98.94	99.26
Sc	9.8	9.5	8.1	6.6	8.9	12.0	10.5	7.5	12.4
V	73.1	74.4	69.8	78.2	70.9	79.0	73.5	71.5	96.1
Cr	19.4	33.9	36.4	82.7	25.5	16.5	16.3	39.9	42.3
Co	11.6	8.5	6.9	9.0	14.4	12.5	10.1	7.7	11.0
Ni	8.1	5.7	2.0	7.3	10.8	9.2	8.4	1.8	18.1
Cu	8.4	17.3	9.0	4.4		7.8	15.7	10.3	22.2
Zn	70.5	74.1	71.7	53.3	65.2	61.6	53.8	72.7	62.8
Ga	17.6	16.6	8.9	17.4	17.2	19.9	14.0	19.4	19.0
Rb	175.9	181.1	154.0	175.4	152.6	149.2	179.1	185.8	214.5
Sr	433.4	521.5	566.1	440.3	545.7	470.5	433.1	572.3	280.1
Y	31.7	31.3	28.7	35.4	26.9	27.3	27.0	30.2	21.7
Zr	155.2	174.5	181.6	171.1	175.1	154.7	148.3	184.0	150.6
Nb	16.9	17.6	15.9	17.0	15.4	13.5	13.6	14.1	15.8
Ba	781.0	703.7	711.9	929.9	739.6	803.6	975.5	1958.8	724.5
La	43.8	30.5	42.0	50.5	48.0	38.0	43.3	43.1	32.0
Ce	77.5	69.8	79.8	88.4	87.1	65.8	74.9	87.4	67.6
Nd	31.6	30.7	37.8	32.5	35.9	29.6	30.0	33.3	25.6
Pb	48.8	43.2	42.5	47.5	46.0	40.7	43.5	49.1	33.8
Th	22.7	21.4	22.7	36.1	28.2	23.7	20.4	30.4	18.4
U		6.1	3.8	5.8				4.9	3.7
cipw									
%AN	41	40	43	39	42	43	36	37	39
Q	15	15	14	14	16	16	14	14	15
or	26	27	25	28	23	23	27	32	27
ab	25	24	26	26	25	25	28	22	25
an	18	16	19	16	18	19	16	13	15
ne									
C									
di	4	5	3	4	4	4	5	6	5
hy	10	10	9	8	10	10	8	9	10
wo									
ol									
mt	1	1	1	1	1	1	1	1	1
il	1	1	1	1	1	1	1	1	1
ap									

APPENDIX C (III)

XRF analyses of the samples from the Central Anatolian Massif.

Pluton	*Celebi*	*Celebi*	*Celebi*	*Celebi*	*Celebi*	*Celebi*	*Celebi*	*Celebi*	*Celebi*
Sample no	**N65**	**N340**	**N68**	**N341**	**N64**	**N77**	**N72**	**N201**	**N218**
Rock type	*qmz*	*qmz*	*qmz*	*qmz*	*qmz*	*qmz*	*qmz*	*qmz*	*qmz*
Geochemical description	*qmz*	*qmz*	*qmz*	*qmz*	*qmz*	*qmz*	*qmz*	*qmz*	*qmz*
SiO_2	64.06	64.17	64.26	64.26	64.27	64.40	64.47	64.53	64.85
TiO_2	0.52	0.48	0.51	0.52	0.50	0.37	0.41	0.38	0.44
Al_2O_3	15.90	15.81	15.63	15.41	16.17	16.39	16.17	16.11	15.91
Fe_2O_3	5.12	4.62	4.94	5.19	4.93	4.13	4.59	4.13	4.16
MnO	0.10	0.09	0.10	0.10	0.10	0.09	0.10	0.09	0.09
MgO	2.10	1.89	2.13	1.96	1.90	1.37	1.52	1.27	1.66
CaO	4.80	4.25	4.56	4.42	4.59	4.13	4.59	4.35	4.18
Na_2O	2.91	2.65	2.99	2.61	2.95	3.14	3.13	3.23	3.07
K_2O	4.33	5.11	4.33	4.71	4.60	5.11	4.47	4.67	4.13
P_2O_5	0.15	0.15	0.15	0.15	0.16	0.12	0.12	0.13	0.13
L.O.I	0.82	0.55	1.11	0.56	0.53	0.63	0.52	0.43	0.61
TOTAL (L.O.I. free)	99.99	99.22	99.60	99.34	100.17	99.25	99.56	98.89	98.62
Sc	6.1	11.1	7.7	11.7	10.8	8.5	6.1	9.6	9.9
V	71.0	64.3	69.1	67.6	68.2	63.3	70.2	64.9	77.8
Cr	22.4	35.0	26.7	32.0	20.1	9.4	14.8	16.3	30.5
Co	14.3	8.3	11.2	10.2	13.3	9.6	9.9	7.3	9.6
Ni	9.3	3.7	9.8	2.4	10.2	7.4	7.6	1.9	7.0
Cu	16.4	13.8	16.6	17.5	7.0	3.1	8.6	13.1	10.0
Zn	64.2	66.3	67.7	68.2	64.5	54.3	49.9	68.6	63.7
Ga	16.0	19.8	17.1	15.3	17.9	16.7	15.7	13.5	16.9
Rb	163.7	180.2	177.8	184.1	183.4	192.6	189.8	189.0	213.0
Sr	529.6	639.1	534.3	516.2	537.4	490.6	430.1	468.6	308.6
Y	32.1	28.2	32.1	27.7	29.8	26.2	30.8	25.7	18.7
Zr	169.8	171.7	167.1	189.9	166.3	133.8	142.5	138.9	168.8
Nb	17.1	13.2	17.6	15.3	16.4	13.7	14.4	15.6	13.4
Ba	839.2	1670.3	804.9	869.9	893.6	1042.0	930.3	830.3	976.7
La	50.8	57.7	43.9	56.2	48.9	46.3	41.4	48.9	29.4
Ce	88.9	99.6	75.7	102.0	103.5	76.2	69.7	81.9	63.0
Nd	30.8	40.9	28.5	39.5	36.0	28.3	22.8	31.4	21.3
Pb	45.1	48.1	44.4	46.9	57.1	50.3	40.1	43.8	30.0
Th	27.0	26.9	26.2	32.8	22.6	32.6	14.1	37.6	23.0
U	4.2	4.7	6.7	5.7			4.1	4.0	4.4
cipw									
%AN	42	42	39	43	41	37	39	36	40
Q	15	16	16	17	15	14	15	15	18
or	26	30	26	28	27	30	26	28	24
ab	25	22	25	22	25	27	26	27	26
an	18	16	16	16	17	16	17	16	17
ne									
C									
di	4	3	4	4	4	4	4	4	2
hy	10	10	10	10	10	8	8	7	9
wo									
ol									
mt	1	1	1	1	1	1	1	1	1
il	1	1	1	1	1	1	1	1	1
ap									

APPENDIX C (III)

XRF analyses of the samples from the Central Anatolian Massif.

Pluton	Celebi	Celebi	Celebi	Celebi	Celebi	Celebi	Celebi	Celebi	Celebi
Sample no	N215	N66a	N111	N75	N74	N202	N67	N203	N208
Rock type	qmz	qmz	gr	gr	gr	gr	gr	gr	gr
Geochemical description	qmz	qmz	grd	qmz	qmz	qmz	qmz	qmz	qmz
SiO_2	64.88	64.91	65.06	65.07	65.20	65.22	65.28	65.43	65.51
TiO_2	0.42	0.43	0.43	0.39	0.38	0.37	0.48	0.38	0.35
Al_2O_3	15.88	15.97	15.22	15.81	16.20	16.58	14.87	16.00	16.39
Fe_2O_3	4.61	4.16	4.65	4.34	4.41	4.02	5.08	4.19	3.85
MnO	0.10	0.08	0.09	0.09	0.10	0.09	0.11	0.10	0.09
MgO	1.61	1.60	2.19	1.46	1.53	1.26	2.04	1.29	1.19
CaO	4.63	4.25	4.61	4.33	4.51	4.13	4.29	4.12	4.04
Na_2O	3.03	2.91	2.55	3.13	3.02	3.18	2.58	3.15	3.29
K_2O	4.41	4.82	4.33	4.54	4.53	5.18	5.06	4.68	4.90
P_2O_5	0.13	0.13	0.15	0.14	0.13	0.13	0.15	0.12	0.12
L.O.I	0.41	0.97	1.20	0.54	0.74	0.76	0.47	0.52	0.60
TOTAL (L.O.I. free)	99.70	99.26	99.28	99.30	100.01	100.16	99.93	99.46	99.72
Sc	9.3	8.1	12.5	8.6	12.7	9.4	9.3	6.1	9.6
V	71.1	60.0	94.1	63.4	63.8	61.2	69.9	68.9	60.1
Cr	25.2	19.8	45.8	7.2	11.0		24.7	15.4	13.4
Co	6.2	8.9	11.0	10.3	10.6	10.9	11.4	7.4	7.1
Ni	0.6	5.1	12.7	8.5	10.2	8.2	8.0	0.1	2.5
Cu	14.3	3.7	4.1	1.3	2.2	5.6	7.8	12.8	13.7
Zn	64.2	49.3	53.2	54.7	56.4	64.3	60.4	62.1	55.3
Ga	13.4	17.5	14.4	18.7	16.0	17.8	17.0	16.9	13.9
Rb	186.7	182.0	173.9	184.8	191.8	186.7	173.9	196.9	194.3
Sr	445.5	569.6	280.9	456.4	454.8	461.0	506.8	426.5	453.7
Y	24.1	20.2	28.7	28.4	23.5	31.8	27.7	25.2	22.7
Zr	146.2	151.0	137.3	144.7	134.4	123.9	173.0	138.5	129.9
Nb	13.6	14.7	13.5	14.0	13.1	13.4	16.1	15.4	15.0
Ba	771.0	1228.5	703.8	787.6	930.1	1103.0	1281.5	699.5	825.9
La	34.7	35.7	33.6	44.3	34.8	40.1	56.2	54.7	47.3
Ce	62.4	69.2	55.8	73.0	49.3	61.0	92.6	99.4	77.4
Nd	24.2	26.9	25.1	27.0	19.3	23.0	37.7	37.2	24.4
Pb	38.9	51.6	28.2	47.4	43.8	57.0	52.2	46.4	39.6
Th	28.7	26.2	19.7	34.4	11.1	29.0	26.0	37.7	34.5
U	4.3	3.0	6.6			2.2		1.0	5.0
cipw									
%AN	39	40	44	37	40	37	39	37	36
Q	17	17	19	17	17	15	17	17	16
or	26	28	26	27	27	31	30	28	29
ab	26	25	22	26	26	27	22	27	28
an	17	16	17	16	17	16	14	16	15
ne									
C									
di	5	3	4	4	4	3	5	3	3
hy	8	8	10	8	8	7	10	8	7
wo									
ol									
mt	1	1	1	1	1	1	1	1	1
il	1	1	1	1	1	1	1	1	1
ap									

APPENDIX C (III)

XRF analyses of the samples from the Central Anatolian Massif.

Pluton	*Celebi*	*Celebi*	*Celebi*	*Celebi*	*Celebi*	*Celebi*	*Celebi*	*Celebi*	*Celebi*
Sample no	**N512**	**N73**	**N109**	**N210**	**N204**	**N209**	**N70**	**N110**	**N114**
Rock type	*gr*	*gr*	*gr*	*gr*	*gr*	*gr*	*gr*	*gr*	*gr*
Geochemical description	*grd*	*qmz*	*qmz*	*qmz*	*qmz*	*qmz*	*qmz*	*grd*	*qmz*
SiO_2	65.56	65.64	65.84	65.97	66.04	66.16	66.18	66.32	66.52
TiO_2	0.48	0.43	0.42	0.36	0.37	0.34	0.41	0.41	0.39
Al_2O_3	15.42	15.59	15.02	15.90	15.80	16.05	16.16	15.18	15.01
Fe_2O_3	4.59	4.49	4.20	4.00	3.88	3.68	4.31	4.21	4.14
MnO	0.09	0.08	0.08	0.10	0.08	0.08	0.10	0.08	0.09
MgO	1.81	1.45	2.26	1.22	1.21	1.13	1.52	2.08	1.88
CaO	4.49	4.06	4.66	4.07	4.08	3.86	4.48	4.31	3.99
Na_2O	2.81	2.99	2.67	3.20	3.13	3.14	3.08	2.64	2.59
K_2O	4.04	4.82	4.45	4.71	4.72	5.27	4.49	4.59	5.11
P_2O_5	0.14	0.11	0.15	0.14	0.10	0.11	0.13	0.13	0.14
L.O.I	0.67	0.62	1.34	0.65	0.72	0.36	0.27	0.92	0.96
TOTAL (L.O.I. free)	99.43	99.67	99.75	99.67	99.41	99.82	100.85	99.96	99.86
Sc	7.9	8.0	8.1	9.2	3.5	7.5	9.3	9.6	8.7
V	67.7	80.1	89.4	63.2	60.4	54.7	68.5	90.7	78.1
Cr	28.2	11.6	45.0	16.4	3.2	17.3	11.5	39.7	36.6
Co	10.0	10.9	8.8	7.2	9.0	6.0	9.3	7.6	10.3
Ni	8.8	5.1	11.6	0.1	6.2		7.6	11.9	12.3
Cu	12.2	7.5	3.5	10.1	5.7	6.7	5.9	2.0	6.9
Zn	60.9	45.1	48.4	55.3	50.9	42.6	52.2	46.7	58.1
Ga	15.8	17.4	15.0	12.1	17.4	2.8	18.1	17.6	15.9
Rb	155.9	179.5	170.5	195.9	186.8	209.9	190.2	191.4	212.5
Sr	539.7	389.5	276.5	436.7	412.0	455.1	445.5	268.3	257.8
Y	26.7	33.4	29.0	24.4	32.4	22.2	27.7	28.9	21.6
Zr	169.0	145.1	133.8	135.2	121.7	129.6	138.8	141.9	158.3
Nb	14.7	13.9	12.9	14.7	15.8	13.9	12.9	13.9	14.5
Ba	754.1	995.4	729.6	818.7	762.6	1158.4	863.7	708.6	710.6
La	93.9	33.4	28.5	44.4	45.0	39.5	43.9	31.7	22.5
Ce	135.3	64.2	54.5	69.5	81.6	69.0	72.2	60.4	53.6
Nd	46.1	24.6	22.4	23.6	26.5	25.7	31.5	17.4	22.8
Pb	45.5	37.5	25.3	41.4	47.2	46.0	44.1	30.7	36.5
Th	32.7	46.8	17.0	36.8	33.9	34.6	27.5	19.0	20.1
U		6.1	5.6	4.2	4.7	3.4		5.0	5.4
cipw									
%AN	42	37	41	36	36	35	39	45	39
Q	20	17	19	17	18	17	18	10	19
or	24	28	26	28	28	31	27	23	30
ab	24	25	23	27	26	27	26	25	22
an	18	15	16	15	15	14	17	20	14
ne									
C									
di	3	4	5	4	4	4	4	10	4
hy	9	8	9	7	7	6	8	10	9
wo									
ol									
mt	1	1	1	1	1	1	1	1	1
il	1	1	1	1	1	1	1	1	1
ap									

APPENDIX C (III)

XRF analyses of the samples from the Central Anatolian Massif.

Pluton	*Celebi*	*Celebi*	*Celebi*	*Celebi*	*Celebi*	*Celebi*	*Celebi*	*Celebi*	*Celebi*
Sample no	**N113**	**N205**	**N200**	**N211**	**N217**	**N206**	**N223**	**N213**	**N214**
Rock type	*gr*	*gr*	*gr*	*gr*	*gr*	*gr*	*gr*	*gr*	*gr*
Geochemical description	*qmz*	*qmz*	*qmz*	*qmz*	*grd*	*qmz*	*grd*	*grd*	*gr*
SiO_2	66.60	66.69	66.95	67.52	67.68	67.68	68.38	68.70	69.39
TiO_2	0.42	0.35	0.33	0.30	0.39	0.32	0.35	0.30	0.26
Al_2O_3	14.99	15.43	15.28	15.84	15.38	15.53	15.00	15.07	14.70
Fe_2O_3	4.14	3.90	3.62	3.21	3.13	3.23	3.20	3.17	2.74
MnO	0.08	0.09	0.08	0.07	0.06	0.07	0.08	0.07	0.06
MgO	1.83	1.18	1.05	0.93	1.40	1.05	1.24	1.03	0.86
CaO	3.74	3.99	3.65	3.68	3.79	3.31	3.05	3.30	2.81
Na_2O	2.61	3.23	3.00	3.21	3.06	3.01	2.91	3.10	2.83
K_2O	4.73	4.43	4.90	4.83	4.50	5.33	4.62	4.81	5.36
P_2O_5	0.11	0.11	0.10	0.11	0.11	0.10	0.10	0.09	0.07
L.O.I	0.65	0.42	0.30	0.38	0.71	0.92	0.63	0.45	0.90
TOTAL (L.O.I. free)	99.25	99.39	98.96	99.70	99.50	99.63	98.93	99.63	99.07
Sc	6.9	10.3	9.4	5.1	3.1	2.7	8.1	3.2	2.6
V	87.8	62.1	61.1	52.1	65.9	49.1	62.0	44.6	39.0
Cr	34.5	16.0	12.0	11.0	20.2		22.2	10.6	
Co	8.5	5.6	6.6	4.7	6.5	5.8	4.0	3.8	4.9
Ni	12.2			3.1	5.7	9.0	3.0	0.6	4.5
Cu	12.0	11.5	10.0	12.4	4.3	4.6	10.2	8.8	5.2
Zn	51.5	62.2	51.3	38.4	33.5	40.0	53.5	53.4	31.5
Ga	15.9	15.1	13.4	16.9	16.9	14.9	18.6	11.2	16.9
Rb	204.6	196.3	210.9	195.4	201.3	202.0	218.3	228.3	215.1
Sr	254.1	382.8	379.2	404.4	255.5	366.9	231.1	327.7	329.1
Y	21.2	24.5	23.7	18.9	29.5	31.8	19.7	21.1	23.9
Zr	151.9	139.3	141.6	115.4	151.0	131.4	144.5	132.8	89.7
Nb	15.1	16.2	15.9	14.7	14.5	14.8	15.7	17.2	11.8
Ba	702.7	480.8	680.5	594.7	825.0	977.6	789.4	576.1	807.6
La	31.9	40.2	45.0	37.2	33.4	46.9	35.8	38.4	34.3
Ce	67.7	77.0	80.8	62.2	57.4	77.7	63.0	66.9	59.0
Nd	27.3	25.0	26.7	20.4	20.7	22.4	23.1	22.3	13.8
Pb	34.5	37.6	41.8	42.2	24.7	42.8	33.1	42.7	42.3
Th	22.0	38.6	36.2	38.1	25.5	33.1	30.1	33.6	33.6
U	6.2	6.3	5.2	5.0	6.7	4.7	5.6	5.1	5.8
cipw									
%AN	41	35	35	35	37	34	37	33	33
Q	21	19	20	20	21	20	24	22	24
or	28	26	29	29	27	31	27	28	32
ab	22	27	25	27	26	25	25	26	24
an	15	15	14	15	15	13	14	13	12
ne									
C									
di	2	4	3	3	3	2		2	2
hy	9	7	6	6	7	6	8	6	5
wo									
ol									
mt	1	1	1			0			
il	1	1	1	1	1	1	1	1	
ap									

APPENDIX C (III)

XRF analyses of the samples from the Central Anatolian Massif.

Pluton	*Celebi*	*Celebi*	*Celebi*	*Baranadag*	*Baranadag*	*Baranadag*	*Baranadag*	*Baranadag*	*Baranadag*
Sample no	**N216**	**N219**	**N212**	**N13**	**N300**	**N27**	**N26**	**N304**	**N307**
Rock type	*gr*	*gr*	*gr*	*mz*	*mz*	*mz*	*mz*	*mz*	*mz*
Geochemical description	*gr*	*gr*	*gr*	*mz*	*mz*	*mz*	*mz*	*mz*	*mz*
SiO_2	69.74	70.91	72.95	55.78	58.20	58.33	58.44	58.52	58.62
TiO_2	0.31	0.28	0.22	0.77	0.68	0.56	0.59	0.56	0.58
Al_2O_3	14.57	14.18	13.87	17.45	16.94	17.63	17.62	17.47	17.78
Fe_2O_3	2.76	2.71	2.24	6.52	6.34	5.17	5.42	5.16	5.33
MnO	0.06	0.06	0.05	0.15	0.16	0.12	0.13	0.12	0.13
MgO	1.07	0.99	0.60	2.30	2.19	1.77	1.85	1.78	1.88
CaO	2.79	2.57	2.22	6.46	6.80	5.56	5.95	5.56	5.82
Na_2O	2.77	2.77	2.74	3.59	4.50	3.71	3.73	3.78	3.76
K_2O	4.90	5.12	5.20	5.69	3.32	5.58	5.52	5.81	5.68
P_2O_5	0.08	0.06	0.05	0.41	0.32	0.25	0.24	0.25	0.26
L.O.I	0.73	0.78	0.62	0.27	0.42	0.58	0.58	0.78	0.46
TOTAL (L.O.I. free)	99.05	99.65	100.14	99.11	99.45	98.69	99.48	99.00	99.84
Sc	6.2	6.3	1.0	12.8	8.2	11.2	11.8	10.4	6.1
V	54.4	40.2	25.6	122.8	117.1	91.5	102.0	103.6	93.7
Cr	7.4	15.6	3.9	4.6	12.1	8.5	5.1	11.3	6.5
Co	6.4	5.0	4.4	17.3	11.2	12.1	11.8	13.9	8.9
Ni	9.3	6.0	7.1	13.8	8.7	8.7	14.1	7.3	6.6
Cu	12.0	6.5	1.4	30.2	7.0	0.8		10.0	7.2
Zn	39.0	41.8	27.1	88.9	100.7	79.4	90.6	81.6	85.7
Ga	14.4	16.8	16.4	18.5	21.6	17.9	21.6	20.3	22.0
Rb	231.4	231.0	210.7	173.3	120.5	199.5	193.4	221.7	204.7
Sr	206.3	184.2	199.4	1088.5	522.0	930.2	911.0	919.5	817.1
Y	30.6	21.8	29.9	37.3	42.2	33.2	35.9	32.7	41.3
Zr	148.3	154.9	111.3	297.8	352.6	244.7	276.8	291.3	253.3
Nb	15.6	16.9	13.9	29.0	29.8	23.6	25.8	23.6	23.3
Ba	652.0	592.1	398.5	854.4	337.0	966.5	933.0	958.9	1033.7
La	38.5	39.6	34.9	78.4	90.4	68.5	79.1	53.9	74.7
Ce	67.1	75.3	63.9	153.4	154.1	101.1	139.0	126.4	126.1
Nd	23.5	25.9	20.7	60.8	54.7	42.3	54.2	45.1	34.0
Pb	41.5	43.4	47.8	38.8	39.8	38.9	39.7	45.8	42.2
Th	39.5	43.5	37.0	22.5	34.1	22.1	27.7	33.0	26.7
U	8.5	8.0	5.6		8.2			6.4	6.0
cipw									
%AN	35	32	31	36	30	32	32	30	32
Q	26	27	30		2	1			
or	29	30	31	34	20	33	33	34	34
ab	23	23	23	26	38	31	32	32	32
an	13	11	10	15	16	15	15	14	15
ne				2					
C									
di		1		12	13	9	11	10	10
hy	6	6	5		8	7	7	6	6
wo									
ol				7				1	1
mt				1	1	1	1	1	1
il	1	1		1	1	1	1	1	1
ap				1	1	1	1	1	1

APPENDIX C (III)

XRF analyses of the samples from the Central Anatolian Massif.

Pluton	*Baranadag*	*Baranadag*	*Baranadag*	*Baranadag*	*Baranadag*	*Baranadag*	*Baranadag*	*Baranadag*	*Baranadag*
Sample no	**N297**	**N28**	**N305**	**N29**	**N30**	**N140**	**N309**	**N306**	**N299**
Rock type	*mz*	*mz*	*mz*	*mz*	*mz*	*mz*	*mz*	*mz*	*mz*
Geochemical description	*mz*	*mz*	*mz*	*mz*	*mz*	*mz*	*mz*	*mz*	*mz*
SiO_2	58.64	59.11	59.27	59.28	59.29	59.29	59.32	59.44	59.76
TiO_2	0.55	0.53	0.49	0.53	0.51	0.57	0.51	0.56	0.49
Al_2O_3	17.63	17.73	17.98	17.68	17.63	17.53	17.42	17.69	17.85
Fe_2O_3	5.15	5.09	4.74	5.08	4.88	5.37	4.81	5.34	4.59
MnO	0.12	0.11	0.11	0.12	0.11	0.14	0.11	0.13	0.10
MgO	1.77	1.64	1.58	1.71	1.65	1.95	1.71	1.84	1.63
CaO	5.58	5.40	5.13	5.46	5.36	4.30	5.11	5.75	4.81
Na_2O	3.76	3.73	3.73	3.67	3.70	3.62	3.41	3.77	3.73
K_2O	5.79	5.76	6.13	5.84	5.87	6.54	6.79	5.70	6.02
P_2O_5	0.24	0.24	0.22	0.23	0.22	0.35	0.23	0.25	0.22
L.O.I	0.52	0.40	0.41	0.76	0.46	0.71	0.42	0.52	0.33
TOTAL (L.O.I. free)	99.23	99.35	99.38	99.61	99.23	99.66	99.42	100.46	99.20
Sc	7.6	10.0	7.2	7.0	4.0	8.9	6.3	8.3	7.1
V	88.5	86.1	77.5	90.9	82.8	92.8	77.4	88.6	73.4
Cr	9.2	5.3	0.4	8.2	4.0	9.6	2.7	9.3	7.9
Co	13.2	9.4	8.1	8.0	12.1	14.1	8.5	8.7	8.2
Ni	6.4	10.7	10.1	10.8	5.6	10.6	10.3	9.4	9.9
Cu	10.0		7.1	21.2	7.9	58.3	20.2	15.3	14.9
Zn	80.8	82.0	79.3	83.3	78.0	95.7	81.9	85.3	73.7
Ga	19.2	20.0	23.4	22.2	17.7	21.1	19.8	19.2	21.7
Rb	209.5	204.8	219.1	213.8	215.7	265.8	246.9	206.1	229.8
Sr	827.4	949.6	861.0	824.0	817.7	516.4	830.2	808.7	811.1
Y	38.6	32.4	34.6	37.1	37.5	32.7	38.4	39.2	34.9
Zr	237.7	226.0	237.2	260.4	235.1	296.8	228.4	227.8	213.9
Nb	22.4	22.3	19.8	23.0	21.3	22.4	21.0	21.6	19.8
Ba	1034.2	1044.4	1120.3	989.1	969.6	590.7	1142.5	991.3	989.1
La	67.2	64.0	51.9	64.1	59.1	70.5	54.3	63.8	54.8
Ce	129.1	108.4	86.1	126.4	110.7	133.5	106.3	108.3	99.8
Nd	36.0	44.2	32.8	46.3	34.5	47.2	36.1	36.7	32.6
Pb	42.9	42.8	43.9	44.1	43.7	60.5	43.7	41.3	43.1
Th	29.6	25.8	23.3	29.5	27.5	27.1	34.8	26.4	21.6
U	5.7		6.4	6.6	4.9	7.1	5.3	4.0	6.5
cipw									
%AN	31	32	31	32	31	29	30	31	31
Q		1		1	1			1	2
or	34	34	36	35	35	39	40	34	36
ab	32	32	32	31	31	31	29	32	32
an	14	15	14	15	14	12	12	15	14
ne									
C									
di	10	9	8	9	9	6	10	10	7
hy	6	7	7	7	6	10	6	7	7
wo									
ol									
mt	1	1	1	1	1	1	1	1	1
il	1	1	1	1	1	1	1	1	1
ap	1	1	1	1	1	1	1	1	1

APPENDIX C (III)

XRF analyses of the samples from the Central Anatolian Massif.

Pluton	Baranadag	Baranadag	Baranadag	Baranadag	Baranadag	Baranadag	Baranadag	Baranadag	Baranadag
Sample no	N301	N298	N19	N18	N303	N155	N15	N16	N152
Rock type	mz	mz	mz	qmz	qmz	qmz	qmz	qmz	qmz
Geochemical description	mz	sy	sy	sy	sy	sy	sy	sy	sy
SiO_2	59.98	60.51	60.93	61.33	61.85	61.93	62.07	62.62	62.67
TiO_2	0.53	0.49	0.51	0.51	0.39	0.46	0.42	0.44	0.42
Al_2O_3	17.25	17.60	17.39	17.35	18.26	17.35	17.43	17.77	17.63
Fe_2O_3	4.85	4.65	4.81	4.59	3.49	4.38	3.97	4.25	3.73
MnO	0.11	0.11	0.12	0.11	0.09	0.10	0.10	0.10	0.09
MgO	1.78	1.47	1.74	1.67	1.13	1.57	1.20	1.34	1.33
CaO	5.17	4.50	4.16	4.24	3.58	3.94	3.90	3.94	3.93
Na_2O	3.66	3.61	3.81	3.88	3.93	3.85	3.83	3.79	3.63
K_2O	5.77	5.85	5.37	5.33	6.68	5.33	5.66	5.39	5.48
P_2O_5	0.23	0.22	0.22	0.21	0.14	0.19	0.17	0.19	0.16
L.O.I	0.64	0.43	0.38	0.65	0.60	0.62	0.77	0.41	0.56
TOTAL (L.O.I. free)	99.32	99.01	99.06	99.22	99.54	99.10	98.75	99.83	99.07
Sc	4.8	5.0	9.0	9.6	6.3	8.2	7.1	8.6	5.2
V	83.2	75.7	73.8	63.9	43.9	69.0	60.1	57.8	49.2
Cr	5.3	5.4	9.8	11.2	7.0	11.6	4.0	7.7	7.1
Co	8.1	8.3	11.4	9.2	4.6	11.0	8.0	7.2	6.6
Ni	9.7	7.9	4.9	8.9	11.7	6.3	9.3	7.5	10.2
Cu	10.7	8.3	5.9	2.0	4.7	6.9	2.7	2.3	4.9
Zn	77.8	75.2	89.0	82.8	65.1	80.5	71.6	71.9	64.2
Ga	18.5	18.7	23.5	22.9	23.3	21.6	20.9	21.4	24.7
Rb	216.1	239.5	213.7	215.4	234.6	225.2	204.3	203.6	205.5
Sr	740.6	790.4	582.7	575.5	565.8	598.5	578.5	579.2	539.6
Y	39.5	35.7	34.4	32.9	36.5	12.0	33.1	30.8	26.9
Zr	231.9	216.6	256.5	249.1	232.8	228.6	218.9	226.2	200.4
Nb	22.6	21.5	20.4	20.2	20.1	15.8	18.1	19.5	15.7
Ba	963.8	963.7	964.5	939.5	1096.9	1013.6	899.3	903.9	884.2
La	55.6	55.2	72.1	74.1	53.9	55.7	50.7	56.8	48.0
Ce	96.7	98.2	117.9	103.9	94.6	99.0	88.9	91.4	78.4
Nd	31.7	34.3	44.8	48.4	31.5	29.3	40.2	32.4	22.5
Pb	51.6	44.6	53.6	52.2	52.3	52.1	52.5	50.5	49.6
Th	28.2	31.3	39.0	36.2	34.7	29.2	24.6	21.4	23.1
U	8.1	7.0			11.7	3.8			5.5
cipw									
%AN	31	32	31	30	27	31	30	33	34
Q	3	4	5	6	3	7	7	8	9
or	34	35	32	31	39	31	33	32	32
ab	31	31	32	33	33	33	32	32	31
an	14	15	14	14	12	14	14	16	16
ne									
C									
di	9	5	4	5	4	3	4	2	2
hy	7	8	9	8	6	9	7	8	7
wo									
ol									
mt	1	1	1	1	1	1	1	1	1
il	1	1	1	1	1	1	1	1	1
ap	1	1	1						

APPENDIX C (III)

XRF analyses of the samples from the Central Anatolian Massif.

Pluton	*Baranadag*	*Baranadag*	*Baranadag*	*Baranadag*	*Baranadag*	*Baranadag*	*Baranadag*	*Baranadag*	*Baranadag*
Sample no	**N153**	**N159**	**N133**	**N154**	**N132**	**N134**	**N151**	**N138**	**N145**
Rock type	*qmz*	*qmz*	*qmz*	*qmz*	*qmz*	*qmz*	*qmz*	*qmz*	*qmz*
Geochemical description	*sy*	*sy*	*sy*	*sy*	*sy*	*sy*	*qmz*	*qmz*	*qmz*
SiO_2	62.85	62.99	63.15	63.19	63.25	63.51	63.51	63.62	63.67
TiO_2	0.45	0.42	0.41	0.40	0.39	0.41	0.44	0.41	0.40
Al_2O_3	17.35	17.20	17.47	17.18	17.65	17.42	16.91	17.35	17.21
Fe_2O_3	4.02	3.83	3.65	3.67	3.58	3.61	4.10	3.53	3.60
MnO	0.10	0.10	0.09	0.09	0.09	0.09	0.10	0.09	0.08
MgO	1.43	1.40	1.24	1.28	1.21	1.22	1.29	1.17	1.21
CaO	4.13	4.03	3.72	3.78	3.49	3.55	3.81	3.57	3.52
Na_2O	3.85	3.79	3.64	3.57	3.63	3.61	3.59	3.94	3.62
K_2O	5.18	5.44	5.85	5.78	6.06	5.84	5.26	5.33	5.61
P_2O_5	0.16	0.16	0.16	0.14	0.19	0.17	0.17	0.14	0.15
L.O.I	0.58	0.64	0.67	0.79	0.51	0.63	0.67	0.43	0.73
TOTAL (L.O.I. free)	99.51	99.36	99.38	99.08	99.54	99.43	99.17	99.15	99.07
Sc	6.6	4.0	4.3	4.6	2.8	4.5	5.9	7.2	4.3
V	53.6	50.7	46.5	47.6	43.6	43.3	60.9	47.7	44.5
Cr	25.9	5.9	9.3	6.1	0.4	3.3	0.7	19.5	5.6
Co	6.3	5.6	7.5	5.2	3.6	5.3	5.3	7.8	5.9
Ni	1.8	8.9	8.4	11.2	11.5	10.0	6.8	2.5	11.3
Cu	9.9	6.4	7.8	8.3	9.1	2.7	5.1	10.4	6.0
Zn	78.5	68.6	69.7	65.6	71.5	64.6	73.3	71.5	66.6
Ga	24.0	18.3	19.6	21.6	23.5	22.0	24.9	20.5	24.3
Rb	200.8	210.8	208.9	205.8	219.8	213.6	208.8	213.1	195.9
Sr	574.0	540.0	550.1	541.2	556.7	536.0	497.6	553.6	523.2
Y	21.9	31.0	30.9	32.7	27.8	32.3	32.2	24.3	36.3
Zr	226.3	216.9	207.8	204.0	201.0	209.2	202.9	219.1	209.7
Nb	15.4	17.5	17.6	18.3	16.4	18.1	17.4	19.1	18.8
Ba	801.1	881.6	1026.0	898.9	1061.1	855.0	844.4	707.1	916.1
La	57.6	45.3	46.8	49.0	40.4	43.1	62.7	49.1	55.1
Ce	108.2	77.9	91.7	82.6	70.3	72.0	100.8	92.9	97.2
Nd	33.4	27.5	35.8	24.3	23.7	28.2	36.1	31.6	31.1
Pb	44.3	52.9	56.8	55.8	58.6	57.6	50.9	47.9	57.7
Th	26.3	31.0	22.1	28.6	25.6	27.5	34.0	29.1	26.8
U	5.1	5.7	7.3	7.9	7.7	8.4	8.0	6.6	5.3
cipw									
%AN	31	30	31	31	31	32	32	29	32
Q	8	8	9	9	8	9	11	10	10
or	31	32	35	34	36	35	31	31	33
ab	33	32	31	30	31	31	30	33	31
an	15	14	14	14	14	14	14	14	14
ne									
C									
di	4	4	3	3	2	2	3	2	2
hy	7	7	7	7	7	7	8	7	7
wo									
ol									
mt	1	1	1	1	1	1	1	1	1
il	1	1	1	1	1	1	1	1	1
ap									

APPENDIX C (III)

XRF analyses of the samples from the Central Anatolian Massif.

Pluton	*Baranadag*	*Baranadag*	*Baranadag*	*Baranadag*	*Baranadag*	*Baranadag*	*Baranadag*	*Baranadag*	*Baranadag*
Sample no	**N136**	**N158**	**N137**	**N143**	**N147**	**N144**	**N146**	**N139**	**N135**
Rock type	*qmz*	*qmz*	*qmz*	*qmz*	*qmz*	*qmz*	*qmz*	*qmz*	*qmz*
Geochemical description	*qmz*	*qmz*	*qmz*	*qmz*	*qmz*	*qmz*	*qmz*	*qmz*	*qmz*
SiO_2	63.80	63.88	63.95	64.10	64.32	64.58	64.60	65.01	65.24
TiO_2	0.41	0.48	0.38	0.43	0.39	0.40	0.37	0.40	0.42
Al_2O_3	16.83	16.75	17.35	16.82	16.86	16.57	16.85	16.95	16.90
Fe_2O_3	3.75	4.06	3.54	3.97	3.53	3.80	3.29	3.64	3.58
MnO	0.09	0.10	0.09	0.09	0.09	0.08	0.08	0.09	0.09
MgO	1.18	1.56	1.16	1.34	1.14	1.22	1.05	1.22	1.12
CaO	3.54	4.31	3.59	3.55	3.42	3.38	3.21	3.35	3.27
Na_2O	3.63	3.75	3.76	3.68	3.73	3.54	3.74	3.69	3.52
K_2O	5.83	5.14	5.71	5.24	5.47	5.18	5.77	5.77	5.51
P_2O_5	0.15	0.17	0.15	0.16	0.14	0.17	0.14	0.14	0.14
L.O.I	1.05	0.73	0.45	0.98	0.85	0.79	0.66	0.87	1.36
TOTAL (L.O.I. free)	99.21	100.20	99.68	99.38	99.09	98.93	99.10	100.26	99.79
Sc	6.9	6.5	5.0	7.0	5.7	7.5	7.4	5.9	3.7
V	54.8	58.8	42.5	61.5	53.9	63.8	46.3	51.2	44.6
Cr	10.1	5.2	7.7	14.1	11.4	14.7	9.7	11.9	11.7
Co	7.5	7.6	5.5	7.5	6.3	9.1	6.8	7.3	7.6
Ni	6.3	6.1	9.4	7.2	5.2	5.5	5.4	6.5	10.5
Cu	5.3	7.9	7.4	4.6	1.5	3.6	7.4	5.0	22.1
Zn	73.8	72.8	65.6	70.3	63.6	68.1	62.9	68.4	84.9
Ga	23.4	20.2	21.6	20.5	20.5	20.2	17.4	19.1	21.4
Rb	231.1	193.7	210.5	203.0	213.1	203.7	220.1	221.6	242.2
Sr	528.5	538.9	539.3	500.1	513.9	501.8	532.5	534.2	1260.7
Y	23.9	35.4	32.4	23.6	23.4	22.3	19.8	21.1	36.4
Zr	230.0	213.9	218.4	229.2	220.0	255.3	201.3	236.1	325.0
Nb	20.5	20.0	18.4	18.7	19.8	18.6	18.3	18.8	36.6
Ba	877.6	926.5	915.0	758.8	781.1	773.3	881.6	849.9	1849.4
La	50.2	59.9	51.4	59.3	57.0	59.0	51.6	54.4	95.9
Ce	103.1	102.0	80.4	113.4	107.7	109.2	84.3	105.6	187.7
Nd	37.1	36.8	29.6	40.8	41.0	39.3	31.3	33.6	51.7
Pb	56.6	49.1	57.1	52.7	49.1	51.3	51.2	53.4	65.1
Th	25.6	32.7	26.9	35.8	31.2	41.4	29.6	35.3	55.4
U	7.0	6.7	4.6	6.5	4.1	5.4	3.8	6.1	14.1
cipw									
%AN	29	30	30	31	29	32	28	29	32
Q	10	10	10	11	11	13	11	11	13
or	34	30	34	31	32	31	34	34	33
ab	31	32	32	31	32	30	32	31	30
an	12	14	14	14	13	14	12	13	14
ne									
C									
di	4	6	3	2	2	1	2	3	1
hy	7	7	7	8	7	8	6	7	7
wo									
ol									
mt	1	1	1	1	1	1		1	1
il	1	1	1	1	1	1	1	1	1
ap									

APPENDIX C (III)

XRF analyses of the samples from the Central Anatolian Massif.

Pluton	*Baranadag*	*Hamit*	*Hamit*	*Hamit*	*Hamit*	*Hamit*	*Hamit*	*Hamit*	*Hamit*
Sample no	**N142**	**N46**	**N45**	**N31**	**N255**	**N296**	**N33**	**N32**	**N252**
Rock type	*qmz*	*pdmzsy*	*pdmzsy*	*nemzsy*	*nemzsy*	*pdmzsy*	*nemzsy*	*nemzsy*	*nemzsy*
Geochemical description	*qmz*	*fmzsy*	*fmzsy*	*fmzsy*	*fmzsy*	*fmzsy*	*fmzsy*	*fmzsy*	*fmzsy*
SiO_2	65.25	52.52	52.83	53.19	53.25	53.25	53.32	53.37	53.58
TiO_2	0.36	0.65	0.62	0.72	0.72	0.62	0.72	0.72	0.74
Al_2O_3	16.71	18.79	19.15	17.99	18.25	19.17	18.09	18.15	18.36
Fe_2O_3	3.25	5.74	5.39	6.41	6.33	5.32	6.49	6.45	6.49
MnO	0.08	0.15	0.14	0.14	0.14	0.14	0.15	0.14	0.14
MgO	1.09	1.58	1.47	2.99	2.93	1.44	2.97	2.80	3.02
CaO	3.31	7.11	6.72	7.15	7.04	6.70	7.01	6.90	6.98
Na_2O	3.68	3.93	4.29	3.29	3.62	4.07	3.37	3.42	3.35
K_2O	5.60	7.82	7.87	6.59	6.61	8.06	6.71	6.36	6.67
P_2O_5	0.14	0.33	0.31	0.42	0.39	0.32	0.42	0.41	0.41
L.O.I	0.91	1.83	1.43	1.23	1.15	1.79	1.05	0.95	1.49
TOTAL (L.O.I. free)	99.47	98.61	98.78	98.90	99.28	99.09	99.25	98.72	99.73
Sc	5.3	11.5	10.2	6.4	6.5	5.6	7.6	11.0	7.3
V	51.4	109.1	97.2	114.2	110.4	83.3	123.2	125.5	120.8
Cr	7.7	1.2	1.3	18.8	18.5	17.0	40.4	19.0	23.8
Co	6.0	11.5	9.8	16.9	14.3	9.4	13.1	14.7	13.2
Ni	4.3	12.6	12.9	18.9	21.1	13.5	15.0	20.3	31.8
Cu	4.5	9.9	6.3	31.0	30.0	27.4	33.8	18.9	28.4
Zn	60.7	93.9	93.4	92.7	83.1	87.2	108.2	84.3	88.6
Ga	19.9	18.7	16.8	17.7	22.1	21.1	25.5	22.3	23.1
Rb	215.6	266.9	264.4	215.3	225.9	296.2	225.6	214.0	215.7
Sr	555.3	1180.6	1259.5	1066.7	1110.4	1085.1	1293.9	1332.3	1073.2
Y	18.9	47.3	44.6	41.4	41.5	52.6	40.1	33.9	42.1
Zr	202.2	442.3	436.1	340.9	332.1	422.4	368.9	341.5	350.8
Nb	17.6	45.3	45.1	30.9	30.3	42.6	27.9	32.0	31.3
Ba	905.2	716.1	948.6	1444.5	1439.1	1134.1	1247.9	1469.6	1492.8
La	42.1	134.7	133.1	105.4	94.8	118.9	103.9	111.1	115.6
Ce	85.2	212.6	207.2	182.6	174.6	195.7	187.3	177.4	187.3
Nd	32.7	90.1	85.2	68.9	60.1	73.0	85.2	74.2	72.8
Pb	52.2	63.4	63.8	50.0	54.2	65.3	45.8	51.8	52.3
Th	28.7	64.7	59.3	46.2	46.1	61.2	49.1	46.5	46.8
U	5.5			9.1	13.3	18.2	8.1		9.9
cipw									
%AN	29	99	93	57	58	90	58	53	58
Q	13								
or	33	46	47	39	39	48	40	38	39
ab	31		1	11	10	1	11	14	11
an	13	11	10	15	14	10	14	15	15
ne		18	19	9	11	18	10	8	9
C									
di	3	19	18	15	15	18	15	13	14
hy	6								
wo									
ol		2	2	7	6	2	7	7	7
mt		1	1	1	1	1	1	1	1
il	1	1	1	1	1	1	1	1	1
ap		1	1	1	1	1	1	1	1

APPENDIX C (III)

XRF analyses of the samples from the Central Anatolian Massif.

Pluton	*Hamit*	*Hamit*	*Hamit*	*Hamit*	*Hamit*	*Hamit*	*Hamit*	*Hamit*	*Hamit*
Sample no	**N293**	**N256**	**N253**	**N295**	**HAMID-II**	**N294**	**N254**	**N287**	**N450**
Rock type	*pdmzsy*	*nemzsy*	*nemzsy*	*pdmzsy*	*pdmzsy*	*pdmzsy*	*nemzsy*	*pho*	*pho*
Geochemical description	*fmzsy*	*fmzsy*	*fmzsy*	*fmzsy*	*fmzsy*	*fmzsy*	*fmzsy*	*fsy*	*fsy*
SiO_2	53.60	53.70	53.77	54.06	54.11	54.23	54.24	54.98	55.46
TiO_2	0.65	0.72	0.72	0.62	0.59	0.62	0.70	0.22	0.30
Al_2O_3	18.90	18.15	18.23	19.15	19.62	18.98	18.13	23.43	21.07
Fe_2O_3	5.52	6.25	6.36	5.30	5.03	5.19	6.10	2.35	3.06
MnO	0.14	0.15	0.15	0.13	0.14	0.13	0.14	0.15	0.14
MgO	1.56	2.90	2.98	1.55	1.00	1.40	2.77	0.25	0.44
CaO	7.17	6.99	6.79	6.98	5.75	6.93	6.59	2.18	3.19
Na_2O	3.92	3.57	3.05	3.81	4.41	3.76	3.45	8.13	6.27
K_2O	7.71	6.65	6.81	8.12	8.10	7.83	6.75	7.99	8.91
P_2O_5	0.33	0.40	0.44	0.33	0.20	0.31	0.40	0.03	0.03
L.O.I	1.86	1.12	1.50	1.79	2.23	2.12	1.18	3.22	2.08
TOTAL (L.O.I. free)	99.51	99.47	99.29	100.05	98.95	99.38	99.27	99.70	98.87
Sc	3.5	7.7	7.9	4.9	10.8	7.0	7.8	3.6	3.5
V	86.7	116.1	112.8	84.7	93.3	74.7	106.7	15.2	36.5
Cr	17.4	23.6	20.2	2.5	0.7	3.4	20.6		6.4
Co	7.6	12.5	15.4	9.2	8.4	9.1	15.8		4.0
Ni	13.9	25.5	26.7	13.3	8.6	14.3	22.5	4.8	6.1
Cu	26.4	34.6	36.8	25.2	7.7	31.8	30.1	7.5	4.4
Zn	93.2	97.7	87.9	82.6	109.2	85.8	88.2	132.4	136.1
Ga	21.4	21.1	24.2	18.1	22.2	17.5	20.8	23.6	30.7
Rb	271.8	229.5	213.0	299.7	283.6	272.5	226.0	346.6	440.4
Sr	1129.1	1095.5	1097.5	1123.1	1277.6	1368.6	1098.7	168.9	536.0
Y	52.2	42.3	40.5	50.8	46.3	49.1	40.7	22.8	30.1
Zr	436.9	340.4	343.5	399.9	599.7	402.7	332.2	817.5	687.6
Nb	42.6	31.0	30.4	39.4	51.2	37.9	31.0	71.9	60.2
Ba	1264.5	1423.7	1461.2	1212.9	1291.0	2082.1	1395.0	89.5	309.7
La	124.6	101.6	103.1	115.3	165.6	113.5	93.7	172.8	154.8
Ce	209.0	192.7	189.9	198.6	250.0	203.5	182.9	271.3	272.4
Nd	73.9	69.5	69.8	75.3	103.8	68.7	56.2	66.7	78.0
Pb	67.3	69.8	55.6	58.2	98.2	60.9	54.2	105.4	119.5
Th	64.1	48.2	50.1	55.8	72.5	56.9	49.9	135.5	96.8
U	17.8	10.8	9.4	15.5		16.4	11.1	44.7	29.7
cipw									
%AN	77	55	56	84	66	68	50	32	36
Q									
or	46	39	40	48	48	46	40	47	53
ab	3	11	13	2	5	5	14	8	5
an	11	14	16	11	10	12	14	4	3
ne	16	10	7	16	18	14	8	33	26
C									
di	19	15	12	18	15	17	13	6	11
hy									
wo									
ol	2	6	8	2	2	1	7	1	
mt	1	1	1	1	1	1	1		
il	1	1	1	1	1	1	1		1
ap	1	1	1	1		1	1		

APPENDIX C (III)

XRF analyses of the samples from the Central Anatolian Massif.

Pluton	*Hamit*	*Hamit*	*Hamit*	*Hamit*	*Hamit*	*Hamit*	*Hamit*	*Hamit*	*Hamit*
Sample no	**N288**	**N283**	**N281**	**N286**	**N43**	**N284**	**N42**	**N285**	**N50**
Rock type	*pho*	*nemzsy*	*nemzsy*	*pho*	*nemzsy*	*nemzsy*	*nemzsy*	*nemzsy*	*nemzsy*
Geochemical description	*fsy*	*fsy*	*fsy*	*fsy*	*fsy*	*fsy*	*fsy*	*fsy*	*fsy*
SiO_2	55.48	55.89	55.93	55.94	56.00	56.06	56.08	56.09	56.45
TiO_2	0.21	0.52	0.52	0.20	0.51	0.51	0.50	0.51	0.43
Al_2O_3	23.21	21.11	20.47	22.83	20.61	20.57	20.62	20.42	20.07
Fe_2O_3	2.21	4.43	4.34	2.20	4.38	4.43	4.36	4.44	3.72
MnO	0.14	0.12	0.12	0.14	0.12	0.12	0.12	0.12	0.12
MgO	0.06	1.07	1.07	0.06	0.99	1.04	1.06	1.08	0.53
CaO	2.05	3.69	3.59	2.03	3.61	3.62	3.54	3.59	4.93
Na_2O	8.32	4.63	4.74	7.92	4.61	5.11	4.54	4.93	4.87
K_2O	8.00	8.01	8.04	8.08	8.08	7.79	7.98	7.99	8.47
P_2O_5	0.01	0.24	0.24	0.02	0.23	0.24	0.23	0.25	0.11
L.O.I	3.55	1.22	1.08	3.12	0.90	0.81	0.96	0.77	1.81
TOTAL (L.O.I. free)	99.70	99.71	99.06	99.42	99.14	99.49	99.03	99.42	99.70
Sc	2.2	3.2	0.7		4.6	7.0	5.5	2.5	6.0
V	35.1	48.6	44.1	32.4	46.1	53.8	66.2	52.1	49.4
Cr	20.5	10.1	11.2	20.6	8.6	24.2		20.6	2.4
Co		5.4	8.0	1.6	7.9	8.9	5.9	7.2	3.9
Ni	12.3	12.4	10.2	12.8	10.2	5.3	5.6	4.8	8.9
Cu	3.1	20.8	22.1	1.0	23.3	29.1	2.7	25.2	
Zn	103.2	82.9	81.7	103.5	80.3	98.3	80.3	96.2	91.1
Ga	27.6	24.7	19.6	27.4	24.0	18.3	19.1	20.3	16.7
Rb	341.2	243.9	246.7	349.6	250.9	258.8	254.1	256.1	290.1
Sr	136.0	1254.7	1209.7	152.6	1211.9	1414.0	1366.5	1391.4	1452.5
Y	42.8	37.6	36.5	42.5	37.7	34.5	27.8	33.4	30.1
Zr	814.1	327.1	328.8	809.2	332.0	397.4	348.6	374.9	423.5
Nb	73.4	37.2	38.3	73.2	37.1	35.9	38.7	35.3	38.2
Ba	77.9	1848.6	1613.8	71.3	1646.2	1353.7	1557.3	1344.7	1469.7
La	168.2	92.2	90.6	168.9	91.3	108.0	102.8	101.8	129.8
Ce	242.8	184.7	172.0	241.4	172.1	204.0	178.4	190.6	193.6
Nd	53.5	53.8	49.4	54.8	54.6	75.4	65.5	67.4	66.0
Pb	110.7	64.9	66.6	110.6	65.9	59.2	70.3	61.4	85.6
Th	131.8	54.3	56.0	130.7	54.9	60.8	55.5	57.6	53.3
U	39.1	11.1	15.2	38.3	13.9	16.7		14.1	
cipw									
%AN	20	46	40	20	42	38	41	38	44
Q									
or	47	47	48	48	48	46	47	47	50
ab	10	16	16	12	16	17	17	16	10
an	2	13	11	3	12	10	12	10	8
ne	33	13	13	30	12	14	11	14	17
C									
di	7	3	5	6	4	5	3	5	13
hy									
wo									
ol		6	5		5	5	5	5	
mt		1	1		1	1	1	1	1
il		1	1		1	1	1	1	1
ap		1	1		1	1		1	

APPENDIX C (III)

XRF analyses of the samples from the Central Anatolian Massif.

Pluton	Hamit	Hamit	Hamit	Hamit	Hamit	Hamit	Hamit	Hamit	Hamit
Sample no	N282	N280	N258	N259	N260	N257	N278	N276	N279
Rock type	nemzsy	nemzsy	kspsy	kspsy	kspsy	kspsy	kspsy	kspsy	kspsy
Geochemical description	fsy	fsy	fsy	fsy	sy	sy	sy	sy	sy
SiO_2	56.48	57.30	57.52	57.78	59.41	60.12	60.96	61.26	61.35
TiO_2	0.52	0.49	0.21	0.21	0.18	0.18	0.41	0.37	0.40
Al_2O_3	20.48	20.66	25.86	25.76	25.20	25.10	18.73	18.80	19.07
Fe_2O_3	4.40	4.17	2.10	1.94	1.90	1.70	2.91	2.81	2.65
MnO	0.12	0.12	0.01	0.01	0.02	0.04	0.13	0.13	0.12
MgO	1.10	1.03	0.31	0.32	0.22	0.18	0.29	0.20	0.18
CaO	3.69	3.37	0.15	0.17	0.58	0.59	2.55	2.66	2.28
Na_2O	4.56	4.40	2.04	1.78	4.24	5.78	3.92	4.00	4.04
K_2O	7.72	8.10	10.88	11.30	7.90	5.86	9.01	9.19	9.26
P_2O_5	0.24	0.22	0.01	0.03	0.02	0.02	0.03	0.03	0.04
L.O.I	1.45	1.18	3.52	3.32	2.70	2.60	0.66	0.83	0.84
TOTAL (L.O.I. free)	99.30	99.86	99.10	99.30	99.67	99.57	98.93	99.45	99.38
Sc	6.7	2.2	2.7	4.3	0.7	1.0	4.3	1.3	2.5
V	52.8	41.6	16.8	24.4	29.4	32.8	46.4	51.8	39.5
Cr	7.9	8.4	52.8	3.3	8.3	7.2	2.0	6.0	
Co	8.6	7.6	1.6	2.6	0.1	1.5	1.5	3.3	1.4
Ni	4.5	10.8	7.3	4.6	5.0	23.6		8.5	
Cu	15.9	19.5	5.1	2.0	2.1	2.1	11.9	4.6	12.3
Zn	86.7	79.8	128.6	156.5	76.8	59.5	61.8	35.2	56.6
Ga	19.5	24.4	38.4	41.0	24.8	25.7	12.2	13.7	20.5
Rb	248.4	264.0	557.3	559.3	391.3	303.2	283.8	295.5	289.3
Sr	1233.0	1154.3	71.8	58.9	84.9	80.7	190.1	165.7	198.6
Y	37.1	36.5	17.1	19.5	21.1	23.8	79.2	104.3	62.8
Zr	332.1	315.9	950.5	996.7	921.7	926.8	269.8	277.1	227.7
Nb	38.0	36.8	96.5	101.0	95.8	87.9	44.5	37.5	41.5
Ba	1671.1	1633.1	138.2	168.8	93.1	71.6	32.0	56.2	23.9
La	96.0	94.6	125.5	182.6	181.8	160.9	94.9	95.1	96.9
Ce	192.7	178.7	232.2	290.3	242.7	232.7	168.6	145.3	171.1
Nd	52.3	49.6	49.1	64.8	46.1	29.2	62.1	52.9	60.6
Pb	64.6	68.3	48.4	59.1	43.7	146.3	53.0	59.6	56.0
Th	59.9	57.9	132.5	139.5	122.4	120.1	67.0	44.1	82.4
U	12.3	12.3	22.3	30.2	13.8	16.5	11.3	8.3	8.7
cipw									
%AN	39	38	4	4	7	5	20	19	19
Q			2	2	2	1			
or	46	48	64	67	47	35	53	54	55
ab	20	20	17	15	36	49	28	27	28
an	13	13	1	1	3	3	7	6	7
ne	10	9					3	4	3
C			10	10	9	8			
di	4	2					5	6	4
hy			4	4	3	3			
wo									
ol	5	6					2	1	2
mt	1	1							
il	1	1					1	1	1
ap	1	1							

APPENDIX C (III)

XRF analyses of the samples from the Central Anatolian Massif.

Pluton	Hamit	Hamit	Hamit	Hamit	Hamit	Hamit	Hamit	Hamit	Hamit
Sample no	N277	N37	N261	N273	N270	N36	N262	N271	N269
Rock type	kspsy	kspsy	kspsy	kspsy	kspsy	kspsy	kspsy	kspsy	kspsy
Geochemical description	sy	sy	sy	sy	sy	sy	sy	sy	sy
SiO_2	61.72	62.23	63.35	63.34	63.36	63.46	63.51	63.58	63.65
TiO_2	0.42	0.35	0.44	0.28	0.27	0.28	0.30	0.25	0.25
Al_2O_3	19.23	19.01	18.23	18.87	18.08	18.80	19.08	18.17	19.05
Fe_2O_3	2.55	2.43	2.39	1.84	2.06	1.91	1.85	1.77	1.78
MnO	0.11	0.08	0.06	0.06	0.11	0.06	0.06	0.08	0.05
MgO	0.25	0.15	0.10	0.14	0.13	0.14	0.03	0.08	0.10
CaO	2.07	1.93	0.98	1.22	1.43	0.95	0.92	1.18	0.80
Na_2O	4.26	4.51	4.45	4.38	3.88	4.30	4.99	4.15	4.66
K_2O	8.91	8.32	9.23	9.29	10.04	9.18	8.51	9.76	8.89
P_2O_5	0.03	0.04	0.06	0.02	0.03	0.04	0.01	0.02	0.02
L.O.I	0.76	0.38	0.87	0.77	0.79	0.47	0.90	0.61	1.00
TOTAL (L.O.I. free)	99.55	99.04	99.29	99.44	99.39	99.12	99.26	99.04	99.26
Sc	1.5	2.5	0.8	3.5	0.1	2.2	3.3	1.5	2.7
V	35.5	38.0	31.1	23.9	35.5	23.0	26.5	27.3	24.7
Cr	0.2		0.8	0.6	2.6	31.8		1.0	
Co	1.7	4.1	0.7	1.3	3.0		2.1	1.0	2.6
Ni	7.4		6.4	4.7	5.1	3.9	5.4	6.4	5.6
Cu	3.2	8.8	7.7	2.7	4.4		3.7	6.2	5.0
Zn	56.8	44.1	49.9	29.9	35.1	30.5	29.5	30.0	37.0
Ga	13.4	18.0	19.1	12.9	17.5	14.5	14.3	16.1	16.0
Rb	275.9	260.4	350.4	281.7	365.1	288.9	270.1	311.3	277.2
Sr	169.5	196.1	184.4	152.1	106.5	158.3	160.5	145.6	146.6
Y	50.9	38.0	28.2	22.0	70.8	26.3	20.7	44.7	19.9
Zr	192.9	116.7	111.8	84.3	280.3	75.0	111.2	134.9	88.8
Nb	45.4	38.2	54.0	32.6	38.6	25.6	36.7	33.0	31.3
Ba	69.6	40.7	101.3	68.7	53.4	65.5	95.2	80.9	88.9
La	103.1	103.4	140.4	95.6	126.4	93.0	123.1	87.9	87.4
Ce	185.1	169.6	222.4	161.8	210.8	188.7	152.9	156.9	161.0
Nd	67.8	53.0	64.7	48.8	58.4	45.6	64.6	39.9	41.2
Pb	63.3	41.9	61.7	50.5	52.1	51.7	46.5	52.3	51.4
Th	93.0	73.7	119.4	93.6	140.5	93.9	75.9	91.3	95.9
U	8.8	5.2	6.5	4.5	8.6		3.4	5.5	5.0
cipw									
%AN	18	16	6	11	7	11	10	6	9
Q									
or	53	49	55	55	59	54	50	58	53
ab	31	37	37	35	31	36	41	34	39
an	7	7	3	4	2	4	4	2	4
ne	3	1		1	1		1	1	
C									
di	3	2	2	1	4			3	
hy						3			1
wo									
ol	2	2	2	2	1		2	1	1
mt									
il	1	1	1	1	1	1	1		
ap									

APPENDIX C (III)

XRF analyses of the samples from the Central Anatolian Massif.

Pluton	*Hamit*	*Hamit*	*Hamit*	*Hamit*	*Hamit*	*Hamit*	*Hamit*	*Hamit*	*Hamit*
Sample no	**N44**	**N267**	**N263**	**N34**	**N40**	**N272**	**N268**	**N264**	**N246**
Rock type	***kspsy***	***kspsy***	***kspsy***	***kspsy***	***kspsy***	***kspsy***	***kspsy***	***kspsy***	***kspsy***
Geochemical description	*sy*	*sy*	*sy*	*sy*	*sy*	*sy*	*sy*	*sy*	*sy*
SiO_2	63.76	63.89	64.19	64.37	64.72	65.06	65.11	65.52	65.56
TiO_2	0.31	0.23	0.19	0.25	0.32	0.28	0.22	0.07	0.05
Al_2O_3	18.45	19.83	18.79	18.33	18.16	18.96	18.83	19.31	19.11
Fe_2O_3	1.86	1.61	1.68	1.53	1.72	0.79	1.21	0.92	0.67
MnO	0.09	0.03	0.04	0.09	0.02	0.04	0.05	0.01	0.02
MgO	0.14	0.03	0.04	0.09	0.04	0.08	0.03	0.04	0.05
CaO	1.14	0.97	0.37	1.03	0.91	0.65	0.35	0.50	0.56
Na_2O	4.17	6.62	4.67	3.93	4.95	4.30	4.87	5.94	4.65
K_2O	9.61	5.99	9.40	10.06	8.29	9.86	8.90	7.63	9.14
P_2O_5	0.03	0.02	0.02	0.04	0.05	0.02	0.02	0.01	0.00
L.O.I	0.58	1.12	0.93	0.48	0.62	0.66	0.91	0.81	1.23
TOTAL (L.O.I. free)	99.57	99.22	99.40	99.71	99.18	100.04	99.60	99.96	99.81
Sc	1.7	3.5	1.9			0.3	1.2	1.8	1.8
V	30.6	26.7	21.4	22.4	32.6	11.0	18.7	6.3	5.0
Cr	6.2		3.3	10.7	29.2	0.2			
Co	1.5	1.5	2.3	0.3			0.7	0.5	0.2
Ni	9.9	1.5	4.7	4.8	5.6	9.2	2.8	2.9	
Cu	5.2	1.2	2.1	0.5	0.7	3.1	3.6	1.1	1.9
Zn	48.9	39.6	42.3	31.9	58.0	26.9	28.0	10.8	44.4
Ga	18.9	20.1	20.4	19.8	19.8	13.6	16.6	15.5	18.6
Rb	418.7	184.4	384.1	398.2	480.0	369.5	269.3	208.7	173.8
Sr	121.6	165.9	131.8	140.4	104.4	161.5	136.6	79.0	69.5
Y	36.8	12.2	10.1	45.0	44.9	28.0	18.5	6.3	4.4
Zr	288.4	99.1	345.4	204.4	278.6	91.8	205.2	324.3	148.3
Nb	46.1	29.6	31.5	26.8	37.7	41.7	31.9	15.1	14.3
Ba	106.6	61.4	89.4	74.3	22.3	148.8	119.3	58.1	123.0
La	84.6	84.1	75.3	112.5	166.5	66.4	75.5	15.3	30.0
Ce	156.9	126.4	142.8	149.6	215.8	118.8	125.9	12.7	41.8
Nd	34.4	32.6	32.0	47.6	58.8	30.1	36.6	5.8	6.3
Pb	68.1	50.8	43.6	53.2	63.1	61.9	49.1	40.8	59.8
Th	93.6	67.9	98.4	84.4	160.2	52.9	65.4	22.7	62.8
U	9.9	5.0	7.5			5.8	4.1	5.8	23.8
cipw									
%AN	8	8	4	7	6	8	4	5	7
Q					2		1		2
or	57	35	56	59	49	58	53	45	54
ab	35	56	39	33	42	36	41	50	39
an	3	5	2	3	3	3	2	2	3
ne									
C		1					1		1
di	2			2	1				
hy				1	2	1	2	1	1
wo									
ol	1	2	2						
mt									
il	1				1	1			
ap									

APPENDIX C (III)

XRF analyses of the samples from the Central Anatolian Massif.

Pluton	Hamit	Hamit	Hamit	Hamit	Hamit	Hamit	Hamit	Hamit	Hamit
Sample no	N48	N247	N47	N251	N49	N266	N291	N290	N289
Rock type	qsy	kspsy	qsy	kspsy	qsy	kspsy	qsy	qsy	qsy
Geochemical description	sy	sy	sy	sy	sy	sy	sy	sy	sy
SiO_2	65.64	65.84	65.88	65.94	66.00	66.16	66.53	66.78	67.02
TiO_2	0.30	0.07	0.30	0.04	0.30	0.04	0.29	0.28	0.31
Al_2O_3	17.11	18.92	17.29	19.12	17.44	19.30	17.16	17.32	17.21
Fe_2O_3	2.04	0.74	2.16	0.45	2.10	0.42	1.92	1.79	2.07
MnO	0.07	0.02	0.07	0.00	0.07	0.01	0.06	0.05	0.07
MgO	0.37	0.03	0.42	0.02	0.39	0.03	0.35	0.29	0.39
CaO	1.80	0.50	1.84	0.37	1.88	0.42	1.73	1.59	1.91
Na_2O	4.38	5.07	4.29	5.82	4.44	6.06	4.24	4.29	4.28
K_2O	7.02	8.67	6.98	7.96	6.97	7.49	7.18	7.30	6.81
P_2O_5	0.06	0.00	0.05	0.01	0.06	0.00	0.04	0.04	0.06
L.O.I	0.27	0.98	0.31	1.14	0.28	0.90	0.39	0.64	0.43
TOTAL (L.O.I. free)	98.80	99.85	99.27	99.73	99.64	99.93	99.50	99.72	100.13
Sc	3.8	1.4	3.6		4.7	1.6	0.3	1.8	1.6
V	23.2	9.5	24.8	0.6	22.3	6.7	28.5	24.5	28.9
Cr	3.9		11.9		3.6		0.8	3.0	5.6
Co	3.2	0.8	0.1	0.8	3.5	0.3	5.6	1.4	5.2
Ni	2.2	2.3	5.8	2.2		0.8	7.9	10.5	10.1
Cu	9.0	3.2	1.1	2.1	6.3	0.4	4.6	2.7	1.5
Zn	48.9	16.4	40.6	17.6	46.8	8.4	33.4	26.7	40.3
Ga	15.3	17.5	21.1	.17.4	21.1	16.6	19.6	19.7	19.9
Rb	355.0	351.4	349.5	362.4	348.4	208.8	364.5	368.8	340.2
Sr	267.0	140.3	270.2	128.1	284.0	66.8	224.9	240.4	255.8
Y	21.4	4.3	36.7	9.7	19.7	2.0	41.5	40.4	43.4
Zr	345.4	106.7	316.9	54.8	367.8	20.2	346.0	316.1	368.4
Nb	37.8	14.8	19.8	12.6	37.5	8.2	35.6	35.2	37.4
Ba	246.8	133.7	295.0	132.5	286.3	38.6	221.7	308.8	294.6
La	87.0	36.7	119.4	38.2	124.7	16.9	96.2	88.6	117.9
Ce	140.7	55.8	159.1	60.4	176.3	6.3	140.5	131.7	154.6
Nd	39.6	13.2	38.1	9.5	43.0	4.1	30.2	23.9	35.2
Pb	57.2	46.8	59.4	55.8	58.5	44.4	60.9	61.3	60.4
Th	108.3	45.9	126.2	54.1	144.2	2.3	111.4	100.7	127.2
U	14.8	2.3		3.3	18.2	1.5	11.5	8.6	11.5
cipw									
%AN	15	5	17	3	16	4	16	15	17
Q	8	2	9	1	8	1	9	9	11
or	41	51	41	47	41	44	42	43	40
ab	37	43	36	49	38	51	36	36	36
an	6	2	7	2	7	2	7	6	8
ne									
C									
di	2		1		2		1	1	1
hy	3	1	3	1	3	1	3	3	3
wo									
ol									
mt									
il	1		1		1		1	1	1
ap									

APPENDIX C (III)

XRF analyses of the samples from the Central Anatolian Massif.

Pluton	*Hamit*	*Hamit*
Sample no	**N292**	**N265**
Rock type	***qsy***	***gr***
Geochemical description	*qmz*	*gr*
SiO_2	67.06	72.24
TiO_2	0.29	0.15
Al_2O_3	17.40	14.50
Fe_2O_3	1.96	1.49
MnO	0.06	0.02
MgO	0.34	0.23
CaO	1.80	1.39
Na_2O	4.25	3.02
K_2O	6.88	6.21
P_2O_5	0.04	0.02
L.O.I	0.41	0.97
TOTAL (L.O.I. free)	100.07	99.27
Sc	1.7	1.9
V	28.2	1.6
Cr	3.0	2.3
Co	3.1	0.2
Ni	8.3	2.2
Cu	2.4	1.8
Zn	35.4	13.7
Ga	19.7	18.1
Rb	317.3	245.8
Sr	236.3	57.7
Y	39.4	2.5
Zr	347.1	67.7
Nb	34.0	9.8
Ba	266.1	39.9
La	108.7	14.6
Ce	152.4	10.4
Nd	30.7	3.6
Pb	62.3	48.7
Th	133.5	10.9
U	13.4	1.1
cipw		
%AN	18	21
Q	11	27
or	41	37
ab	36	26
an	8	7
ne		
C		
di	1	
hy	3	3
wo		
ol		
mt		
il	1	
ap		

APPENDIX C (III)

XRF analyses of the samples from the Central Anatolian Massif.

Pluton	*Cefalikdag*	*Cefalikdag*	*Cefalikdag*	*Cefalikdag*	*Cefalikdag*	*Celebi*	*Celebi*	*Celebi*	*Behrekdag*
Sample no	**N378**	**N419**	**N377**	**N418**	**N412**	**N221**	**N220**	**N222**	**N169**
Characteristic	*mafic dyke*	*mafic dyke*	*mafic dyke*	*mafic dyke*	*phonolitic dyke*	*mafic dyke*	*mafic dyke*	*mafic dyke*	*aplitic dyke*
Rock type									
Geochemical description	*mzdi*	*mzdi*	*mzdi*	*mzdi*	*fsy*	*mz*	*mz*	*mz*	*qmz*
SiO_2	52.29	53.40	53.47	54.98	56.54	56.86	57.21	58.01	69.67
TiO_2	0.56	0.71	0.55	0.70	0.44	0.54	0.55	0.56	0.16
Al_2O_3	19.22	18.77	19.32	19.18	21.12	13.84	14.24	14.32	15.66
Fe_2O_3	8.35	4.35	7.82	4.21	3.00	7.02	6.19	5.78	1.25
MnO	0.21	0.13	0.20	0.10	0.12	0.17	0.13	0.12	0.03
MgO	2.41	2.95	2.42	2.90	0.65	5.87	5.83	5.64	0.38
CaO	9.70	12.37	9.64	11.27	2.41	8.44	8.59	8.68	1.89
Na_2O	3.23	2.46	3.13	2.66	4.93	2.82	2.69	2.91	2.56
K_2O	2.73	4.03	3.07	3.99	9.49	3.77	3.89	3.56	7.35
P_2O_5	0.30	0.09	0.30	0.10	0.06	0.16	0.15	0.16	0.03
L.O.I	1.77	2.52	1.48	1.96	1.93	0.91	0.99	1.07	0.83
TOTAL (L.O.I. free)	99.00	99.25	99.91	100.09	98.76	99.49	99.47	99.73	98.97
Sc	12.9	19.7	15.7	23.4	3.8	18.4	16.9	25.3	3.0
V	98.4	143.5	95.5	147.0	51.0	151.9	147.7	163.1	18.3
Cr	6.0	141.5	6.7	138.3		288.3	274.5	276.9	
Co	23.9	8.3	22.1	13.2	3.1	16.7	15.9	13.1	2.9
Ni	8.7	54.8	9.5	64.6	3.5	47.5	51.1	49.6	
Cu	10.2	4.8	10.4	38.3	8.1	6.6	5.8	3.5	18.1
Zn	125.5	96.8	115.6	71.1	92.9	66.3	58.9	52.8	22.8
Ga	23.9	21.0	23.5	23.7	23.7	13.9	14.7	17.2	9.9
Rb	62.4	157.3	65.5	155.6	305.3	197.6	205.0	192.1	222.1
Sr	822.8	423.3	828.1	415.9	730.2	266.9	309.6	334.4	450.8
Y	31.8	41.9	29.2	35.7	35.6	36.9	33.1	25.1	9.4
Zr	264.8	154.1	161.4	154.2	490.0	126.2	123.5	139.1	59.9
Nb	14.3	15.4	9.6	15.0	63.5	12.6	10.1	11.4	9.1
Ba	1409.9	699.3	1588.3	595.1	323.4	658.2	702.8	655.7	1950.6
La	51.6	33.7	44.9	34.8	129.3	40.6	37.7	30.6	28.8
Ce	147.7	53.0	106.9	63.1	231.4	64.8	55.3	61.1	35.6
Nd	54.5	22.4	47.9	25.5	77.3	32.4	21.6	23.5	12.7
Pb	53.2	49.4	43.7	41.9	82.2	28.8	28.9	36.6	62.1
Th	31.3	13.7	17.0	14.7	88.1	15.2	13.5	13.2	26.2
U	5.7	3.9	3.7	2.7	19.2	3.2	3.2	2.8	3.4
cipw									
%AN	53	65	52	56	42	37	40	39	30
Q						1	2	3	21
or	18	24	16	24	56	22	23	21	43
ab	26	15	27	22	10	24	23	25	22
an	30	28	30	29	7	14	15	15	9
lc									
ne		3			17				
C						22	21	22	
di	14	27	14	22	3	14	13	12	
hy	4		1						3
wo									
ol	5		8	2	3	1	1	1	
mt	1	1	1	1		1	1	1	
il	1	1	1	1	1				
ap			1						

APPENDIX C (III)

XRF analyses of the samples from the Central Anatolian Massif.

Pluton	*Behrekdag*	*Behrekdag*	*Behrekdag*	*Cefalikdag*	*Behrekdag*	*Celebi*	*Celebi*	*Celebi*
Sample no	**N168**	**N178**	**N170**	**N310b**	**N8**	**N119**	**N117**	**N118**
Characteristic	*aplitic dyke*	*pegmatitic dyke*	*aplitic dyke*	*aplitic dyke*	*aplitic dyke*	*aplitic dyke*	*aplitic dyke*	*aplitic dyke*
Rock type								
Geochemical description	*qmz*	*gr*	*gr*	*qmz*	*qmz*	*qmz*	*gr*	*gr*
SiO_2	69.91	76.58	77.05	68.53	69.06	69.58	70.78	71.00
TiO_2	0.15	0.02	0.06	0.27	0.26	0.19	0.18	0.18
Al_2O_3	15.59	12.07	12.38	15.42	14.90	14.84	14.90	14.84
Fe_2O_3	1.07	0.22	0.48	2.68	3.22	2.20	2.00	1.76
MnO	0.03	0.01	0.02	0.06	0.07	0.06	0.05	0.05
MgO	0.31	0.24	0.07	0.93	1.09	0.34	0.23	0.31
CaO	1.51	0.16	0.66	2.24	3.08	2.07	1.86	2.01
Na_2O	2.37	1.41	2.11	2.80	2.51	2.95	2.90	3.00
K_2O	7.97	8.66	6.89	6.16	5.81	6.25	6.41	6.06
P_2O_5	0.02		0.01	0.10	0.08	0.05	0.04	0.04
L.O.I	0.83	0.30	1.03	0.93	0.60	0.65	0.66	0.60
TOTAL (L.O.I. free)	98.93	99.36	99.72	99.19	100.08	98.53	99.35	99.24
Sc	2.7	0.3	3.3	3.5	2.5	4.7	3.3	5.0
V	14.5	0.8	5.9	30.7	43.8	31.2	22.8	25.2
Cr	0.7	18.2	1.2	12.2		1.7	4.1	1.4
Co	3.5	0.2	3.9	3.4	7.4	3.3	3.1	0.2
Ni	0.4	3.9	1.7	4.2	8.3	1.1	2.4	
Cu	16.9	1.5	3.5	4.8	10.5	3.3	2.0	2.3
Zn	22.2	7.1	13.8	45.3	39.8	34.6	42.4	30.0
Ga	10.8	9.2	6.5	18.9	11.0	18.1	14.5	15.4
Rb	239.1	232.1	306.3	202.9	217.4	214.1	218.2	194.2
Sr	462.4	270.5	152.4	343.8	366.1	203.3	198.4	199.8
Y	7.4	3.4	1.7	11.7	19.1	14.4	18.7	15.1
Zr	47.6	5.2	38.5	89.7	92.7	121.5	130.3	104.6
Nb	7.8	3.5	8.4	12.3	8.8	11.5	15.6	12.7
Ba	2277.8	581.2	193.2	798.4	850.6	1135.6	1172.3	1065.1
La	19.8	0.5	7.4	69.0	21.3	25.1	69.0	30.4
Ce	32.1	1.3	8.6	123.1	34.1	37.2	91.7	47.3
Nd	7.4	1.5	1.3	45.6	12.7	8.1	20.1	14.2
Pb	57.8	38.9	43.4	35.1	45.3	51.9	50.3	42.4
Th	26.3	1.4	20.2	41.9	23.2	24.8	34.7	26.2
U	2.7	0.5	5.3	3.3	3.8	5.1	5.0	3.3
cipw								
%AN	27	6	15	31	37	26	26	26
Q	21	34	37	21	23	22	24	25
or	47	51	41	36	34	37	38	36
ab	20	12	18	24	21	25	25	25
an	7	1	3	10	12	9	9	9
lc								
ne								
C						1		
di					2	4	3	3
hy	2	1	1	6	6			
wo								
ol								
mt								
il				1				
ap								

APPENDIX C (III)

XRF analyses of the samples from the Central Anatolian Massif.

Pluton	*Cefalikdag*	*Cefalikdag*	*Cefalikdag*	*Cefalikdag*	*Cefalikdag*	*Cefalikdag*	*Cefalikdag*	*Cefalikdag*
Sample no	**N315**	**N311**	**N241**	**N242**	**N243**	**N312**	**N314**	**N22**
Characteristic	*aplitic dyke*	*aplitic dyke*	*aplitic dyke*	*aplitic dyke*	*aplitic dyke*	*aplitic dyke*	*aplitic dyke*	*aplitic dyke*
Rock type								
Geochemical description	*gr*	*gr*	*gr*	*gr*	*gr*	*gr*	*gr*	*gr*
SiO_2	71.96	71.99	72.35	72.38	72.44	73.06	73.77	75.92
TiO_2	0.24	0.15	0.14	0.14	0.12	0.14	0.19	0.10
Al_2O_3	14.70	14.61	15.13	15.28	15.30	13.83	13.90	12.99
Fe_2O_3	1.81	1.98	1.04	1.09	0.99	1.59	1.46	1.08
MnO	0.04	0.03	0.01	0.01	0.02	0.02	0.03	0.01
MgO	0.52	0.27	0.15	0.19	0.11	0.25	0.35	0.11
CaO	2.33	1.94	1.42	1.01	1.04	1.22	1.56	1.01
Na_2O	2.94	3.00	3.30	3.47	3.42	2.34	2.65	2.35
K_2O	4.65	5.34	5.75	5.67	5.86	6.75	5.42	6.08
P_2O_5	0.07	0.04	0.03	0.03	0.02	0.07	0.05	0.01
L.O.I	0.59	1.40	1.17	0.95	1.40	0.93	0.54	0.34
TOTAL (L.O.I. free)	99.26	99.35	99.32	99.27	99.31	99.27	99.37	99.67
Sc	5.2	5.0	4.2	1.8	3.2	4.2	2.4	2.6
V	16.9	16.5	7.7	16.3	17.8	11.1	10.4	6.4
Cr	4.5	3.0	1.7	0.7	2.1	3.1	0.5	2.3
Co	1.4	0.9	2.2	0.4	3.1	2.8	1.2	
Ni	1.4		2.5	2.2	2.4	1.6	1.9	4.0
Cu		0.5	26.1	22.0	28.3	1.2	1.7	1.2
Zn	37.1	23.9	14.6	9.3	8.8	23.4	35.2	6.9
Ga	17.8	14.0	12.1	14.5	14.3	13.9	15.6	16.2
Rb	156.6	165.0	194.9	180.5	185.3	191.6	188.0	227.6
Sr	333.4	318.9	328.7	349.7	336.2	253.2	276.9	131.0
Y	5.3	2.6	6.4	4.3	9.2	7.2	3.0	15.9
Zr	112.2	105.1	127.6	125.1	109.3	126.7	112.1	59.5
Nb	11.5	7.7	12.8	11.3	12.7	9.1	9.9	2.6
Ba	819.8	754.5	665.7	691.8	643.2	845.0	811.8	193.2
La	19.2	36.5	19.7	25.1	19.5	43.1	15.8	17.6
Ce	40.4	60.0	35.0	42.0	51.2	72.3	23.5	49.0
Nd	13.4	19.9	11.3	14.6	11.5	28.1	10.3	13.1
Pb	35.1	40.9	38.5	26.1	31.0	46.3	37.6	69.2
Th	14.5	16.3	18.2	17.6	17.3	16.6	11.4	24.1
U	2.2	2.2	2.0	3.0	2.7	1.8	2.1	
cipw								
%AN	31	27	20	14	15	22	25	20
Q	30	28	27	27	27	30	33	36
or	27	32	34	34	35	40	32	36
ab	25	25	28	29	29	20	22	20
an	11	9	7	5	5	6	7	5
lc								
ne								
C	1		1	2	1	1	1	1
di								
hy	4	4	2	2	2	3	3	2
wo								
ol								
mt								
il								
ap								

APPENDIX C (III)

XRF analyses of the samples from the Central Anatolian Massif.

Pluton	*Cefalikdag*	*Cefalikdag*	*Celebi*	*Celebi*	*Cefalikdag*	*Celebi*	*Baranadag*
Sample no	**N326**	**N320**	**N120**	**N121**	**N234**	**N207**	**N302**
Characteristic	*aplitic dyke*	*aplitic dyke*	*aplitic dyke*	*aplitic dyke*	*aplitic dyke*	*aplitic dyke*	*microsyenitic dyke*
Rock type							
Geochemical description	*gr*	*gr*	*gr*	*gr*	*gr*	*gr*	*sy*
SiO_2	76.09	76.26	76.81	77.04	77.26	74.07	65.46
TiO_2	0.06	0.06	0.08	0.08	0.13	0.15	0.11
Al_2O_3	12.88	12.79	12.68	12.47	13.12	13.29	19.14
Fe_2O_3	0.94	0.83	0.69	0.75	0.60	1.37	1.63
MnO	0.01	0.01	0.01	0.02	0.01	0.03	0.02
MgO	0.08	0.05	0.04	0.01	0.22	0.36	0.15
CaO	0.89	0.80	0.70	0.74	0.99	1.73	1.94
Na_2O	2.25	2.93	3.38	3.49	2.36	2.61	4.11
K_2O	6.53	5.60	5.03	4.70	5.34	5.74	7.94
P_2O_5	0.01	0.01		0.01	0.01	0.03	0.01
L.O.I	0.55	0.51	0.55	0.48	0.85	0.47	0.29
TOTAL (L.O.I. free)	99.74	99.34	99.43	99.31	100.04	99.38	100.50
Sc	1.4	3.9	3.3	2.4	2.4	4.8	0.6
V	6.1	15.6	2.1	7.0	17.5	24.2	4.7
Cr	0.4	0.4	0.5	0.6	0.6	8.5	
Co	1.4	0.7	1.5	2.0	1.3	2.4	0.8
Ni	2.3		1.8	1.6	1.4	0.5	9.9
Cu	6.2	2.8	4.4	4.9	0.9	6.6	8.7
Zn	14.7	22.6	14.1	8.5	10.4	21.7	18.4
Ga	10.7	14.3	13.3	6.0	6.9	10.2	21.0
Rb	235.7	217.3	524.7	499.8	161.1	263.8	287.4
Sr	87.5	264.2	0.3		693.9	222.4	541.0
Y	3.6	17.4	14.5	12.0	2.7	1.9	17.2
Zr	83.0	159.1	121.3	136.6	18.4	63.1	178.6
Nb	9.3	17.5	30.9	25.6	2.9	11.2	9.2
Ba	118.2	563.7	20.4	21.4	2566.2	222.1	642.8
La	21.0	39.0	21.3	20.6		22.6	11.1
Ce	37.4	70.0	34.6	40.1	8.7	40.9	12.7
Nd	11.2	23.3	11.1	12.3	2.4	5.8	2.4
Pb	66.3	52.9	61.9	57.7	33.7	38.0	58.9
Th	31.8	38.2	40.8	44.9	26.6	33.0	7.1
U	6.4	6.9	.8.0	7.4	2.3	6.1	3.4
cipw							
%AN	19	14	11	11	20	26	22
Q	35	35	36	37	40	32	6
or	39	33	30	28	32	34	47
ab	19	25	29	30	20	22	35
an	4	4	3	4	5	8	10
lc							
ne							
C	1				2		
di						1	
hy	2	1	1	1	1	3	3
wo							
ol							
mt							
il							
ap							

APPENDIX C (III)

XRF analyses of the samples from the Central Anatolian Massif.

Pluton	*Baranadag*	*Baranadag*	*Baranadag*	*Baranadag*	*Behrekdag*	*Behrekdag*	*Behrekdag*
Sample no	**N148**	**N149**	**N150**	**N153**	**N173**	**N103**	**N172**
Characteristic	*aplitic dyke*	*aplitic dyke*	*aplitic dyke*	*aplitic dyke*	*fine-grd enc.*	*fine-grd enc.*	*fine-grd enc.*
Rock type					*qmzdi (*)*	*qmzdi*	*qdi*
Geochemical description					*mz*	*mz*	*mz*
SiO_2	75.79	76.21	76.35	77.12	55.22	56.07	57.97
TiO_2	0.08	0.07	0.06	0.06	0.42	0.76	0.43
Al_2O_3	13.76	12.93	12.68	12.57	16.93	16.11	17.83
Fe_2O_3	0.66	0.81	0.73	0.34	6.53	7.34	6.66
MnO	0.02	0.01	0.01	0.01	0.18	0.18	0.17
MgO	0.05	0.05	0.04	0.02	2.29	4.04	2.45
CaO	0.25	0.68	0.89	0.91	6.32	8.33	6.57
Na_2O	4.82	2.77	2.75	2.44	3.24	2.48	3.28
K_2O	4.15	5.98	5.72	6.07	4.99	4.77	4.64
P_2O_5	0.01	0.01	0.00	0.00	0.27	0.25	0.28
L.O.I	0.49	0.72	0.49	0.91		0.78	0.95
TOTAL (L.O.I. free)	99.59	99.52	99.23	99.54	96.40	100.33	100.28
Sc	2.5	0.9	1.7	3.0	14.7	14.4	18.1
V	7.0	7.7	1.9	1.1	140.3	156.5	147.9
Cr	2.3	0.7	1.2	0.6	11.0	50.9	13.8
Co	0.4	1.3	1.1	1.9	20.7	19.7	16.2
Ni	3.2	1.7	1.4	1.7	9.4	29.3	8.2
Cu	2.7	3.5	1.1	4.4	101.1	57.4	98.0
Zn	18.0	11.5	15.9	15.8	74.0	93.3	72.9
Ga	14.0	14.1	11.5	8.9	18.7	18.0	19.3
Rb	299.6	336.2	259.2	293.3	237.3	193.9	215.4
Sr	146.1	128.6	167.0	24.1	444.4	415.0	441.5
Y	2.6	2.8	1.7	5.1	22.5	40.6	21.6
Zr	65.8	96.6	53.5	92.3	136.8	90.5	143.3
Nb	11.8	11.9	7.2	19.6	10.9	10.2	9.2
Ba	142.4	162.4	93.9	59.9	926.4	1398.6	915.0
La	19.0	16.3	5.1	20.9	31.1	43.2	29.8
Ce	14.6	19.5	1.5	28.2	67.5	83.0	64.3
Nd	2.3	2.8	1.3	6.8	27.9	38.2	28.9
Pb	44.7	46.8	46.1	40.9	58.4	46.6	51.9
Th	31.5	32.7	25.5	36.0	16.0	8.4	14.2
U	7.1	8.1	5.8	7.1	4.4	2.4	3.0
cipw							
%AN	3	12	16	18	38	47	42
Q	31	35	36	38			2
or	25	35	34	36	29	28	27
ab	41	23	23	21	27	21	28
an	1	3	4	5	17	19	20
lc							
ne							
C	1	1					
di					11	17	9
hy	1	1	1	1	7	12	12
wo							
ol					2		
mt					1	1	1
il					1	1	1
ap					1	1	1

APPENDIX C (III)

XRF analyses of the samples from the Central Anatolian Massif.

Pluton	*Behrekdag*	*Behrekdag*	*Celebi*	*Celebi*	*Celebi*	*Behrekdag*	*Behrekdag*
Sample no	**N174**	**N169**	**N66**	**N478**	**N201**	**N139**	**N140**
Characteristic	*fine-grd enc.*	*fine-grd enc.*	*fine-grd enc.*	*fine-grd enc.*	*fine-grd enc.*	*fine-grd enc.*	*fine-grd enc.*
Rock type	*qmzdi*			*qdi*	*qdi*	*qdi*	*qdi*
Geochemical description	*mz*	*qmz*	*mzd*	*mz*	*mz*	*mz*	*mz*
SiO_2	58.44	64.25	53.85	54.32	56.23	58.91	59.29
TiO_2	0.51	0.44	0.89	0.66	0.64	0.58	0.57
Al_2O_3	16.76	15.65	17.81	16.83	16.28	17.50	17.53
Fe_2O_3	6.67	4.97	9.69	7.76	7.22	5.54	5.37
MnO	0.18	0.10	0.20	0.21	0.16	0.14	0.14
MgO	2.54	1.76	3.86	3.11	3.24	1.99	1.95
CaO	5.79	4.61	6.35	7.44	7.19	4.40	4.30
Na_2O	3.16	3.02	4.47	3.14	2.51	3.55	3.62
K_2O	5.43	4.46	2.22	5.23	5.86	6.31	6.54
P_2O_5	0.16	0.14	0.23	0.29	0.15	0.35	0.35
L.O.I	1.05	1.12	2.42	1.56	0.46	0.82	0.71
TOTAL (L.O.I. free)	99.64	99.40	99.56	98.99	99.48	99.27	99.66
Sc	15.1	10.1	15.8	12.5	12.7	10.5	8.9
V	122.8	94.7	120.9	127.8	143.1	91.1	92.8
Cr	16.7	16.3	68.1	9.3	28.8	14.4	9.6
Co	17.3	12.8	29.2	20.3	14.3	12.2	14.1
Ni	12.3	7.6	19.5	9.9	17.6	9.8	10.6
Cu	12.7	19.9	8.0	14.1	34.8	69.6	58.3
Zn	96.8	59.6	131.1	95.1	91.4	104.3	95.7
Ga	14.0	18.8	26.9	20.5	18.9	26.9	21.1
Rb	259.3	168.5	155.2	333.5	231.7	279.5	265.8
Sr	417.6	432.5	520.3	436.5	437.0	515.2	516.4
Y	19.0	23.4	28.4	29.2	29.4	27.4	32.7
Zr	132.0	158.0	210.3	164.6	129.4	302.7	296.8
Nb	13.1	15.4	25.0	16.4	6.9	21.8	22.4
Ba	1200.8	931.6	367.4	780.1	1530.7	603.7	590.7
La	29.5	34.1	35.6	26.3	28.2	77.6	70.5
Ce	59.9	63.4	99.8	64.6	47.5	159.5	133.5
Nd	26.7	24.7	45.0	29.4	21.8	55.9	47.2
Pb	58.5	43.4	24.6	51.1	66.5	61.2	60.5
Th	8.9	24.7	13.0	16.5	0.6	22.9	27.1
U	5.5	3.9	5.3	4.3	3.2	5.4	7.1
cipw							
%AN	37	38	37	42	43	30	29
Q	2	15			35		
or	32	26	13	31	21	37	39
ab	27	26	38	22	16	30	31
an	16	16	22	16		13	12
lc							
ne				2			
C							
di	10	5	7	16	16	5	6
hy	11	9	5		6	10	10
wo							
ol			12	8	4		
mt	1	1	1	1	1	1	1
il	1	1	2	1	1	1	1
ap			1	1		1	1

APPENDIX C (III)

XRF analyses of the samples from the Central Anatolian Massif.

Pluton	*Behrekdag*	*Behrekdag*	*Cefalikdag*	*Cefalikdag*	*Cefalikdag*	*Cefalikdag*
Sample no	**N142**	**N158**	**N508**	**N509**	**N379**	**N381**
Characteristic	*fine-grd enc.*	*fine-grd enc.*	*medium-grd enc.*	*medium-grd enc.*	*medium-grd enc.*	*medium-grd enc.*
Rock type		*ton*		*gb*	*gb*	
Geochemical description	*mz*	*qmz*	*fgb*	*fgb*	*gb*	*gb*
SiO_2	59.66	65.64	42.19	42.86	45.70	46.48
TiO_2	0.62	0.43	1.13	1.06	1.26	1.15
Al_2O_3	17.01	15.59	16.72	17.61	17.77	15.56
Fe_2O_3	5.71	4.49	14.99	14.16	12.94	11.39
MnO	0.15	0.08	0.27	0.26	0.25	0.21
MgO	2.12	1.45	5.46	5.16	5.92	8.77
CaO	4.84	4.06	14.56	14.64	10.34	11.21
Na_2O	3.83	2.99	2.12	1.94	2.80	1.94
K_2O	5.02	4.82	1.52	1.44	1.75	2.18
P_2O_5	0.27	0.11	0.84	0.66	0.38	0.40
L.O.I	1.15	0.73	1.27	1.28	0.78	1.22
TOTAL (L.O.I. free)	99.22	99.67	99.80	99.79	99.11	99.29
Sc	10.1	14.2	38.0	32.6	32.3	34.3
V	83.2	138.2	259.3	241.2	266.9	238.1
Cr	18.2	17.5	9.0	12.6	14.6	270.4
Co	12.2	23.7	51.2	43.8	49.4	43.3
Ni	11.3	13.3	26.6	28.2	22.0	61.4
Cu	23.2	71.7	66.1	74.0	50.7	44.6
Zn	104.9	165.1	149.8	140.0	146.0	129.8
Ga	23.1	31.5	26.9	24.4	27.1	22.3
Rb	205.6	186.4	31.9	30.7	56.1	73.3
Sr	507.7	465.3	869.4	940.7	770.5	760.4
Y	29.7	22.6	36.6	33.0	36.6	33.7
Zr	257.7	286.7	152.3	136.5	163.5	184.9
Nb	25.2	20.0	12.1	9.7	17.6	16.0
Ba	518.6	252.7	319.0	384.5	673.2	774.5
La	57.3	51.2	22.9	21.0	37.0	34.4
Ce	133.4	92.2	104.1	99.2	136.8	108.0
Nd	49.7	22.1	63.9	58.7	80.5	61.8
Pb	52.1	35.6	21.6	15.7	18.7	17.3
Th	27.0	9.8	2.9	0.9	1.2	0.2
U	5.8	4.9	3.1			0.6
cipw						
%AN	31	37	100	100	71	76
Q	3	17				
or	30	28		4	10	13
ab	32	25			13	9
an	14	15	32	35	31	27
lc			7	3		
ne			10	9	6	4
C						
di	7	4	30	28	15	21
hy	10	8				
wo						
ol			16	15	19	20
mt	1	1	2	2	2	2
il	1	1	2	2	2	2
ap	1		2	2	1	1

APPENDIX C (III)

XRF analyses of the samples from the Central Anatolian Massif.

Pluton	*Cefalikdag*	*Cefalikdag*	*Cefalikdag*	*Cefalikdag*	*Cefalikdag*	*Cefalikdag*
Sample no	**N380**	**N241a**	**N228**	**N384**	**N80**	**N227**
Characteristic	*medium-grd enc.*	*medium-grd enc.*	*medium-grd enc.*	*medium-grd enc.*	*medium-grd enc.*	*medium-grd enc.*
Rock type		*gb*			*qdi*	
Geochemical description	*gb*	*mzgb*	*mzgb*	*mzgb*	*mzgb*	*mzgb*
SiO_2	47.36	47.89	47.93	48.23	48.47	48.75
TiO_2	1.14	1.18	1.18	1.24	1.17	1.10
Al_2O_3	15.40	18.29	16.88	18.04	18.38	18.38
Fe_2O_3	11.37	12.32	11.65	11.07	11.05	10.66
MnO	0.21	0.22	0.21	0.25	0.19	0.19
MgO	8.71	5.03	5.49	5.45	4.78	4.99
CaO	11.05	9.51	9.12	9.38	9.65	9.34
Na_2O	1.94	3.17	2.51	3.20	3.19	2.96
K_2O	2.22	1.92	2.55	2.19	2.08	2.45
P_2O_5	0.36	0.31	0.36	0.32	0.33	0.32
L.O.I	0.98	0.67	2.01	1.01	1.21	0.65
TOTAL (L.O.I. free)	99.76	99.84	97.88	99.37	99.28	99.14
Sc	33.3	25.3	23.7	30.2	24.3	30.6
V	249.7	201.7	218.5	174.8	208.3	229.5
Cr	275.5	13.3	32.3	53.9	30.1	27.7
Co	38.1	43.9	36.2	32.9	38.8	33.6
Ni	60.6	4.6	12.9	21.3	24.5	7.5
Cu	42.8	41.3	61.1	36.7	57.0	64.0
Zn	131.9	142.2	132.0	164.5	137.1	123.1
Ga	27.3	23.7	27.2	29.3	19.1	19.6
Rb	72.8	73.3	131.8	102.3	124.7	115.8
Sr	708.6	587.0	760.9	642.0	880.6	787.9
Y	33.9	33.3	27.7	44.2	23.4	28.5
Zr	188.3	147.2	208.3	220.3	193.5	145.9
Nb	16.0	18.7	18.7	24.0	18.8	18.2
Ba	687.7	473.2	1003.4	455.4	688.9	987.2
La	30.1	51.0	32.0	43.0	30.7	35.3
Ce	81.4	128.5	84.9	136.8	75.2	72.8
Nd	53.7	47.1	34.1	70.9	46.2	32.1
Pb	13.9	17.0	29.3	23.0	27.5	31.0
Th	0.1			4.1	1.8	
U	1.6	0.4		0.9	0.3	5.1
cipw						
%AN	71	61	59	60	60	59
Q			15		12	12
or	13	11	19	13	20	20
ab	11	19	27	19	30	29
an	27	30	1	28	4	3
lc						
ne	3	4		5		
C						
di	21	13	13	13	13	18
hy						
wo						
ol	20	18	18	17	16	15
mt	2	2	2	2	2	1
il	2	2	2	2	2	2
ap	1	1	1	1	1	1

APPENDIX C (III)

XRF analyses of the samples from the Central Anatolian Massif.

Pluton	*Cefalikdag*	*Cefalikdag*	*Cefalikdag*	*Cefalikdag*	*Cefalikdag*	*Cefalikdag*	*Cefalikdag*
Sample no	**N364**	**N403**	**N356**	**N355**	**N226a**	**N388**	**N387**
Characteristic	*medium-grd enc.*	*medium-grd enc.*	*medium-grd enc.*	*porphyritic enc.*	*porphyritic enc.*	*porphyritic enc.*	*porphyritic enc.*
Rock type					*qdi*		
Geochemical description	*mzgb*	*mzd*	*mzgb*	*mzgb*	*mzgb*	*gb*	*mzgb*
SiO_2	49.05	49.27	49.34	49.51	49.53	50.07	50.42
TiO_2	1.09	1.22	1.03	0.99	0.99	0.70	0.76
Al_2O_3	17.88	18.80	16.79	18.27	17.59	18.79	17.59
Fe_2O_3	10.85	10.56	10.42	10.35	10.16	9.93	10.50
MnO	0.21	0.23	0.24	0.19	0.21	0.21	0.22
MgO	5.26	4.16	5.82	4.45	5.64	4.07	4.51
CaO	9.57	7.97	9.80	9.75	10.54	9.98	9.69
Na_2O	3.07	3.68	2.80	3.24	2.96	4.00	3.50
K_2O	2.32	2.89	2.52	2.03	2.02	0.90	1.59
P_2O_5	0.29	0.42	0.28	0.26	0.37	0.33	0.27
L.O.I	0.74	1.58	1.63	1.65	0.65	0.84	0.67
TOTAL (L.O.I. free)	99.60	99.20	99.04	99.04	100.00	98.98	99.05
Sc	27.4	22.7	28.2	26.8	25.1	23.3	23.4
V	212.4	168.8	209.0	250.1	187.1	131.9	166.2
Cr	26.9	16.5	65.7	24.4	68.2	10.3	26.3
Co	38.4	28.6	35.7	33.0	26.6	25.4	29.7
Ni	15.8	16.3	17.9	18.0	31.2	14.5	21.1
Cu	31.2	125.6	53.0	25.0	96.1	68.9	97.8
Zn	142.0	164.6	134.4	124.6	128.2	128.9	136.8
Ga	23.1	28.8	21.5	24.5	23.1	25.1	26.3
Rb	118.4	165.1	113.2	85.3	122.5	29.7	49.5
Sr	717.8	529.1	634.6	810.6	817.9	676.9	589.4
Y	28.0	46.2	32.1	30.0	34.2	46.8	41.3
Zr	166.4	299.7	239.8	218.4	124.0	144.6	159.7
Nb	17.9	28.4	19.9	13.9	13.1	20.1	19.4
Ba	865.1	341.2	867.1	883.0	687.0	94.0	252.3
La	26.6	65.0	25.2	29.8	38.3	39.5	32.7
Ce	77.9	164.3	59.9	83.6	72.3	128.2	110.4
Nd	42.8	88.1	38.3	45.3	47.8	70.4	62.3
Pb	33.2	35.1	26.7	27.5	25.4	35.6	32.6
Th	2.7	12.8	0.8		2.8	1.1	2.5
U	2.2	1.3	0.6	1.3	1.2	1.2	3.6
cipw							
%AN	59	55	58	56	59	50	50
Q					12		
or	14	17	15	12	20	19	9
ab	19	21	19	23	29	23	28
an	28	26	26	29	3	24	28
lc							
ne	4	5	3	2		1	1
C							
di	15	9	17	15	18	15	16
hy							
wo							
ol	16	16	15	14	15	14	14
mt	2	2	2	2	1	1	2
il	2	2	2	2	2	2	1
ap	1	1	1	1	1	1	1

APPENDIX C (III)

XRF analyses of the samples from the Central Anatolian Massif.

Pluton	*Cefalikdag*	*Cefalikdag*	*Cefalikdag*	*Cefalikdag*	*Cefalikdag*	*Cefalikdag*	*Cefalikdag*
Sample no	**N375**	**N389**	**N401**	**N402b**	**N385**	**N402**	**N398**
Characteristic	*porphyritic enc.*	*porphyritic enc.*	*porphyritic enc.*	*porphyritic enc.*	*porphyritic enc.*	*porphyritic enc.*	*porphyritic enc.*
Rock type		*qdi*					
Geochemical description	*mzgb*	*mzd*	*mzd*	*mz*	*di*	*mz*	*mz*
SiO_2	50.72	51.44	52.53	54.48	55.44	56.91	58.55
TiO_2	0.82	0.83	0.87	0.85	0.86	0.63	0.58
Al_2O_3	18.36	17.00	16.00	15.53	16.55	15.87	15.57
Fe_2O_3	9.95	9.68	10.24	9.63	8.09	8.00	6.97
MnO	0.20	0.23	0.26	0.24	0.17	0.20	0.18
MgO	4.57	4.73	4.48	4.26	4.27	3.34	3.27
CaO	9.03	8.73	7.44	7.03	7.95	6.17	5.74
Na_2O	3.14	3.02	2.88	2.85	2.84	2.82	2.78
K_2O	1.87	3.14	4.02	3.81	2.58	5.04	5.08
P_2O_5	0.25	0.23	0.24	0.24	0.22	0.25	0.24
L.O.I	1.26	0.77	0.96	1.14	1.10	0.86	0.92
TOTAL (L.O.I. free)	98.91	99.03	98.96	98.92	98.97	99.23	98.96
Sc	22.5	20.9	24.6	18.8	24.5	18.5	15.2
V	117.7	188.6	153.7	151.8	133.6	120.9	100.1
Cr	9.6	29.4	35.9	34.5	59.8	30.6	43.9
Co	30.0	31.2	29.9	30.5	23.7	21.2	17.7
Ni	18.1	24.1	18.0	14.8	17.0	15.1	19.1
Cu	41.4	84.6	414.9	460.4	12.7	233.2	224.0
Zn	120.7	127.9	142.1	131.9	107.2	106.3	93.6
Ga	22.9	25.1	20.9	24.9	19.9	19.7	20.4
Rb	88.5	87.4	138.8	139.0	104.2	156.3	163.8
Sr	430.0	605.5	462.2	460.1	633.4	506.9	515.1
Y	41.5	36.2	47.9	41.9	28.9	43.6	41.8
Zr	190.1	159.2	160.2	153.6	193.6	193.5	193.3
Nb	17.3	19.0	27.5	25.4	16.7	21.2	18.4
Ba	462.6	732.3	571.1	575.7	814.7	685.2	915.3
La	25.7	37.6	33.7	28.8	34.5	35.8	33.8
Ce	86.5	110.4	98.6	88.5	84.4	93.9	82.7
Nd	49.2	56.3	71.9	58.7	37.8	56.1	49.9
Pb	18.6	37.8	46.5	43.2	34.7	63.6	52.2
Th	1.6	3.1	3.6	5.3	6.2	28.5	40.3
U	2.6	0.6	1.7	4.1	2.6	2.3	3.9
cipw							
%AN	53	50	44	43	51	40	39
Q					4	1	4
or	11	19	24	23	15	30	30
ab	27	23	24	24	24	24	24
an	30	24	19	18	25	16	15
lc							
ne		1					
C							
di	11	15	14	13	11	11	10
hy	5			16	17	15	13
wo							
ol	12	14	14	2			
mt	1	1	1	1	1	1	1
il	2	2	2	2	2	1	1
ap	1	1	1	1	1	1	1

APPENDIX C (III)

XRF analyses of the samples from the Central Anatolian Massif.

Area	*Kaman*	*Kaman*	*Kaman*	*Kaman*	*Kaman*	*Kaman*	*Kaman*
Sample no	**N365**	**N370**	**N362**	**N491**	**N490**	**C-1**	**C-2**
Rock type	*marble*	*meta-greywacke*	*meta-greywacke*	*meta-greywacke*	*meta-greywacke*	*semi-pelite*	*semi-pelite*
SiO_2	56.88	69.66	72.94	74.29	74.96	77.26	77.52
TiO_2	0.01	0.42	0.67	0.03	0.17	0.38	0.39
Al_2O_3		14.48	12.71	13.17	12.52	11.30	11.21
Fe_2O_3	0.25	3.47	4.61	1.45	1.61	3.88	3.87
MnO	0.00	0.06	0.09	0.03	0.02	0.06	0.06
MgO	15.31	1.62	1.85	0.71	0.71	2.16	2.10
CaO	27.78	4.04	2.39	1.65	1.57	0.44	0.45
Na_2O	0.24	3.19	2.21	2.54	2.14	0.74	0.74
K_2O	0.01	1.99	1.46	5.13	5.58	2.76	2.84
P_2O_5		0.07	0.05	0.04	0.03	0.06	0.07
L.O.I	-2.79	0.92	1.80	1.33	1.12	2.52	2.57
TOTAL (L.O.I. free)	100.48	98.99	98.97	99.03	99.32	99.03	99.25
Sc	41.1	10.0	8.8	4.1	4.7	4.9	6.8
V	1.5	53.3	105.6	16.7	18.7	69.4	75.8
Cr	2.8	30.3	85.3	4.0	4.6	1236.4	489.8
Co	1.7	5.1	8.7	0.5	0.9	6.4	6.2
Ni	7.2	10.1	31.2	2.3	2.0	102.0	95.8
Cu	3.8	7.0	20.6	3.8	19.9	28.4	26.2
Zn	13.5	49.8	47.3	16.0	11.9	54.5	53.9
Ga	3.7	18.1	16.5	14.2	11.9	19.8	18.8
Rb	1.1	89.6	59.0	261.2	261.6	128.4	124.5
Sr	38.1	237.7	179.4	76.7	84.5	51.4	51.0
Y	1.5	5.7	41.6	17.4	20.7	18.5	17.3
Zr	9.8	130.4	241.8	136.6	124.2	137.9	130.8
Nb	1.7	9.8	15.1	15.3	13.5	13.5	12.8
Ba	7.5	394.1	361.4	500.9	662.1	466.2	485.9
La	1.1	15.4	40.8	25.2	21.5	15.5	23.6
Ce	5.5	26.9	78.6	45.7	34.4	37.4	58.1
Nd	2.3	12.5	37.6	18.2	12.8	13.0	23.3
Pb	50.6	21.8	18.9	39.8	32.8	15.5	17.6
Th	1.2	21.7	21.0	26.5	22.5	7.8	6.2
U	2.1	4.4	1.9	2.6	1.9	1.7	1.0
cipw							
%AN		42	38	27	30	22	22
Q	4	30	44	34	36	56	56
or		12	9	30	33	16	17
ab		27	19	21	18	6	6
an		19	12	8	8	2	2
lc							
ne							
C			3	1		6	6
di	83						
hy		9	11	4	4	11	11
wo	13						
ol							
mt		1	1			1	1
il		1	1			1	1
ap							

APPENDIX C (III)

XRF analyses of the samples from the Central Anatolian Massif.

Area	*Kaman*	*Kaman*	*Kaman*	*Kaman*
Sample no	**N353**	**N464**	**N364**	**N463**
Rock type	*meta-greywacke*	*meta-greywacke*	*meta-greywacke*	*meta-greywacke*
SiO_2	81.02	83.65	83.78	87.13
TiO_2	0.76	0.37	0.69	0.31
Al_2O_3	7.11	6.79	6.44	4.87
Fe_2O_3	4.81	3.75	3.97	3.33
MnO	0.07	0.14	0.06	0.09
MgO	1.75	1.77	1.51	1.09
CaO	0.89	0.19	0.95	0.33
Na_2O	1.35	0.62	0.82	0.74
K_2O	1.41	1.79	0.79	1.19
P_2O_5	0.02	0.02	0.03	0.07
L.O.I	1.30	2.16	1.91	1.47
TOTAL (L.O.I. free)	99.19	99.09	99.04	99.15
Sc	7.7	5.4	6.3	5.6
V	111.5	169.3	122.2	33.7
Cr	64.6	49.7	63.2	27.9
Co	10.1	13.3	6.9	6.8
Ni	30.7	37.1	23.7	26.3
Cu	25.3	8.7	19.3	4.4
Zn	48.3	51.9	40.7	35.4
Ga	13.8	17.5	11.6	13.7
Rb	63.7	65.2	31.9	39.0
Sr	89.7	34.8	48.1	36.9
Y	28.5	18.6	29.3	17.9
Zr	431.3	69.2	461.0	58.1
Nb	15.4	8.3	15.7	5.6
Ba	438.6	182.1	155.3	141.7
La	41.5	28.6	37.4	20.5
Ce	81.9	78.2	65.5	38.2
Nd	35.9	23.6	32.4	16.9
Pb	10.5	6.4	3.9	5.0
Th	18.5	8.4	11.4	7.3
U	1.5	2.7	1.7	1.8
cipw				
%AN	27	13	39	16
Q	60	68	69	74
or	8	11	5	7
ab	11	5	7	6
an	4	1	5	1
lc				
ne				
C	2	4	3	2
di				
hy	11	10	9	8
wo				
ol				
mt	1	1	1	
il	1	1	1	1
ap				

(*)=pellet result

APPENDIX C (IV-I)- ICP-MS whole-rock dataset

APPENDIX C (IV-1)

XRF and ICP-MS whole-rock results of the samples from the Central Anatolian Massif.

Pluton	*Behrekdag*	*Behrekdag*	*Behrekdag*	*Behrekdag*	*Behrekdag*	*Cefalikdag*	*Cefalikdag*	*Cefalikdag*	*Cefalikdag*	*Cefalikdag*	*Cefalikdag*	*Cefalikdag*	*Celebi*	*Celebi*	*Celebi*
Sample no	**N2**	**N99**	**N107**	**N5**	**N6**	**N225**	**N233**	**N78**	**N85**	**N20**	**N310**	**N395**	**N24**	**N71**	**N75**
Characteristic															
Rock type	*qmz*	*qmz*	*qmz*	*gr*	*gr*	*mzdi*	*mzdi*	*qmzdi*	*qmzdi*	*qmz*	*qmz*	*gr*	*qmz*	*qmz*	*gr*
Geochemical description	*mz*	*mz*	*qmz*	*qmz*	*qmz*	*mzgb*	*mzdi*	*mzdi*	*mzdi*	*mz*	*mz*	*gr*	*qmz*	*qmz*	*qmz*
SiO_2	60.11	60.15	60.20	63.58	63.61	50.45	51.36	53.86	58.17	61.82	63.27	71.53	63.71	63.72	65.07
TiO_2	0.61	0.63	0.61	0.45	0.42	1.08	0.93	0.85	0.67	0.61	0.52	0.20	0.47	0.42	0.39
Al_2O_3	16.49	16.38	16.29	16.19	16.29	18.04	18.08	17.70	17.94	16.36	16.87	14.37	16.32	16.04	15.81
Fe_2O_3	6.04	6.11	5.87	4.93	4.68	9.71	9.08	8.22	6.27	5.77	4.94	1.98	4.79	4.65	4.34
MnO	0.12	0.12	0.12	0.10	0.10	0.18	0.17	0.15	0.13	0.12	0.12	0.05	0.10	0.10	0.09
MgO	2.42	2.26	2.33	1.83	1.69	5.09	4.15	3.74	2.80	2.52	2.06	0.61	1.85	1.60	1.46
CaO	6.38	6.21	6.50	4.72	4.79	9.34	8.94	8.22	6.30	5.14	4.42	1.97	5.01	4.51	4.33
Na_2O	2.94	2.92	3.03	2.93	3.05	2.90	3.10	2.99	3.31	2.99	3.61	2.82	3.01	3.31	3.13
K_2O	3.89	4.22	4.04	4.89	4.51	2.80	2.56	3.23	3.62	4.19	3.58	5.37	3.91	4.54	4.54
P_2O_5	0.18	0.18	0.15	0.14	0.13	0.29	0.30	0.27	0.20	0.19	0.15	0.06	0.14	0.14	0.14
L.O.I	0.37	0.55	0.57	0.51	0.54	0.49	0.66	0.78	0.90	0.51	1.06	0.79	0.39	0.49	0.54
TOTAL (L.O.I. free)	99.18	99.19	99.15	99.77	99.27	99.88	98.67	99.24	99.41	99.71	99.54	98.96	99.31	99.02	99.30
Rb	135.8	145.0	131.4	168.8	160.3	114.4	85.6	93.2	121.7	143.3	134.3	159.7	148.3	172.3	186.7
Sr	546.2	528.9	539.7	475.3	482.1	825.9	899.1	891.1	636.1	507.7	474.4	335.6	466.5	425.1	461.8
Y	24.4	29.0	26.3	24.8	25.3	28.8	28.5	25.6	29.2	29.7	24.4	6.9	25.2	24.2	24.9
Zr	200.3	204.3	183.9	167.5	155.3	227.7	240.5	233.9	231.4	220.3	169.0	128.7	178.8	172.4	162.1
Nb	15.4	17.0	15.3	16.0	15.5	17.5	19.9	17.9	16.5	18.3	15.7	8.3	16.0	15.7	18.0
Cs	6.0	10.0	6.1	4.1	4.2	3.1	2.6	2.2	7.9	6.5	5.4	6.3	6.8	7.7	5.8
Ba	1019.2	1091.7	1098.9	1217.4	1182.6	1220.2	1078.3	1386.3	1080.8	993.4	1091.6	705.8	794.5	983.6	800.7
La	56.60	49.00	47.36	49.97	47.09	37.76	44.79	43.64	67.57	59.18	43.87	25.27	41.25	46.16	49.86
Ce	95.69	86.45	86.50	85.33	82.81	72.11	86.87	82.10	116.02	103.27	81.29	45.19	71.52	78.93	91.06
Pr	10.59	10.17	9.85	9.71	9.51	9.19	10.76	10.04	13.02	12.05	9.50	5.00	8.44	9.03	10.53
Nd	35.59	36.74	35.16	34.10	33.39	36.31	40.67	38.40	45.44	42.19	33.86	16.50	30.50	31.02	36.35
Sm	5.84	6.40	6.41	5.79	5.75	7.51	7.88	7.20	7.23	7.14	6.30	2.50	5.58	5.60	6.04
Eu	1.37	1.37	1.40	1.14	1.20	1.77	1.94	1.83	1.61	1.40	1.31	0.41	1.14	1.10	1.17
Gd	4.59	5.17	4.83	4.33	4.66	6.55	6.35	5.96	6.23	5.61	4.87	1.57	4.47	3.98	4.36
Tb	0.73	0.84	0.77	0.73	0.71	0.95	0.93	0.85	0.89	0.88	0.76	0.22	0.73	0.69	0.69
Dy	3.98	4.71	4.32	4.00	4.14	5.41	4.92	4.67	4.83	4.86	4.17	1.18	3.92	3.87	3.78
Ho	0.79	0.97	0.89	0.81	0.86	1.07	0.96	0.89	0.96	0.94	0.83	0.23	0.82	0.80	0.78
Er	2.14	2.58	2.35	2.20	2.20	2.59	2.53	2.42	2.53	2.68	2.07	0.60	2.25	2.19	2.10
Tm	0.36	0.43	0.41	0.39	0.38	0.41	0.39	0.34	0.41	0.44	0.35	0.11	0.37	0.38	0.36
Yb	2.18	2.55	2.50	2.33	2.39	2.46	2.27	2.14	2.52	2.74	2.20	0.68	2.39	2.46	2.31
Lu	0.36	0.43	0.40	0.39	0.39	0.39	0.37	0.34	0.41	0.45	0.35	0.12	0.37	0.42	0.39
Hf	5.16	5.24	4.61	4.34	4.15	5.05	5.70	5.43	5.65	5.82	4.43	3.21	4.65	4.63	4.38
Ta	0.96	1.32	0.77	1.26	1.12	0.82	1.24	0.85	0.92	1.32	0.70	0.28	1.23	1.11	1.49
Pb	41.74	56.49	49.41	43.30	58.98	28.13	30.47	34.08	32.52	43.19	29.62	37.72	41.08	47.37	47.55
Th	22.34	19.42	19.75	24.44	22.33	8.21	8.04	11.17	21.31	23.23	21.87	14.88	27.21	29.12	36.89
U	4.48	4.57	4.25	4.34	5.60	2.01	2.59	3.08	3.86	5.07	3.80	2.90	7.12	5.59	5.69

APPENDIX C (IV-1)

XRF and ICP-MS whole-rock results of the samples from the Central Anatolian Massif.

Pluton	Celebi	Celebi	Baranadag	Baranadag	Baranadag	Baranadag	Baranadag	Baranadag	Baranadag	Hamit	Hamit	Hamit	Hamit	Hamit	Hamit
Sample no	N206	N214	N26	N304	N19	N18	N303	N15	N16	N45	N33	N252	N294	N287	N286
Characteristic														foid-bear. dyke	foid-bear. dyke
Rock type	gr	gr	mz	mz	mz	qmz	qmz	qmz	qmz	pdmzsy	nemzsy	nemzsy	pdmzsy	pho	pho
Geochemical description	qmz	gr	mz	mz	sy	sy	sy	sy	sy	fmzsy	fmzsy	fmzsy	fmzsy	fsy	fsy
SiO_2	67.68	69.39	58.44	58.52	60.93	61.33	61.85	62.07	62.62	52.83	53.32	53.58	54.23	54.98	55.94
TiO_2	0.32	0.26	0.59	0.56	0.51	0.51	0.39	0.42	0.44	0.62	0.72	0.74	0.62	0.22	0.20
Al_2O_3	15.53	14.70	17.62	17.47	17.39	17.35	18.26	17.43	17.77	19.15	18.09	18.36	18.98	23.43	22.83
Fe_2O_3	3.23	2.74	5.42	5.16	4.81	4.59	3.49	3.97	4.25	5.39	6.49	6.49	5.19	2.35	2.20
MnO	0.07	0.06	0.13	0.12	0.12	0.11	0.09	0.10	0.10	0.14	0.15	0.14	0.13	0.15	0.14
MgO	1.05	0.86	1.85	1.78	1.74	1.67	1.13	1.20	1.34	1.47	2.97	3.02	1.40	0.25	0.06
CaO	3.31	2.81	5.95	5.56	4.16	4.24	3.58	3.90	3.94	6.72	7.01	6.98	6.93	2.18	2.03
Na_2O	3.01	2.83	3.73	3.78	3.81	3.88	3.93	3.83	3.79	4.29	3.37	3.35	3.76	8.13	7.92
K_2O	5.33	5.36	5.52	5.81	5.37	5.33	6.68	5.66	5.39	7.87	6.71	6.67	7.83	7.99	8.08
P_2O_5	0.10	0.07	0.24	0.25	0.22	0.21	0.14	0.17	0.19	0.31	0.42	0.41	0.31	0.03	0.02
L.O.I	0.92	0.90	0.58	0.78	0.38	0.65	0.60	0.77	0.41	1.43	1.05	1.49	2.12	3.22	3.12
TOTAL (L.O.I. free)	99.63	99.07	99.48	99.00	99.06	99.22	99.54	98.75	99.83	98.78	99.25	99.73	99.38	99.70	99.42
Rb	197.4	212.5	191.8	203.8	202.7	207.7	230.3	222.5	193.8	288.4	212.9	210.5	211.3	336.7	337.2
Sr	385.7	347.7	882.4	920.2	571.6	569.3	628.7	579.1	568.7	1203.9	1252.9	1199.7	1558.8	169.4	152.0
Y	22.9	15.3	31.1	30.6	30.4	28.4	27.3	25.8	26.7	33.4	31.7	31.0	22.9	25.8	21.6
Zr	148.0	123.5	308.3	305.3	276.3	272.1	272.1	253.7	264.8	426.8	366.3	343.4	376.3	793.8	785.4
Nb	16.8	13.4	28.1	26.6	24.2	23.7	23.0	21.8	21.6	56.8	40.6	38.1	48.5	83.6	82.6
Cs	4.3	3.8	6.7	6.9	10.1	10.4	8.1	6.7	8.6	19.5	10.5	9.3	15.7	35.9	33.9
Ba	970.6	826.8	920.5	974.9	984.4	939.2	1134.0	930.3	912.6	1053.0	1451.0	1437.4	1953.2	130.5	122.2
La	50.83	44.28	89.24	64.30	80.80	70.02	63.32	59.36	69.08	122.09	112.68	116.51	92.40	152.60	149.24
Ce	88.27	70.89	157.48	135.35	136.62	120.81	120.58	111.19	123.50	223.53	208.86	171.51	172.00	220.79	216.60
Pr	9.75	7.41	17.75	16.17	14.97	13.79	13.89	12.85	14.11	24.24	23.03	23.22	20.54	23.12	22.29
Nd	32.90	23.68	60.12	57.65	52.37	47.59	48.46	44.12	47.94	86.42	76.77	83.44	73.54	63.05	59.99
Sm	5.53	3.81	9.90	9.53	8.69	7.75	8.03	6.91	8.02	13.77	13.57	13.67	11.90	7.41	6.79
Eu	1.09	0.80	2.01	2.00	1.60	1.47	1.58	1.54	1.55	2.88	2.89	2.96	2.67	1.03	0.92
Gd	3.91	2.46	6.39	6.98	6.39	5.84	5.11	4.75	5.51	12.00	9.58	9.91	8.35	4.67	4.12
Tb	0.61	0.44	1.01	0.98	0.96	0.87	0.81	0.80	0.84	1.25	1.00	1.24	1.08	0.71	0.59
Dy	3.43	2.30	5.20	5.26	5.14	4.81	4.45	4.11	4.49	6.00	5.16	5.87	5.35	3.65	2.94
Ho	0.72	0.49	0.97	1.01	1.02	0.93	0.89	0.83	0.89	1.04	0.83	1.03	0.93	0.72	0.58
Er	1.90	1.33	2.60	2.45	2.64	2.46	2.28	2.12	2.20	2.77	2.14	2.61	2.45	2.19	1.74
Tm	0.34	0.25	0.43	0.43	0.41	0.39	0.40	0.37	0.40	0.43	0.32	0.41	0.39	0.40	0.32
Yb	2.31	1.53	2.64	2.71	2.43	2.29	2.49	2.36	2.41	2.50	2.25	2.41	2.27	2.67	2.19
Lu	0.39	0.26	0.42	0.41	0.39	0.36	0.39	0.38	0.37	0.37	0.32	0.37	0.34	0.42	0.35
Hf	4.24	3.47	6.91	6.72	6.67	6.57	6.58	6.36	6.53	8.25	7.32	8.26	8.33	13.61	13.56
Ta	1.05	1.06	1.74	1.33	1.17	1.42	1.32	1.59	1.34	3.09	2.13	2.22	2.89	3.11	3.02
Pb	44.31	48.33	38.69	42.89	52.62	51.69	55.36	54.06	52.59	63.05	51.51	55.45	69.30	137.99	129.32
Th	36.99	37.81	30.19	36.71	42.90	39.81	37.37	32.72	32.55	59.89	50.91	51.77	28.46	133.72	130.12
U	4.27	5.96	5.29	7.86	6.77	6.28	11.30	6.59	5.70	18.46	13.72	11.75	19.26	48.56	46.19

APPENDIX C (IV-2)

ICP-MS mineral results of the intrusive samples from the Central Anatolian Massif.

Pluton	*Behrekdag*	*Cefalikdag*	*Cefalikdag*	*Celebi*	*Baranadag*	*Cefalikdag*	*Behrekdag*	*Cefalikdag*	*Cefalikdag*	*Celebi*	*Celebi*
Sample no	**N2**	**N78**	**N85**	**N214**	**N26**	**N85**	**N2**	**N78**	**N85**	**N75**	**N214**
Mineral	*amp*	*amp*	*amp*	*amp*	*amp*	*bi*	*pl*	*pl*	*pl*	*pl*	*pl*
SiO_2 of the host rock	60.11	53.86	58.17	58.17	58.44	58.17	60.11	53.86	58.17	65.07	69.09
Rb	31.1	50.8	138.8	26.5	19.4	107.6	127.3	136.7	120.6	107.5	205.0
Sr	85.3	288.5	107.9	212.0	179.3	247.7	957.1	1339.7	1088.7	1033.8	966.2
Y	64.8	48.3	99.7	69.0	53.3	55.8	5.3	1.9	1.4	1.6	1.0
Zr	84.5	72.6	124.2	298.1	166.2	182.2	13.0	8.3	5.5	7.2	5.7
Nb	24.5	25.0	40.1	49.5	37.1	24.9	4.0	1.0	0.4	0.6	0.5
Cs	2.8	1.9	11.3	0.9	0.7	10.4	5.3	2.5	4.0	2.0	1.8
Ba	177.7	352.4	246.0	32.1	41.1	181.5	2361.8	2063.8	3316.8	3567.1	5142.2
La	67.61	70.79	56.20	155.5	119.29	111.51	21.60	15.72	17.23	14.11	7.74
Ce	138.60	137.36	154.80	281.6	262.10	196.42	32.29	19.70	21.30	16.93	8.04
Pr	14.91	14.74	19.76	25.0	24.62	18.91	2.74	1.47	1.56	1.32	0.62
Nd	64.75	65.01	94.38	92.8	95.08	74.63	9.99	5.08	5.11	4.48	2.16
Sm	13.36	13.03	21.35	15.7	15.37	13.29	1.52	0.66	0.58	0.57	0.31
Eu	1.69	2.65	2.65	1.9	3.07	1.96	2.06	1.35	2.39	2.45	2.60
Gd	14.08	13.26	21.47	16.7	15.96	14.28	1.79	0.93	0.94	0.89	0.47
Tb	2.15	1.88	3.46	2.1	1.89	1.96	0.20	0.07	0.06	0.06	0.03
Dy	10.76	8.87	17.41	10.2	8.75	9.58	0.96	0.32	0.24	0.26	0.16
Ho	2.10	1.63	3.30	2.0	1.63	1.82	0.17	0.06	0.04	0.05	0.03
Er	6.43	4.70	9.79	6.5	4.94	5.48	0.50	0.17	0.12	0.14	0.09
Yb	6.06	3.93	8.68	7.2	5.05	5.14	0.46	0.15	0.11	0.13	0.08
Lu	0.89	0.56	1.20	1.1	0.79	0.73	0.06	0.02	0.02	0.02	0.01
Hf	3.32	2.53	4.29	10.4	6.01	5.14	0.40	0.20	0.17	0.19	0.16
Ta	1.25	1.14	2.21	4.0	2.00	1.59	0.44	0.08	0.06	0.06	0.05
Pb	22.62	15.26	13.03	38.8	11.22	12.26	49.15	58.56	58.48	59.46	81.17
Th	12.59	11.69	12.43	88.6	16.09	25.00	4.44	3.58	1.69	3.64	2.77
U	3.64	4.71	5.35	31.6	5.05	5.04	1.66	0.87	0.67	0.75	0.63

APPENDIX C (IV-2)

ICP-MS mineral results of the intrusive samples from the Central Anatolian Massif.

Pluton	*Behrekdag*	*Cefalikdag*	*Celebi*	*Celebi*	*Baranadag*
Sample no	**N2**	**N85**	**N75**	**N214**	**N18**
Mineral	*ksp*	*ksp*	*ksp*	*ksp*	*ksp*
SiO_2 of the host rock	60.11	58.17	65.07	69.09	61.33
Rb	149.8	259.7	269.2	237.9	341.9
Sr	120.1	71.2	83.1	110.2	92.3
Y	3.9	1.1	2.3	1.6	1.4
Zr	6.6	7.7	3.2	10.9	13.6
Nb	2.4	0.5	1.3	0.9	0.6
Cs	5.3	4.5	3.9	3.4	6.3
Ba	2510.5	6475.6	5000.5	2170.7	2488.5
La	25.07	6.39	5.72	5.24	8.82
Ce	34.91	7.40	7.59	7.03	10.34
Pr	2.77	0.57	0.72	0.62	0.77
Nd	9.52	1.94	2.89	2.22	2.73
Sm	1.31	0.32	0.56	0.38	0.41
Eu	2.02	2.50	2.51	1.19	1.57
Gd	1.65	0.43	0.60	0.42	0.48
Tb	0.15	0.04	0.08	0.05	0.04
Dy	0.67	0.16	0.36	0.24	0.20
Ho	0.12	0.03	0.07	0.05	0.04
Er	0.36	0.10	0.21	0.15	0.12
Yb	0.32	0.09	0.18	0.16	0.11
Lu	0.05	0.01	0.03	0.03	0.02
Hf	0.20	0.21	0.11	0.30	0.30
Ta	0.29	0.08	0.15	0.10	0.05
Pb	54.94	89.23	86.99	61.97	92.03
Th	7.06	1.83	4.45	5.88	1.82
U	1.97	0.87	0.59	0.95	1.07

APPENDIX C (IV-3)- Partition coefficient (mineral/whole-rock) data

APPENDIX C (IV-3)

Mineral/whole-rock partition coeffients of amphibole, biotite, plagioclase and alkali feldspars.

Pluton	*Behrekdag*	*Cefalikdag*	*Cefalikdag*	*Celebi*	*Baranadag*	*Cefalikdag*	*Behrekdag*	*Cefalikdag*	*Cefalikdag*	*Celebi*	*Celebi*
Sample no	**N2**	**N78**	**N85**	**N214**	**N26**	**N85**	**N2**	**N78**	**N85**	**N75**	**N214**
Mineral/whole-rock	*amp/wr*	*amp/wr*	*amp/wr*	*amp/wr*	*amp/wr*	*bi/wr*	*pl/wr*	*pl/wr*	*pl/wr*	*pl/wr*	*pl/wr*
Rb	0.23	0.55	1.14	0.12	0.10	0.88	0.04	0.05	0.10	0.22	0.15
Sr	0.16	0.32	0.17	0.61	0.20	0.39	1.75	1.50	1.71	2.24	2.78
Y	2.66	1.88	3.42	4.50	1.71	1.91	0.22	0.07	0.05	0.07	0.07
Zr	0.42	0.31	0.54	2.41	0.54	0.79	0.06	0.04	0.02	0.04	0.05
Nb	1.60	1.39	2.43	3.68	1.32	1.51	0.26	0.06	0.02	0.03	0.04
Cs	0.47	0.86	1.43	0.25	0.11	1.32	0.88	1.12	0.51	0.33	0.47
Ba	0.17	0.25	0.23	0.04	0.04	0.17	0.20	0.23	0.38	0.82	0.63
La	1.19	1.62	0.83	3.51	1.34	1.65	0.38	0.36	0.25	0.28	0.17
Ce	1.45	1.67	1.33	3.97	1.66	1.69	0.34	0.24	0.18	0.19	0.11
Pr	1.41	1.47	1.52	3.37	1.39	1.45	0.26	0.15	0.12	0.12	0.08
Nd	1.82	1.69	2.08	3.92	1.58	1.64	0.28	0.13	0.11	0.12	0.09
Sm	2.29	1.81	2.95	4.11	1.55	1.84	0.26	0.09	0.08	0.09	0.08
Eu	1.24	1.44	1.67	2.37	1.55	1.24	1.37	0.65	1.31	1.81	2.66
Gd	3.07	2.23	3.44	6.80	2.50	2.29	0.39	0.16	0.15	0.20	0.19
Tb	2.95	2.22	3.87	4.80	1.87	2.20	0.27	0.09	0.06	0.09	0.08
Dy	2.70	1.90	3.60	4.45	1.68	1.98	0.24	0.07	0.05	0.07	0.07
Ho	2.67	1.83	3.43	4.14	1.67	1.89	0.22	0.06	0.04	0.06	0.06
Er	3.00	1.95	3.87	4.91	1.90	2.17	0.23	0.07	0.05	0.07	0.07
Yb	2.78	1.83	3.45	4.70	1.92	2.04	0.21	0.07	0.04	0.05	0.06
Lu	2.51	1.65	2.93	4.42	1.86	1.79	0.18	0.07	0.04	0.05	0.05
Hf	0.64	0.47	0.76	2.99	0.87	0.91	0.08	0.04	0.03	0.04	0.04
Ta	1.31	1.34	2.39	3.78	1.15	1.73	0.46	0.09	0.07	0.04	0.05
Pb	0.54	0.45	0.40	0.80	0.29	0.38	1.18	1.72	1.80	1.25	1.68
Th	0.56	1.05	0.58	2.34	0.53	1.17	0.20	0.32	0.08	0.10	0.07
U	0.81	1.53	1.39	5.30	0.95	1.30	0.37	0.28	0.17	0.13	0.11

APPENDIX C (IV-3)

Mineral/whole-rock partition coeffients of amphibole, biotite, plagioclase and alkali feldspars.

Pluton	*Behrekdag*	*Cefalikdag*	*Celebi*	*Celebi*	*Baranadag*
Sample no	**N2**	**N85**	**N75**	**N214**	**N18**
Mineral/whole-rock	*ksp/wr*	*ksp/wr*	*ksp/wr*	*ksp/wr*	*ksp/wr*
Rb	1.10	2.13	1.44	1.12	1.65
Sr	0.22	0.11	0.18	0.32	0.16
Y	0.16	0.04	0.09	0.10	0.05
Zr	0.03	0.03	0.02	0.05	0.05
Nb	0.16	0.03	0.07	0.07	0.03
Cs	0.88	0.57	0.67	0.91	0.61
Ba	2.46	5.99	6.25	2.63	2.65
La	0.44	0.09	0.11	0.12	0.13
Ce	0.36	0.06	0.08	0.10	0.09
Pr	0.26	0.04	0.07	0.08	0.06
Nd	0.27	0.04	0.08	0.09	0.06
Sm	0.22	0.04	0.09	0.10	0.05
Eu	1.48	1.20	1.73	1.48	0.92
Gd	0.36	0.07	0.14	0.17	0.08
Tb	0.21	0.04	0.11	0.12	0.05
Dy	0.17	0.03	0.09	0.10	0.04
Ho	0.15	0.03	0.09	0.09	0.04
Er	0.17	0.04	0.10	0.11	0.05
Yb	0.15	0.03	0.08	0.10	0.05
Lu	0.14	0.03	0.07	0.10	0.06
Hf	0.04	0.04	0.02	0.09	0.05
Ta	0.30	0.08	0.10	0.09	0.03
Pb	1.32	2.74	1.83	1.26	1.78
Th	0.32	0.09	0.12	0.16	0.05
U	0.44	0.23	0.10	0.16	0.17